Scuola Internazionale Superiore di Studi Avanzati - Trieste

Doctoral Thesis

Aspects of the Symmetry Approach to Neutrino Masses and Mixing

Candidate : João Tiago Neves Penedo

Supervisors : Prof. S. T. Petcov

Prof. A. Romanino

Academic Year 2017 – 2018

SISSA - Via Bonomea 265 - 34136 TRIESTE - ITALY

À memoria da minha avó, Maria de Lurdes

Abstract

In the present thesis we investigate distinct facets of the symmetry approach to neutrino masses and neutrino mixing. Regarding the symmetry approach to neutrino masses, we focus on lepton number violation, namely its relation to Froggatt-Nielsen symmetry in a low-scale seesaw model and its potential observability in future neutrinoless double beta decay experiments. As for the symmetry approach to neutrino mixing, we consider the effects of non-Abelian discrete flavour symmetries in the lepton sector, which may be consistently combined with CP symmetry. We further discuss, in a bottom-up approach, the implications of a broken modular symmetry for neutrino masses and mixing.

Keywords: Neutrino Physics; Neutrino masses; Neutrino mixing; Majorana neutrinos; CP violation; Neutrinoless double beta decay; Seesaw mechanism; Froggatt-Nielsen mechanism; Discrete symmetries; Generalised CP symmetry; Modular symmetry.

List of Publications

This thesis is based on the following publications and preprints, listed in chronological order:

- J. T. Penedo, S. T. Petcov and A. V. Titov, *Neutrino mixing and leptonic CP violation from S_4 flavour and generalised CP symmetries*, *JHEP* **12** (2017) 022 [arXiv:1705.00309],
- J. T. Penedo, S. T. Petcov and T. T. Yanagida, *Low-Scale Seesaw and the CP Violation in Neutrino Oscillations*, *Nucl. Phys.* **B929** (2018) 377 [arXiv:1712.09922],
- J. T. Penedo and S. T. Petcov, *The 10^{-3} eV Frontier in Neutrinoless Double Beta Decay*, Accepted for publication in *Phys. Lett. B* [arXiv: 1806.03203],
- J. T. Penedo and S. T. Petcov, *Lepton Masses and Mixing from Modular S_4 Symmetry*, [arXiv: 1806.11040].

The research performed by the author during his PhD studies has also lead to the publication

- P. Baratella, J. Elias-Miro, J. Penedo and A. Romanino, *A closer look to the sgoldstino interpretation of the diphoton excess*, *JHEP* **06** (2016) 086 [arXiv:1603.05682],

as well as to the following contribution to conference proceedings:

- J. T. Penedo, S. T. Petcov and A. V. Titov, *Neutrino Mixing and Leptonic CP Violation from S_4 and Generalised CP Symmetries*, in *Prospects in Neutrino Physics (NuPhys2017) London, United Kingdom, December 20-22, 2017*, 2018, [arXiv:1803.11009].

Contents

Abstract **iii**

List of Publications **v**

1 Introduction **1**

1.1 Neutrino Masses and Mixing . . . 3

1.1.1 Neutrino Oscillations . . . 3

1.1.2 State of the Art Overview . . . 4

1.2 Symmetry and Neutrino Masses . . . 9

1.3 Symmetry and Neutrino Mixing . . . 11

1.3.1 The Discrete Symmetry Approach . . . 11

1.3.2 Combining CP with Discrete Symmetries . . . 14

1.3.3 A New Approach: Modular Symmetry . . . 16

1.4 Outline . . . 16

2 Symmetry-protected Low-scale Seesaw **19**

2.1 Symmetry-protected Setup . . . 19

2.2 Froggatt-Nielsen Realisation . . . 23

2.3 Neutrino Mixing . . . 25

2.4 Predictions for CPV Phases . . . 25

2.5 Phenomenology . . . 29

2.5.1 Neutrino Mass Matrix and Non-unitarity Bounds . . . 30

2.5.2 LFV Observables and Higgs Decays . . . 32

2.6 Leptogenesis . . . 34

2.7 Chapter Summary . . . 35

3 Neutrinoless Double Beta Decay **37**

3.1 Description and Half-lives . . . 37

3.2 The Effective Majorana Mass . . . 38

3.3 The Absolute Neutrino Mass Scale . . . 40

3.4 The Case of Normal Ordering . . . 40

3.5 CP and Generalised CP . . . 43

3.6 Chapter Summary . . . 48

4 S_4 Flavour and gCP **49**
4.1 Motivation and Overview . . . 49
4.2 The Framework . . . 51
4.2.1 The PMNS Matrix from $G_e = Z_2$ and $G_\nu = Z_2 \times H^\nu_{\rm CP}$ . . . 51
4.2.2 Conjugate Residual Symmetries . . . 55
4.2.3 Phenomenologically Non-Viable Cases . . . 55
4.3 Mixing Patterns from $S_4 \rtimes H_{\rm CP}$ Broken to $G_e = Z_2$ and $G_\nu = Z_2 \times H^\nu_{\rm CP}$ . . . 56
4.3.1 S_4 Group and Residual Symmetries . . . 56
4.3.2 Explicit Forms of the PMNS Matrix . . . 58
4.3.3 Extracting Mixing Parameters and Statistical Analysis . . . 59
4.3.4 Results and Discussion . . . 62
4.4 Neutrinoless Double Beta Decay . . . 86
4.5 Chapter Summary . . . 92

5 Modular Invariance **95**
5.1 The Framework . . . 95
5.1.1 Generators of Modular Forms of Level $N = 4$ . . . 97
5.2 Phenomenology . . . 99
5.2.1 Model I ($k_L = 1$) . . . 101
5.2.2 Model II ($k_L = 2$) . . . 102
5.3 Chapter Summary . . . 105

6 Summary and Conclusions **107**

A S_4 Group Theory **109**
A.1 Presentation and Basis . . . 109
A.2 Clebsch-Gordan Coefficients . . . 110
A.3 Conjugate Pairs of S_4 Elements . . . 111

B S_4 Flavour and gCP **113**
B.1 Equivalent Cases . . . 113
B.2 Correspondence with Earlier Results . . . 114

C Modular Forms **117**
C.1 q-expansions of Lowest Weight $N = 4$ Modular Forms . . . 117
C.2 Forms of Higher Weight and Constraints . . . 117

Bibliography **132**

Introduction 1

> The miracle of the appropriateness of the language of mathematics for the formulation of the laws of physics is a wonderful gift which we neither understand nor deserve.
>
> Eugene Wigner (1902-1995) [1]

Symmetry plays a central role in modern theoretical physics. Commonly, symmetry is understood as a property of a beautiful and well-coordinated unity. In a technical sense, instead, symmetry is taken to mean invariance under specified operations. The description of such operations and of their relations relies on the language of group theory.

Gauge symmetries, in particular, are at heart of our current understanding of the subatomic world, which relies on the Standard Model (SM) of particle physics. Aside from the postulated gauge symmetry, it possesses what one may call accidental or automatic global symmetries, such as lepton number (L) and baryon number (B). Although L and B are individually anomalous, i.e. they do not hold as symmetries at the quantum level, the combination $B - L$ is a bona fide, unbroken symmetry of the SM.

The SM has been spectacularly [2] (and perhaps excessively [3]) successful. The recent discovery of the Higgs boson at the Large Hadron Collider (LHC) by the ATLAS and CMS collaborations [4, 5] represents a significant milestone in our search to describe fundamental interactions. The SM cannot however provide a complete description of Nature for several reasons. Aside from not including gravity, it does not provide a viable dark matter candidate. It suffers from the hierarchy and strong CP problems. It is additionally incomplete in the sense that it gives no justification for the quantum numbers in its construction, no pretext for the hierarchies between the masses of different generations of fermions, and no raison d'être for the observed pattern of quark mixing. Most relevant to the present discussion is the fact that in the renormalisable SM, with no additions to its usual field content, neutrinos are massless and no physical neutrino mixing is possible. Such a conclusion would be in clear contradiction with the large body of experimental evidence on neutrino oscillations accumulated in the last 20 years.

Unveiling the properties of neutrinos and of their interactions is of importance to particle physics, nuclear physics, astrophysics and cosmology. Neutrinos are very light neutral fermions, with masses at least six orders of magnitude smaller than the electron mass. By definition, a neutrino of a certain flavour is the particle which is produced alongside a charged antilepton of the same flavour (e^+, μ^+, τ^+) and which produces a charged lepton of the same flavour (e^-, μ^-, τ^-) in a charged current (CC) weak

interaction. The fact that neutrinos mix means neutrino states of a certain flavour – a Lorentz-invariant property – are not in direct correspondence with the states of definite mass. Neutrino mixing can in part be described by three mixing angles. Two of these angles are quite large, $\theta_{12} \sim 33^\circ$ and $\theta_{23} \sim 45^\circ$, while the third is rather small, $\theta_{13} \sim 8^\circ$. Nonetheless, the mixing in the lepton sector is relatively large with respect to the mixing in the quark sector. In fact, the largest angle parameterising quark mixing, the Cabibbo angle $\theta_C \sim 13^\circ$, is comparable to the smallest angle parameterising lepton mixing. The above observations set neutrinos apart from the rest of the SM charged matter content, suggesting that mechanisms other than electroweak symmetry breaking (EWSB) are responsible for the generation of neutrino masses and mixing.

Presently, the SM is seen as an effective description of Nature (see, e.g., [6]), i.e. as the low-energy limit of a more complete, as-yet-unknown theory. A tower of non-renormalisable operators, compatible with the SM gauge symmetry group, is expected to be present in the physical action. These operators are understood to provide a good description of physical effects at energies sufficiently below the effective field theory cutoff. Different new-physics scales may suppress different operators, depending on their respective origins in the context of a particular ultraviolet (UV) completion of the SM. If one refrains from treating $B - L$ as sacrosanct and unbroken, the lowest floor of the effective theory operator tower is populated by a single inhabitant: the dimension-5 Weinberg operator [7]. The presence of the Weinberg operator generically leads to non-zero neutrino masses and mixing.[1] Without further insight into the origin of this operator, however, it seems impossible to explain the peculiarities of the observed pattern of neutrino mixing. Moreover, it is not clear if the smallness of neutrino masses should be primarily attributed to the largeness of the energy scale governing the overall magnitude of the Weinberg operator, or whether some mechanism which suppresses the operator coefficients is in play.

The smallness of neutrino masses can naturally be tied to a small breaking of a symmetry, viz. lepton number. A symmetry principle connecting the three lepton generations may also be at work in shaping neutrino mixing. Refusing symmetry, one may embrace instead the anarchy approach to the flavour puzzle, in which the neutrino mass matrix is assumed structureless [8]. However, the qualitative features of the observed pattern of neutrino masses and mixing are not in correspondence with the most generic expectations within this scheme. In particular, the random matrix scan of Ref. [8] shows that only 3% of the randomly generated mass matrices (or less, depending on the assumed nature and origin of neutrino masses) pass the criteria of jointly presenting a hierarchy of mass-squared differences (see further) and having two large θ_{12} and θ_{23} plus one small θ_{13} mixing angles. The quantitative statement of these cuts as originally formulated in Ref. [8] is compatible with the current experimental situation. We argue that the observed smallness of θ_{13} is enough to lend credibility to the use of flavour symmetries as guiding principles in model building.

In the present thesis, we approach the puzzle of neutrino masses and mixing through the exploration of the possible roles of different symmetries, namely: lepton number, the Abelian Froggatt-Nielsen symmetry, non-Abelian discrete symmetries combined with generalised CP symmetry, and modular symmetry.

[1] Neutrino masses thus generated will be of Majorana nature (see also Section 1.2). Scenarios can be devised where operators of higher dimension with respect to that of the Weinberg operator provide the leading-order contribution to neutrino masses and mixing.

1.1 Neutrino Masses and Mixing

1.1.1 Neutrino Oscillations

The fact that neutrinos mix has a remarkable observable consequence: neutrino oscillations. The idea that neutrinos could undergo oscillations was theorised more than 60 years ago by Bruno Pontecorvo [9, 10]. The suggestion that the electron and muon neutrinos could be admixtures of neutrinos with different mass was put forward by Ziro Maki, Masami Nakagawa, and Shoichi Sakata [11]. Further development of the early theory of neutrino oscillations is due to Pontecorvo, Gribov, Eliezer, Swift, Fritzsch, Minkowski, and Bilenky [12–18].

Neutrino oscillations are transitions in flight between neutrinos of definite flavour. In oscillation experiments, the processes of neutrino production and neutrino detection are not typically sensitive to the individual neutrino masses, since detectable neutrinos are ultrarelativistic. This allows one to consistently define the neutrino flavour states

$$|\nu_\alpha\rangle \equiv (U_{\text{PMNS}})^*_{\alpha k} |\nu_k\rangle , \tag{1.1}$$

where $|\nu_k\rangle$ is a neutrino state with definite mass m_k and U_{PMNS} is a unitary matrix, known as the Pontecorvo-Maki-Nakagawa-Sakata (PMNS) mixing matrix. A conjugate relation can also be written for antineutrino states, which by definition are produced alongside a charged lepton or produce a charged antilepton in a CC weak interaction.

The probability that an ultrarelativistic neutrino in the flavour state $|\nu_\alpha\rangle$, produced at a certain source in a beam with energy E, is detected in the flavour state $|\nu_\beta\rangle$ a distance L from said source is given by:

$$P_{\alpha\beta} = \left|\langle\nu_\beta| e^{-i\mathcal{H}_0 L} |\nu_\alpha\rangle\right|^2 = \left|U_{\beta k}\, U^*_{\alpha k}\, e^{-iE_k L}\right|^2 = U^*_{\alpha k}\, U_{\beta k}\, U_{\alpha j}\, U^*_{\beta j}\, \exp\left(-i\frac{\Delta m^2_{kj} L}{2E}\right) , \tag{1.2}$$

where we have assumed that the neutrino is travelling in vacuum, such that $\mathcal{H}_0$ is the free Hamiltonian. In the above expression, we have defined $\Delta m^2_{kj} \equiv m^2_k - m^2_j$ and have additionally abbreviated $U_{\text{PMNS}} \to U$. Equation (1.2) can also be written in the form:

$$P_{\alpha\beta} = \delta_{\alpha\beta} - 4\sum_{k>j} \text{Re}\left(U^*_{\alpha k}\, U_{\beta k}\, U_{\alpha j}\, U^*_{\beta j}\right) \sin^2\left(\frac{\Delta m^2_{kj} L}{4E}\right) + 2\sum_{k>j} \text{Im}\left(U^*_{\alpha k}\, U_{\beta k}\, U_{\alpha j}\, U^*_{\beta j}\right) \sin\left(\frac{\Delta m^2_{kj} L}{2E}\right) . \tag{1.3}$$

These equations, whose rigorous derivation is possible by treating neutrinos as propagating wave packets [19], already allow for the extraction of some general conclusions. By inspection, one sees that i) neutrino oscillations are not sensitive to individual neutrino masses, but instead depend on the mass-squared differences Δm^2_{kj}, and ii) while oscillation experiments can measure the angles and phases entering U_{PMNS}, they are insensitive to rephasings from the left or from the right, e.g. $U_{\text{PMNS}} \to U_{\text{PMNS}}\ \text{diag}(\dots, e^{i\varphi_k}, \dots)$, meaning they cannot decipher the nature (Dirac or Majorana) of massive neutrinos [20].

The formula for the antineutrino oscillation probability $P_{\bar\alpha\bar\beta}$ can be obtained by taking $U \to U^*$ in Eqs. (1.2) and (1.3). Knowing that $P_{\alpha\beta}$ transforms to $P_{\bar\alpha\bar\beta}$ under a CP transformation and to $P_{\bar\beta\bar\alpha}$ under a CPT one leads to an additional conclusion, namely that a so-called *disappearance* experiment measuring

the *survival* probability $P_{\alpha\alpha}$ (which due to CPT invariance, and as can be checked explicitly, equals $P_{\bar{\alpha}\bar{\alpha}}$) is not sensitive to CP violation (CPV). In the search for CPV effects, one has thus to consider *appearance* experimental setups, in which *conversion* probabilities $P_{\alpha\beta}$ with $\alpha \neq \beta$ are measured.

It is instructive to briefly consider the simple case of two neutrino flavours, for which:

$$P^{(2\nu)}_{\alpha\alpha} \;=\; 1 - \sin^2 2\theta \, \sin^2 \frac{\Delta m^2_{21} L}{4E} \,, \tag{1.4}$$

with $P^{(2\nu)}_{\alpha\beta}\,(\beta \neq \alpha) \;=\; 1 - P^{(2\nu)}_{\alpha\alpha}$, and where the 2-flavour mixing matrix has been parameterised as

$$U^{(2\nu)}_{\rm PMNS} \;=\; \begin{pmatrix} \cos\theta & \sin\theta \\ -\sin\theta & \cos\theta \end{pmatrix} \begin{pmatrix} e^{i\lambda} & 0 \\ 0 & 1 \end{pmatrix} \,, \tag{1.5}$$

with $\theta \in [0, \pi/2]$ and $\lambda \in [0, \pi)$. As anticipated above, phases to the right of $U_{\rm PMNS}$ are irrelevant in neutrino oscillations. Depending on the specific experimental setup, one mass-squared difference may be the dominant source of oscillations with respect to another mass-squared difference, and the full expression of $P_{\alpha\beta}$ may reduce to a simple function of two-neutrino oscillation probabilities. This can happen either because the oscillation length $\ell_{\rm osc} \equiv 4\pi E/\Delta m^2$ corresponding to the neglected Δm^2 is very large compared to L and no oscillations have taken place, or because $L \gg \ell_{\rm osc}$, in which case the corresponding oscillations are averaged out due to limitations in energy resolution.

So far we have discussed neutrino oscillations in vacuum. However, the expressions thus derived do not hold when neutrinos propagate through matter, where they can scatter coherently. The effect of coherent forward elastic scattering can be described by an effective potential, which modifies the relevant Hamiltonian, $\mathcal{H} = \mathcal{H}_0 + \mathcal{H}_{\rm int}$ [21]. In the case of ordinary matter, $\mathcal{H}_{\rm int}$ depends on the (possibly varying) number density N_e of electrons in the medium. The aforementioned conclusion that neutrino oscillation experiments cannot decipher the nature (Dirac or Majorana) of massive neutrinos also holds in the presence of matter [22]. Matter effects in neutrino oscillations are crucial in understanding the flavour composition of the flux of solar neutrinos arriving at the Earth. In fact, it is not the oscillations in vacuum between the outer solar layers and the Earth which determine the experimentally observed flavour conversion of solar electron neutrinos. Instead, the transitions are enhanced in solar matter due to the Mikheyev–Smirnov–Wolfenstein (MSW) effect [21, 23]. Matter effects additionally play a role in long baseline and atmospheric neutrino oscillation experiments.

For reviews on the theory of neutrino oscillations and neutrino mixing phenomenology, the reader is further referred to Refs. [24, 25].

1.1.2 State of the Art Overview

The first conclusive evidence for neutrino oscillations in the atmosphere was presented by the Super-Kamiokande (Super-K) collaboration in 1998 [26] . For the flavour conversion of neutrinos coming from the Sun, clear evidence was obtained by the Sudbury Neutrino Observatory (SNO) collaboration in 2001 [27]. In Table 1.1 we list the different types of experiment according to the energy and length scales involved.

At present (2018), we are already entering a precision era for neutrino physics. The paradigm of three-flavour neutrino (3ν) mixing – with $\alpha = e, \mu, \tau$ and $k = 1, 2, 3$ in Eq. (1.1) – which we consider

Experiment type	ν at source	L	E	Δm^2 sensitivity
Solar	ν_e	$\sim 10^8$ km	0.2−15 MeV	$\sim 10^{-12}$ eV^2
Atmospheric	$\nu_{\mu,e}, \bar{\nu}_{\mu,e}$	20−10^4 km	0.5−10^2 GeV	$\sim 10^{-4}$ eV^2
Accelerator	$\nu_\mu, \bar{\nu}_\mu$			
short baseline (π dec. in flight)		~ 1 km	~ 1 GeV	~ 1 eV^2
short baseline (μ dec. at rest)		~ 10 m	~ 10 MeV	~ 1 eV^2
long baseline		$\sim 10^2$−10^3 km	~ 1 GeV	$\sim 10^{-3}$ eV^2
Reactor	$\bar{\nu}_e$			
short baseline		~ 10 m	~ 1 MeV	~ 0.1 eV^2
long baseline		~ 1 km	~ 1 MeV	$\sim 10^{-3}$ eV^2
very-long baseline		~ 100 km	~ 1 MeV	$\sim 10^{-5}$ eV^2

Table 1.1: Oscillation experiment types and typical lengths L and energies E involved [24, 25].

in what follows, provides a consistent description of most of the available data. The SM, being a chiral model, incorporates the three neutrino flavours by means of the left-handed two-component spinor fields $\nu_{\alpha L}$, which together with left-handed charged-lepton fields $\ell_{\alpha L}$ make up weak isospin doublets L_α. Such a minimal, parity-violating inclusion is consistent with the supposed masslessness of neutrinos within the SM and with the fact that flavour neutrinos (antineutrinos) have only been observed in Nature as states of negative (positive) helicity. Naturally, neutrino fields in the mass basis are related to those in the flavour basis through[2] $\nu_{\alpha L}(x) = (U_{\rm PMNS})_{\alpha k}\, \nu_{kL}(x)$, cf. Eq. (1.1). Neutrino mixing emerges in the CC weak interaction following the diagonalisation of the neutrino mass matrix arising in an appropriate extension of the SM:

$$\mathcal{L}_{\rm CC} \,=\, -\frac{g}{\sqrt{2}}\, \overline{\ell_{\alpha L}}\, \gamma^\mu\, \nu_{\alpha L}\, W^\dagger_\mu \,+\, \text{h.c.} \,=\, -\frac{g}{\sqrt{2}}\, \overline{\ell_{\alpha L}}\, \gamma^\mu\, (U_{\rm PMNS})_{\alpha k}\, \nu_{kL}\, W^\dagger_\mu \,+\, \text{h.c.}\,, \tag{1.6}$$

where g is the $\mathrm{SU}(2)_L$ gauge coupling and the spacetime dependence of fields is implied. The PMNS matrix in the 3ν case is given in its standard parameterisation by [25]:

$$U_{\rm PMNS} \,=\, \begin{pmatrix} c_{12}c_{13} & s_{12}c_{13} & s_{13}e^{-i\delta} \\ -s_{12}c_{23} - c_{12}s_{23}s_{13}e^{i\delta} & c_{12}c_{23} - s_{12}s_{23}s_{13}e^{i\delta} & s_{23}c_{13} \\ s_{12}s_{23} - c_{12}c_{23}s_{13}e^{i\delta} & -c_{12}s_{23} - s_{12}c_{23}s_{13}e^{i\delta} & c_{23}c_{13} \end{pmatrix} \mathrm{diag}(1, e^{i\alpha_{21}/2}, e^{i\alpha_{31}/2})\,, \tag{1.7}$$

where $c_{ij} \equiv \cos\theta_{ij}$ and $s_{ij} \equiv \sin\theta_{ij}$, with the three mixing angles $\theta_{ij} \in [0, \pi/2]$. Here, $\delta \in [0, 2\pi)$ denotes the Dirac CPV phase, while α_{21} and α_{31} are Majorana CPV phases [20, 28, 29], with $\alpha_{ij} \in [0, 2\pi)$. The latter phases are only physical if neutrinos are Majorana particles. The last term in Eq. (1.3) encodes CPV effects in neutrino oscillations and is proportional to $\sin\delta$, since the imaginary parts of the PMNS quartets coincide up to a sign with the rephasing invariant $\mathcal{J}_{\rm CP}$ associated with the Dirac phase δ [30]:

$$\left|\mathrm{Im}\left(U^*_{\alpha k}\, U_{\beta k}\, U_{\alpha j}\, U^*_{\beta j}\right)\right| \,=\, |\mathcal{J}_{\rm CP}| \,=\, \frac{1}{8}\, \sin 2\theta_{12}\, \sin 2\theta_{13}\, \sin 2\theta_{23}\, \cos\theta_{13}\, |\sin\delta|\,. \tag{1.8}$$

The quantity $\mathcal{J}_{\rm CP}$ is the leptonic analog of the rephasing invariant associated with the CP violating phase in the Cabibbo-Kobayashi-Maskawa (CKM) quark mixing matrix, introduced in Ref. [31].

[2] Neutrinos with definite flavour are defined in the basis in which the charged-lepton mass matrix is diagonal.

As anticipated, within the 3ν paradigm, oscillation experiments are able to provide information on the 2 mass-squared differences, on the 3 mixing angles and on the Dirac phase. As we will see, the mass-squared difference $\Delta m^2_{\odot}$ responsible for solar ν_e and very-long baseline reactor $\bar{\nu}_e$ oscillations is much smaller than the mass-squared difference $\Delta m^2_{\rm A}$ responsible for atmospheric and accelerator ν_μ and $\bar{\nu}_\mu$ and long baseline reactor $\bar{\nu}_e$ oscillations, $\Delta m^2_{\odot}/|\Delta m^2_{\rm A}| \sim 1/30$. It is important to note that the sign of $\Delta m^2_{\rm A}$ cannot be determined from the existing data. The two possible signs of $\Delta m^2_{\rm A}$ correspond to two types of neutrino mass spectrum: $\Delta m^2_{\rm A} > 0$ – a spectrum with normal ordering (NO), $\Delta m^2_{\rm A} < 0$ – a spectrum with inverted ordering (IO). In the widely-used convention which we also employ, $\Delta m^2_{\odot} \equiv \Delta m^2_{21} > 0$, and the lightest neutrino mass is m_1 (m_3) for a spectrum with NO (IO). We then have:

- $m_1 < m_2 < m_3, \qquad \Delta m^2_{31} \equiv \Delta m^2_{\rm A} > 0, \qquad$ for NO, and
- $m_3 < m_1 < m_2, \quad -\Delta m^2_{23} \equiv \Delta m^2_{\rm A} < 0, \qquad$ for IO.

For either ordering, $|\Delta m^2_{\rm A}| = \max(|m^2_i - m^2_j|)$, $i, j = 1, 2, 3$. Determination of the neutrino mass ordering may, e.g., be possible in long baseline and atmospheric neutrino experiments owing to the dependence of $\overset{(-)}{\nu}_\mu \to \overset{(-)}{\nu}_e$ oscillations in matter on the sign of $\Delta m^2_{\rm A}$. Information regarding the absolute scale of neutrino masses must be obtained through means other than the study of neutrino oscillations. We postpone this discussion to Section 3.3.

Global fits to neutrino data have been performed by several independent groups in recent years [32–39]. Interestingly, the first hints for a non-zero θ_{13} were extracted from a global analysis [40]. By combining data from several independent sources, such analyses are able to provide an overall picture of the status of 3ν oscillations. Our present knowledge of $\Delta m^2_{\odot}$, $|\Delta m^2_{\rm A}|$, $\sin^2\theta_{12}$, $\sin^2\theta_{23}$ and $\sin^2\theta_{13}$ is rather precise. The value of $\sin^2\theta_{23}$ presents the largest relative uncertainty among these parameters, while its octant remains undetermined. At 3σ CL, about half of the defining region for the Dirac CPV phase, namely $0 \lesssim \delta \lesssim \pi$, is excluded for both orderings [39]. There is a hint for a close to maximally CP violating Dirac phase, $\delta \sim 3\pi/2$ [35]. Direct information on CP violation in neutrino oscillations is obtained from the data of the T2K and NOνA experiments. The most recent fits show a preference of the data for a spectrum with NO over IO at the 2σ CL [36,38] and even above the 3σ CL [37,39].

Due to their fast update rate, the work comprising this thesis relies on two global analyses of neutrino data, performed by the Bari group in 2017 [38] and 2018 [39]. The latest of the two, as opposed to the first, makes use of official Super-K χ^2 maps and includes updated solar neutrino data from the Borexino (Boron solar neutrino) and Super-K experiments. The main differences in the results correspond to: i) a reduced uncertainty in the determination of $\sin^2\theta_{23}$, with a change in octant preference (for the NO case), ii) an increased preference for a spectrum with NO over IO (from $\sim 2\sigma$ to $\sim 3\sigma$), iii) a small shift in the ranges for $\Delta m^2_{\rm A}$, and iv) a slightly improved 3σ range for δ. Bounds on the oscillation parameters for these two analyses are shown in Figures 1.1 (2017) and 1.2 (2018), in terms of standard deviations, $n\sigma = \sqrt{\chi^2 - \chi^2_{\rm min}}$, for both orderings. The corresponding $n\sigma$ ranges, with $n = 1, 2, 3$, are collected in Tables 1.2 and 1.3, respectively.

In closing, we briefly mention the existence of anomalies which have challenged the 3ν mixing paradigm, and have not been resolved so far. These anomalies have been interpreted as possible signs for

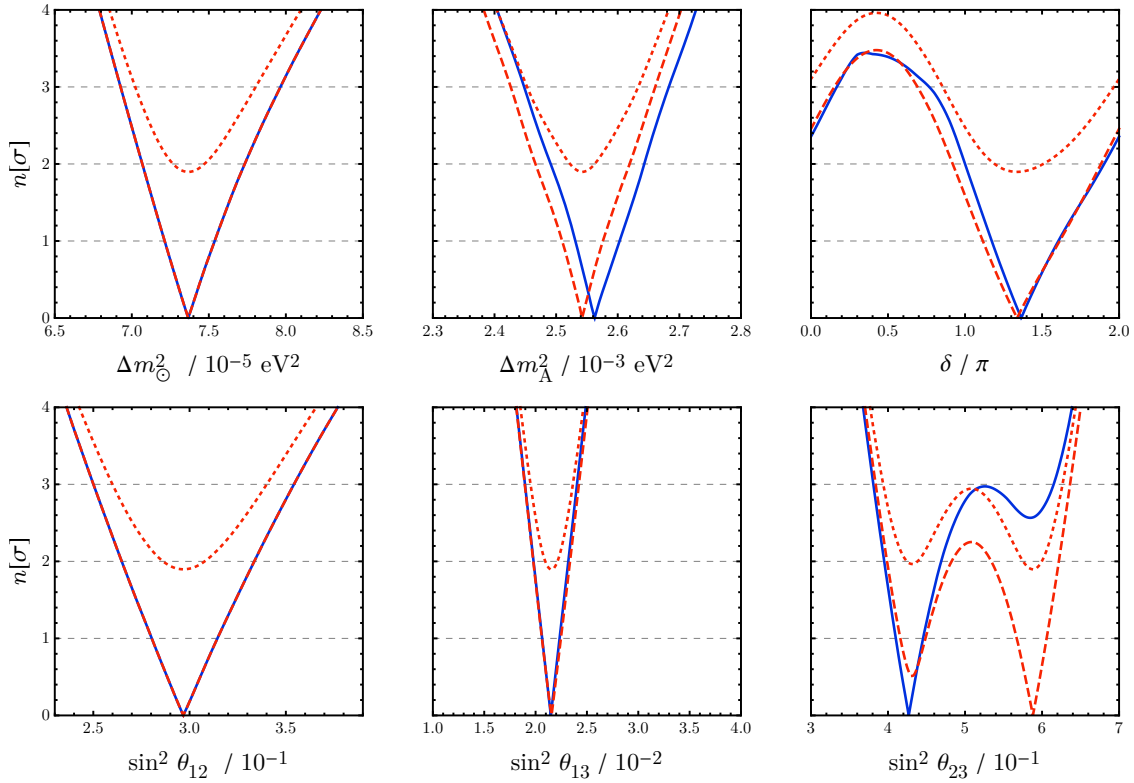

Figure 1.1: Bounds on neutrino oscillation parameters in terms of n standard deviations, obtained from the 2017 global analysis of Ref. [38]. Blue solid (red dashed) curves correspond to a spectrum with NO (IO). The red dotted line corresponds to the IO case and includes the likelihood offset with respect to NO. For each ordering, $\Delta m^2_{\rm A}$ is obtained from the quantities defined in Ref. [38] using the best-fit value of $\Delta m^2_\odot$.

Parameter	Ordering	Best fit	1σ range	2σ range	3σ range
$\Delta m^2_\odot/10^{-5}$ eV^2	Any	7.37	7.21 – 7.54	7.07 – 7.73	6.93 – 7.96
$\lvert\Delta m^2_{\rm A}\rvert/10^{-3}$ eV^2	NO	2.56	2.53 – 2.60	2.49 – 2.64	2.45 – 2.68
	IO	2.54	2.51 – 2.58	2.47 – 2.62	2.43 – 2.66
$\sin^2\theta_{12}/10^{-1}$	Any	2.97	2.81 – 3.14	2.65 – 3.34	2.50 – 3.54
$\sin^2\theta_{13}/10^{-2}$	NO	2.15	2.08 – 2.22	1.99 – 2.31	1.90 – 2.40
	IO	2.16	2.07 – 2.24	1.98 – 2.33	1.90 – 2.42
$\sin^2\theta_{23}/10^{-1}$	NO	4.25	4.10 – 4.46	3.95 – 4.70	3.81 – 6.15
	IO	5.89	$[4.17, 4.48]$ $\cup\,[5.67, 6.05]$	$[3.99, 4.83]$ $\cup\,[5.33, 6.21]$	3.84 – 6.36
δ/π	NO	1.38	1.18 – 1.61	1.00 – 1.90	$[0, 0.17] \cup [0.76, 2]$
	IO	1.31	1.12 – 1.62	0.92 – 1.88	$[0, 0.15] \cup [0.69, 2]$

Table 1.2: Best-fit values and $n\sigma$ ($n = 1, 2, 3$) ranges for neutrino oscillation parameters, obtained from the 2017 global analysis of Ref. [38], see Figure 1.1.

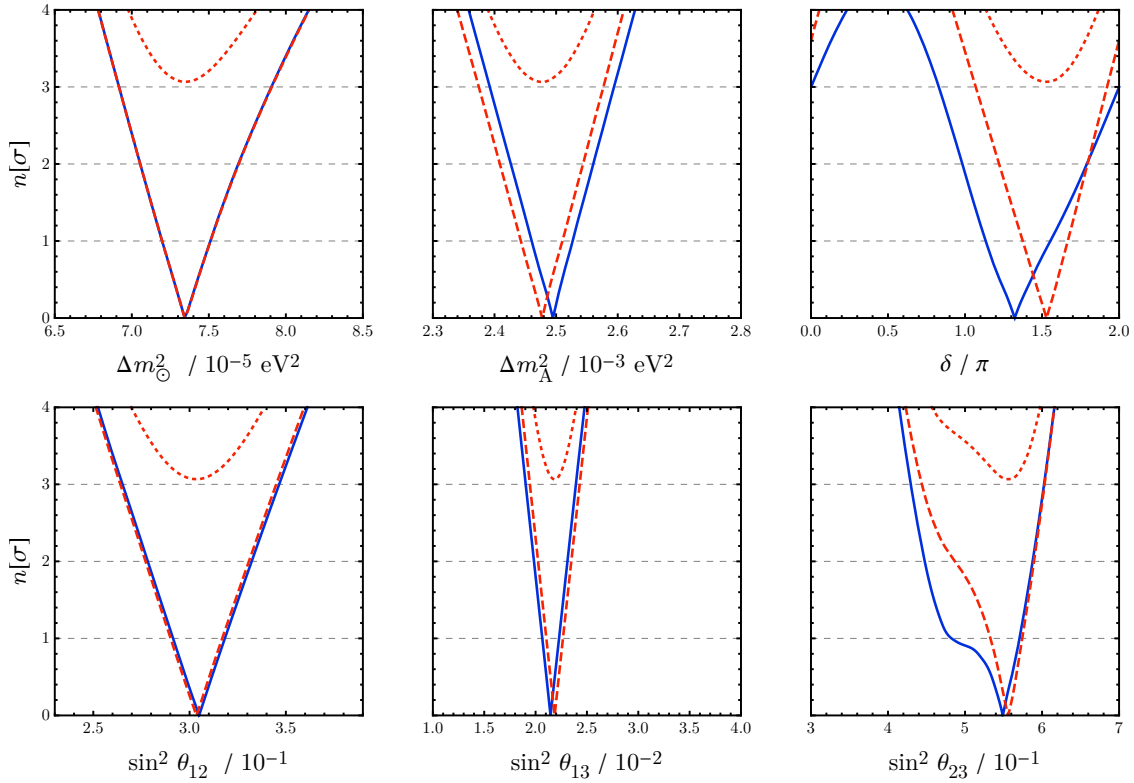

Figure 1.2: Bounds on neutrino oscillation parameters in terms of n standard deviations, obtained from the 2018 global analysis of Ref. [39]. Blue solid (red dashed) curves correspond to a spectrum with NO (IO). The red dotted line corresponds to the IO case and includes the likelihood offset with respect to NO. For each ordering, $\Delta m^2_{\rm A}$ is obtained from the quantities defined in Ref. [39] using the best-fit value of $\Delta m^2_\odot$.

Parameter	Ordering	Best fit	1σ range	2σ range	3σ range
$\Delta m^2_\odot/10^{-5}$ eV^2	Any	7.34	7.20 – 7.51	7.05 – 7.69	6.92 – 7.91
$\lvert\Delta m^2_{\rm A}\rvert/10^{-3}$ eV^2	NO	2.49	2.46 – 2.53	2.43 – 2.56	2.39 – 2.59
	IO	2.48	2.44 – 2.51	2.41 – 2.54	2.38 – 2.58
$\sin^2\theta_{12}/10^{-1}$	NO	3.04	2.91 – 3.18	2.78 – 3.32	2.65 – 3.46
	IO	3.03	2.90 – 3.17	2.77 – 3.31	2.64 – 3.45
$\sin^2\theta_{13}/10^{-2}$	NO	2.14	2.07 – 2.23	1.98 – 2.31	1.90 – 2.39
	IO	2.18	2.11 – 2.26	2.02 – 2.35	1.95 – 2.43
$\sin^2\theta_{23}/10^{-1}$	NO	5.51	4.81 – 5.70	4.48 – 5.88	4.30 – 6.02
	IO	5.57	5.33 – 5.74	4.86 – 5.89	4.44 – 6.03
δ/π	NO	1.32	1.14 – 1.55	0.98 – 1.79	0.83 – 1.99
	IO	1.52	1.37 – 1.66	1.22 – 1.79	1.07 – 1.92

Table 1.3: Best-fit values and $n\sigma$ ($n = 1, 2, 3$) ranges for neutrino oscillation parameters, obtained from the 2018 global analysis of Ref. [39], see Figure 1.2.

the presence of *sterile* neutrino species – neutral fermions which do not take part in weak interactions, but may mix with the three known *active* neutrino species. They are the LSND anomaly, the MiniBooNE excesses, the reactor neutrino anomaly, and the Gallium anomaly (see, e.g., [25]).

1.2 Symmetry and Neutrino Masses

In 3+1 spacetime dimensions, the (restricted-)Lorentz-irreducible building blocks of spin-1/2 fermion fields are two-component (Weyl) spinors. These come in two possible chiralities, namely left- and right-handed spinor representations. A fermion mass term in the physical action connects left- and right-handed spinors, ψ_L and ψ_R respectively. If these are two *independent* spinors, the massive particle in question is a Dirac fermion, and the mass term reads:

$$-\mathcal{L}_D \,=\, m\,\overline{\psi_L}\,\psi_R \,+\, \text{h.c.} \,=\, m\,\overline{\psi}\,\psi\,, \tag{1.9}$$

in 4-component notation, with $\psi = \psi_L + \psi_R$ and $m > 0$ without loss of generality. Instead, as implied by the work of Ettore Majorana [41], there exists a more economical possibility in which the spinors are *not independent* from each other. One chirality of the Majorana fermion is built from the other, say $\psi_R = C\,\overline{\psi_L}^T \equiv (\psi_L)^C$, C being the charge conjugation matrix, so that half of the number of degrees of freedom is needed with respect to the Dirac case. The corresponding Majorana mass term reads:

$$-\mathcal{L}_M \,=\, \frac{1}{2}\,m\,\overline{\psi_L}\,(\psi_L)^C \,+\, \text{h.c.} \,=\, \frac{1}{2}\,m\,\overline{\psi}\psi\,, \tag{1.10}$$

with $m > 0$, and $\psi = \psi_L + (\psi_L)^C$ satisfying $\psi^C = \psi$. This last condition implies the equality between particle and antiparticle, and is incompatible with a conserved fermion number. Of the known particles, only neutrinos can be Majorana fermions since they do not carry any unbroken gauge quantum numbers of colour or electric charge. The question of weather massive neutrinos are of Dirac or Majorana nature remains unanswered.

At this point, one may wonder if it is possible that combinations of active neutrinos pair up to form a Dirac fermion. This is the Zeldovich-Konopinski-Mahmoud (ZKM) idea [42, 43], originally stated for the pairing of electron and muon neutrinos. Other choices, involving combinations of all three active neutrinos [44], may be closer to reality. Unfortunately, these options cannot be realised exactly since they would imply a mass degeneracy in contradiction with our knowledge of oscillation data. To make such scenarios realistic one needs e.g. the addition of perturbations in the neutrino mass matrix and corrections from the charged lepton sector [45]. In such a case, neutrinos are not strictly Dirac but are instead of Majorana nature, with a very small splitting between the masses of the two Majorana neutrinos. This splitting is much smaller than the masses themselves and in this case one has what is usually referred to as a "pseudo-Dirac" neutrino [44, 46].

In the context of the SM, a Majorana mass term for the left-handed (LH) neutrino fields cannot be introduced directly, since it would violate weak isospin by one unit. Indeed, three conserved family lepton numbers L_α ($\alpha = e, \mu, \tau$), and thus a conserved (standard) lepton number $L \equiv L_e + L_\mu + L_\tau$,

exist automatically in the SM at the renormalisable level.[3] As mentioned, such conserved charges are incompatible with neutrinos of Majorana nature. However, the SM has to be extended due to the existence of neutrino masses and mixing. Neutrino oscillation data then imply that each of the family numbers $L_{e,\mu,\tau}$ is not a good symmetry individually, since all conversion probabilities $P_{\alpha\beta}$ with $\alpha \neq \beta$ are non-vanishing in the 3ν framework.

A lepton-number charge can still be unbroken in the relevant SM extension. In this case, massive neutrinos cannot be Majorana and must instead be of Dirac nature. If, however, the SM extension brings about lepton-number-violating interactions, massive neutrinos can be of Majorana nature.

A straightforward extension of the SM accommodating neutrino masses and mixing consists in adding to it so-called right-handed (RH) fermion fields, which are singlets under the SM gauge group. Their presence does not affect the cancellation of gauge anomalies, meaning their number is not constrained a priori. They also fit neatly into matter multiplets of SO(10) grand unified theories (GUTs). Due to the presence of these extra, independent chiral fields, Yukawa interactions analogous to those of up-type quarks can be introduced in the Lagrangian (density), leading to Dirac mass terms for neutrinos after EWSB. Without further modifications to the model, the smallness of neutrino masses would be a consequence of the (unexplained) smallness of these Yukawa couplings y_ν.

In contrast to the case of LH fields, the SM gauge structure does not forbid direct Majorana terms for the RH singlets. Once Majorana terms are present, they generically "infect" the Dirac-type terms, i.e., after mass-matrix diagonalisation, the fields with definite masses will be of Majorana nature. The case where the direct Majorana masses M are large with respect to the electroweak scale, $v = 174$ GeV, corresponds to the celebrated type I seesaw mechanism [47–51]. In this case, neutrino masses are parametrically given by $m_k \sim y_\nu^2\, v^2/M$. Realisations of the seesaw mechanism with non-singlet fields exist, such as the type II [28, 52–55], type III [56] and radiative [57, 58] seesaws (see, e.g., [59, 60]). Integrating out the heavy fields, an imprint of $(B-)L$ violation is left at low energies in the form of Majorana neutrino masses, encoded in the aforementioned Weinberg operator:

$$\mathcal{L}_W \,=\, \frac{1}{2}\,\frac{w_{\alpha\beta}}{\Lambda}\,\left(\overline{L_\alpha^C}\,H^{c*}\right)\,\left(H^{c\dagger}\,L_\beta\right) \,+\, \text{h.c.}\,, \tag{1.11}$$

where H^c is the Higgs conjugate doublet, Λ is the cutoff scale of the effective operator, and the $w_{\alpha\beta}$ are (in general) complex coefficients. One has the matching $w/\Lambda \sim y_\nu^2/M$ (see, e.g., [61]).

It is possible to have instead Dirac neutrinos in a SM extension. A necessary and sufficient condition for the existence of Dirac massive neutrinos is the presence of a conserved lepton number $\mathrm{U}(1)_{L'}$ as a symmetry of the mass matrix and weak interactions [46,62]. Examples of such a conserved lepton number are $L' = L_e - L_\mu$ for the ZKM model, and $L' = L_e - L_\mu \pm L_\tau$ for the models of Refs. [44] and [45], respectively. In realistic models extending the SM, however, one expects that if such a (classically) conserved charge exists, it is of the form $L' = L + \ldots$, where the ellipsis refers to new fields carrying lepton number. In passing we note that, at the level of the full Lagrangian, a discrete version of this symmetry is possible. Dirac neutrinos are present in the model of Ref. [63] where the continuous $\mathrm{U}(1)_{L'}$ is a symmetry of the mass matrix and weak interactions but is broken to a discrete subgroup in Yukawa-type

[3] While this discussion focuses on L and the L_α ($\alpha = e, \mu, \tau$), one should keep in mind that in the SM the non-anomalous quantities are $B/3 - L_\alpha$ and consequently $B - L$, as previously noted.

couplings and in the scalar potential.

Throughout this thesis, we focus on what are ultimately Majorana neutrino masses. As we have seen, there is a connection between symmetry and the nature of neutrino masses. Thus, small neutrino Majorana masses can arise as a result of a small breaking of such a symmetry. This connection is explored in the low-scale seesaw scenario of Chapter 2.

The breaking of lepton number may have played a central role in generating the baryon asymmetry of the Universe (BAU), out of which we are fundamentally born. A dynamical origin of the BAU requires C, CP and (naturally) B violation, as well as a departure from thermal equilibrium [64]. Baryogenesis through leptogenesis [65] is based on the possibility that electroweak sphaleron processes [66, 67] convert an asymmetry in lepton number into an asymmetry in B, thus sourcing the BAU. We discuss, also in Chapter 2, the possibility of incorporating baryogenesis in the context of the studied seesaw model.

Finally, we mention that, due to the $V - A$ structure of weak interactions, the ability to distinguish experimentally between the unknown Dirac or Majorana nature of neutrinos disappears as their masses go to zero. This implies that the rate of processes which would allow to make the Dirac vs. Majorana distinction are suppressed by the smallness of neutrino masses, and this is sometimes referred to as the "Practical Dirac-Majorana Confusion Theorem" [68]. The most promising tool to unveil the nature of neutrino masses is the search for neutrinoless double beta ($(\beta\beta)_{0\nu}$-)decay, whose observation would imply that the lepton number L is violated and also that neutrinos are Majorana particles. We dedicate Chapter 3 to the investigation of the conditions under which this decay, generated by standard contributions, may potentially be observable in far-future experiments.

1.3 Symmetry and Neutrino Mixing

1.3.1 The Discrete Symmetry Approach

The pattern of mixing that has emerged from neutrino oscillation data may offer a window into the origins of flavour. In the flavour sector of the (extended) SM there are 20 unexplained mass and mixing low-energy parameters – 6 lepton and 6 quark masses, 6 angles and 2 Dirac CPV phases – plus 2 Majorana phases in the leptonic sector if neutrinos are Majorana fermions. Confronted with such a multitude of quantities, one may wonder about the existence of some organising principle which constrains the flavour sector. Finding such a principle means solving a piece of the so-called flavour puzzle.

Flavour symmetries may provide the sought-after guiding principle. These are also known as horizontal symmetries, since they unify fermions of different generations, as opposed to the GUT philosophy, where unification happens "vertically" inside each generation, see Figure 1.3. Although we focus on the lepton sector, extensions of the flavour symmetry to the quark sector are welcome and needed to create a unified portrayal of fermion masses and mixing. In such a scenario, the radical disparities in the mixing patterns of quarks and leptons should be justified.

If the flavour symmetry group is Abelian, all its irreducible representations (irreps) are one-dimensional, meaning different families are not unified inside multiplets. Nevertheless, such unequal treatment of generations proves useful if one aims at explaining hierarchical structures. The Froggatt-Nielsen (FN)

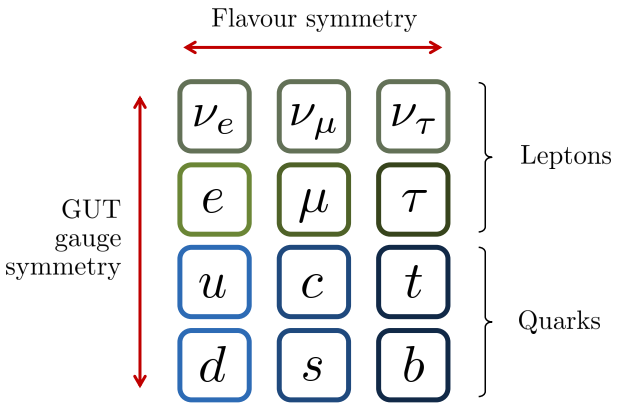

Figure 1.3: Schematic comparison of flavour symmetries, which act "horizontally" across different generations, and GUT gauge symmetries, which act "vertically" inside each generation. The representations into which the chiral fields fit are model dependent.

construction [69] makes use of a continuous symmetry $\mathrm{U}(1)_{\mathrm{FN}}$ and is used to justify fermion hierarchies. In a minimal FN setup, a SM-neutral scalar field S is introduced. This field has a FN charge assignment of opposite sign with respect to that of the usual Yukawa terms, say $Q_{\mathrm{FN}}(S) = -1$ and $-Q_{\mathrm{FN}}(\psi_{iL}) + Q_{\mathrm{FN}}(\psi_{jR}) = n_{ij} > 0$. In this way, direct Yukawa terms are forbidden and only arise from effective operators once S acquires a vacuum expectation value (VEV) and breaks the $\mathrm{U}(1)_{\mathrm{FN}}$ symmetry:

$$\mathcal{L} \supset k_{ij} \left(\frac{S}{\Lambda_{\mathrm{FN}}}\right)^{n_{ij}} \overline{\psi_{iL}}\, H\, \psi_{jR} \qquad \rightarrow \qquad k_{ij}\, \epsilon^{n_{ij}}\, \overline{\psi_{iL}}\, H\, \psi_{jR}\,, \tag{1.12}$$

where H is the Higgs doublet and we have defined $\epsilon \equiv \langle S \rangle / \Lambda_{\mathrm{FN}}$. The scale Λ_{FN} is associated with other flavoured heavy fields not playing a role at low energies (see also [70]). The key insight here is that ϵ may be sufficiently smaller than unity and thus work as an expansion parameter. Then, hierarchical spectra can naturally be accommodated by selecting appropriate combinations n_{ij} of charges. One should keep in mind that although this is a valuable mechanism to explain hierarchies, entries of the mass matrices with the same suppression in terms of powers of ϵ may still present $\mathcal{O}(1)$ uncertainties between themselves, as the coefficients k_{ij} are not precisely determined.

While the FN approach is appropriate for a qualitative characterisation of fermion masses when hierarchies are present, non-Abelian discrete symmetries are able to provide a quantitative picture of mixing. In fact, precise relations between parameters can be predicted if different generations of fermions are unified in a multiplet of the *non-Abelian* symmetry group G_f, which admits larger-dimensional irreps. The three $\mathrm{SU}(2)_L$ lepton doublets are naturally arranged into triplet irreps. Such horizontal unification allows for the presence of large mixing angles in the lepton sector. Also, *discrete* symmetries are a simple and economical choice when compared to continuous ones. The former can be embedded in the latter and may allow to naturally obtain the needed vacuum alignments. Extensions of the SM encompassing non-Abelian discrete flavour symmetries have been considered extensively in attempts to unravel the flavour puzzle. For reviews on this subject, the reader is referred to Refs. [71–74].

The breaking of the flavour symmetry is needed to distinguish the leptons, but may proceed in such a way that invariance under some elements of the group remains at low energy. Said invariances are called *residual symmetries* and typically yield predictions for the values of – and/or correlations between

– low-energy neutrino mixing parameters.

To understand the low-energy implications of the presence of a flavour symmetry, consider the lepton-sector Lagrangian in an arbitrary flavour basis (no mixing in $\mathcal{L}_{\rm CC}$):

$$\mathcal{L}_\ell \,=\, -\frac{1}{2}\left(M_\nu\right)_{ij}\overline{\nu_{iR}^C}\,\nu_{jL} - \left(M_e\right)_{ij}\overline{\ell_{iL}}\,\ell_{jR} + \text{h.c.}\,, \tag{1.13}$$

where M_e and M_ν are the charged-lepton Dirac and neutrino Majorana mass matrices, respectively, and $\nu_{iR}^C \equiv (\nu_{iL})^C$. As suggested, the lepton doublets $L_i = (\nu_{iL}, \ell_{iL})^T$ are assumed to transform under a three-dimensional irrep of the flavour group. Under the action of an element $g \in G_f$ one then has $L_i \to (\rho_L(g))_{ij}\, L_j$, where ρ_L denotes the representation matrix.

Residual symmetries manifest themselves as *independent* symmetries of the mass matrices M_e and M_ν, under remnant groups G_e and G_ν, respectively. The knowledge of which symmetries survive may be enough to severely constrain the shape of $U_{\rm PMNS}$. In particular, G_e and G_ν must be subgroups of the maximal exact symmetries the corresponding mass matrices may possess. Considering the case of Majorana neutrinos with non-zero and non-degenerate masses, the largest symmetries M_e and M_ν can have are U(1)×U(1) and the Klein symmetry $Z_2 \times Z_2$, respectively [75]. This group structure can be inferred in the mass basis. Note also that a joint rephasing (sign flip) of all ℓ_{iL} (ν_{iL}) plays no role in constraining the shapes of the mass matrices, which is why only subgroups of SU(3) need to be considered. For $g_e \in G_e$ and $g_\nu \in G_\nu$, one has the invariance conditions:

$$\rho_L(g_\nu)^T\, M_\nu\, \rho_L(g_\nu) \,=\, M_\nu\,, \tag{1.14}$$

$$\rho_L(g_e)^\dagger\, M_e\, M_e^\dagger\, \rho_L(g_e) \,=\, M_e\, M_e^\dagger\,, \tag{1.15}$$

which imply the vanishing of commutators $[M_e\, M_e^\dagger, \rho_L(g_e)] = [M_\nu^\dagger\, M_\nu, \rho_L(g_\nu)] = 0$, meaning $M_e\, M_e^\dagger$ ($M_\nu^\dagger\, M_\nu$) and $\rho_L(g_e)$ ($\rho_L(g_\nu)$) are diagonalised by the same matrix. Recall than in an arbitrary flavour basis we have $U_{\rm PMNS} = U_e^\dagger\, U_\nu$, with

$$U_\nu^T\, M_\nu\, U_\nu \,=\, \text{diag}(m_1, m_2, m_3) \quad \Rightarrow \quad U_\nu^\dagger\, M_\nu^\dagger\, M_\nu\, U_\nu \,=\, \text{diag}(m_1^2, m_2^2, m_3^2)\,, \tag{1.16}$$

$$U_e^\dagger\, M_e\, M_e^\dagger\, U_e \,=\, \text{diag}(m_e^2, m_\mu^2, m_\tau^2)\,. \tag{1.17}$$

Thus, up to permutations, rephasings, and unitary rotations in subspaces of degenerate eigenvalues of the ρ_L, the matrices $U_{e,\nu}$ are obtained from those diagonalising (the given) $\rho_L(g_{e,\nu})$.

To close, we go through two simple examples of applications of the non-Abelian discrete symmetry paradigm. The first is $\mu - \tau$ exchange symmetry [76, 77]. In this case, the residual symmetries are taken to be $G_e = Z_3 = \{1, T, T^2\}$ and $G_\nu = Z_2 = \{1, U'\}$, with the representation matrices

$$\rho_L(T) \,=\, \begin{pmatrix} 1 & 0 & 0 \\ 0 & \omega^2 & 0 \\ 0 & 0 & \omega \end{pmatrix}\,, \qquad \rho_L(U') \,=\, \begin{pmatrix} 1 & 0 & 0 \\ 0 & 0 & 1 \\ 0 & 1 & 0 \end{pmatrix}\,, \tag{1.18}$$

in a certain basis, and $\omega \equiv e^{2\pi i/3}$. The Z_3 symmetry is enough to distinguish the charged-leptons and render the corresponding mass matrix diagonal in the chosen basis. Up to permutations and unphysical rephasings, one has $U_e = \mathbb{1}$. On the other hand, one sees that

$$\Omega^\dagger\, \rho_L(U')\, \Omega \,=\, \text{diag}(1, 1, -1)\,, \quad \text{with } \Omega \,=\, \begin{pmatrix} 1 & 0 & 0 \\ 0 & 1/\sqrt{2} & -1/\sqrt{2} \\ 0 & 1/\sqrt{2} & 1/\sqrt{2} \end{pmatrix}\,, \tag{1.19}$$

meaning that, up to permutations and rephasings, one has:

$$U_{\rm PMNS} \,=\, U_\nu \,=\, \Omega\, U_{12}(\theta_{12},\delta_{12}) \,=\, \begin{pmatrix} \cos\theta_{12} & \sin\theta_{12} & 0 \\ -\sin\theta_{12}/\sqrt{2} & \cos\theta_{12}/\sqrt{2} & -1/\sqrt{2} \\ -\sin\theta_{12}/\sqrt{2} & \cos\theta_{12}/\sqrt{2} & 1/\sqrt{2} \end{pmatrix} , \tag{1.20}$$

where $U_{12}(\theta_{12},\delta_{12})$ is a unitary rotation matrix in the 1-2 plane parameterised by an angle θ_{12} and a phase δ_{12}, the latter having been absorbed in the undetermined Majorana phase matrix (not shown). In this scenario, one predicts maximal $\theta_{23} = \pi/4$ and $\theta_{13} = 0$, while θ_{12} remains unconstrained. Extending G_ν to the full Klein symmetry allows to fix the value of θ_{12}. This brings us to our second example, where the mixing pattern is predicted to be tribimaximal (TBM) [78]. TBM mixing is achievable for instance if $G_f = A_4$ [79] or $G_f = S_4$ [80] – in the former case, one of the Z_2 factors arises accidentally. If we take $G_f = S_4$ (see also Chapter 4 and appendix A), the flavour group includes elements S, T and U which in a certain basis correspond to the representation matrices:

$$\rho_L(S) \,=\, \frac{1}{3}\begin{pmatrix} -1 & 2 & 2 \\ 2 & -1 & 2 \\ 2 & 2 & -1 \end{pmatrix} , \quad \rho_L(T) \,=\, \begin{pmatrix} 1 & 0 & 0 \\ 0 & \omega^2 & 0 \\ 0 & 0 & \omega \end{pmatrix} , \quad \rho_L(U) \,=\, -\begin{pmatrix} 1 & 0 & 0 \\ 0 & 0 & 1 \\ 0 & 1 & 0 \end{pmatrix} . \tag{1.21}$$

Taking the residual symmetries to be $G_e = Z_3 = \{1, T, T^2\}$ and $G_\nu = Z_2 \times Z_2 = \{1, S, U, SU\}$, implies a further constraint on the matrix of Eq. (1.20), yielding

$$U_{\rm PMNS} \,=\, U_{\rm TBM} \,\equiv\, \begin{pmatrix} \sqrt{2/3} & 1/\sqrt{3} & 0 \\ -1/\sqrt{6} & 1/\sqrt{3} & -1/\sqrt{2} \\ -1/\sqrt{6} & 1/\sqrt{3} & 1/\sqrt{2} \end{pmatrix} . \tag{1.22}$$

In this setup, one finds $\theta_{12} = \arccos\left(\sqrt{2/3}\right) \simeq 35^\circ$, with $\sin^2\theta_{12} = 1/3$.

Taken at face value, both examples considered above predict $\theta_{13} = 0$ (and the vanishing of $\mathcal{J}_{\rm CP}$) and are presently excluded. While these simple patterns do not give a good fit to the data, they can nevertheless be interpreted as leading order results, subject to corrections. These corrections may arise, for instance, in the form of charged-lepton rotations (perhaps $G_e = Z_3$ is too strict a condition), renormalisation group running, or higher-order operators in a UV complete model.

1.3.2 Combining CP with Discrete Symmetries

An interesting extension of the discrete symmetry framework outlined above comes from additionally considering invariance under CP transformations. Crucial to this approach is the recognition that the most general CP transformation one can impose on fermion multiplets ψ acts non-trivially in flavour space [81–84]:

$$\psi(x) \,\to\, i\, X\, \gamma^0\, C\, \overline{\psi(x_P)}^{\,T} , \tag{1.23}$$

where X is a unitary matrix carrying flavour indices and $x = (x^0, \vec{x})$ goes into $x_P = (x^0, -\vec{x})$ under parity. CP transformations with non-trivial flavour rotations $X \neq \mathbb{1}$ are often referred to as generalised CP (gCP) transformations, as opposed to canonical ones (for which $X = \mathbb{1}$).

If such gCP transformations represent residual symmetries, we are led to new invariance conditions on the mass matrices. Suppose that, in the unbroken phase, the matrix X_L appears in a gCP symmetry transformation of the lepton-doublet flavour multiplet. The requirement that M_ν preserves such a

symmetry at low energy implies:

$$X_L^T \, M_\nu \, X_L \, = \, M_\nu^* \, , \tag{1.24}$$

in some flavour basis. Thus, the presence of just a residual gCP symmetry may lead by itself to interesting predictions. This is the case for the so-called $\mu - \tau$ reflection symmetry [85, 86] (distinct from the aforementioned exchange symmetry), which corresponds to taking

$$X_L \, = \, \begin{pmatrix} 1 & 0 & 0 \\ 0 & 0 & 1 \\ 0 & 1 & 0 \end{pmatrix} \tag{1.25}$$

as the residual gCP symmetry matrix in the neutrino sector. Then, Eq. (1.24) constrains the mass matrix to have the form:

$$M_\nu \, = \, \begin{pmatrix} a & b & b^* \\ b & c & d \\ b^* & d & c^* \end{pmatrix} \, , \tag{1.26}$$

with $a, d \in \mathbb{R}$ and $b, c \in \mathbb{C}$. This in turn implies $|(U_{\rm PMNS})_{\mu k}| = |(U_{\rm PMNS})_{\tau k}|$, for $k = 1, 2, 3$ (see Ref. [86] for a proof), from which maximal atmospheric mixing follows, $\theta_{23} = \pi/4$, while θ_{12} and θ_{13} remain unconstrained. If furthermore $\theta_{13} \neq 0$ (as is known to be the case), then $\cos\delta = 0$, meaning a maximal Dirac CPV phase, $\delta = \pi/2, 3\pi/2$, is predicted. Additionally, knowing that neutrinos are non-degenerate, the Majorana phases can be shown to take the CP-conserving values $\alpha_{21,31} = 0, \pi$ [86].

In what follows, we will consider scenarios where both a non-Abelian discrete symmetry and some gCP symmetry are present in the flavour model. The concurrent presence of flavour and gCP symmetries constrains the possible form of the gCP matrices. In particular, given the flavour symmetry group G_f acting as before in the lepton sector, the X_L matrix must obey the so-called *consistency condition* [87,88]:

$$X_L \, \rho_L(g)^* \, {X_L}^{-1} \, = \, \rho_L(u(g)) \, , \tag{1.27}$$

where u is a class-inverting automorphism of G_f, mapping an element $g \in G_f$ into $g' = u(g) \in G_f$, the latter belonging to the conjugacy class of g^{-1} [89]. This condition is obtained by applying in sequence a gCP transformation, followed by a flavour transformation associated with the group element $g \in G_f$, and finally an inverse gCP transformation, and noticing that the resulting transformation must correspond to an element of G_f since the Lagrangian is unchanged. Failing to satisfy such a condition means one has misidentified the full flavour symmetry of the model [88].

The approach of combining gCP and flavour symmetries, which we discuss further in Chapter 4, is powerful in that it allows to constrain Majorana phases, something flavour symmetries cannot achieve by themselves. As an application of this setup, consider the example of combining $G_f = S_4$ flavour and gCP symmetries. Here, using the same presentation of S_4 as before, $G_e = Z_3 = \{1, T, T^2\}$, and $G_\nu = Z_2 \times H^\nu_{\rm CP}$, with $Z_2 = \{1, S\}$ and $H^\nu_{\rm CP}$ being the group of residual CP transformations in the neutrino sector, containing a single non-trivial element X_ν. One possible choice for this element is $X_\nu = \rho(U)$, and it leads to maximal atmospheric mixing, $\sin^2\theta_{23} = 1/2$, maximal Dirac phase, $\delta = \pi/2, 3\pi/2$ and CP-conserving Majorana phases, $\alpha_{21,31} = 0, \pi$, while predicting the interesting correlation [87, 90]:

$$\sin^2\theta_{12} \, = \, \frac{1}{3\cos^2\theta_{13}} \, . \tag{1.28}$$

In this scenario, mixing is determined up to an unknown continuous parameter. We note that at present (see Table 1.3), however, taking $\sin^2\theta_{23}$ in its full 3σ range, a value of $\sin^2\theta_{12}$ satisfying the above relation lies outside the corresponding 2σ range.

1.3.3 A New Approach: Modular Symmetry

A generalisation of the discrete symmetry approach based on modular symmetry has recently been put forward in Ref. [91] and further explored in Refs. [92–95]. In this setup, invariance under finite subgroups Γ_N ($N > 1$) of the modular group shapes the relevant mass matrices. Fields carrying a non-trivial representation under Γ_N are assigned a modular weight, transforming with a scale factor in addition to the usual unitary rotation representing the discrete group. To build an invariant action under such transformations, special functions of the modular field with the appropriate scaling properties (modular forms) need to be present in order to provide compensating factors. By setting modular weights to zero, the construction reduces to a regular, flavour-symmetric one.

The models considered are supersymmetric (SUSY) and predictive. In their minimal realisation, only one complex VEV breaks the modular symmetry and, together with superpotential parameters, it fixes the neutrino and charged-lepton mass matrices, determining not only mixing and CPV phases, but also masses and mass-squared differences. There is a limited number of sources for deviations from the leading-order predictions in such models, such as SUSY breaking and renormalisation group running.

A systematic exploration of the modular invariance paradigm in bottom-up approaches to the flavour puzzle is desirable but still lacking at the moment. The predictive power of the present approach and the existence of successful benchmarks make this model-building avenue worthy of future study.

1.4 Outline

In the four chapters which follow we consider distinct facets of what has so far been described as the symmetry approach to neutrino masses and to neutrino mixing.

In Chapter 2, we present a low-scale seesaw scenario in which a connection exists between symmetry and neutrino masses. In particular, the smallness of these masses is related to the smallness of Yukawa couplings protected by an approximately conserved (non-standard) lepton number. The specific realisation of such a scenario considers yet another kind of symmetry, the aforementioned (Abelian) Froggatt-Nielsen symmetry, which in a certain limit mimics the required lepton number symmetry.

In Chapter 3, we analyse neutrinoless double-beta decay, a process whose existence signals the Majorana nature of massive neutrinos and the rupture of the standard lepton number symmetry L. After considering a generic situation, we look into bounds on the $(\beta\beta)_{0\nu}$-decay rate for choices of Majorana phases in line with predictive schemes combining flavour and generalised CP symmetries.

In Chapter 4, we look into a more flexible scheme combining flavour and gCP symmetries. Our analysis is based on the flavour group $G_f = S_4$ and on particular, small residual symmetry groups. We focus on correlations between mixing parameters, following from the symmetry breaking pattern.

In Chapter 5, we explore the predictions of minimalistic models based on the modular group $\Gamma_4 \simeq S_4$.

In this setup, modular symmetry breaking determines mixing angles, CPV phases and ratios of masses and of mass-squared differences.

Chapter 6 contains our concluding remarks.

Symmetry-protected Low-scale Seesaw

2

The seesaw mechanism explains naturally the smallness of neutrino masses, which in the standard type I scenario has its origin in large lepton-number violating Majorana masses of right-handed neutrinos. An appealing aspect of this setup is that one can relate the existence of large Majorana masses of the RH neutrino fields to a spontaneous breaking of some high-scale symmetry, say GUT symmetry. However, direct tests of the standard seesaw mechanism are almost impossible due to the largeness of the scales involved with respect to the electroweak scale.

In the present chapter, following Ref. [96], we consider a symmetry-protected seesaw scenario where small Majorana neutrino masses arise as a result of an approximately conserved (non-standard) lepton number. We first establish our setup independently of the origin of the considered Yukawa and mass matrix structures. Afterwards, we detail a Froggatt-Nielsen scenario where such structures are realised, predicting relations between magnitudes of Yukawa couplings. In this context, we further discuss predictions for CPV phases, aspects of the low-energy phenomenology and the possibility of successful leptogenesis.

2.1 Symmetry-protected Setup

We minimally extend the Standard Model by adding two RH neutrinos, i.e., two chiral fields $\nu_{aR}(x)$, $a = 1, 2$, which are singlets under the SM gauge symmetry group. Following the notations of Refs. [97–100], the relevant low-energy Lagrangian is

$$\mathcal{L}_\nu \,=\, -\,\overline{\nu_{aR}}\,(M_D^T)_{a\alpha}\,\nu_{\alpha L} \,-\, \frac{1}{2}\,\overline{\nu_{aR}}\,(M_N)_{ab}\,\nu_{bL}^C \,+\, \text{h.c.}\,, \tag{2.1}$$

with $\nu_{aL}^C \equiv (\nu_{aR})^C \equiv C\,\overline{\nu_{aR}}^T$. $M_N = (M_N)^T$ is the 2×2 Majorana mass matrix of RH neutrinos, while M_D denotes the 3×2 neutrino Dirac mass matrix, generated from the Yukawa couplings of neutrinos following the breaking of electroweak symmetry. These Yukawa interactions read

$$\mathcal{L}_Y \,=\, -\,\overline{\nu_{aR}}\,(Y_D^T)_{a\alpha}\,H^{c\dagger}\,L_\alpha \,+\, \text{h.c.}\,, \qquad M_D \,=\, v\,Y_D\,, \tag{2.2}$$

where $L_\alpha(x) = (\nu_{\alpha L}(x), \ell_{\alpha L}(x))^T$, the Higgs conjugate doublet is defined as $H^c \equiv i\sigma_2 H^*$, and $H = (H^+, H^0)^T$ is the Higgs doublet field whose neutral component acquires a VEV $v = \langle H^0 \rangle = 174$ GeV. The matrix of neutrino Yukawa couplings has the form

$$Y_D \,\equiv\, \begin{pmatrix} g_{e1} & g_{e2} \\ g_{\mu 1} & g_{\mu 2} \\ g_{\tau 1} & g_{\tau 2} \end{pmatrix}\,, \tag{2.3}$$

where $g_{\alpha a}$ denotes the coupling of $L_\alpha(x)$ to $\nu_{aR}(x)$, $\alpha = e, \mu, \tau$, $a = 1, 2$.

The full 5×5 neutrino Dirac-Majorana mass matrix, given below in the (ν_L, ν_L^C) basis, can be made block-diagonal by use of a unitary matrix Ω,

$$\Omega^T \begin{pmatrix} 0 & M_D \\ M_D^T & M_N \end{pmatrix} \Omega = \begin{pmatrix} U_\nu^* \hat{m} U_\nu^\dagger & 0 \\ 0 & V^* \hat{M} V^\dagger \end{pmatrix}, \tag{2.4}$$

where $\hat{m} \equiv \mathrm{diag}(m_1, m_2, m_3)$ contains the masses m_i of the light Majorana neutrino mass eigenstates ν_i, while $\hat{M} \equiv \mathrm{diag}(M_1, M_2)$ contains the masses $M_{1,2}$ of the heavy Majorana neutrinos, $N_{1,2}$. Here, U_ν and V are 3×3 and 2×2 unitary matrices, respectively. The matrix Ω can be parametrised as [97, 101]:

$$\Omega = \exp \begin{pmatrix} 0 & R \\ -R^\dagger & 0 \end{pmatrix} = \begin{pmatrix} \mathbb{1} - \frac{1}{2} R R^\dagger & R \\ -R^\dagger & \mathbb{1} - \frac{1}{2} R^\dagger R \end{pmatrix} + \mathcal{O}(R^3), \tag{2.5}$$

under the assumption that the elements of the 3×2 complex matrix R are small, which will be justified later. At leading order in R, the following relations hold [97]:

$$R^* \simeq M_D M_N^{-1}, \tag{2.6}$$

$$M_\nu \equiv U_\nu^* \hat{m} U_\nu^\dagger \simeq R^* M_N R^\dagger - R^* M_D^T - M_D R^\dagger = - R^* M_N R^\dagger, \tag{2.7}$$

$$V^* \hat{M} V^\dagger \simeq M_N + \frac{1}{2} R^T R^* M_N + \frac{1}{2} M_N R^\dagger R \simeq M_N, \tag{2.8}$$

where we have used Eq. (2.6) to get the last equality in Eq. (2.7).[1] From the first two we recover the well-known seesaw formula for the light neutrino mass matrix,

$$M_\nu = - M_D M_N^{-1} M_D^T. \tag{2.9}$$

We are interested in the case where only the lepton-number-conserving Majorana mass term of $\nu_{1R}(x)$ and $\nu_{2R}(x)$, $M \nu_{1R}^T C^{-1} \nu_{2R}$, with $M > 0$ and, e.g., $L'(\nu_{1R}) = -1$ and $L'(\nu_{2R}) = +1$, L' being the total lepton charge, is present in the Lagrangian. The conserved charge is a non-standard lepton charge which is expressed in terms of the individual lepton charges L_α, $\alpha = e, \mu, \tau$, and $L_a(\nu_{bR}) = -\delta_{ab}$, $a, b = 1, 2$, as:

$$L' = L_e + L_\mu + L_\tau + L_1 - L_2, \tag{2.10}$$

with $L'(\nu_{1R}) = L_1(\nu_{1R}) = -1$ and $L'(\nu_{2R}) = -L_2(\nu_{2R}) = +1$. We will drop the prime in L' in what follows. In this case the Majorana mass matrix of RH neutrinos $\nu_{1R}(x)$ and $\nu_{2R}(x)$ reads:

$$M_N = \begin{pmatrix} 0 & M \\ M & 0 \end{pmatrix}. \tag{2.11}$$

Using Eqs. (2.2), (2.3) and Eq. (2.9), we get the following expression for the light neutrino Majorana mass matrix M_ν:

$$M_\nu = - \frac{v^2}{M} \begin{pmatrix} 2\, g_{e1}\, g_{e2} & g_{\mu 1}\, g_{e2} + g_{e1}\, g_{\mu 2} & g_{\tau 1}\, g_{e2} + g_{e1}\, g_{\tau 2} \\ g_{\mu 1}\, g_{e2} + g_{e1}\, g_{\mu 2} & 2\, g_{\mu 1}\, g_{\mu 2} & g_{\tau 1}\, g_{\mu 2} + g_{\mu 1}\, g_{\tau 2} \\ g_{\tau 1}\, g_{e2} + g_{e1}\, g_{\tau 2} & g_{\tau 1}\, g_{\mu 2} + g_{\mu 1}\, g_{\tau 2} & 2\, g_{\tau 1}\, g_{\tau 2} \end{pmatrix}. \tag{2.12}$$

[1] The factors 1/2 in the two terms $\propto R^T R^* M_N$ and $\propto M_N R^\dagger R$ in Eq. (2.8) are missing in the corresponding expression in Ref. [97]. These two terms provide a sub-leading correction to the leading term M_N and have been neglected in the discussion of the phenomenology in Ref. [97]. We will also neglect them in the phenomenological analysis we perform.

With the assignments $L(\nu_{1R}) = -1$ and $L(\nu_{2R}) = +1$ made, the requirement of conservation of the total lepton charge L leads to $g_{\alpha 1} = 0$, $\alpha = e, \mu, \tau$. In this limit of $g_{\alpha 1} = 0$, we have $M_\nu = 0$, the light neutrino masses vanish and ν_{1R} and ν_{2L}^C combine to form a Dirac fermion N_D of mass $\tilde{M} = \sqrt{M^2 + v^2 \sum_\alpha |g_{\alpha 2}|^2}$,

$$N_D = \frac{N_1 \pm i\, N_2}{\sqrt{2}} = \nu_{1R} + \nu_{2L}^C \,, \tag{2.13}$$

with $N_k = N_{kL} + N_{kR} \equiv N_{kL} + (N_{kL})^C = C\,\overline{N_k}^T$, $k = 1, 2$, and $\nu_{1R} = (N_{1R} \pm i\, N_{2R})/\sqrt{2}$, $\nu_{2L}^C = (N_{1L} \pm i\, N_{2L})/\sqrt{2}$. These general results can be inferred just from the form of the conserved non-standard lepton charge of Eq. (2.10). In particular, $\min(n_+, n_-)$ and $|n_+ - n_-|$ are the numbers of massive Dirac and massless neutrinos, respectively, n_+ (n_-) being the number of charges entering into the expression for L with positive (negative) sign [62].

Thus, the massive fields $N_k(x)$ are related to the fields $\nu_{aR}(x)$ by $\nu_{aR}(x) \simeq V_{ak}^*\, N_{kR}(x)$, where

$$V = \frac{1}{\sqrt{2}} \begin{pmatrix} 1 & \mp i \\ 1 & \pm i \end{pmatrix} , \tag{2.14}$$

where the upper (lower) signs correspond to the case with the upper (lower) signs in Eq. (2.13) and in the expressions for ν_{1R} and ν_{2L}^C given after it. We will adhere to the upper-sign convention further on.

Small L-violating couplings $g_{\alpha 1} \neq 0$ split the Dirac fermion N_D into two Majorana fermions N_1 and N_2 which have very close but different masses, $M_1 \neq M_2$, $|M_2 - M_1| \ll M_{1,2}$. As a consequence, N_D corresponds to a pseudo-Dirac particle [44,46]. Of the three light massive neutrinos, one remains massless (at tree level) while the other two acquire non-zero and different masses. The splitting between the masses of N_1 and N_2 is of the order of one of the light neutrino mass differences and thus is extremely difficult to resolve in practice.

More specifically, in the case of a neutrino mass spectrum with normal ordering, we have (at tree level) keeping terms up to 4th power in the Yukawa couplings $g_{\alpha 1}$ and $g_{\alpha 2}$ and taking $g_{\alpha a}$ to be real for simplicity:

$$m_1 = 0 \,, \quad m_{2,3} \simeq \frac{1}{M} \left[\sqrt{\Delta} \left(1 - \frac{D(A^2 + \Delta)}{2M^2 \Delta} \right) \mp A \left(1 - \frac{D}{M^2} \right) \right] + \mathcal{O}(g_{\alpha a}^6) \,, \tag{2.15}$$

where

$$D \equiv v^2 \left(g_{e1}^2 + g_{\mu 1}^2 + g_{\tau 1}^2 + g_{e2}^2 + g_{\mu 2}^2 + g_{\tau 2}^2 \right) , \tag{2.16}$$

$$\Delta \equiv v^4 \left(g_{e1}^2 + g_{\mu 1}^2 + g_{\tau 1}^2 \right) \left(g_{e2}^2 + g_{\mu 2}^2 + g_{\tau 2}^2 \right) , \tag{2.17}$$

$$A \equiv v^2 \left(g_{e1}\, g_{e2} + g_{\mu 1}\, g_{\mu 2} + g_{\tau 1}\, g_{\tau 2} \right) . \tag{2.18}$$

The heavy neutrino mass spectrum is given by:

$$M_{1,2} \simeq M \left[1 + \frac{D}{2M^2} - \frac{1}{2M^4} \left(\Delta + 2A^2 + \frac{D^2}{4} \right) \right] \mp \frac{A}{M} \left(1 - \frac{D}{M^2} \right) + \mathcal{O}(g_{\alpha a}^6) \,. \tag{2.19}$$

The values of $m_{2,3}$ and $M_{1,2}$ given in Eqs. (2.15) and (2.19) can be obtained as approximate solutions of the *exact* mass-eigenvalue equation:

$$\lambda^4 - \lambda^2 \left(M^2 + D \right) - 2\,\lambda\, M\, A - \left(\Delta - A^2 \right) = 0 \,. \tag{2.20}$$

Note that, as it follows from Eqs. (2.15) and (2.19), we have [97]: $M_2 - M_1 \simeq 2(A/M)(1 - D/M^2) = m_3 - m_2$. Therefore, the splitting between M_2 and M_1, as we have already noted, is exceedingly small. Indeed, for a neutrino mass spectrum with normal ordering and $m_1 = 0$, we have $m_2 = \sqrt{\Delta m^2_{21}} \simeq 8.6 \times 10^{-3}$ eV, $m_3 = \sqrt{\Delta m^2_{31}} \simeq 0.051$ eV, and

$$M_2 - M_1 \,=\, m_3 - m_2 \,\simeq\, 0.042 \text{ eV}\,, \tag{2.21}$$

where we have used the best-fit values of Δm^2_{21} and Δm^2_{31} determined in the global analysis of neutrino oscillation data of Ref. [38] (see Fig. 1.1 and Table 1.2). Even though in the present chapter we consistently rely on the global analysis of Ref. [38], as in the original work we report on, our conclusions are unchanged when considering the updated data. The corrections to the matrix V which diagonalises M_N are of the order of AD/M^4 and are negligible, as was noticed also in [97].

To leading order in (real) $g_{\alpha 1}$ and $g_{\alpha 2}$, the expressions in Eqs. (2.15) and (2.19) simplify significantly [97]:

$$m_1 \,=\, 0\,, \quad m_2 \,\simeq\, \frac{1}{M}\left(\sqrt{\Delta} - A\right)\,, \quad m_3 \,\simeq\, \frac{1}{M}\left(\sqrt{\Delta} + A\right)\,, \tag{2.22}$$

$$M_1 \,\simeq\, M\left(1 + \frac{D}{2M^2}\right) - \frac{A}{M}\,, \quad M_2 \,\simeq\, M\left(1 + \frac{D}{2M^2}\right) + \frac{A}{M}\,. \tag{2.23}$$

The low-energy phenomenology involving the pseudo-Dirac neutrino N_D, or equivalently the Majorana neutrinos N_1 and N_2, is controlled by the matrix RV of couplings of N_1 and N_2 to the charged leptons in the weak charged lepton current (see Section 2.5). When both $g_{\alpha 1}$ and $g_{\alpha 2}$ couplings are present, this matrix is given by:

$$RV \,\simeq\, \frac{1}{\sqrt{2}}\,\frac{v}{M}\,\begin{pmatrix} g^*_{e1} + g^*_{e2} & i\,(g^*_{e1} - g^*_{e2}) \\ g^*_{\mu 1} + g^*_{\mu 2} & i\,(g^*_{\mu 1} - g^*_{\mu 2}) \\ g^*_{\tau 1} + g^*_{\tau 2} & i\,(g^*_{\tau 1} - g^*_{\tau 2}) \end{pmatrix}\,. \tag{2.24}$$

It follows from the preceding discussion that the generation of non-zero light neutrino masses may be directly related to the generation of the L-non-conserving neutrino Yukawa couplings $g_{\alpha 1} \neq 0$, $\alpha = e, \mu, \tau$. Among the many possible mechanisms leading to $g_{\alpha 1} \neq 0$ there is one we will discuss further, that can lead to exceedingly small $g_{\alpha 1}$, say $|g_{\alpha 1}| \sim 10^{-12} - 10^{-8}$. In this case the RH neutrinos can have masses in the few GeV to a few TeV range and the neutrino Yukawa couplings $|g_{\alpha 2}|$ can be much larger than $|g_{\alpha 1}|$, of the order $|g_{\alpha 2}| \sim 10^{-4} - 10^{-2}$, leading to interesting low-energy phenomenology. For these ranges of $|g_{\alpha 2}|$ and M, the approximations $D/M^2 \ll 1$ and $\tilde{M} \simeq M$ are valid and will be used in what follows, i.e., we will use Eqs. (2.22) and (2.23).

Thus, in the scenario we are interested in with two RH neutrinos possessing a Majorana mass term which conserves the total lepton charge L, the smallness of the light Majorana neutrino masses is related to the smallness of the L-non-conserving neutrino Yukawa couplings $g_{\alpha 1}$ and not to the RH neutrinos having large Majorana masses in the range of $\sim (10^{10} - 10^{14})$ GeV. Moreover, in contrast to the standard seesaw scenario, the heavy Majorana neutrinos of the scenario of interest, having masses at the TeV or lower scale, are in principle directly observable in collider (LHC, future $e^+ - e^-$ and $p - p$) experiments.

The low-scale type I seesaw scenario of interest with two RH neutrinos ν_{1R} and ν_{2R} with L-conserving Majorana mass term and L-conserving (L-non-conserving) neutrino Yukawa couplings $g_{\alpha 2}$ ($g_{\alpha 1}$) of ν_{2R} (of ν_{1R}) was considered in Ref. [97] on purely phenomenological grounds (see also, e.g., [102,103]). It was

pointed out in Ref. [97], in particular, that the strong hierarchy $|g_{\alpha 1}| \ll |g_{\beta 2}|$, $\alpha, \beta = e, \mu, \tau$, is a perfectly viable possibility from the point of view of generation of the light Majorana neutrino masses and that in this case the L-non-conserving effects would be hardly observable. In the next section we provide a possible theoretical justification of the strong hierarchy between the L-conserving and L-non-conserving neutrino Yukawa couplings based on the Froggatt-Nielsen approach to the flavour problem.

2.2 Froggatt-Nielsen Realisation

We work in a supersymmetric (SUSY) framework and consider a global broken $\mathrm{U}(1)_{\mathrm{FN}}$ Froggatt-Nielsen flavour symmetry, whose charge assignments we motivate below. We will show how an approximate $\mathrm{U}(1)_L$ symmetry, related to the L-conservation, may arise in such a model, with $g_{\alpha 1} \neq 0$ as the leading L-breaking effect responsible for neutrino masses.

In our setup, one of the RH neutrino chiral superfields has a negative charge under $\mathrm{U}(1)_{\mathrm{FN}}$, namely $Q_{\mathrm{FN}}(\hat{N}_2) = -1$, while the other carries a positive FN charge, $Q_{\mathrm{FN}}(\hat{N}_1) \equiv n > 0$. The FN mechanism is (as usual) realised thanks to the VEV of the lowest component S of a chiral superfield $\hat{S}$, which is a singlet under the SM gauge symmetry group and carries negative FN charge, $Q_{\mathrm{FN}}(\hat{S}) = -1$. Charges for the $\hat{L}_\alpha$ superfields follow a standard lopsided assignment [104], namely $Q_{\mathrm{FN}}(\hat{L}_e) = 2$, $Q_{\mathrm{FN}}(\hat{L}_\mu) = 1$, and $Q_{\mathrm{FN}}(\hat{L}_\tau) = 1$, which allows for large $\nu_\mu - \nu_\tau$ mixing. For definiteness we take $Q_{\mathrm{FN}}(\hat{H}_u) = 0$, $Q_{\mathrm{FN}}(\hat{e}^c) = 4$, $Q_{\mathrm{FN}}(\hat{\mu}^c) = 2$, and $Q_{\mathrm{FN}}(\hat{\tau}_c) = 0$. The FN suppression parameter $\epsilon = \langle S \rangle / \Lambda_{\mathrm{FN}}$ is thus chosen to be close to the sine of the Cabibbo angle λ_C, specifically $\epsilon = 0.2$, in order to reproduce the hierarchies between charged lepton masses (see also [105, 106]). Here, Λ_{FN} is the FN flavour dynamics scale. The charge assignments under $\mathrm{U}(1)_{\mathrm{FN}}$ relevant to the present study are summarised in Table 2.1.

	$\hat{S}$	$\hat{N}_1$	$\hat{N}_2$	$\hat{H}_u$	$\hat{L}_e$	$\hat{L}_\mu$	$\hat{L}_\tau$	$\hat{e}^c$	$\hat{\mu}^c$	$\hat{\tau}^c$
Q_{FN}	-1	n	-1	0	2	1	1	4	2	0

Table 2.1: Charge assignments of lepton superfields under the $\mathrm{U}(1)_{\mathrm{FN}}$ symmetry group.

The effective superpotential for the neutrino sector reads:[2]

$$W_\nu \sim M_0 \left(\epsilon^{2n} \hat{N}_1 \hat{N}_1 + \epsilon^{n-1} \hat{N}_1 \hat{N}_2\right) + \left(\epsilon \hat{L}_e + \hat{L}_\mu + \hat{L}_\tau\right) \left(\epsilon^{n+1} \hat{N}_1 + g_2 \hat{N}_2\right) \hat{H}_u \,, \tag{2.25}$$

where $M_0 \sim \Lambda_{\mathrm{FN}}$ and g_2 is an *a priori* $\mathcal{O}(1)$ coupling. Due to the condition of holomorphicity of the superpotential, no quadratic term for $\hat{N}_2$ is allowed, justifying the absence of the Majorana mass term $M \nu_{2R}^T C^{-1} \nu_{2R}$. This framework may naturally arrange for the suppression $(M_N)_{11} \ll (M_N)_{12}$, as well as for a hierarchy between RH masses and the FN scale, $M \sim \epsilon^{n-1} \Lambda_{\mathrm{FN}} \ll \Lambda_{\mathrm{FN}}$, provided the charge n is sufficiently large.

The limit of a large $\hat{N}_1$ charge, $n \gg 1$, is quite interesting. In this limit, one finds an accidental (approximate) $\mathrm{U}(1)_L$ symmetry, with assignments $L(\hat{N}_{1,2}) = \pm 1$. Furthermore, the desired hierarchy between (would-be) L-breaking and (would-be) L-conserving Yukawa couplings, $|g_{\alpha 1}| \sim \epsilon^{n+1} \ll |g_{\beta 2}|$,

[2] The presence of an R-parity preventing the usual L- and B-violating terms in the MSSM superpotential is assumed.

is manifestly achieved. Finally, the mass term for $\hat{N}_1$ is suppressed with respect to $\Lambda_{\rm FN}$ by the FN parameter to the power of $2n \gg 1$. This observation and the holomorphicity of the superpotential justify the absence of diagonal Majorana mass terms $M\,\nu_{aR}^T\,C^{-1}\,\nu_{aR}$, $a = 1, 2$, in Eq. (2.11) which could push up the light neutrino masses to unwanted heavy scales. We will focus on the case of a sufficiently large charge n in what follows.

The lopsided choice of FN charges for the lepton doublets is responsible for the structure $|g_{e2}| : |g_{\mu 2}| : |g_{\tau 2}| \simeq \epsilon : 1 : 1$ of Yukawa couplings of ν_{2R}. However, due to the large FN charge of ν_{1R}, such FN flavour structure might be diluted in the L-violating Yukawa couplings. Indeed, for each insertion of $\hat{S}$, a factor of ϵ is in principle accompanied by an $\mathcal{O}(1)$ factor. This uncertainty makes it impossible to have an unambiguous prediction for the ratios $|g_{e1}| : |g_{\mu 1}| : |g_{\tau 1}|$ in the model under discussion. This is in contrast to the case of the $g_{\alpha 2}$ couplings.

Thus, in the present setup, the Yukawa matrix Y_D obeys the following structure (up to phases):

$$Y_D \sim \begin{pmatrix} g_{e1} & \epsilon\, g_2 \\ g_{\mu 1} & g_2 \\ g_{\tau 1} & g_2 \end{pmatrix} \sin\beta\,, \tag{2.26}$$

with $\sin\beta = \left\langle H_u^0 \right\rangle / v$, and where $g_{\alpha 1}, g_2 > 0$, and the hierarchy $g_{\alpha 1} \ll g_2 \lesssim 1$ is naturally realised. We see from Eq. (2.12) that the scale of light neutrino masses depends on the size of the product $g_{\alpha 1}\, g_2$, namely

$$(M_\nu)_{\alpha\beta} \sim \frac{v^2\,\sin^2\beta}{M}\,(g_{\alpha 1} + g_{\beta 1})\, g_2\,. \tag{2.27}$$

The $g_{\alpha 1}$ couplings represent a linear-like [107] contribution to light neutrino masses. In the FN realisation, the RH neutrino Majorana mass matrix reads

$$M_N = \begin{pmatrix} \mu & M \\ M & 0 \end{pmatrix}, \tag{2.28}$$

with an inverse-like [108–110] component μ, which gives a subleading contribution to light neutrino masses. Despite being suppressed, the quadratic term for $\hat{N}_1$, and thus the Majorana mass term $\mu\,\nu_{1R}^T\,C^{-1}\,\nu_{1R}$, may still play a non-negligible role, for instance, in studies of leptogenesis. A complete suppression of μ can be achieved through the modification of our setup which we summarise in the following. Consider (4+1) dimensions where the extra dimension is compactified on an S^1/Z_2 orbifold. This extra dimension has two fixed points, y_1 and y_2, where an enhanced symmetry may arise. We localize all SM fields on y_1, a new chiral superfield $\hat{\Phi}$ (with lowest component Φ) on y_2, and allow the FN field S and both RH neutrino fields to propagate in the bulk. We impose, aside from the aforementioned FN symmetry ($Q_{\rm FN}(\Phi) = 0$), an $\mathrm{U}(1)_{B-\hat{L}}$ symmetry with the charge assignments $(B - \hat{L})(\nu_{1,2R}) = -1$ and $(B - \hat{L})(\Phi) = +2$. Notice that $\hat{L}$ does not coincide with the previously defined lepton charge L.[3] Then, interactions of the type $\Phi\,\nu_{aR}^T\,C^{-1}\,\nu_{bR}\,(a, b = 1, 2)$ are allowed, provided a sufficient number of insertions of S are considered. They generate mass terms for the RH neutrinos once Φ develops a non-zero VEV, $\langle\Phi\rangle \neq 0$. The Yukawa couplings $g_{\alpha a}$ are allowed and retain their FN hierarchy. Assuming an enhanced $\mathrm{U}(1)_L$ symmetry at y_2 with charges $L(\nu_{1R}) = -1$, $L(\nu_{2R}) = +1$ and $L(\Phi) = 0$, diagonal Majorana mass

[3] Indeed, we have $\hat{L}(\nu_{1R}) = \hat{L}(\nu_{2R}) = +1$ while $L(\nu_{1R}) = -L(\nu_{2R}) = -1$ (see Section 2.1).

terms for $\nu_{1,2R}$ are thus forbidden. The situation is that of Section 2.1, where FN plays the role of an approximate lepton number.

2.3 Neutrino Mixing

The addition of the terms of Eq. (2.1) to the SM Lagrangian leads to a PMNS neutrino mixing matrix, $U_{\rm PMNS}$, which is not unitary. Indeed, the charged and neutral current weak interactions involving the light Majorana neutrinos ν_i read:

$$\mathcal{L}^{\nu}_{\rm CC} \;=\; -\frac{g}{\sqrt{2}}\,\overline{\ell_{\alpha L}}\,\gamma_\mu\left(U_e^\dagger(\mathbb{1}+\eta)U_\nu\right)_{\alpha i}\,\nu_{iL}\,W^\mu \;+\; \text{h.c.}\,, \tag{2.29}$$

$$\mathcal{L}^{\nu}_{\rm NC} \;=\; -\frac{g}{2c_w}\,\overline{\nu_{iL}}\,\gamma_\mu\left(U_\nu^\dagger(\mathbb{1}+2\eta)U_\nu\right)_{ij}\,\nu_{jL}\,Z^\mu\,, \tag{2.30}$$

where $\alpha = e,\mu,\tau$, c_w is the cosine of the Weinberg angle, and U_e is the unitary matrix originating from the diagonalisation of the charged lepton mass matrix and $\eta \equiv -\,R\,R^\dagger/2$. The transformation U_e does not affect the power counting in the structure of Eq. (2.26), though it may provide a source of deviations. We then choose to work in the charged lepton mass basis, in which $U_e = \mathbb{1}$. In this basis the neutrino mixing matrix is given by: $U_{\rm PMNS} = (\mathbb{1}+\eta)U_\nu$, where U_ν is the unitary matrix diagonalising the Majorana neutrino mass matrix generated by the seesaw mechanism and η describes the deviation from unitarity of the PMNS matrix. As we will see further, the experimental constraints on the elements of η imply $|\eta_{\alpha\beta}| \lesssim 10^{-3}$, $\alpha,\beta = e,\mu,\tau$.

Due to the structure of the matrix of Yukawa couplings Y_D given in Eq. (2.26), in the scheme we are considering, a spectrum with normal ordering, $m_1 < m_2 < m_3$, is favoured over inverted ordering. We henceforth consider the NO case, for which, as we have already commented, we have $m_1 = 0$, $m_2 = \sqrt{\Delta m^2_{21}}$, and $m_3 = \sqrt{\Delta m^2_{31}}$. Working in the basis of a diagonal charged-lepton mass term and neglecting the deviations from unitarity, which are parametrised by η, we identify the PMNS mixing matrix with the unitary matrix U_ν which diagonalises M_ν, $U_{\rm PMNS} \simeq U_\nu$. Given that one neutrino is massless (at tree level), the neutrino mixing matrix can be parametrised as (cf. Eq. (1.7)):

$$U_{\rm PMNS} \;=\; \begin{pmatrix} c_{12}c_{13} & s_{12}c_{13} & s_{13}e^{-i\delta} \\ -s_{12}c_{23} - c_{12}s_{23}s_{13}e^{i\delta} & c_{12}c_{23} - s_{12}s_{23}s_{13}e^{i\delta} & s_{23}c_{13} \\ s_{12}s_{23} - c_{12}c_{23}s_{13}e^{i\delta} & -c_{12}s_{23} - s_{12}c_{23}s_{13}e^{i\delta} & c_{23}c_{13} \end{pmatrix} \text{diag}(1, e^{i\alpha/2}, 1)\,, \tag{2.31}$$

where δ and α denote the Dirac and Majorana CPV phases, respectively, $\delta,\alpha \in [0, 2\pi)$.

2.4 Predictions for CPV Phases

It proves convenient for our further analysis to use the Casas-Ibarra parametrisation [111] of the Dirac mass matrix M_D (neutrino Yukawa matrix Y_D):

$$M_D \;=\; v\,Y_D \;=\; i\,U^*_{\rm PMNS}\,\sqrt{\hat{m}}\,O\,\sqrt{\hat{M}}\,V^\dagger\,, \tag{2.32}$$

where $\hat{m} = \mathrm{diag}(m_1, m_2, m_3)$ and O is a complex orthogonal matrix. In the scheme with two heavy RH Majorana neutrinos the matrix O has the form [112, 113]:

$$O = \begin{pmatrix} 0 & 0 \\ \cos\hat{\theta} & \pm\sin\hat{\theta} \\ -\sin\hat{\theta} & \pm\cos\hat{\theta} \end{pmatrix}, \quad \text{for NO mass spectrum,} \tag{2.33}$$

$$O = \begin{pmatrix} \cos\hat{\theta} & \pm\sin\hat{\theta} \\ -\sin\hat{\theta} & \pm\cos\hat{\theta} \\ 0 & 0 \end{pmatrix}, \quad \text{for IO mass spectrum,} \tag{2.34}$$

where $\hat{\theta} \equiv \omega - i\xi$. The O-matrix in the case of NO spectrum of interest can be decomposed as follows:[4]

$$O = \frac{e^{i\hat{\theta}}}{2}\begin{pmatrix} 0 & 0 \\ 1 & \mp i \\ i & \pm 1 \end{pmatrix} + \frac{e^{-i\hat{\theta}}}{2}\begin{pmatrix} 0 & 0 \\ 1 & \pm i \\ -i & \pm 1 \end{pmatrix} = O_+ + O_- \,. \tag{2.35}$$

The Dirac neutrino mass matrix can be presented accordingly as $M_D = M_{D+} + M_{D-}$, in a self-explanatory notation. For the elements of $M_{D+} = v\,Y_{D+}$ and $M_{D-} = v\,Y_{D-}$ we get:

$$v\,(Y_D)_{\alpha a} = v\,(Y_{D+})_{\alpha a} + v\,(Y_{D-})_{\alpha a} = v\,g^{(+)}_{\alpha a} + v\,g^{(-)}_{\alpha a}\,, \quad \alpha = e,\mu,\tau,\ a = 1,2\,, \tag{2.36}$$

where

$$v\,g^{(+)}_{\alpha 1} \simeq i\,\frac{e^{i\omega}e^{\xi}}{2\sqrt{2}}\left(\sqrt{M_1} \pm \sqrt{M_2}\right)\left(\sqrt{m_2}\,U^*_{\alpha 2} + i\,\sqrt{m_3}\,U^*_{\alpha 3}\right), \tag{2.37}$$

$$v\,g^{(+)}_{\alpha 2} \simeq i\,\frac{e^{i\omega}e^{\xi}}{2\sqrt{2}}\left(\sqrt{M_1} \mp \sqrt{M_2}\right)\left(\sqrt{m_2}\,U^*_{\alpha 2} + i\,\sqrt{m_3}\,U^*_{\alpha 3}\right), \tag{2.38}$$

$$v\,g^{(-)}_{\alpha 1} \simeq i\,\frac{e^{-i\omega}e^{-\xi}}{2\sqrt{2}}\left(\sqrt{M_1} \mp \sqrt{M_2}\right)\left(\sqrt{m_2}\,U^*_{\alpha 2} - i\,\sqrt{m_3}\,U^*_{\alpha 3}\right), \tag{2.39}$$

$$v\,g^{(-)}_{\alpha 2} \simeq i\,\frac{e^{-i\omega}e^{-\xi}}{2\sqrt{2}}\left(\sqrt{M_1} \pm \sqrt{M_2}\right)\left(\sqrt{m_2}\,U^*_{\alpha 2} - i\,\sqrt{m_3}\,U^*_{\alpha 3}\right), \tag{2.40}$$

with the abbreviation $U_{\rm PMNS} \to U$, used also in what follows. Given the fact that $(\sqrt{M_2} - \sqrt{M_1})/(\sqrt{M_2} + \sqrt{M_1}) \simeq (m_3 - m_2)/(4M) \ll 1$ and, e.g., for $M = 10$ (100) GeV, $(m_3 - m_2)/(4M) \simeq 10^{-12}$ (10^{-13}), it is clear from Eqs. (2.37) – (2.40) that for $\xi = 0$ we have (barring accidental cancellations): $|g^{(-)}_{\alpha 1}| \ll |g^{(+)}_{\beta 1}|$, $|g^{(+)}_{\alpha 2}| \ll |g^{(-)}_{\beta 2}|$, $|g^{(+)}_{\alpha 1}| \sim |g^{(-)}_{\beta 2}|$, and thus $|g_{\alpha 1}| \sim |g_{\beta 2}|$, where we have used the upper signs in the expressions for $g^{(\pm)}_{\alpha 1}$ and $g^{(\pm)}_{\beta 2}$. Unless otherwise stated we will employ this sign choice in the discussion which follows.

Taking for definiteness $\xi < 0$, it follows from Eqs. (2.37) – (2.40) that $|g^{(-)}_{\alpha a}|$ ($|g^{(+)}_{\alpha a}|$) grows (decreases) exponentially with $|\xi|$.[5] Therefore, for sufficiently large $|\xi|$ we will have

$$\frac{|g^{(+)}_{\alpha 1}|}{|g^{(-)}_{\beta 2}|} = e^{-2|\xi|}\,r_{\alpha\beta} \ll 1\,, \quad r_{\alpha\beta} \equiv \frac{\left|\sqrt{m_2}\,U^*_{\alpha 2} + i\,\sqrt{m_3}\,U^*_{\alpha 3}\right|}{\left|\sqrt{m_2}\,U^*_{\beta 2} - i\,\sqrt{m_3}\,U^*_{\beta 3}\right|}\,, \quad \alpha,\beta = e,\mu,\tau\,. \tag{2.41}$$

Using the 3σ allowed ranges of the neutrino oscillation parameters found in the global analysis of the neutrino oscillation data in Ref. [38] and given in Table 1.2 and varying the CP violation phases in the

[4] A similar decomposition exists for the IO spectrum [98].

[5] Obviously, if $\xi > 0$, $|g^{(+)}_{\alpha a}|$ ($|g^{(-)}_{\alpha a}|$) will grow (decrease) exponentially with ξ.

PMNS matrix in their defining intervals it is not difficult to show that the ratios r in Eq. (2.41) vary in the interval $r_{\alpha\beta} = (0.04 - 22.5)$.

Therefore even for the maximal cited value of $r_{\alpha\beta}$ we would have $|g^{(+)}_{\alpha 1}| \ll |g^{(-)}_{\beta 2}|$ for a sufficiently large value of $|\xi|$. At the same time the inequalities $|g^{(-)}_{\alpha 1}|/|g^{(-)}_{\beta 2}| \ll 1$ and $|g^{(+)}_{\alpha 2}|/|g^{(-)}_{\beta 2}| \ll 1$, $\alpha, \beta = e, \mu, \tau$, hold. Thus, for $\xi < 0$ and sufficiently large $|\xi|$ we get the hierarchy of Yukawa couplings: $|g_{\alpha 1}| \simeq |g^{(+)}_{\alpha 1}| \ll |g_{\beta 2}| \simeq |g^{(-)}_{\beta 2}|$. For $|\xi| = 9$, for example, we find for $r_{\alpha\beta} \simeq 1$: $|g_{\alpha 1}|/|g_{\beta 2}| \simeq |g^{(+)}_{\alpha 1}|/|g^{(-)}_{\beta 2}| \simeq 1.5 \times 10^{-8}$, which is in the range of values relevant for our discussion (see Section 2.1). We get the same hierarchy of Yukawa couplings, $|g_{\alpha 1}| \ll |g_{\beta 2}|$, $\alpha, \beta = e, \mu, \tau$, in the case of the lower signs in the expressions in Eqs. (2.37) – (2.40) for sufficiently large $\xi > 0$. In this case $|g_{\alpha 1}| \simeq |g^{(-)}_{\alpha 1}| \ll |g_{\beta 2}| \simeq |g^{(+)}_{\beta 2}|$.

We will show next that, given the present neutrino oscillation data, enforcing the flavour pattern specified in Eq. (2.26) results in preferences for a Dirac phase δ close to $\pi/4$, $3\pi/4$, $5\pi/4$, $7\pi/4$, and for a Majorana phase α close to zero.

As we have seen, the matrix of neutrino Yukawa couplings Y_D can be reconstructed up to normalization, a complex parameter, and a sign using Eqs. (2.32) and (2.35) (for NO spectrum). For the cases of interest, with sufficiently large values of $|\xi|$, necessary to ensure the requisite hierarchy of Yukawa couplings $|g_{\alpha 1}| \ll |g_{\beta 2}|$, $\alpha, \beta = e, \mu, \tau$, the ratios of (absolute values of) Yukawa couplings read:

$$R^{(1)}_{\alpha\beta} \equiv \frac{|g_{\alpha 1}|}{|g_{\beta 1}|} \simeq \frac{\left|\sqrt{m_2}\, U^*_{\alpha 2} \pm i \sqrt{m_3}\, U^*_{\alpha 3}\right|}{\left|\sqrt{m_2}\, U^*_{\beta 2} \pm i \sqrt{m_3}\, U^*_{\beta 3}\right|}\,, \tag{2.42}$$

$$R^{(2)}_{\alpha\beta} \equiv \frac{|g_{\alpha 2}|}{|g_{\beta 2}|} \simeq \frac{\left|\sqrt{m_2}\, U^*_{\alpha 2} \mp i \sqrt{m_3}\, U^*_{\alpha 3}\right|}{\left|\sqrt{m_2}\, U^*_{\beta 2} \mp i \sqrt{m_3}\, U^*_{\beta 3}\right|}\,, \tag{2.43}$$

where the upper and lower signs correspond to the case with $\xi < 0$ and upper signs in Eq. (2.35) and to the case with $\xi > 0$ and lower signs in Eq. (2.35), respectively. Recall that $|g_{\alpha 1}| \simeq |g^{(+)}_{\alpha 1}|$, $|g_{\alpha 2}| \simeq |g^{(-)}_{\alpha 2}|$ in the former case ($\xi < 0$), and $|g_{\alpha 1}| \simeq |g^{(-)}_{\alpha 1}|$, $|g_{\alpha 2}| \simeq |g^{(+)}_{\alpha 2}|$ in the latter ($\xi > 0$).

One sees that the dependence on the complex parameter $\hat{\theta}$ drops out in the ratios $R^{(1,2)}_{\alpha\beta}$, which are determined by the light neutrino masses m_2 and m_3 and by neutrino mixing parameters only, once the sign in O in Eq. (2.35) (or equivalently in Eqs. (2.37) – (2.40)) is fixed. In particular, the flavour structure depends on the elements $U_{\alpha 2}$ and $U_{\alpha 3}$ of the PMNS matrix. Given the fact that $m_2 = \sqrt{\Delta m^2_{21}}$, $m_3 = \sqrt{\Delta m^2_{31}}$, and that Δm^2_{21}, Δm^2_{31} and the three neutrino mixing angles θ_{12}, θ_{23} and θ_{13} have been determined in neutrino oscillation experiments with a rather high precision, the quantities $R^{(1)}_{\alpha\beta}$ and $R^{(2)}_{\alpha\beta}$ depend only on the CPV phases δ and α once the sign of ξ is fixed. This means that knowing any two of the ratios $|g_{\alpha 1}|/|g_{\beta 1}|$ or $|g_{\alpha 2}|/|g_{\beta 2}|$, $\alpha \neq \beta = e, \mu, \tau$ allows to determine both phases δ and α.

In Figs. 2.1 and 2.2 we present the ratios $R^{(1,2)}_{\alpha\beta}$ as a function of δ for the case $\xi < 0$ and two representative values of the Majorana phase α. Figure 2.1 is obtained using the best-fit values of $\Delta m^2_{21,31}$ and $\sin^2\theta_{ij}$ taken from Table 1.2. In Fig. 2.2 we show the ranges in which $R^{(1,2)}_{\alpha\beta}$ vary when $\Delta m^2_{21,31}$ and the $\sin^2\theta_{ij}$ are varied in their respective 3σ allowed intervals given in Table 1.2. In Table 2.2 we report the respective intervals in which each of the six ratios can lie. As Table 2.2 indicates, certain specific simple patterns cannot be realised within the scheme considered. Among those are, for example, the patterns $|g_{e1}| : |g_{\mu 1}| : |g_{\tau 1}| \simeq 1 : 1 : 1$ and $|g_{e2}| : |g_{\mu 2}| : |g_{\tau 2}| \simeq 1 : 1 : 1$.

The flavour structure of Eq. (2.26), which is naturally realised in the model of Section 2.2, corresponds

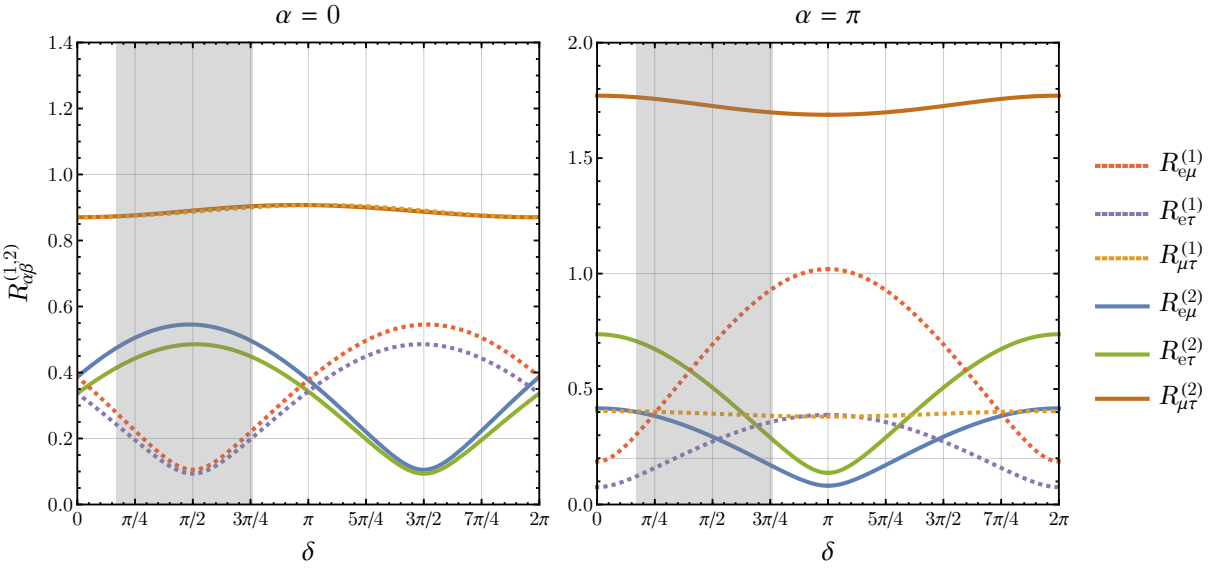

Figure 2.1: Ratios $R^{(1,2)}_{\alpha\beta}$ of (absolute values of) Yukawa couplings for a NO neutrino spectrum as a function of the Dirac phase δ for a Majorana phase $\alpha = 0$ (left panel) and $\alpha = \pi$ (right panel), in the case $\xi < 0$. The figure is obtained using the best-fit values of $\Delta m^2_{21,31}$ and $\sin^2\theta_{ij}$ quoted in Table 1.2. The vertical grey band indicates values of δ which are disfavoured at 3σ. The case $\xi > 0$ is obtained by exchanging $R^{(1)}_{\alpha\beta}$ and $R^{(2)}_{\alpha\beta}$.

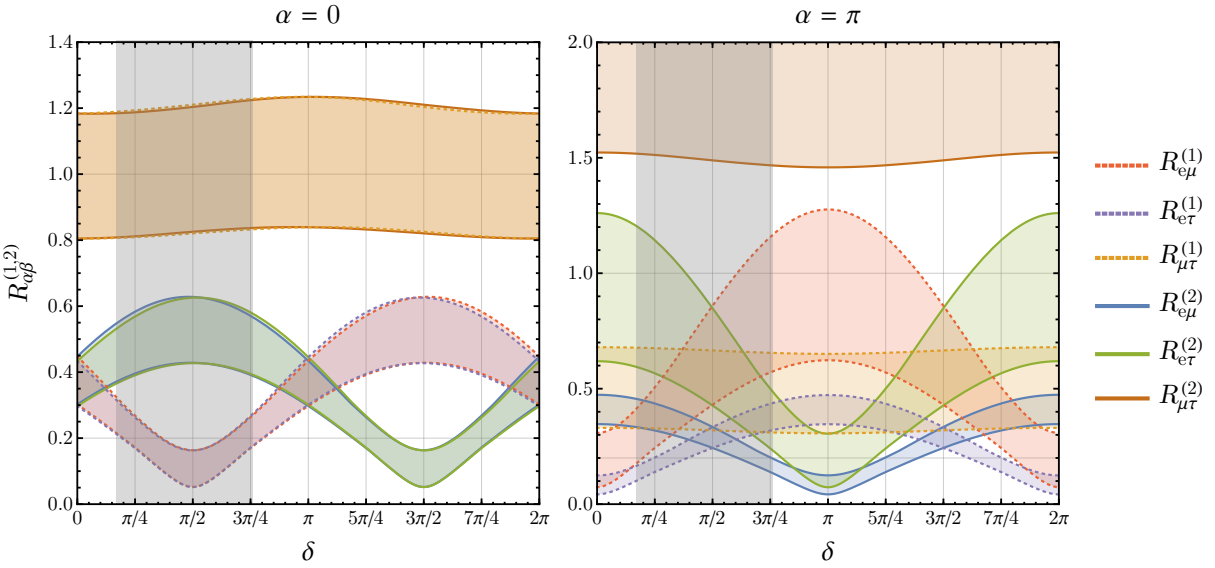

Figure 2.2: Ratios $R^{(1,2)}_{\alpha\beta}$ of (absolute values of) Yukawa couplings for a NO neutrino spectrum as a function of the Dirac phase δ for a Majorana phase $\alpha = 0$ (left panel) and $\alpha = \pi$ (right panel), in the case $\xi < 0$. Bands are obtained by varying $\Delta m^2_{21,31}$ and the $\sin^2\theta_{ij}$ in their respective 3σ allowed ranges given in Table 1.2. In the case $\alpha = \pi$, the upper boundary of the $R^{(2)}_{\mu\tau}$ band (not shown) is located at $R^{(2)}_{\mu\tau} \simeq 3.0 - 3.2$. The vertical grey band indicates values of δ which are disfavoured at 3σ. The case $\xi > 0$ is obtained by exchanging $R^{(1)}_{\alpha\beta}$ and $R^{(2)}_{\alpha\beta}$.

Ratio	Allowed range
$R^{(1)}_{e\mu}$	$0.05 - 1.28$
$R^{(1)}_{e\tau}$	$0.04 - 0.63$
$R^{(1)}_{\mu\tau}$	$0.31 - 1.23$
$R^{(2)}_{e\mu}$	$0.04 - 0.63$
$R^{(2)}_{e\tau}$	$0.05 - 1.26$
$R^{(2)}_{\mu\tau}$	$0.80 - 3.21$

Table 2.2: Ranges for the ratios of absolute values of Yukawa couplings, obtained by varying $\Delta m^2_{21,31}$, the $\sin^2\theta_{ij}$, and δ in their respective 3σ allowed ranges and α in its defining range, for $\xi < 0$. The case $\xi > 0$ is obtained by exchanging $R^{(1)}_{\alpha\beta}$ and $R^{(2)}_{\alpha\beta}$.

to the pattern $|g_{e2}| : |g_{\mu 2}| : |g_{\tau 2}| \simeq \epsilon : 1 : 1$, and thus to $R^{(2)}_{e\mu} \simeq R^{(2)}_{e\tau} \simeq \epsilon$ and $R^{(2)}_{\mu\tau} \simeq 1$. The requirement of having $R^{(2)}_{\mu\tau} \simeq 1$ favours α close to zero.[6] As can be inferred from Fig. 2.1, given the best-fit values of neutrino mass-squared differences and mixing parameters, the requirement of $R^{(2)}_{e\mu} \simeq R^{(2)}_{e\tau} \simeq \epsilon = 0.2$ leads, for $\xi < 0$, to the prediction of $\delta \simeq 5\pi/4,\, 7\pi/4$.[7] Taking into account the 3σ allowed ranges of $\Delta m^2_{21,31}$ and $\sin^2\theta_{ij}$ leads, as Fig. 2.2 shows, to δ lying in narrow intervals around the values $5\pi/4$ and $7\pi/4$, if $\alpha \simeq 0$. Allowing for a somewhat smaller value of ϵ, e.g., $\epsilon = 0.15$, we find that δ should lie in the interval $\delta \simeq [5\pi/4,\, 7\pi/4]$ which includes the value $3\pi/2$ (see Fig. 2.2).

For $\delta \simeq 5\pi/4,\, 7\pi/4$, $\alpha = 0$ and the best-fit values of $\Delta m^2_{21,31}$ and of the $\sin^2\theta_{ij}$ we get the following pattern of the Yukawa couplings of ν_{1R}: $|g_{e1}| : |g_{\mu 1}| : |g_{\tau 1}| \sim 0.5 : 1 : 1$.

For $\xi > 0$, using the same arguments we obtain instead $\delta \simeq \pi/4, 3\pi/4$, or $\delta \simeq [\pi/4, 3\pi/4]$. According to global analyses, however, these values of δ are strongly disfavoured by data.

In a more phenomenological approach, we get $\delta \simeq 3\pi/2$ provided, e.g., $|g_{e2}| : |g_{\mu 2}| : |g_{\tau 2}| \simeq 0.14 : 1 : 1$ and $\alpha \simeq \pi/5$. In this case, the remaining ratios read $|g_{e1}| : |g_{\mu 1}| : |g_{\tau 1}| \simeq 0.5 : 0.7 : 1$. In the GUT-inspired scenario of Ref. [115], a different FN charge assignment leads to $\epsilon = 0.06$, in which case $\delta \simeq 3\pi/2$ is favoured.

2.5 Phenomenology

The low-energy phenomenology of the model of interest resembles that of the model with two heavy Majorana neutrinos $N_{1,2}$ forming a pseudo-Dirac pair considered in [97–99], in which the splitting between the masses of $N_{1,2}$ is exceedingly small. For this model, direct and indirect constraints on the model parameters, which do not depend on the splitting between the masses of N_1 and N_2, as well as expected sensitivities of future lepton colliders have been analysed, e.g., in Refs. [97–99,116,117] (see also [118–120]).

Due to the mixing of LH and RH neutrino fields, i) the PMNS neutrino mixing matrix, as we have already noted, is not unitary, as also the expressions for the charged and neutral current weak interaction

[6] Marginalizing over δ (either in its defining or in its 3σ range) and varying $\Delta m^2_{21,31}$ and the $\sin^2\theta_{ij}$ in their respective 3σ allowed ranges, the requirement that $|R^{(2)}_{\mu\tau} - 1| < 0.1$ implies $\alpha < 0.36\pi \vee \alpha > 1.64\pi$, independently of the sign of ξ. However, if we require that the relative probability of α having a given value in the indicated intervals is not less than 0.15, then we have $\alpha < 0.2\pi$ or $\alpha > 1.8\pi$. For these values of α and $\epsilon = 0.2$, the predictions for δ can be read off from the plots where $\alpha = 0$.

[7] Similar predictions for CPV phases δ and α were obtained in a different context in Ref. [114].

of the light Majorana neutrinos ν_i given in Eqs. (2.29) and (2.30) show, and ii) the heavy Majorana neutrinos $N_{1,2}$ also participate in charged and neutral current weak interactions with the $W^{\pm}$ and Z^0 bosons:

$$\mathcal{L}^{N}_{\rm CC} \;=\; -\frac{g}{\sqrt{2}}\,\overline{\ell_{\alpha L}}\,\gamma_\mu\,\left(RV\right)_{\alpha k}\,N_{kL}\,W^{\mu} \;+\; \text{h.c.}\,, \tag{2.44}$$

$$\mathcal{L}^{N}_{\rm NC} \;=\; -\frac{g}{2c_w}\,\overline{\nu_{\alpha L}}\,\gamma_\mu\,\left(RV\right)_{\alpha k}\,N_{kL}\,Z^{\mu} \;+\; \text{h.c.}\,. \tag{2.45}$$

Due to the Yukawa interactions, see Eq. (2.2), there are interactions of the heavy Majorana neutrinos $N_{1,2}$ with the SM Higgs boson h as well (see [100]):

$$\mathcal{L}^{N}_{\rm H} \;=\; -\,\frac{M_k}{v}\,\overline{\nu_{\alpha L}}\,\left(RV\right)_{\alpha k}\,N_{kR}\,h \;+\; \text{h.c.}\,. \tag{2.46}$$

2.5.1 Neutrino Mass Matrix and Non-unitarity Bounds

The first constraint on the RV elements follows from the fact that the elements of the light neutrino Majorana mass matrix, $(M_\nu)_{\alpha\beta}$, have rather small maximal values. Indeed, as follows from Eq. (2.7), we have [97]:

$$|(M_\nu)_{\alpha\beta}| = |U^{*}_{\alpha j}\,m_j\,U^{*}_{\beta j}| \simeq \left|\sum_a (RV)^{*}_{\alpha a}\,M_a\,(RV)^{*}_{\beta a}\right|\,,\;\alpha,\beta = e,\mu,\tau\,, \tag{2.47}$$

where the sum is effectively over $j = 2, 3$ since in the model considered $m_1 = 0$.[8] The elements of the neutrino Majorana mass matrix depend, apart from $m_2 = \sqrt{\Delta m^2_{21}} \simeq 8.6 \times 10^{-3}$ eV, $m_3 = \sqrt{\Delta m^2_{31}} \simeq 0.051$ eV, θ_{12}, θ_{23}, θ_{13}, on the CPV phases δ and α. The maximal value a given element of M_ν can have depends on its flavour indices. It is not difficult to derive these maximal values using the results reported in Table 1.2. We have:

i) $|(M_\nu)_{ee}| \lesssim 4.3 \times 10^{-3}$ eV ($\alpha + 2\delta = 0$);

ii) $|(M_\nu)_{e\mu}| \lesssim 9.2 \times 10^{-3}$ eV ($\delta = \pi$, $\alpha = \pi$);

iii) $|(M_\nu)_{e\tau}| \lesssim 9.2 \times 10^{-3}$ eV ($\delta = 0$, $\alpha = \pi$);

iv) $|(M_\nu)_{\mu\mu}| \lesssim 3.4 \times 10^{-2}$ eV ($\delta = \pi$, $\alpha = 0$);

v) $|(M_\nu)_{\mu\tau}| \lesssim 2.9 \times 10^{-2}$ eV ($\delta = 3\pi/2$, $\alpha = \pi$);

vi) $|(M_\nu)_{\tau\tau}| \lesssim 3.5 \times 10^{-2}$ eV ($\delta = 0$, $\alpha = 0$).

The quoted maximal values are reached for the values of the CPV phases given in the brackets. It should be added that the dependence of $\max(|(M_\nu)_{\alpha\beta}|)$, $\alpha,\beta = \mu,\tau$, on CPV phases is rather weak since the terms involving δ always include the suppressing factor $\sin\theta_{13}$, while the term $\propto m_2$ is considerably smaller (typically by a factor of 10) than the term $\propto m_3$, as $m_2/m_3 \simeq 0.17$. We will consider $|(M_\nu)_{ee}| \lesssim 4 \times 10^{-3}$ eV, $|(M_\nu)_{e\mu}|, |(M_\nu)_{e\tau}| \lesssim 9 \times 10^{-3}$ eV, and $|(M_\nu)_{\alpha\beta}| \lesssim 3 \times 10^{-2}$ eV, $\alpha,\beta = \mu,\tau$, as reference maximal values in the numerical analysis which follows.

[8] Strictly speaking, we have $m_1 = 0$ only at tree level. Higher order corrections lead to a non-zero value of m_1, which is however negligibly small.

From the expression for RV given in Eq. (2.24) and Eq. (2.47), and taking into account the mass splitting between N_1 and N_2, we get to leading order in $|g_{\alpha 1}|$, $|g_{\beta 2}|$ and $|g_{\alpha 1} g_{\beta 2}|$:

$$|(M_\nu)_{\alpha\beta}| \simeq \frac{v^2}{M} |g_{\alpha 1} g_{\beta 2} + g_{\alpha 2} g_{\beta 1}| + \mathcal{O}(g_{\alpha 1} g_{\beta 1}) , \tag{2.48}$$

which coincides (up to higher order corrections) with the form given in Eq. (2.12). Thus, for a given value of M, the upper bounds on $|(M_\nu)_{\alpha\beta}|$ lead via Eq. (2.47) to upper bounds on the magnitude of the product of the neutrino Yukawa couplings of ν_{1R} and ν_{2R}, $g_{\alpha 1}$ and $g_{\beta 2}$. As we have seen, these bounds depend on the flavour of the lepton doublet to which ν_{1R} and ν_{2R} are coupled.

For $M = 100$ GeV (1 TeV), for example, the constraint of interest $|(M_\nu)_{ee}| \lesssim 4 \times 10^{-3}$ eV implies $2|g_{e1} g_{e2}| \lesssim 1.3 \times 10^{-14}$ (1.3×10^{-13}). This upper limit can be satisfied for, e.g., $|g_{e1}| \sim 0.65 \times 10^{-12}$ (0.65×10^{-11}) and $|g_{e2}| \sim 10^{-2}$. The upper bounds on $|g_{e1} g_{\alpha 2} + g_{\alpha 1} g_{e2}|$, $\alpha = \mu, \tau$, are approximately by a factor of 2 larger than the quoted upper bound on $2|g_{e1} g_{e2}|$, while those on $|g_{\alpha 1} g_{\beta 2} + g_{\alpha 2} g_{\beta 1}|$, $\alpha, \beta = \mu, \tau$ are larger approximately by a factor of 8.

In Refs. [97, 98] the constraint in Eq. (2.47) is satisfied by finding a region, in the general parameter space of the model considered, in which to leading order $\sum_{a=1,2} (RV)^*_{\alpha a} M_a (RV)^*_{\beta a} = 0$, i.e., the two terms in the sum cancel. In the version of the low-scale type I seesaw model with two RH neutrinos we are considering the constraint in Eq. (2.47) is satisfied due to smallness of the product of Yukawa couplings $|g_{\alpha 1}|$ and $|g_{\beta 2}|$. In the model under consideration one gets $\sum_{a=1,2} (RV)^*_{\alpha a} M_a (RV)^*_{\beta a} = 0$ in the limit of negligible couplings $g_{\alpha 1}$. Indeed, setting $g_{\alpha 1} = 0$ we get $M_1 = M_2$ and the expression for the matrix RV takes the form:

$$RV = \frac{1}{\sqrt{2}} \frac{v}{M} \begin{pmatrix} g^*_{e2} & -i\, g^*_{e2} \\ g^*_{\mu 2} & -i\, g^*_{\mu 2} \\ g^*_{\tau 2} & -i\, g^*_{\tau 2} \end{pmatrix} . \tag{2.49}$$

This implies

$$(RV)_{\alpha 1} = -i\, (RV)_{\alpha 2} , \quad \alpha = e, \mu, \tau , \tag{2.50}$$

which together with the equality $M_1 = M_2$ leads to $\sum_{a=1,2} (RV)^*_{\alpha a} M_a (RV)^*_{\beta a} = 0$.

As we have already discussed, the matrix $\eta \equiv -R\, R^\dagger/2 = -(RV)\, (RV)^\dagger/2 = \eta^\dagger$ parametrises the deviations from unitary of the PMNS matrix. The elements of η are constrained by precision electroweak data and data on flavour observables. For heavy Majorana neutrino masses above the electroweak scale the most updated set of constraints on the absolute values of the elements of η at 2σ C.L. reads [121,122]:

$$|\eta| < \begin{pmatrix} 1.3 \times 10^{-3} & 1.2 \times 10^{-5} & 1.4 \times 10^{-3} \\ 1.2 \times 10^{-5} & 2.2 \times 10^{-4} & 6.0 \times 10^{-4} \\ 1.4 \times 10^{-3} & 6.0 \times 10^{-4} & 2.8 \times 10^{-3} \end{pmatrix} . \tag{2.51}$$

The upper bound on the $e-\mu$ elements is relaxed to $|\eta_{e\mu}| < 3.4 \times 10^{-4}$ for heavy Majorana neutrino masses below the electroweak scale (but still above the kaon mass, $M_k \gtrsim 500$ MeV) due to the restoration of a GIM cancellation [123]. The above constraints on η justify the assumption made in Section 2.1 regarding the smallness of the elements of R.

Using the expression for RV given in Eq. (2.24) we find that, to leading order in $g_{\alpha 1}$, $g_{\beta 2}$, $|g_{\alpha 1}| \ll |g_{\beta 2}|$, we have:

$$|\eta_{\alpha\beta}| \simeq \frac{1}{2} \frac{v^2}{M^2} |g_{\alpha 2}\, g_{\beta 2}| + \mathcal{O}(g_{\alpha 1}\, g_{\beta 2}, g_{\beta 1}\, g_{\alpha 2}) . \tag{2.52}$$

As a consequence, if M is given, the experimental limits on $|\eta|$ cited in Eq. (2.51), in contrast to the limits on $|(M_\nu)_{\alpha\beta}|$, imply upper bounds on $|g_{\alpha 2}\, g_{\beta 2}|$, i.e., on the Yukawa couplings of ν_{2R}. For, e.g., $M = 100$ GeV we find, depending on the flavour indices, $|g_{\alpha 2}\, g_{\beta 2}|^{1/2} \lesssim (2.8 \times 10^{-3} - 4.3 \times 10^{-2})$, i.e., $|g_{\alpha 2}|$ can be relatively large. This can lead to interesting low-energy phenomenology involving the heavy Majorana neutrinos $N_{1,2}$.

2.5.2 LFV Observables and Higgs Decays

The predictions of the model under discussion for the rates of the lepton flavour violating (LFV) $\mu \to e\gamma$ and $\mu \to eee$ decays and $\mu - e$ conversion in nuclei, as can be shown, depend on $|(RV)^*_{\mu 1}(RV)_{e1} + (RV)^*_{\mu 2}(RV)_{e2}|^2 \simeq 4\,|(RV)^*_{\mu 2}(RV)_{e2}|^2$, where we have used Eq. (2.50), and on the masses $M_1 \simeq M_2 \simeq M$ of the heavy Majorana neutrinos N_1 and N_2. The expressions for the $\mu \to e\gamma$ and $\mu \to eee$ decay branching ratios, $\mathrm{BR}(\mu \to e\gamma)$ and $\mathrm{BR}(\mu \to eee)$, and for the relative $\mu - e$ conversion in a nucleus X, $\mathrm{CR}(\mu X \to eX)$, coincide with those given in Refs. [98,99]. The best experimental limits on $\mathrm{BR}(\mu \to e\gamma)$, $\mathrm{BR}(\mu \to eee)$ and $\mathrm{CR}(\mu X \to eX)$ have been obtained by the MEG [124], SINDRUM [125] and SINDRUM II [126,127] collaborations:

$$\mathrm{BR}(\mu \to e\gamma) \;<\; 4.2 \times 10^{-13}\ (90\%\ \mathrm{C.L.})\,, \tag{2.53}$$

$$\mathrm{BR}(\mu \to eee) \;<\; 1.0 \times 10^{-12}\ (90\%\ \mathrm{C.L.})\,, \tag{2.54}$$

$$\mathrm{CR}(\mu\,\mathrm{Ti} \to e\,\mathrm{Ti}) \;<\; 4.3 \times 10^{-12}\ (90\%\ \mathrm{C.L.})\,, \tag{2.55}$$

$$\mathrm{CR}(\mu\,\mathrm{Au} \to e\,\mathrm{Au}) \;<\; 7 \times 10^{-13}\ (90\%\ \mathrm{C.L.})\,. \tag{2.56}$$

The planned MEG II update of the MEG experiment [128] is expected to reach sensitivity to $\mathrm{BR}(\mu \to e\gamma) \simeq 4 \times 10^{-14}$. The sensitivity to $\mathrm{BR}(\mu \to eee)$ is expected to experience a dramatic increase of up to four orders of magnitude with the realisation of the Mu3e Project [129], which aims at probing values down to $\mathrm{BR}(\mu \to eee) \sim 10^{-16}$ in its phase II of operation. Using an aluminium target, the Mu2e [130] and COMET [131] collaborations plan to ultimately be sensitive to $\mathrm{CR}(\mu\,\mathrm{Al} \to e\,\mathrm{Al}) \sim 6 \times 10^{-17}$. The PRISM/PRIME project [132] aims at an impressive increase of sensitivity to the $\mu - e$ conversion rate in titanium, planning to probe values down to $\mathrm{CR}(\mu\,\mathrm{Ti} \to e\,\mathrm{Ti}) \sim 10^{-18}$, an improvement of six orders of magnitude with respect to the bound of Eq. (2.55).

We show in Fig. 2.3 the limits on $|g_{\mu 2}\, g_{e2}|$ implied by the experimental bounds in Eqs. (2.53) – (2.56), as a function of the mass M, as well as the prospective sensitivity of the future planned experiments MEG II, Mu3e, Mu2e, COMET and PRISM/PRIME. The data from these experiments, as Fig. 2.3 indicates, will allow to test for values of $|g_{\mu 2}\, g_{e2}|$ quite smaller than the existing limits, with a significant potential for a discovery.

For reference, the most stringent bounds on the branching ratios for the LFV processes $\tau \to e\gamma$, $\tau \to \mu\gamma$ and $\tau \to \mu\mu\mu$ at present are obtained by the BaBar [133] and Belle [134] collaborations, respectively:

$$\mathrm{BR}(\tau \to e\gamma) < 3.3 \times 10^{-8}\ (90\%\ \mathrm{C.L.})\,, \tag{2.57}$$

$$\mathrm{BR}(\tau \to \mu\gamma) < 4.4 \times 10^{-8}\ (90\%\ \mathrm{C.L.})\,, \tag{2.58}$$

$$\mathrm{BR}(\tau \to \mu\mu\mu) < 2.1 \times 10^{-8}\ (90\%\ \mathrm{C.L.})\,. \tag{2.59}$$

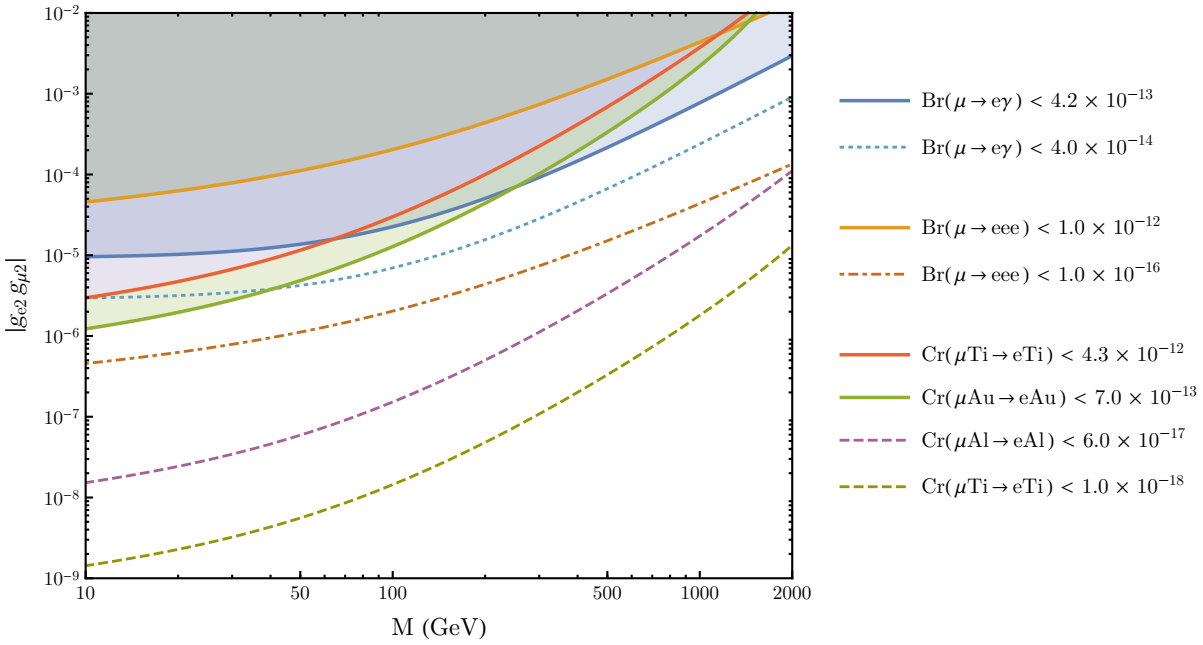

Figure 2.3: Present limits (solid lines) and expected future sensitivities (dotted, dashed and dot-dashed lines) on $|g_{\mu 2}||g_{e2}|$ from data on muon LFV processes, as a function of the mass M of heavy Majorana neutrinos.

Even taking into account the prospective sensitivity of next generation experiments, non-unitarity considerations dominate the constraints on $|g_{e2}g_{\tau 2}|$ and $|g_{\mu 2}g_{\tau 2}|$.

The interactions given in Eq. (2.46) open up novel decay channels for the Higgs boson, provided the masses of the heavy neutrinos $N_{1,2}$ are below the Higgs boson mass, m_h. For $M_{1,2} < m_h \simeq 125.1\,\text{GeV}$, the new Higgs decay modes are those into one light and one heavy neutrino, $h \to \nu_{\alpha L}\, N_k$, $\alpha = e, \mu, \tau$, $k = 1, 2$. The phenomenology of the Higgs decays $h \to \nu_{\alpha L}\, N_k$ in the model considered in this chapter is similar to that of the same decay investigated in detail in Ref. [100] in the model discussed in Ref. [98]. The rate of the decay $h \to \nu_{\alpha L}\, N_{1,2}$ to any $\nu_{\alpha L}$ and N_1 or N_2 is given in Ref. [100] and in the limit of zero mass splitting of $N_{1,2}$ ($M_1 = M_2 = M$) reads:

$$\Gamma(h \to \nu\, N) \;=\; \frac{m_h}{16\pi}\left(1 - \frac{M^2}{m_h^2}\right)^2 \frac{M^2}{v^2} \sum_{\alpha,k} \left|\left(RV\right)_{\alpha k}\right|^2 , \tag{2.60}$$

where in the model considered by us

$$\frac{M^2}{v^2} \sum_{\alpha,k} \left|\left(RV\right)_{\alpha k}\right|^2 \simeq |g_{e2}|^2 + |g_{\mu 2}|^2 + |g_{\tau 2}|^2 , \tag{2.61}$$

and we have used Eqs. (2.49) and (2.50). The dominant decay mode of the SM Higgs boson is into bottom quark-antiquark pair, $b - \bar{b}$. The decay rate is given by:

$$\Gamma(h \to b\,\bar{b}) = \frac{3 m_h}{16\pi}\left(\frac{m_b}{v}\right)^2 \left(1 - \frac{4m_b^2}{m_h^2}\right)^{3/2} , \tag{2.62}$$

$m_b \simeq 4.18$ GeV being the b quark mass (in the $\overline{\text{MS}}$ scheme). The SM branching ratio of this decay is 58.4% [135]. The formula for $\Gamma(h \to b\bar{b})$ offers an interesting parallel with the one for $\Gamma(h \to \nu N)$.

Namely, they are structurally identical save for the exponents 2 and 3/2, a difference which has its origin in the phase space integration. The total SM decay width of the Higgs boson is rather small [135]: $\Gamma^{\rm SM}_{\rm tot} \simeq 4.07 \times 10^{-3}$ GeV.

The upper bound on $(\sum_\alpha |g_{\alpha 2}|^2)$ is determined essentially by the upper bound on $|g_{\tau 2}|^2 = 2|\eta_{\tau\tau}|M^2/v^2$, which is less stringent than the upper bounds on $|g_{e2}|^2$ and $|g_{\mu 2}|^2$. Using the bound $|\eta_{\tau\tau}| < 2.8 \times 10^{-3}$ quoted in Eq. (2.51), we get for $M = 100$ GeV the upper bound $|g_{\tau 2}|^2 < 1.8 \times 10^{-3}$. For the Higgs decay rate $\Gamma(h \to \nu N)$ in the case of $M = 100$ GeV and, e.g., $(\sum_\alpha |g_{\alpha 2}|^2) = 10^{-3}$, we get $\Gamma(h \to \nu N) = 3.2 \times 10^{-4}$ GeV. This decay rate would lead to an increase of the total SM decay width of the Higgs boson by approximately 8%. Thus, the presence of the $h \to \nu N$ decay would modify the SM prediction for the branching ratio for any generic (allowed in the SM) decay of the Higgs particle [100], decreasing it.

We briefly comment on neutrinoless double beta decay. The relevant observable is the absolute value of the effective neutrino Majorana mass $|\langle m \rangle|$ (see, e.g., [136]), which receives an extra contribution from the exchange of heavy Majorana neutrinos N_1 and N_2. This contribution should be added to the one due to light Majorana neutrino exchange [137,138] (see also [97,139]). The sum of the two contributions can lead, in principle, to $|\langle m \rangle|$ that differs significantly from the one due to light Majorana neutrino exchange. The contribution due to the $N_{1,2}$ exchange in $|\langle m \rangle|$ in the model considered is proportional, in particular, to the difference between the masses of N_1 and N_2, which form a pseudo-Dirac pair. For $M \gtrsim 1$ GeV, as can be shown, it is strongly suppressed in the present setup due to the extremely small $N_{1,2}$ mass difference, the stringent upper limit on $|g_{e2}|^2$, and the values of the relevant nuclear matrix elements (NME), which at $M = 1$ GeV are smaller approximately by a factor of 6×10^{-2} than the NME for the light neutrino exchange and scale with M as $(0.9\ \text{GeV}/M)^2$. As a consequence, the contribution to $|\langle m \rangle|$ due to the exchange of N_1 and N_2 is significantly smaller than the contribution from the exchange of light Majorana neutrinos ν_i. Thus, the analysis of the standard $(\beta\beta)_{0\nu}$-decay rate performed in the following chapter of this thesis is applicable to the case at hand.

2.6 Leptogenesis

Finally, we discuss the issue of leptogenesis. For temperatures above the electroweak phase transition (EWPT), the Higgs VEV vanishes and thus, in the considered setup, the splitting between the masses of heavy neutrinos originates from the (suppressed) Majorana mass term $\mu\, \nu_{1R}^T\, C^{-1}\, \nu_{1R}$, with $\mu \sim \epsilon^{n+1} M \sim |g_{\alpha 1}| M$. This component of the heavy neutrino mass matrix – which in our case presents a subleading contribution to neutrino masses – is then crucial for resonant leptogenesis to proceed (see, e.g., [140]). The resonant condition reads $\mu \simeq \Gamma/2$, where Γ denotes the average heavy neutrino decay width. However, the values of μ, Γ and neutrino masses are tightly connected in the FN model we analyse, which, together with the required smallness of μ, prevents reproducing the observed baryon asymmetry of the Universe (BAU), $\eta_B^{\rm obs} \simeq (6.09 \pm 0.06) \times 10^{-10}$ [141].

One may instead successfully generate the observed BAU through the mechanism of anti-leptogenesis [142] (also known as "neutrino-assisted GUT baryogenesis"). In this case, an excess of both baryon

number B and lepton number $\hat{L}$ (see Section 2.2) is produced at a high energy scale ($T > 10^{12}$ GeV, possibly related to grand unification), while conserving $B - \hat{L}$. If there are new $\hat{L}$-violating interactions in thermal equilibrium at such high temperature, they may erase the lepton number excess while leaving the baryon number excess untouched, since sphalerons are not efficient at these times. At later times, sphalerons are responsible for only a partial conversion of the baryon number excess into a lepton number excess, while some of the baryon excess remains.

Unlike resonant leptogenesis, the anti-leptogenesis mechanism relies on a suppression of the $\hat{L}$-violating heavy neutrino mass splitting above the EWPT, in order not to wash-out the asymmetry generated at a high scale. Modifying our setup as detailed in the end of Section 2.2, the Majorana mass term $\mu\, \nu_{1R}^T\, C^{-1}\, \nu_{1R}$ is forbidden and the heavy neutrinos are degenerate above the EWPT. One then adds a third RH neutrino in the bulk with $(B-\hat{L})(\nu_{3R}) = -1$ and vanishing $\mathrm{U}(1)_L$ charge, such that its Yukawa couplings, which violate lepton number, are allowed, and such that the mass term $M_3\, \nu_{3R}^T\, C^{-1}\, \nu_{3R}$ is generated, $M_3 \sim \langle\Phi\rangle$. Notice that only one such RH neutrino is needed to erase lepton number at high temperatures ($M_3 \sim (10^{12} - 10^{13})$ GeV), and that there is a large region of parameter space where the new contribution to the neutrino mass matrix is negligible [143]. Given these conditions, successful (anti-)leptogenesis may proceed.

2.7 Chapter Summary

In the present chapter we have explored a symmetry-protected scenario of neutrino mass generation, where two RH neutrinos are added to the SM. In the class of models considered, the main source of L-violation responsible for the neutrino masses are small lepton-charge violating Yukawa couplings $g_{\alpha 1}$ ($\alpha = e, \mu, \tau$) to one of the RH neutrinos, ν_{1R}. Thus, the smallness of the light Majorana neutrino masses is related to the smallness of the $g_{\alpha 1}$ and not to the RH neutrinos having large Majorana masses in the range of $\sim (10^{10} - 10^{14})$ GeV as in the standard seesaw scenario. We have considered heavy Majorana neutrinos forming a pseudo-Dirac pair with masses $M_{1,2} \simeq M$ at the TeV or lower scale, which are potentially observable in collider experiments.

The setup described above can be realised in a Froggatt-Nielsen (FN) scheme, as detailed in Section 2.2. In such a model, no $\mathrm{U}(1)_L$ symmetry is imposed, and instead the suppression of L-violating operators arises in the limit of a large FN charge for ν_{1R}, which mimics lepton number conservation. The FN charge assignments are partly motivated by large $\nu_\mu - \nu_\tau$ mixing. The structure of the Yukawa couplings $g_{\alpha a}$ ($a = 1, 2$) is then determined by the FN charges, and yields $|g_{e2}| : |g_{\mu 2}| : |g_{\tau 2}| \simeq \epsilon : 1 : 1$, where $\epsilon \simeq \lambda_C \simeq 0.2$ is the FN suppression parameter, while no unambiguous prediction may be extracted for the ratios $|g_{e1}| : |g_{\mu 1}| : |g_{\tau 1}|$.

It is interesting to point out that, given the exceedingly small splitting between heavy neutrinos, the dependence on the Casas-Ibarra complex parameter drops out in the ratios between absolute values of Yukawa couplings to the same RH neutrino. These ratios are then determined (up to the exchange of $g_{\alpha 1}$ and $g_{\alpha 2}$) by neutrino low-energy parameters alone, namely, by neutrino masses, mixing angles and CPV phases δ and α. Given the Yukawa structure of our model, $|g_{e2}| : |g_{\mu 2}| : |g_{\tau 2}| \simeq \epsilon : 1 : 1$ with

$\epsilon \simeq \lambda_C \simeq 0.2$, the Dirac CPV phase δ is predicted to have approximately one of the values $\delta \simeq \pi/4$, $3\pi/4$, or $5\pi/4$, $7\pi/4$, or to lie in an interval around one of these values, while a Majorana CPV phase $\alpha \simeq 0$ is preferred (Figs. 2.1 and 2.2).

In the considered scenario, the maximal values of the elements of the neutrino mass matrix lead to constraints on the combinations $|g_{\alpha 1} g_{\beta 2} + g_{\beta 1} g_{\alpha 2}|$, $\alpha, \beta = e, \mu, \tau$, which depend on products of L-conserving and L-violating Yukawa couplings (see Section 2.5.1). Deviations from unitarity of the PMNS matrix constrain instead the products $|g_{\alpha 2} g_{\beta 2}|$ of L-conserving couplings alone. In particular, the product $|g_{\mu 2} g_{e 2}|$ is constrained by data on muon lepton flavour violating (LFV) processes. Data from future LFV experiments (MEG II, Mu3e, Mu2e, COMET, PRISM/PRIME) will allow to probe values of $|g_{\mu 2}\, g_{e 2}|$ significantly smaller than the existing limits (Fig. 2.3). The decay of the Higgs boson into one light and one heavy neutrino can have a rate $\Gamma(h \to \nu N)$ as large as 8% of the total SM Higgs decay width. This decay mode can lead to a change of the Higgs branching ratios with respect to the SM predictions. Concerning neutrinoless double beta decay in the considered model, the contribution due to $N_{1,2}$ exchange is found to be negligible when compared to the contribution from the exchange of light Majorana neutrinos, which is the subject of the following chapter.

3 Neutrinoless Double Beta Decay

Observations of flavour oscillations in experiments with solar, atmospheric, reactor, and accelerator neutrinos imply both non-trivial mixing in the leptonic sector and above-meV masses for at least two of the light neutrinos. However, as noted, neutrino oscillations are blind to the absolute scale of neutrino masses and to the nature – Dirac or Majorana – of massive neutrinos. The observation of neutrinoless double beta decay would instead allow to establish lepton number violation and the Majorana nature of neutrinos. The rate of this process in the case of 3-neutrino mixing is controlled by the neutrinoless double beta decay effective Majorana mass $|\langle m \rangle|$.

In the present chapter, following Ref. [144] and taking into account up-to-date neutrino oscillation data (see Fig. 1.2 and Table 1.3), we give the conditions under which the effective Majorana mass in the case of 3-neutrino mixing exceeds the millielectronvolt value. We consider both the generic case, where Majorana and Dirac CPV phases are unconstrained, as well as a set of cases in which these phases take particular values, motivated by predictive schemes combining generalised CP and flavour symmetries. Our study is a natural continuation of the one performed in Ref. [145].

3.1 Description and Half-lives

In order to uncover the possible Majorana nature of neutrinos, searches for the lepton-number violating process of neutrinoless double beta are underway (for recent reviews, see e.g. [146, 147]). This decay corresponds to a transition between the isobars (A, Z) and $(A, Z+2)$, accompanied by the emission of two electrons but – unlike usual double beta decay – without the emission of two (anti)neutrinos, see Figure 3.1a. If observed, neutrinos are of Majorana nature as a consequence of the "black-box" theorem [148]: whatever is the process generating $(\beta\beta)_{0\nu}$-decay, it invariably contributes to the neutrino Majorana mass matrix, see Figure 3.1b.[1]

A potential observation of $(\beta\beta)_{0\nu}$-decay is feasible, in principle, whenever single beta decay is energetically forbidden, as is the case for certain even-even nuclei. The searches for $(\beta\beta)_{0\nu}$-decay have a long history (see, e.g., [150]). The best lower limits on the half-lives $T^{0\nu}_{1/2}$ of this decay have been obtained for the isotopes of germanium-76, tellurium-130, and xenon-136: $T^{0\nu}_{1/2}(^{76}\mathrm{Ge}) > 8.0 \times 10^{25}$ yr reported by the GERDA-II collaboration [151], $T^{0\nu}_{1/2}(^{130}\mathrm{Te}) > 1.5 \times 10^{25}$ yr obtained from the combined results of the Cuoricino, CUORE-0, and CUORE experiments [152], and $T^{0\nu}_{1/2}(^{136}\mathrm{Xe}) > 1.07 \times 10^{26}$ yr reached by the

[1] This four-loop diagram is not expected to be the leading contribution to neutrino masses (see, e.g., [149]).

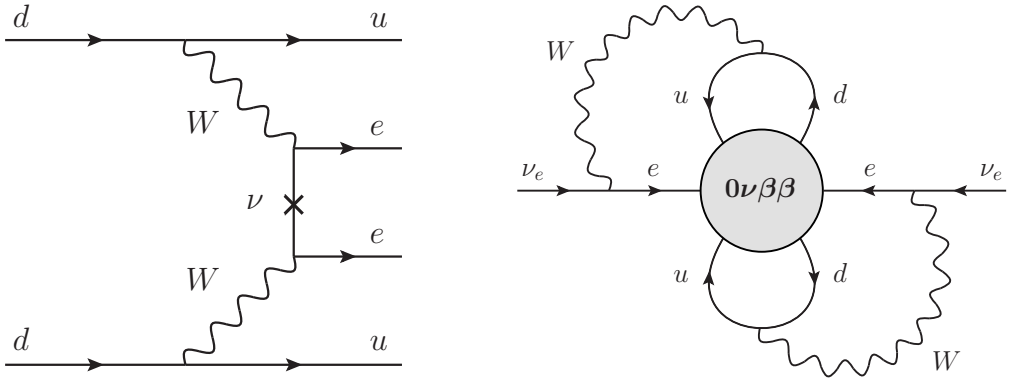

Figure 3.1: (a) Diagram of the standard light Majorana neutrino exchange contribution to $(\beta\beta)_{0\nu}$-decay, at the quark level. The process is allowed do to the neutrino (Majorana) mass insertion, which allows for a chirality flip. (b) Diagrammatic illustration of the black-box theorem of Ref. [148].

KamLAND-Zen collaboration [153], with all limits given at the 90% CL.

In the standard scenario where the exchange of three Majorana neutrinos ν_k ($k = 1, 2, 3$) with masses $m_k < 10$ MeV provides the dominant contribution to the decay rate, the $(\beta\beta)_{0\nu}$-decay rate is proportional to the so-called effective Majorana mass $|\langle m \rangle|$ (see next section). Given the present knowledge of neutrino oscillation data, the effective Majorana mass is bounded from below in the case of a neutrino mass spectrum with inverted ordering [154], $|\langle m \rangle|_{\rm IO} > 1.4 \times 10^{-2}$ eV. Instead, in the case of a spectrum with normal ordering, $|\langle m \rangle|$ can be exceptionally small: depending on the values of the lightest neutrino mass and of the CP violation Majorana phases we can have $|\langle m \rangle|_{\rm NO} \ll 10^{-3}$ eV (see, e.g., [25]). Recall that recent global analyses show a preference of the data for NO spectrum over IO spectrum at the 3σ CL.

New-generation experiments seek to probe and possibly cover the IO region of parameter space, working towards the $|\langle m \rangle| \sim 10^{-2}$ eV frontier. Such experiments include, aside from upgrades to the ones mentioned above (see, e.g., [146, 147]): CANDLES (^{48}Ca), MAJORANA and LEGEND (^{76}Ge), SuperNEMO and DCBA (^{82}Se, ^{150}Nd), ZICOS (^{96}Zr), AMoRE and MOON (^{100}Mo), COBRA (^{116}Cd,^{130} Te), SNO+ (^{130}Te), and NEXT, PandaX-III and nEXO (^{136}Xe). In case these searches produce a negative result, the next frontier in the quest for $(\beta\beta)_{0\nu}$-decay will correspond to $|\langle m \rangle| \sim 10^{-3}$ eV.

3.2 The Effective Majorana Mass

Taking the dominant contribution to the $(\beta\beta)_{0\nu}$-decay rate $\Gamma_{0\nu}$ to be due to the exchange of three Majorana neutrinos ν_k ($m_k < 10$ MeV; $k = 1, 2, 3$), one can write the inverse of the decay half-life, $(T^{0\nu}_{1/2})^{-1} = \Gamma_{0\nu} / \ln 2$, as

$$\left(T^{0\nu}_{1/2}\right)^{-1} = G_{0\nu}(Q, Z) \left|\mathcal{M}_{0\nu}(A, Z)\right|^2 |\langle m \rangle|^2 , \tag{3.1}$$

where $G_{0\nu}$ denotes the phase-space factor, which depends on the Q-value of the nuclear transition, and $\mathcal{M}_{0\nu}$ is the nuclear matrix element (NME) of the decay. The former can be computed with relatively

good accuracy whereas the latter remains the predominant source of uncertainty in the extraction of $|\langle m\rangle|$ from the data (see, e.g., [146, 155]).

The effective Majorana mass $|\langle m\rangle|$ is given by (see, e.g., [136]):

$$|\langle m\rangle| \,=\, \left| \sum_{k=1}^{3} (U_{\rm PMNS})^2_{ek}\, m_k \right| . \tag{3.2}$$

The first row of $U_{\rm PMNS}$ is the one relevant for $(\beta\beta)_{0\nu}$-decay and reads, in the standard parametrization (cf. Eq. (1.7)),

$$(U_{\rm PMNS})_{ek} = \left(c_{12}\, c_{13}\,, \quad s_{12}\, c_{13}\, e^{i\alpha_{21}/2}\,, \quad s_{13}\, e^{-i\delta}\, e^{i\alpha_{31}/2} \right)_k . \tag{3.3}$$

The most stringent upper limit on the effective Majorana mass was reported by the KamLAND-Zen collaboration. Using the lower limit on the half-life of ^{136}Xe obtained by the collaboration and quoted in the previous section, and taking into account the estimated uncertainties in the NMEs of the relevant process, the limit reads [153]:

$$|\langle m\rangle| < (0.061 - 0.165)\ \text{eV} . \tag{3.4}$$

We will henceforth make use of the notations given in Section 1.1, and additionally define $m_{\rm min} \equiv m_1\,(m_3)$ in the NO (IO) case. A NO or IO mass spectrum is said to be normal hierarchical (NH) or inverted hierarchical (IH) if respectively $m_1 \ll m_{2,3}$ or $m_3 \ll m_{1,2}$. In the converse limit of relatively large $m_{\rm min}$, $m_{\rm min} \gtrsim 0.1$ eV, the spectrum is said to be quasi-degenerate (QD) and $m_1 \simeq m_2 \simeq m_3$. In this last case, the distinction between NO and IO spectra is blurred and $\Delta m^2_{\odot}$ and $|\Delta m^2_{\rm A}|$ can usually be neglected with respect to $m^2_{\rm min}$.

In terms of the lightest neutrino mass, CPV phases, neutrino mixing angles, and neutrino mass-squared differences, the effective Majorana mass reads:

$$|\langle m\rangle|_{\rm NO} = \left| m_{\rm min}\, c^2_{12}\, c^2_{13} + \sqrt{\Delta m^2_{\odot} + m^2_{\rm min}}\, s^2_{12}\, c^2_{13}\, e^{i\alpha_{21}} + \sqrt{\Delta m^2_{\rm A} + m^2_{\rm min}}\, s^2_{13}\, e^{i\alpha'_{31}} \right| , \tag{3.5}$$

$$|\langle m\rangle|_{\rm IO} = \left| \sqrt{|\Delta m^2_{\rm A}| - \Delta m^2_{\odot} + m^2_{\rm min}}\, c^2_{12}\, c^2_{13} + \sqrt{|\Delta m^2_{\rm A}| + m^2_{\rm min}}\, s^2_{12}\, c^2_{13}\, e^{i\alpha_{21}} + m_{\rm min}\, s^2_{13}\, e^{i\alpha'_{31}} \right| , \tag{3.6}$$

where we have defined $\alpha'_{31} \equiv \alpha_{31} - 2\delta$.

It proves useful to recast $|\langle m\rangle|_{\rm NO}$ and $|\langle m\rangle|_{\rm IO}$ given above in the form

$$|\langle m\rangle| = \left| \widetilde{m}_1 + \widetilde{m}_2\, e^{i\alpha_{21}} + \widetilde{m}_3\, e^{i\alpha'_{31}} \right| , \tag{3.7}$$

with $\widetilde{m}_i > 0$ $(i = 1, 2, 3)$. It is then clear that the effective Majorana mass is the length of the vector sum of three vectors in the complex plane, whose relative orientations are given by the angles α_{21} and α'_{31}.

For the IO case, taking into account the 3σ ranges of Δm^2_{32}, Δm^2_{21}, $\sin^2\theta_{12}$, and $\sin^2\theta_{13}$ summarised in Table 1.3, one finds that there is a hierarchy between the lengths of the three vectors, $\widetilde{m}_3 < 0.1\,\widetilde{m}_2$ and $\widetilde{m}_2 < 0.6\,\widetilde{m}_1$, which holds for all values of $m_{\rm min}$. In particular, $\widetilde{m}_3 = m_{\rm min}\, s^2_{13}$ can be neglected with respect to the other terms since $s^2_{13} \ll \cos 2\theta_{12}$.[2] The above implies that extremal values of $|\langle m\rangle|_{\rm IO}$ are obtained when the three vectors are aligned ($\alpha_{21} = \alpha'_{31} = 0$, $|\langle m\rangle|_{\rm IO}$ is maximal) or when $\widetilde{m}_1$ is anti-aligned with $\widetilde{m}_{2,3}$ ($\alpha_{21} = \alpha'_{31} = \pi$, $|\langle m\rangle|_{\rm IO}$ is minimal). It then follows that there is a lower bound

[2] It follows from the current data that $\cos 2\theta_{12} > 0.30$ at 3σ CL.

on $|\langle m\rangle|_{\rm IO}$ for every value of $m_{\rm min}$ [154]. This bound reads: $|\langle m\rangle|_{\rm IO} \gtrsim \sqrt{|\Delta m^2_{\rm A}| + m^2_{\rm min}}\, c^2_{13} \cos 2\theta_{12} > \sqrt{|\Delta m^2_{\rm A}|}\, c^2_{13} \cos 2\theta_{12}$, $|\langle m\rangle|_{\rm IO} > 1.4{\times}10^{-2}$ eV, for variations of oscillation parameters in their respective 3σ ranges. In the limit of negligible $m_{\rm min}$ (IH spectrum), $m^2_{\rm min} \ll |\Delta m^2_{\rm A}|$, one has $|\langle m\rangle|_{\rm IO} \in [1.4, 4.9] \times 10^{-2}$ eV.

3.3 The Absolute Neutrino Mass Scale

Before proceeding to the analysis of the NO case, let us comment on present constraints on the absolute neutrino mass scale. The "conservative" upper limit of Eq. (3.4), $|\langle m\rangle|^{\rm max}_{\rm exp} = 0.165$ eV, which is in the range of the QD spectrum, implies, as it is not difficult to show, the following upper limit on the absolute Majorana neutrino mass scale (i.e., on the lightest neutrino mass): $m_{\rm min} \simeq m_{1,2,3} < 0.60$ eV, with $m_{\rm min} \lesssim |\langle m\rangle|^{\rm max}_{\rm exp}/(\cos 2\theta_{12} - s^2_{13})$, taking into account the 3σ ranges of $\cos 2\theta_{12}$ and $\sin^2\theta_{13}$.

Measurements of the end-point electron spectrum in tritium beta decay experiments constrain the combination $m_\beta \equiv \sum_k |U_{ek}|^2\, m_k$. The most stringent upper bounds on m_β, $m_\beta < 2.1$ eV and $m_\beta < 2.3$ eV, both at the 95% CL, are given by the Troitzk [156] and Mainz [157] collaborations, respectively. The KATRIN experiment [158] is planned to either improve this bound by an order of magnitude, or discover $m_\beta > 0.35$ eV. Taking into account the 3σ ranges for the relevant mixing angles and mass-squared differences, the Troitzk bound constrains the lightest neutrino mass to be $m_{\rm min} < 2.1$ eV.

Cosmological and astrophysical data constrain instead the sum $\Sigma \equiv \sum_k m_k$. Depending on the likelihood function and data set used, the upper limit on Σ reported by the Planck collaboration [159] varies in the interval $\Sigma < [0.34, 0.72]$ eV, 95% CL. Including data on baryon acoustic oscillations lowers this bound to $\Sigma < 0.17$ eV, 95% CL. Taking into account the 3σ ranges for the mass-squared differences, this last bound implies $m_{\rm min} < 0.05\,(0.04)$ eV in the NO (IO) case. One should note that the Planck collaboration analysis is based on the ΛCDM cosmological model. The quoted bounds may not apply in non-standard cosmological scenarios (see, e.g., [160]).

3.4 The Case of Normal Ordering

We henceforth restrict our discussion to the effective Majorana mass $|\langle m\rangle|_{\rm NO}$, for which there is no lower bound. In fact, unlike in the IO case, here the ordering of the lengths of the $\widetilde{m}_i$ depends on the value of $m_{\rm min}$ and cancellations in $|\langle m\rangle|_{\rm NO}$ are possible: one risks "falling" inside the "well of unobservability".[3]

For convenience, we reproduce in Table 3.1 the $n\sigma$ ($n = 1, 2, 3$) ranges for the oscillation parameters relevant to $(\beta\beta)_{0\nu}$-decay in the NO case, obtained in the recent global analysis of Ref. [39]. Considering variations of oscillation parameters in the corresponding 3σ ranges, for $m_{\rm min} \leq 5 \times 10^{-2}$ eV there is an upper bound $|\langle m\rangle|_{\rm NO} \leq 5.1 \times 10^{-2}$ eV (obtained for $\alpha_{21} = \alpha'_{31} = 0$). In the limit of negligible $m_{\rm min}$, $m^2_{\rm min} \ll |\Delta m^2_{\rm A}|$, one has $|\langle m\rangle|_{\rm NO} \in [0.9, 4.2] \times 10^{-3}$ eV.

From inspection of Eqs. (3.5) and (3.7), the vector lengths explicitly read $\widetilde{m}_1 = m_{\rm min}\, c^2_{12}\, c^2_{13}$, $\widetilde{m}_2 = \sqrt{\Delta m^2_\odot + m^2_{\rm min}}\, s^2_{12}\, c^2_{13}$, and $\widetilde{m}_3 = \sqrt{\Delta m^2_{\rm A} + m^2_{\rm min}}\, s^2_{13}$. In Figure 3.2, these lengths are plotted as func-

[3] For the consequences of not observing $(\beta\beta)_{0\nu}$-decay with $|\langle m\rangle|_{\rm NO} \gtrsim 10^{-3}$ eV, see Ref. [161].

Parameter	1σ range	2σ range	3σ range
Δm^2_{21} / (10^{-5} eV^2)	$7.20 - 7.51$	$7.05 - 7.69$	$6.92 - 7.91$
Δm^2_{31} / (10^{-3} eV^2)	$2.46 - 2.53$	$2.43 - 2.56$	$2.39 - 2.59$
$\sin^2\theta_{12}$ / 10^{-1}	$2.91 - 3.18$	$2.78 - 3.32$	$2.65 - 3.46$
$\sin^2\theta_{13}$ / 10^{-2}	$2.07 - 2.23$	$1.98 - 2.31$	$1.90 - 2.39$

Table 3.1: Ranges for the relevant oscillation parameters in the case of a NO neutrino spectrum, at the $n\sigma$ ($n = 1, 2, 3$) CLs, taken from the 2018 global analysis of Ref. [39] (part of Table 1.3).

tions of $m_{\rm min}$ for 3σ variations of oscillation parameters.

The requirement of having the effective Majorana mass above a reference value $|\langle m\rangle|_0$ is geometrically equivalent to not being able to form a quadrilateral with sides $\widetilde{m}_1$, $\widetilde{m}_2$, $\widetilde{m}_3$, and $|\langle m\rangle|_0$. This happens whenever one of the lengths exceeds the sum of the other three. If however $|\langle m\rangle|_0 > \sum_i \widetilde{m}_i$, it follows that $|\langle m\rangle| \leq \sum_i \widetilde{m}_i < |\langle m\rangle|_0$. Thus, for values of $m_{\rm min}$ and oscillation parameters for which $\widetilde{m}_2 > \widetilde{m}_1 + \widetilde{m}_3 + |\langle m\rangle|_0$ or $\widetilde{m}_1 > \widetilde{m}_2 + \widetilde{m}_3 + |\langle m\rangle|_0$ (see Figure 3.2) one is guaranteed to have $|\langle m\rangle|_{\rm NO} > |\langle m\rangle|_0$ independently of the choice of CPV phases α_{21} and α'_{31}. There are instead values of $m_{\rm min}$ for which the conditions $\widetilde{m}_2 < \widetilde{m}_1 + \widetilde{m}_3 + |\langle m\rangle|_0$ and $\widetilde{m}_1 < \widetilde{m}_2 + \widetilde{m}_3 + |\langle m\rangle|_0$ hold independently of the values of oscillation parameters within a given range. In such a case, values of α_{21} and α'_{31} such that $|\langle m\rangle|_{\rm NO} < |\langle m\rangle|_0$ are sure to exist.

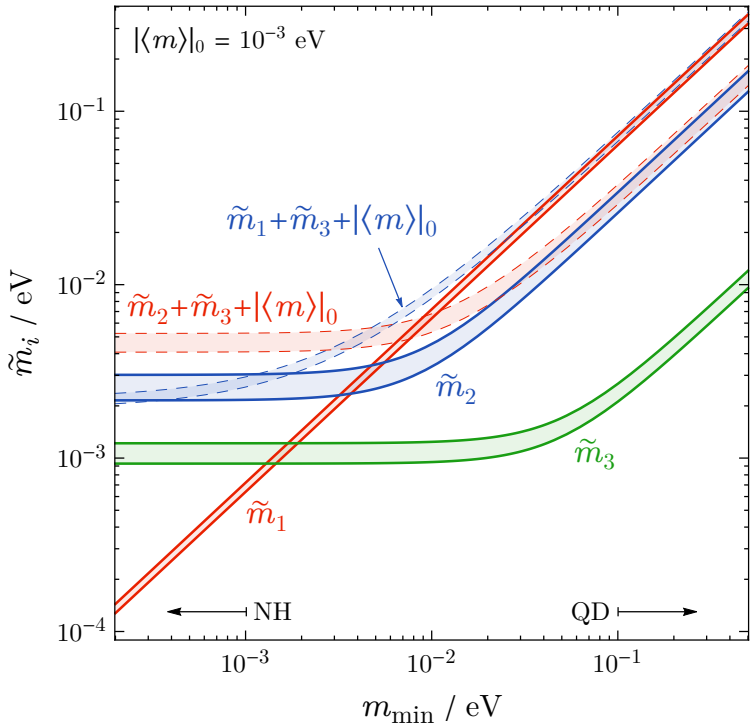

Figure 3.2: Lengths $\widetilde{m}_i$ of the complex vectors entering the expression of $|\langle m\rangle|_{\rm NO}$ as a function of the lightest neutrino mass $m_{\rm min}$, for NO spectrum. For comparison, the sums $\widetilde{m}_1 + \widetilde{m}_3 + |\langle m\rangle|_0$ and $\widetilde{m}_2 + \widetilde{m}_3 + |\langle m\rangle|_0$ are also shown (see text), with $|\langle m\rangle|_0 = 10^{-3}$ eV. Bands are obtained by varying the mixing angles and mass-squared differences in their respective 3σ ranges (see Table 3.1). See text for details.

We summarise in Figure 3.3 the ranges of $m_{\rm min}$ for which these different conditions apply (see caption). We vary oscillation parameters in their respective $n\sigma$ ($n = 1, 2, 3$) intervals and focus on the millielectronvolt "threshold", $|\langle m\rangle|_0 = 10^{-3}$ eV. We find that, for 3σ variations of the $\sin^2\theta_{ij}$ and Δm^2_{ij}, one is guaranteed to have $|\langle m\rangle|_{\rm NO} > 10^{-3}$ eV if $m_{\rm min} > 1.10 \times 10^{-2}$ eV. This corresponds to the lower bound $\Sigma > 0.07$ eV on the sum of neutrino masses. For 2σ variations, having $m_{\rm min} < 2 \times 10^{-4}$ eV or $m_{\rm min} > 9.9 \times 10^{-3}$ eV is enough to ensure $|\langle m\rangle|_{\rm NO} > 10^{-3}$ eV.

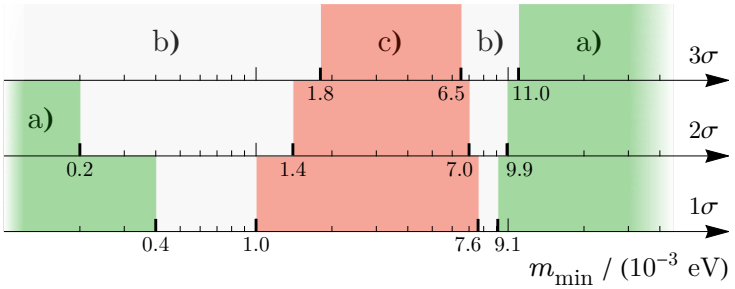

Figure 3.3: Ranges of $m_{\rm min}$ for a NO spectrum and for oscillation parameters inside their $n\sigma$ ($n = 1, 2, 3$) intervals (see Table 3.1) for which: in green, a) $|\langle m\rangle|_{\rm NO} > |\langle m\rangle|_0 = 10^{-3}$ eV for all values of θ_{ij}, Δm^2_{ij}, and $\alpha^{(\prime)}_{ij}$ from the corresponding allowed or defining intervals; in grey, b) there exist values of θ_{ij}, Δm^2_{ij} from the 1σ, 2σ and 3σ allowed intervals and values of $\alpha^{(\prime)}_{ij}$ such that $|\langle m\rangle|_{\rm NO} < |\langle m\rangle|_0 = 10^{-3}$ eV; and in red, c) for all values of θ_{ij} and Δm^2_{ij} from the corresponding allowed intervals there exist values of the phases α_{21} and α'_{31} for which $|\langle m\rangle|_{\rm NO} < |\langle m\rangle|_0 = 10^{-3}$ eV.

If one takes instead the higher value $|\langle m\rangle|_0 = 5\times10^{-3}$ eV and allows the relevant oscillation parameters to vary in their respective 3σ ranges, $|\langle m\rangle|_{\rm NO} > |\langle m\rangle|_0$ is guaranteed provided $m_{\rm min} > 2.3 \times 10^{-2}$ eV, which corresponds to the lower bound $\Sigma > 0.10$ eV on the sum of neutrino masses. This lower bound on Σ practically coincides with $\min(\Sigma)$ in the case of IO spectrum. Thus, if Σ is found to satisfy $\Sigma > 0.10$ eV, that would imply that $|\langle m\rangle|$ exceeds 5×10^{-3} eV, unless there exist additional contributions to the $(\beta\beta)_{0\nu}$-decay amplitude which cancel at least partially the contribution due to the 3 light neutrinos. If instead $m_{\rm min} < 1.4\times10^{-2}$ eV, for all (3σ allowed) values of oscillation parameters there is a choice of α_{21} and α'_{31} such that $|\langle m\rangle|_{\rm NO} < |\langle m\rangle|_0 = 5 \times 10^{-3}$ eV. These results are shown graphically in Figure 3.4.

Let us briefly remark on the dependence of $|\langle m\rangle|_{\rm NO}$ on the CPV phases. For the present discussion, 3σ variations of oscillation parameters are considered. For all values of α'_{31} and $\epsilon > 0$ there exist values of α_{21} and $m_{\rm min}$ such that $|\langle m\rangle|_{\rm NO} < \epsilon$, i.e. such that $|\langle m\rangle|_{\rm NO}$ is arbitrarily small. This is a consequence of the fact that, for any fixed oscillation parameters and α'_{31}, there is always a point $m^*_{\rm min}$ at which $|\widetilde{m}_1(m^*_{\rm min}) + \widetilde{m}_3(m^*_{\rm min})\, e^{i\alpha'_{31}}| = \widetilde{m}_2(m^*_{\rm min})$. Instead, there are values of α_{21} and $\epsilon > 0$ for which, independently of α'_{31} and $m_{\rm min}$, one has $|\langle m\rangle|_{\rm NO} > \epsilon$, i.e. for which $|\langle m\rangle|_{\rm NO}$ cannot be arbitrarily small. This conclusion may be anticipated from the graphical results of Ref. [162], where the structure of the $|\langle m\rangle|_{\rm NO}$ "well" has been studied as a function of $m_{\rm min}$ and α_{21}. In fact, we find that for $\alpha_{21} \lesssim 0.81\pi$ or $\alpha_{21} \gtrsim 1.19\pi$, $|\langle m\rangle|_{\rm NO}$ cannot be zero at tree-level since $|\widetilde{m}_1 + \widetilde{m}_2\, e^{i\alpha_{21}}| > \widetilde{m}_3$, strictly.

In Figure 3.5 we highlight the region of the $(m_{\rm min}, \alpha_{21})$ plane in which $|\langle m\rangle|_{\rm NO}$ is guaranteed to satisfy

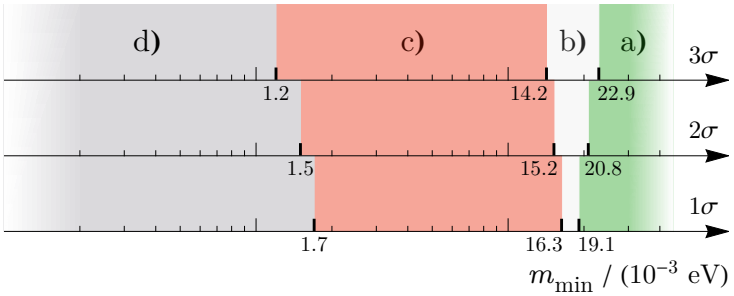

Figure 3.4: The same as in Figure 3.3, but for the reference value $|\langle m\rangle|_0 = 5\times10^{-3}$ eV: in green, a) $|\langle m\rangle|_{\rm NO} > |\langle m\rangle|_0 = 5\times10^{-3}$ eV for all values of θ_{ij}, Δm^2_{ij}, and $\alpha^{(\prime)}_{ij}$ from the corresponding allowed or defining intervals; in grey, b) there exist values of θ_{ij}, Δm^2_{ij} from the 1σ, 2σ and 3σ allowed intervals and values of $\alpha^{(\prime)}_{ij}$ such that $|\langle m\rangle|_{\rm NO} < |\langle m\rangle|_0 = 5\times10^{-3}$ eV; and in red, c) for all values of θ_{ij} and Δm^2_{ij} from the corresponding allowed intervals there exist values of the phases α_{21} and α'_{31} for which $|\langle m\rangle|_{\rm NO} < |\langle m\rangle|_0 = 5\times10^{-3}$ eV. In the darker grey ranges d) of $m_{\rm min}$, one has $|\langle m\rangle|_{\rm NO} < |\langle m\rangle|_0 = 5\times10^{-3}$ eV independently of the values of oscillation parameters and CPV phases.

$|\langle m\rangle|_{\rm NO} > 5\times10^{-3}$ eV, independently of α'_{31} and of variations of oscillation parameters inside their 3σ ranges.

3.5 CP and Generalised CP

Given the strong dependence of $|\langle m\rangle|$ on α_{21} and α'_{31}, some principle which determines these phases is welcome. The requirement of CP invariance constrains the values of the CPV phases α_{21}, α_{31}, and δ to integer multiples of π [163–165], meaning the relevant CP-conserving values are α_{21}, $\alpha'_{31} = 0, \pi$. Non-trivial predictions for the leptonic CPV phases may instead arise from the breaking of a discrete symmetry combined with a generalised CP symmetry. We focus on schemes with large enough residual symmetry such that the PMNS matrix depends at most on one real parameter θ [87] and realisations thereof where the predictions for the CPV phases are unambiguous, i.e. independent of θ. For symmetry groups with less than 100 elements, aside from the aforementioned CP-conserving values, the non-trivial values α_{21}, $\alpha'_{31} = \pi/2, 3\pi/2$ are possible predictions [166–172].

In what follows, we analyse the behaviour of $|\langle m\rangle|_{\rm NO}$ and $|\langle m\rangle|_{\rm IO}$ for each of 16 different $(\alpha_{21}, \alpha'_{31})$ pairs, with the relevant phases taking gCP-compatible values: $\alpha_{21}, \alpha'_{31} \in \{0, \pi/2, \pi, 3\pi/2\}$.[4] As can be seen from Eq. (3.7), some pairs are redundant as they lead to the same values of $|\langle m\rangle|$. We are left with 10 inequivalent pairs of phases: $(\alpha_{21}, \alpha'_{31}) = (\pi/2, 0) \sim (3\pi/2, 0)$, $(\pi/2, \pi) \sim (3\pi/2, \pi)$, $(0, \pi/2) \sim (0, 3\pi/2)$, $(\pi, \pi/2) \sim (\pi, 3\pi/2)$, $(\pi/2, \pi/2) \sim (3\pi/2, 3\pi/2)$, and $(\pi/2, 3\pi/2) \sim (3\pi/2, \pi/2)$.

The 2σ-allowed values of the effective Majorana mass $|\langle m\rangle|$ are presented in Figure 3.6 as a function of $m_{\rm min}$, for both orderings. Regions corresponding to different pairs $(\alpha_{21}, \alpha'_{31})$ with CP-conserving phases, $\alpha_{21}, \alpha'_{31} = 0, \pi$, are singled out. The predictions for the remaining pairs of fixed phases, containing at

[4] Given our scope and the available literature, we find that if $\alpha'_{31} = \pi/2, 3\pi/2$, then necessarily $\alpha_{21} = \pi/2, 3\pi/2$ is predicted. We nevertheless take all 16 pairs of phases into consideration.

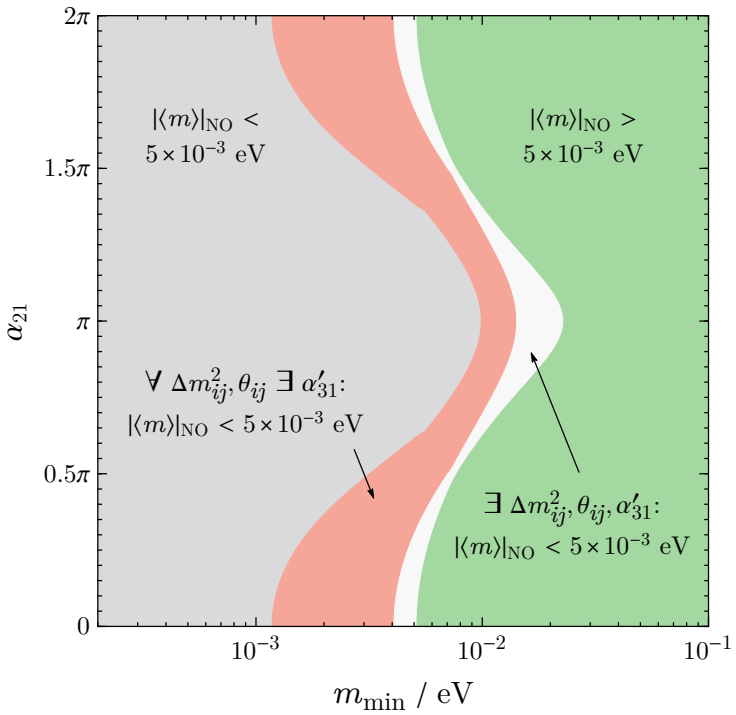

Figure 3.5: Regions in the $(m_{\rm min}, \alpha_{21})$ plane where different conditions on $|\langle m\rangle|_{\rm NO}$ apply. In the green (dark grey) region, $|\langle m\rangle|_{\rm NO}$ satisfies $|\langle m\rangle|_{\rm NO} > 5 \times 10^{-3}$ eV ($|\langle m\rangle|_{\rm NO} < 5 \times 10^{-3}$ eV) for all values of θ_{ij}, Δm^2_{ij}, and α'_{13} from the corresponding 3σ or defining intervals. In the red and grey regions, conditions analogous to those described in the caption of Figure 3.3 apply and are indicated. This figure is to be contrasted with Figure 3.4, where the dependence on α_{21} is not explicit.

least one phase which is gCP-compatible but not CP-conserving, are shown in Figure 3.7 for IO and in Figures 3.8 and 3.9 for NO (for one CP-conserving phase and for no CP-conserving phases, respectively). Allowed values of $|\langle m\rangle|$ are found by constructing an approximate χ^2 function from the sum of the one-dimensional projections in Ref. [39], and varying mixing angles and mass-squared differences while keeping $\chi^2(\theta_{ij}, \Delta m^2_{ij}) \lesssim 9.72$ (2σ CL, for joint estimation of 4 parameters).

From Figures 3.6 – 3.9, one sees that for each value of $m_{\rm min}$ there exist values of the effective Majorana mass which are incompatible with CP conservation. Some of these points may nonetheless be compatible with gCP-based predictive models. For IO, one sees there is substantial overlap between the bands with $(\alpha_{21}, \alpha'_{31}) = (0, 0)$ and $(0, \pi)$, between those of $(\pi, 0)$ and (π, π), and between the four bands $(\pi/2, k\,\pi/2)$, with $k = 0, 1, 2, 3$. In the case of NO, it is interesting to note that, for a fixed, gCP-compatible but not CP-conserving pair $(\alpha_{21}, \alpha'_{31})$, $|\langle m\rangle|_{\rm NO}$ is bounded from below at the 2σ CL, with the lower bound at or above the meV value, $|\langle m\rangle|_{\rm NO} \gtrsim 10^{-3}$ eV. We collect in Table 3.2 information on the lower bound on $|\langle m\rangle|_{\rm NO}$ for each pair of phases.

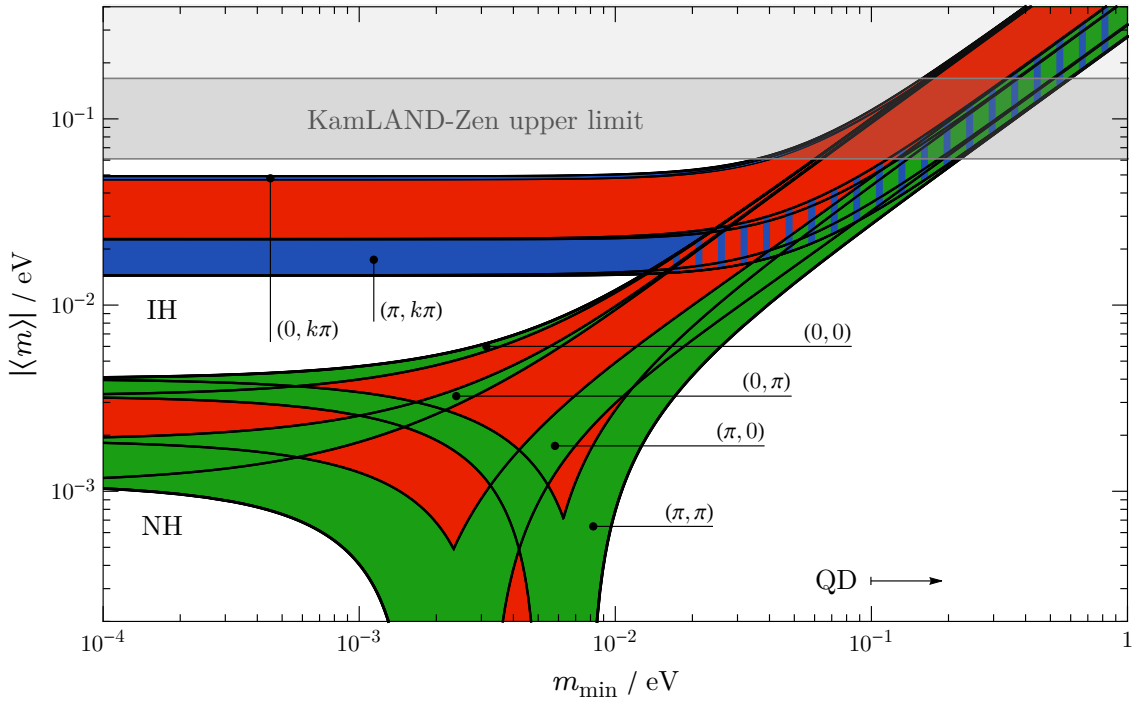

Figure 3.6: The effective Majorana mass $|\langle m \rangle|$ as a function of $m_{\rm min}$, for both orderings, allowing for variations of mixing angles and mass-squared differences at the 2σ CL (see text). The phases α_{21} and $\alpha'_{31} = \alpha_{31} - 2\delta$ are varied in the interval $[0,\, 2\pi]$. Blue and green bands correspond to (the indicated, with $k = 0, 1$) CP-conserving values of the phases $(\alpha_{21},\, \alpha'_{31})$, for IO and NO neutrino mass spectra, respectively, while in red regions at least one of the phases takes a CP-violating value. Blue hatching is used to locate CP-conserving bands in the case of IO spectrum whenever IO and NO spectra regions overlap. The KamLAND-Zen bound of Eq. (3.4) is indicated. See also Refs. [25, 145].

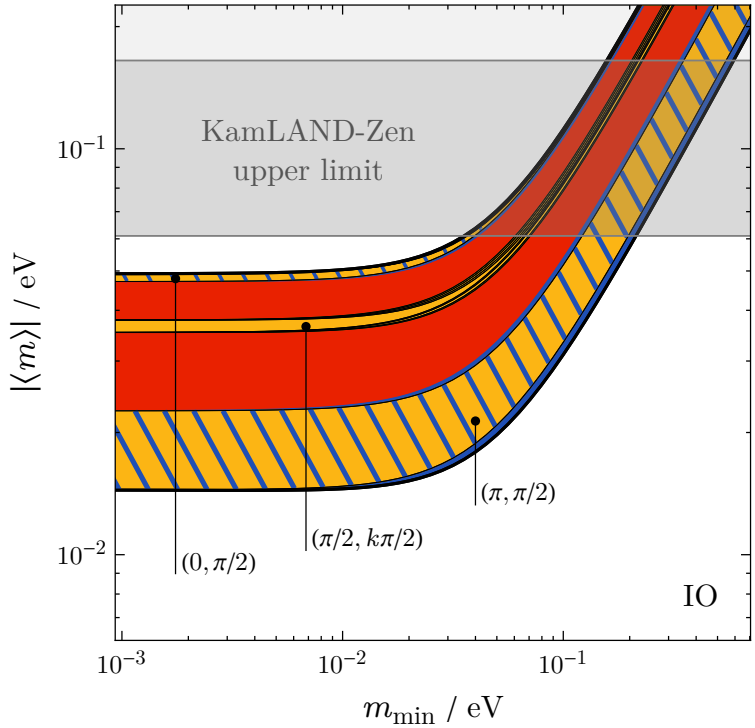

Figure 3.7: The effective Majorana mass $|\langle m\rangle|$ as a function of $m_{\rm min}$, for IO spectrum, allowing for variations of mixing angles and mass-squared differences at the 2σ CL (see text). Yellow bands correspond to (the indicated, $k = 0, 1, 2, 3$) gCP-compatible but not CP-conserving values of the phases (α_{21}, α'_{31}). Blue bands correspond to CP-conserving phases (see Figure 3.6) and hatching indicates overlap with such regions, while red regions are not gCP-compatible (for the models under consideration, see text). The KamLAND-Zen bound of Eq. (3.4) is also indicated.

	α'_{31}			
α_{21}	0	$\pi/2$	π	$3\pi/2$
0	3.1 (3.3)	2.4 (2.4)	1.0 (1.1)	$\sim (0,\, \pi/2)$
$\pi/2$	2.4 (2.4)	3.1 (3.3)	2.1 (2.2)	$\sim (3\pi/2,\, \pi/2)$
π	no bound[a]	0.91 (0.95)[b]	no bound[c]	$\sim (\pi,\, \pi/2)$
$3\pi/2$	$\sim (\pi/2,\, 0)$	1.0 (1.1)	$\sim (\pi/2,\, \pi)$	$\sim (\pi/2,\, \pi/2)$

[a] $|\langle m\rangle|_{\rm NO} > 1$ meV if $m_{\rm min} > 5.8\,(m_{\rm min} \notin [0.1, 5.3])$ meV.
[b] Only bounded case where $|\langle m\rangle|_{\rm NO}$ is not strictly at or above the meV value,for $m_{\rm min} \in [2.9, 5.9]([3.2, 5.3])$ meV. $|\langle m\rangle|_{\rm NO} > 1$ meV if e.g. $\sin^2\theta_{13} > 2.04 \times 10^{-2}$.
[c] $|\langle m\rangle|_{\rm NO} > 1$ meV if $m_{\rm min} \notin [3.1, 11.5]([3.4, 10.6])$ meV.

Table 3.2: Lower bounds on $|\langle m\rangle|_{\rm NO}$ given at the 3σ (2σ) CL, where applicable, for different fixed values of the phases α_{21} and α'_{31}. A tilde denotes equivalence between cases. All bounds are given in meV.

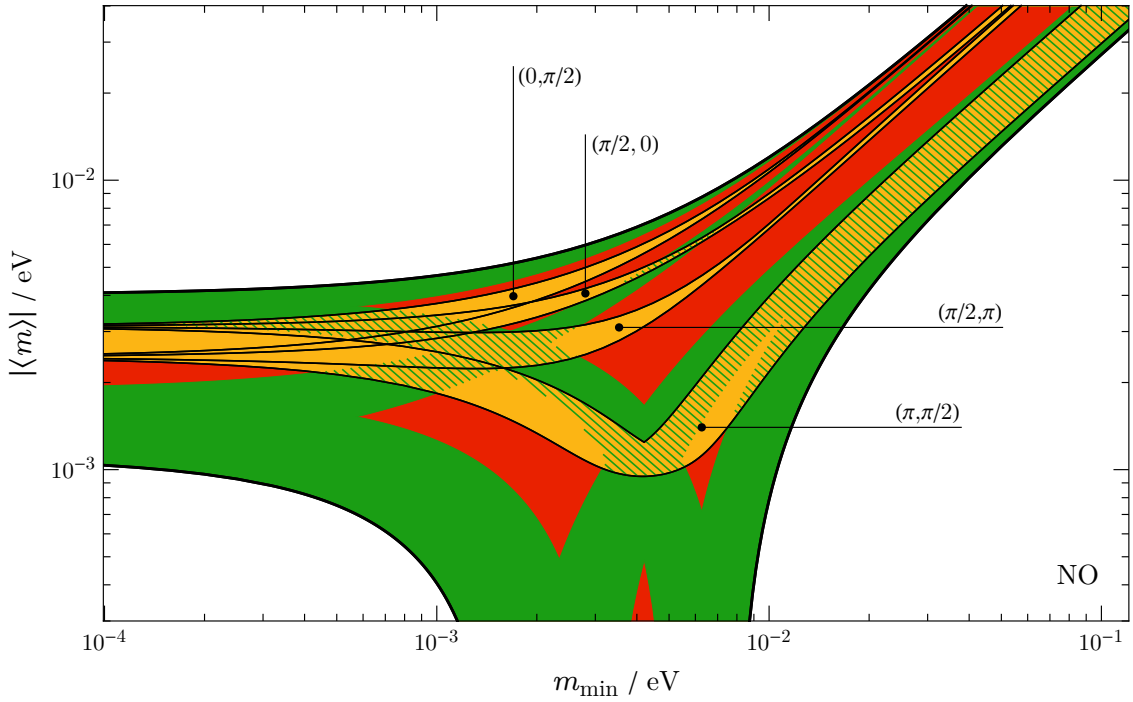

Figure 3.8: The effective Majorana mass $|\langle m\rangle|$ as a function of $m_{\rm min}$, for NO spectrum, allowing for variations of mixing angles and mass-squared differences at the 2σ CL (see text). Yellow bands correspond to (the indicated) pairs $(\alpha_{21},\, \alpha'_{31})$ of phases, with one CP-conserving, the other being gCP-compatible but not CP-conserving. Green bands correspond to CP-conserving phases (see Figure 3.6) and hatching indicates overlap with such regions, while red regions are not gCP-compatible (for the models under consideration, see text).

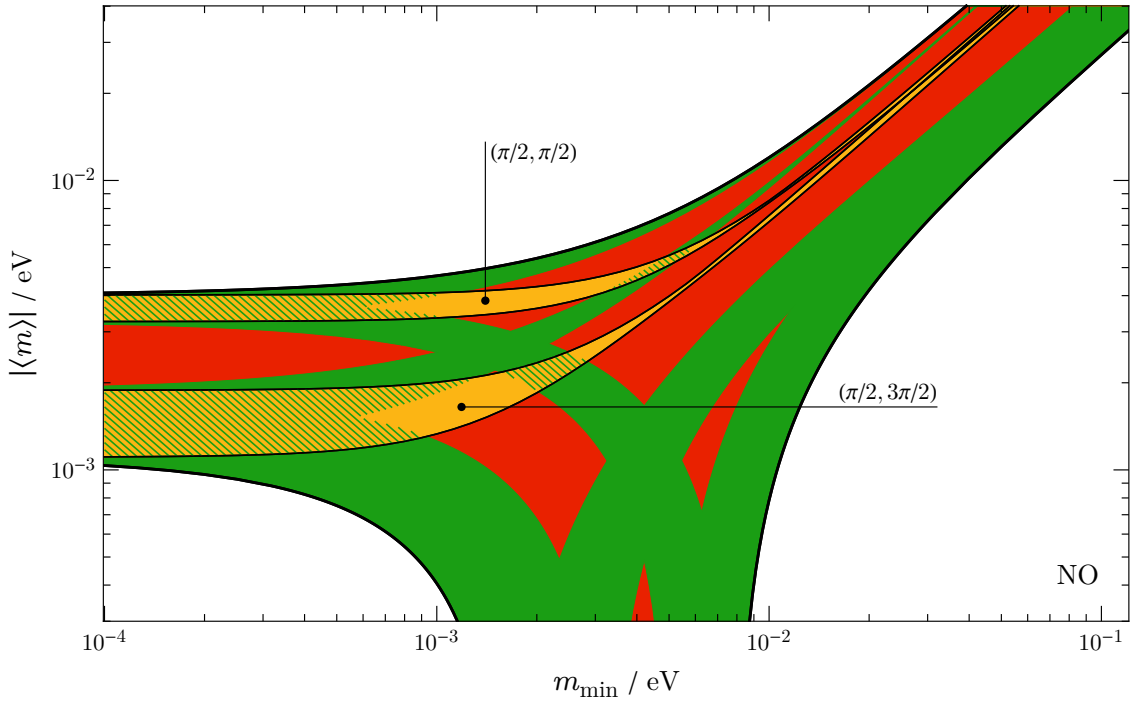

Figure 3.9: The same as in Figure 3.8, with yellow bands corresponding to pairs $(\alpha_{21},\, \alpha'_{31})$ with both phases being gCP-compatible but not CP-conserving.

3.6 Chapter Summary

The observation of $(\beta\beta)_{0\nu}$-decay would allow to establish lepton number violation and the Majorana nature of neutrinos. In the standard scenario of three light neutrino exchange dominance, the rate of this process is controlled by the effective Majorana mass $|\langle m\rangle|$. In the case of neutrino mass spectrum with inverted ordering (IO) the effective Majorana mass is bounded from below, $|\langle m\rangle|_{\rm IO} > 1.4 \times 10^{-2}$ eV. In the NO case, the effective Majorana mass $|\langle m\rangle|_{\rm NO}$, under certain conditions, can be exceedingly small, $|\langle m\rangle|_{\rm NO} \ll 10^{-2}$ eV, suppressing the $(\beta\beta)_{0\nu}$-decay rate.

Taking into account updated global-fit data, we have determined the conditions under which the effective Majorana mass in the NO case $|\langle m\rangle|_{\rm NO}$ exceeds the 10^{-3} eV (5×10^{-3} eV) value. For variations of θ_{12}, θ_{13}, Δm^2_{21} and Δm^2_{31} in their $n\sigma$ ($n = 1, 2, 3$) intervals, we have determined the ranges of the lightest neutrino mass $m_{\rm min}$ such that (see Figures 3.3 – 3.5):

a) $|\langle m\rangle|_{\rm NO} > 10^{-3}$ (5×10^{-3}) eV independently of the values of α_{21} and α'_{31}; $|\langle m\rangle|_{\rm NO} > 5 \times 10^{-3}$ eV is fulfilled when $m_{\rm min} > 2.3 \times 10^{-2}$ eV (for 3σ variations),

b) for some values of the θ_{ij} and Δm^2_{ij} there are choices of the CPV phases α_{21} and α'_{31} such that $|\langle m\rangle|_{\rm NO} < 10^{-3}$ (5×10^{-3}) eV,

c) for all values of the θ_{ij} and Δm^2_{ij} there are choices of the CPV phases α_{21} and α'_{31} such that $|\langle m\rangle|_{\rm NO} < 10^{-3}$ (5×10^{-3}) eV, and

d) $|\langle m\rangle|_{\rm NO} < 5 \times 10^{-3}$ eV independently of the values of α_{21} and α'_{31}.

We have shown, in particular, that if the sum of the three neutrino masses is found to satisfy the lower bound $\Sigma > 0.10$ eV, one has $|\langle m\rangle|_{\rm NO} > 5 \times 10^{-3}$ eV for any values of the CPV phases α_{21} and α'_{31}, unless there exist additional contributions to the $(\beta\beta)_{0\nu}$-decay amplitude which cancel at least partially the contribution due to the 3 light neutrinos.

We have additionally studied the predictions for $|\langle m\rangle|_{\rm IO}$ and $|\langle m\rangle|_{\rm NO}$ in cases where the leptonic CPV phases are fixed to particular values, α_{21}, $\alpha_{31} - 2\delta \in \{0, \pi/2, \pi, 3\pi/2\}$, which are either CP conserving (see Figure 3.6) or may arise in predictive schemes combining generalised CP and flavour symmetries (see Figures 3.7 – 3.9). The quantitative lower bounds on the effective mass $|\langle m\rangle|_{\rm NO}$ for such choices of phases are given in Table 3.2. We find that $|\langle m\rangle|_{\rm NO} \gtrsim 10^{-3}$ eV for all gCP-compatible but not CP-conserving pairs of the relevant phases.

Searches for lepton number non-conservation are of fundamental importance – as important as the searches for baryon number non-conservation in the form of, e.g., proton decay. Therefore if current and next-generation $(\beta\beta)_{0\nu}$-decay experiments seeking to probe the IO region of parameter space produce a negative result, the quest for $(\beta\beta)_{0\nu}$-decay should continue towards the $|\langle m\rangle| \sim 5 \times 10^{-3}$ eV and possibly the $|\langle m\rangle| \sim 10^{-3}$ eV frontier.

S_4 Flavour and gCP

4

In this chapter, we consider a class of models of neutrino mixing with S_4 lepton flavour symmetry combined with a generalised CP symmetry, which are broken to residual Z_2 and $Z_2 \times H^{\nu}_{\rm CP}$ symmetries in the charged lepton and neutrino sectors, respectively, $H^{\nu}_{\rm CP}$ being a remnant CP symmetry of the neutrino Majorana mass term. In this setup, the neutrino mixing angles and CP violation phases of the neutrino mixing matrix depend on three real parameters – two angles and a phase. Following Ref. [173], we classify all phenomenologically viable mixing patterns and derive predictions for the Dirac and Majorana CPV phases. Further, we use the results obtained on the neutrino mixing angles and leptonic CPV phases to derive predictions for the effective Majorana mass in neutrinoless double beta decay (see previous chapter).

4.1 Motivation and Overview

The idea of extending the Standard Model with a non-Abelian discrete flavour symmetry has been widely exploited in attempts to make progress towards the understanding the origin of flavour (see Section 1.3.1). Recall that in this approach one assumes the theory to possess a flavour symmetry at a certain high-energy scale, which is broken at lower energies to residual symmetries of the charged lepton and neutrino sectors, yielding certain predictions for the values of, and/or correlations between, the low-energy neutrino mixing parameters. In the reference 3ν mixing scheme we consider, i) the values of certain pairs of, or of all three, neutrino mixing angles are predicted to be correlated, and/or ii) there is a correlation between the value of the Dirac phase δ and the values of the three neutrino mixing angles, which includes also symmetry-dependent fixed parameters (see, e.g., [174–182] and references therein). These correlations are referred to as "neutrino mixing sum rules" in the literature and they can be tested experimentally [175, 179, 183–185]. Sufficiently precise experimental data on the neutrino mixing angles and on the Dirac CPV phase can also be used to distinguish between different possible underlying flavour symmetries leading to viable patters of neutrino mixing.

While in the discrete flavour symmetry approach at least some of the neutrino mixing angles and/or the Dirac phase are determined (directly or indirectly) by the flavour symmetry, the Majorana CPV phases α_{21} and α_{31} remain unconstrained. The values of the Majorana CPV phases are instead constrained to lie in certain narrow intervals, or are predicted, in theories which in addition to a flavour symmetry possess at a certain high-energy scale a generalised CP symmetry (see Section 1.3.2). The gCP symmetry

should be implemented in a way that is consistent with the flavour symmetry. At low energies, the gCP symmetry is broken, in general, to residual CP symmetries of the charged lepton and neutrino sectors.

In the scenarios involving a gCP symmetry which were most widely explored so far (see, e.g., [87, 90, 186–189]), a non-Abelian flavour symmetry G_f consistently combined with a gCP symmetry $H_{\rm CP}$ is broken to residual Abelian symmetries $G_e = Z_n$, $n > 2$, or $Z_m \times Z_k$, m, $k \geq 2$, and $G_\nu = Z_2 \times H^\nu_{\rm CP}$ of the charged lepton and neutrino mass terms, respectively.[1] The factor $H^\nu_{\rm CP}$ in G_ν stands for a remnant gCP symmetry of the neutrino mass term. In such a setup, G_e fixes completely the form of the unitary matrix U_e which diagonalises the product $M_e M_e^\dagger$ and enters into the expression of the PMNS matrix, M_e being the charged lepton mass matrix, in the conventions of Eq. (1.13). At the same time, G_ν fixes the unitary matrix U_ν, diagonalising the neutrino Majorana mass matrix M_ν up to a single free real parameter – a rotation angle θ^ν. Given the fact that the PMNS neutrino mixing matrix $U_{\rm PMNS}$ is given by the product

$$U_{\rm PMNS} = U_e^\dagger \, U_\nu \,, \tag{4.1}$$

all three neutrino mixing angles are expressed in terms of this rotation angle. In this class of models, one obtains specific correlations between the values of the three neutrino mixing angles, while the leptonic CPV phases are typically predicted to be exactly 0 or π, or else $\pi/2$ or $3\pi/2$ (recall the discussion in Section 3.5).

An example of such a setup was given at the end of Section 1.3.2, which, as we have noted, predicts a value of $\sin^2\theta_{12}$ outside its corresponding 2σ range. Other examples of one-parametric models can be found in the extensive study performed in Ref. [190], in which the authors have considered two different residual symmetry patterns. The first pattern is the one described in Section 1.3.2, namely with $G_e = Z_3$ and $G_\nu = Z_2 \times H^\nu_{\rm CP}$, while the second pattern has $G_e = Z_2 \times H^e_{\rm CP}$ and $G_\nu = Z_2 \times Z_2 \times H^\nu_{\rm CP}$ as residual symmetries in the charged lepton and neutrino sectors, respectively. The authors have performed an exhaustive scan over discrete groups of order less than 2000, which admit faithful 3-dimensional irreducible representations, and classified phenomenologically viable mixing patterns.

Models based on the approach to neutrino mixing that combines discrete symmetries and gCP invariance in which the neutrino mixing angles and the leptonic CPV phases are functions of two or three parameters have also been considered in the literature (see, e.g., [191–194]). In these models, the residual symmetry G_e of the charged lepton mass term is typically assumed to be a Z_2 symmetry or to be fully broken. In spite of the larger number of parameters in terms of which the neutrino mixing angles and the leptonic CPV phases are expressed, the values of the CPV phases are still predicted to be correlated with the values of the three neutrino mixing angles. A setup with $G_e = Z_2 \times H^e_{\rm CP}$ and $G_\nu = Z_2 \times H^\nu_{\rm CP}$ has been considered in Ref. [194]. The resulting PMNS matrix in such a scheme depends on two free real parameters – two angles θ^ν and θ^e. The authors have obtained several phenomenologically viable neutrino mixing patterns from $G_f = S_4$ combined with $H_{\rm CP}$, broken to all possible residual symmetries of the type indicated above. Models allowing for three free parameters have been investigated in Refs. [191–193]. In Ref. [192], the author has considered $G_f = A_5$ combined with $H_{\rm CP}$ and broken to $G_e = Z_2$ and $G_\nu = Z_2 \times H^\nu_{\rm CP}$. In this case, the matrix U_e depends on an angle θ^e and a phase δ^e, while

[1] We note that in Refs. [186,187] the residual symmetry G_e of the charged lepton mass term is augmented with a remnant CP symmetry $H^e_{\rm CP}$ as well.

the matrix U_ν depends on an angle θ^ν. In the above two scenarios the leptonic CPV phases possess non-trivial values.

The specific correlations between the values of the three neutrino mixing angles, which characterise the one-parameter models based on $G_e = Z_n$, $n > 2$, or $Z_m \times Z_k$, $m, k \geq 2$, and $G_\nu = Z_2 \times H^\nu_{\rm CP}$, do not hold in the two- and three-parameter models. In addition, the Dirac CPV phase in the two- and three-parameter models is predicted to have non-trivial values which are correlated with the values of the three neutrino mixing angles and differ from 0, π, $\pi/2$ and $3\pi/2$, although the deviations from, say, $3\pi/2$ can be relatively small. The indicated differences between the predictions of the models based on $G_e = Z_n$, $n > 2$, or $Z_m \times Z_k$, $m, k \geq 2$, and on $G_e = Z_2$ symmetries make it possible to distinguish between them experimentally by improving the precision on each of the three measured neutrino mixing angles θ_{12}, θ_{23} and θ_{13}, and by performing a sufficiently precise measurement of the Dirac phase δ. In case the predictions based on general residual symmetry considerations are experimentally vindicated, one is then compelled to further investigate concrete models of neutrino masses and lepton flavour realising said symmetries.

In what follows, we investigate the possible neutrino mixing patterns generated by a $G_f = S_4$ symmetry combined with an $H_{\rm CP}$ symmetry when these symmetries are broken down to $G_e = Z_2$ and $G_\nu = Z_2 \times H^\nu_{\rm CP}$, a rather simple setup not previously explored in the literature on the subject. In the following section, we describe a general framework for deriving the form of the PMNS matrix, dictated by the chosen residual symmetries, which we then apply, in Section 4.3, to $G_f = S_4$ combined with $H_{\rm CP}$ to obtain all phenomenologically viable mixing patterns.

4.2 The Framework

We start by considering a non-Abelian flavour symmetry group G_f, which admits a faithful irreducible 3-dimensional representation ρ. The three generations of left-handed leptons are assigned to this representation. Apart from that, the high-energy theory respects also the gCP symmetry $H_{\rm CP}$, which is implemented consistently along with the flavour symmetry. At some flavour symmetry breaking scale $G_f \rtimes H_{\rm CP}$ gets broken down to residual symmetries G_e and G_ν of the charged lepton and neutrino mass terms, respectively. The residual flavour symmetries are Abelian subgroups of G_f. The symmetries G_e and G_ν significantly constrain the form of the neutrino mixing matrix $U_{\rm PMNS}$, as we demonstrate below.

4.2.1 The PMNS Matrix from $G_e = Z_2$ and $G_\nu = Z_2 \times H^\nu_{\rm CP}$

We choose G_e to be a Z_2 symmetry. We will denote it as $Z_2^{g_e} \equiv \{1, g_e\}$, $g_e^2 = 1$ being an element of G_f of order two, generating the $Z_2^{g_e}$ subgroup. The invariance of the charged lepton mass term under G_e implies

$$\rho(g_e)^\dagger M_e M_e^\dagger \, \rho(g_e) = M_e M_e^\dagger \, . \tag{4.2}$$

Below we show how this invariance constrains the form of the unitary matrix U_e, diagonalising $M_e M_e^\dagger$ through

$$U_e^\dagger M_e M_e^\dagger \, U_e = {\rm diag}(m_e^2, m_\mu^2, m_\tau^2) \, . \tag{4.3}$$

Let Ω_e be a diagonalising unitary matrix of a given $\rho(g_e)$, such that

$$\Omega_e^\dagger \, \rho(g_e) \, \Omega_e = \rho(g_e)^{\rm d} \equiv {\rm diag}(1,-1,-1) \, . \tag{4.4}$$

The form of the diagonal matrix is obtained as follows. The diagonal entries of $\rho(g_e)^{\rm d}$ are constrained to be ± 1, since this matrix must still furnish a representation of Z_2 and hence its square is the identity. We have assumed that the trace of $\rho(g_e)$ is -1, for the relevant elements g_e, as it is the case for the 3-dimensional representation of S_4 we will consider later on.[2] Note that we can take the order of the eigenvalues of $\rho(g_e)$ as given in Eq. (4.4) without loss of generality, as will become clear later.

Expressing $\rho(g_e)$ as in Eq. (4.4) and substituting it in Eq. (4.2), we obtain

$$\rho(g_e)^{\rm d} \, \Omega_e^\dagger \, M_e M_e^\dagger \, \Omega_e \, \rho(g_e)^{\rm d} = \Omega_e^\dagger \, M_e M_e^\dagger \, \Omega_e \, . \tag{4.5}$$

This equation implies that $\Omega_e^\dagger \, M_e M_e^\dagger \, \Omega_e$ has the block-diagonal form

$$\begin{pmatrix} \times & 0 & 0 \\ 0 & \times & \times \\ 0 & \times & \times \end{pmatrix} \, , \tag{4.6}$$

and, since this matrix is hermitian, it can be diagonalised by a unitary matrix with a $U(2)$ transformation acting on the 2-3 block. In the general case, the $U(2)$ transformation can be parametrised as follows:

$$\begin{pmatrix} \cos\theta^e & -\sin\theta^e \, e^{-i\delta^e} \\ \sin\theta^e \, e^{i\delta^e} & \cos\theta^e \end{pmatrix} \begin{pmatrix} e^{i\beta_1^e} & 0 \\ 0 & e^{i\beta_2^e} \end{pmatrix} \, . \tag{4.7}$$

The diagonal phase matrix is, however, unphysical, since it can be eliminated by rephasing the charged lepton fields, and we will not keep it. Thus, we arrive to the conclusion that the matrix U_e diagonalising $M_e M_e^\dagger$ reads

$$U_e = \Omega_e \, U_{23}(\theta^e, \delta^e)^\dagger \, P_e^T \, , \tag{4.8}$$

with

$$U_{23}(\theta^e, \delta^e) = \begin{pmatrix} 1 & 0 & 0 \\ 0 & \cos\theta^e & \sin\theta^e \, e^{-i\delta^e} \\ 0 & -\sin\theta^e \, e^{i\delta^e} & \cos\theta^e \end{pmatrix} \, , \tag{4.9}$$

and P_e being one of six permutation matrices, which need to be taken into account, since in the approach under consideration the order of the charged lepton masses is unknown. The six permutation matrices read:

$$P_{123} = \begin{pmatrix} 1 & 0 & 0 \\ 0 & 1 & 0 \\ 0 & 0 & 1 \end{pmatrix} \, , \quad P_{132} = \begin{pmatrix} 1 & 0 & 0 \\ 0 & 0 & 1 \\ 0 & 1 & 0 \end{pmatrix} \, , \quad P_{213} = \begin{pmatrix} 0 & 1 & 0 \\ 1 & 0 & 0 \\ 0 & 0 & 1 \end{pmatrix} \, , \tag{4.10}$$

$$P_{231} = \begin{pmatrix} 0 & 1 & 0 \\ 0 & 0 & 1 \\ 1 & 0 & 0 \end{pmatrix} \, , \quad P_{312} = \begin{pmatrix} 0 & 0 & 1 \\ 1 & 0 & 0 \\ 0 & 1 & 0 \end{pmatrix} \, , \quad P_{321} = \begin{pmatrix} 0 & 0 & 1 \\ 0 & 1 & 0 \\ 1 & 0 & 0 \end{pmatrix} \, . \tag{4.11}$$

Note that the order of indices in P_{ijk} stands for the order of rows, i.e., when applied from the left to a matrix, it gives the desired order, i-j-k, of the matrix rows.

[2] For the other 3-dimensional irreducible representation of S_4 the trace can be either -1 or $+1$, depending on g_e. Choosing $+1$ would simply imply a change of sign of $\rho(g_e)^{\rm d}$, which however does not lead to new constraints. The conclusions we reach in what follows are then independent of the choice of 3-dimensional representation.

For the neutrino sector we consider a $G_\nu = Z_2 \times H^\nu_{\rm CP}$ residual symmetry. We denote the Z_2 symmetry of the neutrino mass matrix as $Z_2^{g_\nu} \equiv \{1, g_\nu\}$, with $g_\nu^2 = 1$ being an element of G_f, generating the $Z_2^{g_\nu}$ subgroup. $H^\nu_{\rm CP} = \{X_\nu\}$ is the set of remnant gCP unitary transformations X_ν forming a residual CP symmetry of the neutrino mass matrix. $H^\nu_{\rm CP}$ is contained in $H_{\rm CP} = \{X\}$ which is the gCP symmetry of the high-energy theory consistently defined along with the flavour symmetry G_f. It is worth to comment here on the notation $H^\nu_{\rm CP}$ used. By $H^\nu_{\rm CP} = \{X_{\nu 1}, X_{\nu 2}\}$ we mean a set of gCP transformations ($X_{\nu 1}$ and $X_{\nu 2}$) compatible with the residual flavour $Z_2^{g_\nu}$ symmetry. However, when writing $G_\nu = Z_2^{g_\nu} \times H^\nu_{\rm CP}$, $H^\nu_{\rm CP}$ is intended to be a group generated by $X_{\nu 1}$. Namely, following Ref. [87] (Appendix B within), $H^\nu_{\rm CP}$ is isomorphic to $\{\mathcal{I}, \mathcal{X}_{\nu 1}\}$, where $\mathcal{I}$ is the 6×6 unit matrix and

$$\mathcal{X}_{\nu 1} = \begin{pmatrix} 0 & X_{\nu 1} \\ X^*_{\nu 1} & 0 \end{pmatrix} , \tag{4.12}$$

both acting on $(\varphi, \varphi^*)^T$. Then, $Z_2^{g_\nu}$ is isomorphic to $\{\mathcal{I}, \mathcal{G}_\nu\}$, where

$$\mathcal{G}_\nu = \begin{pmatrix} \rho(g_\nu) & 0 \\ 0 & \rho(g_\nu)^* \end{pmatrix} \tag{4.13}$$

acts again on $(\varphi, \varphi^*)^T$. Finally, it is not difficult to convince oneself that the full residual symmetry group G_ν is given by a direct product $Z_2^{g_\nu} \times H^\nu_{\rm CP}$, and there is a second gCP transformation $X_{\nu 2} = \rho(g_\nu)\, X_{\nu 1}$ contained in it. The same logic applies to the notation $H_{\rm CP}$, and, as has been shown in Ref. [87], the full symmetry group is a semi-direct product $G_f \rtimes H_{\rm CP}$.

The invariance under G_ν of the neutrino mass matrix implies that the following two equations hold:

$$\rho(g_\nu)^T M_\nu\, \rho(g_\nu) = M_\nu \,, \tag{4.14}$$

$$X_\nu^T M_\nu\, X_\nu = M_\nu^* \,. \tag{4.15}$$

In addition, the consistency condition between $Z_2^{g_\nu}$ and $H^\nu_{\rm CP}$ has to be respected, namely:

$$X_\nu\, \rho(g_\nu)^*\, X_\nu^{-1} = \rho(g_\nu) \,. \tag{4.16}$$

To derive the form of the unitary matrix U_ν diagonalising the neutrino Majorana mass matrix M_ν as

$$U_\nu^T M_\nu\, U_\nu = {\rm diag}(m_1, m_2, m_3) \,, \tag{4.17}$$

$m_k > 0$ being the neutrino masses, we will follow the method presented in Ref. [194].

Let $\Omega_{\nu 1}$ be a diagonalising unitary matrix of $\rho(g_\nu)$, such that

$$\Omega^\dagger_{\nu 1}\, \rho(g_\nu)\, \Omega_{\nu 1} = \rho(g_\nu)^{\rm d} \equiv {\rm diag}(1, -1, -1) \,. \tag{4.18}$$

Expressing $\rho(g_\nu)$ from this equation and substituting it in the consistency condition, Eq. (4.16), we find

$$\rho(g_\nu)^{\rm d}\, \Omega^\dagger_{\nu 1}\, X_\nu\, \Omega^*_{\nu 1}\, \rho(g_\nu)^{\rm d} = \Omega^\dagger_{\nu 1}\, X_\nu\, \Omega^*_{\nu 1} \,, \tag{4.19}$$

meaning that $\Omega^\dagger_{\nu 1}\, X_\nu\, \Omega^*_{\nu 1}$ is a block-diagonal matrix, having the form of Eq. (4.6). Moreover, this matrix is symmetric, since the gCP transformations X_ν have to be symmetric in order for all the three neutrino

masses to be different [87,90], as is required by the data (see, e.g., Ref. [195] for an explicit proof). Being a complex (unitary) symmetric matrix, it is diagonalised by a unitary matrix $\Omega_{\nu 2}$ via the transformation:

$$\Omega_{\nu 2}^{\dagger}\,(\Omega_{\nu 1}^{\dagger}\,X_{\nu}\,\Omega_{\nu 1}^{*})\,\Omega_{\nu 2}^{*} = (\Omega_{\nu 1}^{\dagger}\,X_{\nu}\,\Omega_{\nu 1}^{*})^{\rm d}\,. \tag{4.20}$$

The matrix $(\Omega_{\nu 1}^{\dagger}\,X_{\nu}\,\Omega_{\nu 1}^{*})^{\rm d}$ is, in general, a diagonal phase matrix. However, we can choose $(\Omega_{\nu 1}^{\dagger}\,X_{\nu}\,\Omega_{\nu 1}^{*})^{\rm d} = \mathbb{1}$, as the phases of $(\Omega_{\nu 1}^{\dagger}\,X_{\nu}\,\Omega_{\nu 1}^{*})^{\rm d}$ can be moved to the matrix $\Omega_{\nu 2}$. With this choice we obtain the Takagi factorisation of the X_{ν} (valid for unitary symmetric matrices):

$$X_{\nu} = \Omega_{\nu}\,\Omega_{\nu}^{T}\,, \tag{4.21}$$

with $\Omega_{\nu} = \Omega_{\nu 1}\,\Omega_{\nu 2}$.

Since, as we have noted earlier, $\Omega_{\nu 1}^{\dagger}\,X_{\nu}\,\Omega_{\nu 1}^{*}$ has the form of Eq. (4.6), the matrix $\Omega_{\nu 2}$ can be chosen without loss of generality to have the same form with a unitary 2×2 matrix in the 2-3 block. This implies that the matrix $\Omega_{\nu} = \Omega_{\nu 1}\,\Omega_{\nu 2}$ also diagonalises $\rho(g_{\nu})$. Indeed,

$$\Omega_{\nu}^{\dagger}\,\rho(g_{\nu})\,\Omega_{\nu} = \Omega_{\nu 2}^{\dagger}\,\rho(g_{\nu})^{\rm d}\,\Omega_{\nu 2} = \rho(g_{\nu})^{\rm d}\,, \tag{4.22}$$

where we have used Eq. (4.18).

We substitute next X_{ν} from Eq. (4.21) in the gCP invariance condition of the neutrino mass matrix, Eq. (4.15), and find that the matrix $\Omega_{\nu}^{T}\,M_{\nu}\,\Omega_{\nu}$ is real. Furthermore, this is a symmetric matrix, since the neutrino Majorana mass matrix M_{ν} is symmetric. A real symmetric matrix can be diagonalised by a real orthogonal transformation. Employing Eqs. (4.22) and (4.14), we have

$$\rho(g_{\nu})^{\rm d}\,\left(\Omega_{\nu}^{T}\,M_{\nu}\,\Omega_{\nu}\right)\,\rho(g_{\nu})^{\rm d} = \Omega_{\nu}^{T}\,M_{\nu}\,\Omega_{\nu}\,, \tag{4.23}$$

implying that $\Omega_{\nu}^{T}\,M_{\nu}\,\Omega_{\nu}$ is a block-diagonal matrix as in Eq. (4.6). Thus, the required orthogonal transformation is a rotation in the 2-3 plane by an angle θ^{ν}:

$$R_{23}(\theta^{\nu}) = \begin{pmatrix} 1 & 0 & 0 \\ 0 & \cos\theta^{\nu} & \sin\theta^{\nu} \\ 0 & -\sin\theta^{\nu} & \cos\theta^{\nu} \end{pmatrix}\,. \tag{4.24}$$

Finally, the matrix U_{ν} diagonalising M_{ν} reads

$$U_{\nu} = \Omega_{\nu}\,R_{23}(\theta^{\nu})\,P_{\nu}\,Q_{\nu}\,, \tag{4.25}$$

where P_{ν} is one of the six permutation matrices, which accounts for different order of the m_k, and the matrix Q_{ν} renders them positive. Without loss of generality Q_{ν} can be parametrised as follows:

$$Q_{\nu} = {\rm diag}(1, i^{k_1}, i^{k_2})\,, \quad \text{with} \quad k_{1,2} = 0, 1\,. \tag{4.26}$$

Assembling together the results for U_e and U_{ν}, Eqs. (4.8) and (4.25), we obtain for the form of the PMNS matrix:

$$U_{\rm PMNS} = P_e\,U_{23}(\theta^{e}, \delta^{e})\,\Omega_{e}^{\dagger}\,\Omega_{\nu}\,R_{23}(\theta^{\nu})\,P_{\nu}\,Q_{\nu}\,. \tag{4.27}$$

Thus, in the approach we are following the PMNS matrix depends on three free real parameters – the two angles θ^e and θ^ν and the phase δ^e.[3] One of the elements of the PMNS matrix is fixed to be a constant by the residual symmetries. We note finally that, since $R_{23}(\theta^\nu + \pi) = R_{23}(\theta^\nu)\,\mathrm{diag}(1,-1,-1)$, where the diagonal matrix can be absorbed into Q_ν, and $U_{23}(\theta^e + \pi, \delta^e) = \mathrm{diag}(1,-1,-1)\,U_{23}(\theta^e, \delta^e)$, where the diagonal matrix contributes to unphysical charged lepton phases, it is sufficient to consider θ^e and θ^ν in the interval $[0, \pi)$.

4.2.2 Conjugate Residual Symmetries

In this subsection we briefly recall why the residual symmetries G'_e and G'_ν conjugate to G_e and G_ν, respectively, under the same element of the flavour symmetry group G_f lead to the same PMNS matrix (see, e.g., [87, 186]). Two pairs of residual symmetries $\{Z_2^{g_e}, Z_2^{g_\nu}\}$ and $\{Z_2^{g'_e}, Z_2^{g'_\nu}\}$ are conjugate to each other under $h \in G_f$ if

$$h\, g_e\, h^{-1} = g'_e \quad \text{and} \quad h\, g_\nu\, h^{-1} = g'_\nu\,. \tag{4.28}$$

At the representation level this means

$$\rho(h)\,\rho(g_e)\,\rho(h)^\dagger = \rho(g'_e) \quad \text{and} \quad \rho(h)\,\rho(g_\nu)\,\rho(h)^\dagger = \rho(g'_\nu)\,. \tag{4.29}$$

Substituting $\rho(g_e)$ and $\rho(g_\nu)$ from these equalities to Eqs. (4.2) and (4.14), respectively, one obtains

$$\rho(g'_e)^\dagger M'_e M'^\dagger_e\, \rho(g'_e) = M'_e M'^\dagger_e \quad \text{and} \quad \rho(g'_\nu)^T M'_\nu\, \rho(g'_\nu) = M'_\nu\,, \tag{4.30}$$

where the primed mass matrices are related to the original ones as

$$M'_e M'^\dagger_e = \rho(h)\, M_e M_e^\dagger\, \rho(h)^\dagger \quad \text{and} \quad M'_\nu = \rho(h)^*\, M_\nu\, \rho(h)^\dagger\,. \tag{4.31}$$

As can be understood from Eq. (4.15) (or Eq. (4.16)), the matrix M'_ν will respect a remnant CP symmetry X'_ν, which is related to X_ν as follows:

$$X'_\nu = \rho(h)\, X_\nu\, \rho(h)^T\,. \tag{4.32}$$

The unitary transformations U'_e and U'_ν diagonalising the primed mass matrices are given by

$$U'_e = \rho(h)\, U_e \quad \text{and} \quad U'_\nu = \rho(h)\, U_\nu\,, \tag{4.33}$$

thus yielding, as promised,

$$U'_{\mathrm{PMNS}} = U'^\dagger_e\, U'_\nu = U_e^\dagger\, U_\nu = U_{\mathrm{PMNS}}\,. \tag{4.34}$$

4.2.3 Phenomenologically Non-Viable Cases

Here we show that at least two types of residual symmetries $\{G_e, G_\nu\} = \{Z_2^{g_e}, Z_2^{g_\nu} \times H^\nu_{\mathrm{CP}}\}$, characterised by certain elements g_e and g_ν, cannot lead to phenomenologically viable form of the PMNS matrix.

[3] The matrix $\Omega_{\nu 2}$ in Eq. (4.20) with $(\Omega_{\nu 1}^\dagger\, X_\nu\, \Omega_{\nu 1}^*)^{\mathrm{d}} = \mathbb{1}$, and thus the matrix $\Omega_\nu = \Omega_{\nu 1}\,\Omega_{\nu 2}$ in Eq. (4.21), is determined up to multiplication by an orthogonal matrix O on the right. The matrix $\Omega_{\nu 2}\, O$ must be unitary since it diagonalises a complex symmetric matrix, which implies that O must be unitary in addition of being orthogonal, and therefore must be a real matrix. Eq. (4.22) restricts further this real orthogonal matrix O to have the form of a real rotation in the 2-3 plane, which can be "absorbed" in the $R_{23}(\theta^\nu)$ matrix in Eq. (4.27).

• **Type I: $g_e = g_\nu$.** In this case, we can choose $\Omega_e = \Omega_\nu P$, with P_{123} or P_{132}. Then, Eq. (4.27) yields

$$U_{\rm PMNS} = P_e\, U_{23}(\theta^e, \delta^e)\, P\, R_{23}(\theta^\nu)\, P_\nu\, Q_\nu\,. \tag{4.35}$$

This means that up to permutations of the rows and columns $U_{\rm PMNS}$ has the form of Eq. (4.6), i.e., it contains four zero entries, which are ruled out by neutrino oscillation data.

• **Type II: $g_e, g_\nu \in Z_2 \times Z_2 \subset G_f$.** Now we consider two different order two elements $g_e \neq g_\nu$, which belong to the same Klein subgroup of G_f, $Z_2 \times Z_2 = \{1, g_e, g_\nu, g_e\, g_\nu\}$. In this case, since g_e and g_ν commute, there exists a unitary matrix simultaneously diagonalising both $\rho(g_e)$ and $\rho(g_\nu)$. Note, however, that the order of eigenvalues in the resulting diagonal matrices must be different, since the elements differ. Namely, let $\Omega_{\nu 1}$ be a diagonalising matrix of $\rho(g_\nu)$ and $\rho(g_e)$, and let $\Omega_{\nu 1}$ diagonalise $\rho(g_\nu)$ as in Eq. (4.18). Then, $\Omega_{\nu 1}^\dagger\, \rho(g_e)\, \Omega_{\nu 1}$ can yield either $\mathrm{diag}(-1,1,-1)$ or $\mathrm{diag}(-1,-1,1)$, but not $\mathrm{diag}(1,-1,-1)$. Hence, Ω_e diagonalising $\rho(g_e)$ as in Eq. (4.4), must read

$$\Omega_e = \Omega_{\nu 1}\, P\,, \quad \text{with} \quad P = P_{213} \text{ or } P_{312} \quad \text{if} \quad \Omega_{\nu 1}^\dagger\, \rho(g_e)\, \Omega_{\nu 1} = \mathrm{diag}(-1,1,-1)\,, \tag{4.36}$$

$$\text{and} \quad P = P_{231} \text{ or } P_{321} \quad \text{if} \quad \Omega_{\nu 1}^\dagger\, \rho(g_e)\, \Omega_{\nu 1} = \mathrm{diag}(-1,-1,1)\,. \tag{4.37}$$

Taking into account that $\Omega_\nu = \Omega_{\nu 1}\, \Omega_{\nu 2}$, with $\Omega_{\nu 2}$ of the block-diagonal form given in Eq. (4.6), we obtain

$$U_{\rm PMNS} = P_e\, U_{23}(\theta^e, \delta^e)\, P^T\, \Omega_{\nu 2}\, R_{23}(\theta^\nu)\, P_\nu\, Q_\nu\,, \tag{4.38}$$

where $P^T\, \Omega_{\nu 2}$, depending on P, can take one of the following forms:

$$\begin{pmatrix} 0 & \times & \times \\ \times & 0 & 0 \\ 0 & \times & \times \end{pmatrix} \quad \text{or} \quad \begin{pmatrix} 0 & \times & \times \\ 0 & \times & \times \\ \times & 0 & 0 \end{pmatrix}\,. \tag{4.39}$$

As a consequence, up to permutations of the rows and columns, $U_{\rm PMNS}$ has the form

$$\begin{pmatrix} 0 & \times & \times \\ \times & \times & \times \\ \times & \times & \times \end{pmatrix}\,, \tag{4.40}$$

containing one zero element, which is ruled out by data.

4.3 Mixing Patterns from $S_4 \rtimes H_{\rm CP}$ Broken to $G_e = Z_2$ and $G_\nu = Z_2 \times H_{\rm CP}^\nu$

4.3.1 S_4 Group and Residual Symmetries

S_4 is the symmetric group of permutations of four objects. This group is isomorphic to the group of rotational symmetries of the cube. S_4 can be defined in terms of three generators S, T and U, satisfying [196] (see also Appendix A):

$$S^2 = T^3 = U^2 = (ST)^3 = (SU)^2 = (TU)^2 = (STU)^4 = 1\,. \tag{4.41}$$

Out of the 24 group elements, there are nine elements of order two which belong to two of five conjugacy classes of S_4 (see, e.g., [90]):

$$3\,\mathcal{C}_2 : \{S\,,\ TST^2\,,\ T^2ST\}\,, \tag{4.42}$$

$$6\,\mathcal{C}_2' : \{U\,,\ TU\,,\ SU\,,\ T^2U\,,\ STSU\,,\ ST^2SU\}\,. \tag{4.43}$$

Each of these nine elements generates a corresponding Z_2 subgroup of S_4. Each subgroup can furnish the residual symmetry of $M_e M_e^\dagger$, and, combined with compatible CP transformations, yield the residual symmetry of M_ν. Hence, we have 81 possible pairs of residual flavour symmetries. Many of them, however, being conjugate to each other, will lead to the same form of the PMNS matrix, as explained in Section 4.2.2. Thus, we first identify the pairs of elements $\{g_e, g_\nu\}$, which are not related by the similarity transformation given in Eq. (4.28). We find nine distinct cases for which $\{g_e, g_\nu\}$ can be chosen as

$$\{S,S\}\,,\quad \{U,U\}\,,\quad \{T^2ST,S\}\,,\quad \{S,U\}\,,\quad \{U,S\}\,,\quad \{SU,U\}\,, \tag{4.44}$$

$$\{S,TU\}\,,\quad \{TU,S\}\,,\quad \{TU,U\}\,. \tag{4.45}$$

The pair $\{S,S\}$ is clearly conjugate to $\{TST^2,TST^2\}$ and $\{T^2ST,T^2ST\}$, while $\{U,U\}$ is conjugate to $\{g_e,g_\nu\}$ with $g_e = g_\nu$ being one of the remaining 5 elements from conjugacy class $6\,\mathcal{C}_2'$ given in Eq. (4.43). The pairs $\{T^2ST,S\}$, $\{S,U\}$, $\{U,S\}$ and $\{SU,U\}$ are conjugate to 5 pairs each, and $\{S,TU\}$ and $\{TU,S\}$ to 11 pairs each. Finally, $\{TU,U\}$ is conjugate to 23 pairs. The complete lists of pairs of elements which are conjugate to each of these nine pairs are given in Appendix A.3.

The cases in Eq. (4.44) do not lead to phenomenologically viable results. The first two of them belong to the cases of Type I (see Section 4.2.3). The remaining four belong to Type II, since S_4 contains $Z_2^S \times Z_2^{TST^2} = \{1,\, S,\, TST^2\,, T^2ST\}$ and $Z_2^S \times Z_2^U = \{1,\, S,\, U\,, SU\}$ subgroups (see, e.g., [197]). Thus, we are left with three cases in Eq. (4.45).

We have chosen g_ν in such a way that it is S, U or TU for all the cases in Eq. (4.45). Now one needs to identify the remnant CP transformations X_ν compatible with each of these three elements. It is known that a gCP symmetry X compatible with $G_f = S_4$ is of the same form of G_f itself [88], i.e.,

$$X = \rho(g), \quad g \in S_4\,. \tag{4.46}$$

Thus, to find X_ν compatible with the g_ν of interest, we need to select those $X_\nu = \rho(g)$, which i) satisfy the consistency condition in Eq. (4.16) and ii) are symmetric in order to avoid a partially degenerate neutrino mass spectrum, as previously noted. The result reads:[4]

$$X_\nu = 1\,,\ (S)\,,\ U\,,\ (SU)\,,\ TST^2U\,,\ (T^2STU) \quad \text{for} \quad g_\nu = S\,; \tag{4.47}$$

$$X_\nu = 1\,,\ (U)\,,\ S\,,\ (SU) \quad \text{for} \quad g_\nu = U\,; \tag{4.48}$$

$$X_\nu = U\,,\ (T)\,,\ STS\,,\ (T^2STU) \quad \text{for} \quad g_\nu = TU\,. \tag{4.49}$$

Here, a gCP transformation in parentheses arises automatically as a remnant CP symmetry of M_ν if the X_ν preceding it is a remnant CP symmetry. This is a consequence of Eqs. (4.14) and (4.15), which imply that if X_ν is a residual CP symmetry of M_ν, then $\rho(g_\nu)X_\nu$ is a residual CP symmetry as well. Therefore,

[4] For notational simplicity, the representation symbol ρ is omitted.

there are three sets of remnant CP transformations compatible with Z_2^S, namely $H^\nu_{\rm CP} = \{1, S\}$, $\{U, SU\}$, and $\{TST^2U, T^2STU\}$, two sets compatible with Z_2^U, which are $H^\nu_{\rm CP} = \{1, U\}$ and $\{S, SU\}$, and two sets consistent with Z_2^{TU}, which read $H^\nu_{\rm CP} = \{U, T\}$ and $\{STS, T^2STU\}$.

To summarise, there are 7 possible triplets (g_e, g_ν, X_ν), with $\{g_e, g_\nu\}$ as in Eq. (4.45). In what follows, we will consider them one by one and classify the phenomenologically viable mixing patterns they lead to. Before starting, however, let us point out that the study to which the present chapter pertains, unless otherwise noted, makes use of the results of the global analysis of Ref. [38]. Adopting these results, the 3σ ranges of the absolute values of the PMNS matrix elements read:

$$|U_{\rm PMNS}|_{3\sigma} = \begin{pmatrix} 0.796 \to 0.855 & 0.497 \to 0.587 & 0.140 \to 0.153 \\ 0.245 \to 0.513 & 0.543 \to 0.709 & 0.614 \to 0.768 \\ 0.244 \to 0.510 & 0.456 \to 0.642 & 0.624 \to 0.776 \end{pmatrix} \tag{4.50}$$

for a neutrino mass spectrum with normal ordering, and

$$|U_{\rm PMNS}|_{3\sigma} = \begin{pmatrix} 0.796 \to 0.855 & 0.497 \to 0.587 & 0.140 \to 0.153 \\ 0.223 \to 0.503 & 0.452 \to 0.703 & 0.614 \to 0.783 \\ 0.257 \to 0.526 & 0.464 \to 0.712 & 0.605 \to 0.775 \end{pmatrix} \tag{4.51}$$

for a neutrino mass spectrum with inverted ordering.

4.3.2 Explicit Forms of the PMNS Matrix

First, we present an explicit example of constructing the PMNS matrix in the case of $g_e = S$, $g_\nu = TU$ and $H^\nu_{\rm CP} = \{U, T\}$. We work in the basis for S_4 from Ref. [198], in which the matrices for the generators S, T and U in the 3-dimensional representation read (cf. Eq. (1.21)):

$$S = \frac{1}{3}\begin{pmatrix} -1 & 2 & 2 \\ 2 & -1 & 2 \\ 2 & 2 & -1 \end{pmatrix}, \quad T = \begin{pmatrix} 1 & 0 & 0 \\ 0 & \omega^2 & 0 \\ 0 & 0 & \omega \end{pmatrix} \quad \text{and} \quad U = -\begin{pmatrix} 1 & 0 & 0 \\ 0 & 0 & 1 \\ 0 & 1 & 0 \end{pmatrix}, \tag{4.52}$$

where $\omega = e^{2\pi i/3}$, and for simplicity we use the same notation for generators and their 3-dimensional representation matrices. A matrix Ω_e diagonalising $\rho(g_e) = S$ (see Eq. (4.4)) is given by

$$\Omega_e = \frac{1}{\sqrt{6}}\begin{pmatrix} \sqrt{2} & -\sqrt{3} & -1 \\ \sqrt{2} & 0 & 2 \\ \sqrt{2} & \sqrt{3} & -1 \end{pmatrix}. \tag{4.53}$$

The matrix Ω_ν, such that $\Omega_\nu\, \Omega_\nu^T = X_\nu = U$ (see Eq. (4.21)), reads

$$\Omega_\nu = \frac{1}{\sqrt{2}}\begin{pmatrix} 0 & 0 & \sqrt{2}i \\ e^{\frac{2\pi i}{3}} & -e^{\frac{i\pi}{6}} & 0 \\ e^{\frac{i\pi}{3}} & e^{-\frac{i\pi}{6}} & 0 \end{pmatrix}. \tag{4.54}$$

Using the master formula in Eq. (4.27) one obtains that, up to permutations of the rows and columns, $U_{\rm PMNS}$ has the form

$$\begin{pmatrix} \frac{i}{\sqrt{2}} & \times & \times \\ \times & \times & \times \\ \times & \times & \times \end{pmatrix}, \tag{4.55}$$

where "$\times$" entries are functions of the free parameters θ^ν, θ^e and δ^e. Taking into account Eqs. (4.50) and (4.51), the fixed element with the absolute value of $1/\sqrt{2} \simeq 0.707$ can be $(U_{\rm PMNS})_{\mu 2}$, $(U_{\rm PMNS})_{\mu 3}$,

$(U_{\rm PMNS})_{\tau 2}$ or $(U_{\rm PMNS})_{\tau 3}$. Note that $|(U_{\rm PMNS})_{\tau 2}| = 0.707$ is outside the 3σ range in the case of the NO neutrino mass spectrum, while $|(U_{\rm PMNS})_{\mu 2}| = 0.707$ is at the border of the 3σ allowed ranges for both the NO and IO spectra.

Let us consider as an example the first possibility, i.e., $P_e = P_\nu = P_{213}$, leading to $|(U_{\rm PMNS})_{\mu 2}| = 1/\sqrt{2}$. In this case the mixing angles are related to the free parameters θ^ν, θ^e and δ^e as follows:

$$\sin^2\theta_{13} = |(U_{\rm PMNS})_{e3}|^2 = \frac{1}{24}\Big[\cos 2\theta^\nu\left(\sin 2\theta^e\left(3\sin\delta^e + 4\sqrt{3}\cos\delta^e\right) + 4\cos 2\theta^e - 1\right) + \sqrt{2}\sin 2\theta^\nu\left(\sin 2\theta^e\left(\sqrt{3}\cos\delta^e - 6\sin\delta^e\right) + \cos 2\theta^e + 2\right) - 3\sin\delta^e\sin 2\theta^e + 9\Big]\,, \tag{4.56}$$

$$\sin^2\theta_{23} = \frac{|(U_{\rm PMNS})_{\mu 3}|^2}{1 - |(U_{\rm PMNS})_{e3}|^2} = \frac{3 - 2\sqrt{2}\sin 2\theta^\nu + \cos 2\theta^\nu}{12\cos^2\theta_{13}}\,, \tag{4.57}$$

$$\sin^2\theta_{12} = \frac{|(U_{\rm PMNS})_{e2}|^2}{1 - |(U_{\rm PMNS})_{e3}|^2} = \frac{1 + \sin\delta^e\sin 2\theta^e}{4\cos^2\theta_{13}}\,. \tag{4.58}$$

Moreover, from $|(U_{\rm PMNS})_{\mu 2}| = 1/\sqrt{2}$ we obtain a "sum rule" for $\cos\delta$:

$$\cos\delta = \frac{2\cos^2\theta_{12}\cos^2\theta_{23} + 2\sin^2\theta_{12}\sin^2\theta_{23}\sin^2\theta_{13} - 1}{\sin 2\theta_{12}\sin 2\theta_{23}\sin\theta_{13}}\,. \tag{4.59}$$

Once one of the elements of the PMNS matrix is fixed, there are still 4 possible configurations, namely, a permutation of the two remaining columns, a permutation of the two remaining rows and a joint permutation of both. For instance, in the case considered above, aside from $P_e = P_\nu = P_{213}$, we can have a fixed $(U_{\rm PMNS})_{\mu 2}$ with $(P_e, P_\nu) = (P_{213}, P_{231})$, (P_{312}, P_{213}) and (P_{312}, P_{231}). These combinations of the permutation matrices will not lead, however, to different mixing patterns by virtue of the following relations:

$$R_{23}\left(\theta^\nu\right) P_{231} = R_{23}\left(\theta^\nu + \pi/2\right) P_{213}\ {\rm diag}\left(-1,1,1\right)\,, \tag{4.60}$$

$$P_{312}\, U_{23}\left(\theta^e, \delta^e\right) = {\rm diag}\left(e^{i\delta^e}, 1, -e^{-i\delta^e}\right) P_{213}\, U_{23}\left(\theta^e + \pi/2, \delta^e\right)\,. \tag{4.61}$$

Indeed, e.g., in the case of $(P_e, P_\nu) = (P_{312}, P_{231})$, defining $\hat{\theta}^\nu = \theta^\nu + \pi/2$, $\hat{\theta}^e = \theta^e + \pi/2$ and absorbing the matrix ${\rm diag}\left(-1,1,1\right)$ in the matrix Q_ν, we obtain the same PMNS matrix as in the case of $(P_e, P_\nu) = (P_{213}, P_{213})$:

$$U_{\rm PMNS} = P_{213}\, U_{23}(\hat{\theta}^e, \delta^e)\, \Omega_e^\dagger\, \Omega_\nu\, R_{23}(\hat{\theta}^\nu)\, P_{213}\, Q_\nu\,. \tag{4.62}$$

The phases in the matrix ${\rm diag}\left(e^{i\delta^e}, 1, -e^{-i\delta^e}\right)$ in Eq. (4.61) are unphysical and are not shown.

We list in Table 4.1 the matrices Ω_e and Ω_ν for all 7 phenomenologically viable pairs of residual symmetries $\{G_e, G_\nu\} = \{Z_2^{g_e}, Z_2^{g_\nu} \times H^\nu_{\rm CP}\}$. It turns out, however, that 4 of these 7 pairs, namely, $\{G_e, G_\nu\} = \{Z_2^S, Z_2^{TU} \times H^\nu_{\rm CP}\}$ with $H^\nu_{\rm CP} = \{U, T\}$ and $\{STS, T^2STU\}$, and $\{G_e, G_\nu\} = \{Z_2^{TU}, Z_2^S \times H^\nu_{\rm CP}\}$ with $H^\nu_{\rm CP} = \{U, SU\}$ and $\{TST^2U, T^2STU\}$, lead to the same predictions for the mixing parameters. We demonstrate this in Appendix B.1.

4.3.3 Extracting Mixing Parameters and Statistical Analysis

In this subsection we perform a statistical analysis of the predictions for the neutrino mixing angles and CPV phases for each of the 4 distinctive sets of the residual flavour and CP symmetries, which are:

g_e, Ω_e	g_ν	$H^\nu_{\rm CP}$	Ω_ν
$g_e = S$ $\frac{1}{\sqrt{6}}\begin{pmatrix}\sqrt{2} & -\sqrt{3} & -1\\ \sqrt{2} & 0 & 2\\ \sqrt{2} & \sqrt{3} & -1\end{pmatrix}$	TU	$\{U, T\}$	$\frac{1}{\sqrt{2}}\begin{pmatrix}0 & 0 & \sqrt{2}i\\ e^{\frac{2\pi i}{3}} & -e^{\frac{i\pi}{6}} & 0\\ e^{\frac{i\pi}{3}} & e^{-\frac{i\pi}{6}} & 0\end{pmatrix}$
		$\{STS, T^2STU\}$	$\frac{1}{\sqrt{6}}\begin{pmatrix}0 & 2i & \sqrt{2}\\ \sqrt{3}e^{\frac{i\pi}{6}} & e^{\frac{i\pi}{6}} & -\sqrt{2}e^{-\frac{i\pi}{3}}\\ \sqrt{3}e^{-\frac{i\pi}{6}} & -e^{-\frac{i\pi}{6}} & -\sqrt{2}e^{\frac{i\pi}{3}}\end{pmatrix}$
$g_e = TU$ $\frac{1}{\sqrt{2}}\begin{pmatrix}0 & 0 & \sqrt{2}\\ e^{\frac{i\pi}{3}} & e^{-\frac{2\pi i}{3}} & 0\\ 1 & 1 & 0\end{pmatrix}$	S	$\boldsymbol{\{1, S\}}$	$\frac{1}{\sqrt{6}}\begin{pmatrix}\sqrt{2} & -\sqrt{3} & -1\\ \sqrt{2} & 0 & 2\\ \sqrt{2} & \sqrt{3} & -1\end{pmatrix}$
		$\boldsymbol{\{U, SU\}}$	$\frac{i}{\sqrt{6}}\begin{pmatrix}\sqrt{2} & -2 & 0\\ \sqrt{2} & 1 & -\sqrt{3}i\\ \sqrt{2} & 1 & \sqrt{3}i\end{pmatrix}$
		$\{TST^2U, T^2STU\}$	$\frac{1}{\sqrt{3}}\begin{pmatrix}1 & i & 1\\ 1 & e^{-\frac{i\pi}{6}} & -e^{-\frac{i\pi}{3}}\\ 1 & -e^{\frac{i\pi}{6}} & -e^{\frac{i\pi}{3}}\end{pmatrix}$
	U	$\boldsymbol{\{1, U\}}$	$\frac{1}{\sqrt{2}}\begin{pmatrix}0 & 0 & \sqrt{2}\\ -1 & 1 & 0\\ 1 & 1 & 0\end{pmatrix}$
		$\boldsymbol{\{S, SU\}}$	$-\frac{i}{\sqrt{6}}\begin{pmatrix}0 & \sqrt{2}i & -2\\ \sqrt{3} & \sqrt{2}i & 1\\ -\sqrt{3} & \sqrt{2}i & 1\end{pmatrix}$

Table 4.1: The matrices Ω_e and Ω_ν dictated by the residual symmetries $G_e = Z_2^{g_e}$ and $G_\nu = Z_2^{g_\nu} \times H^\nu_{\rm CP}$ for all seven phenomenologically viable pairs of G_e and G_ν. For each pair $H^\nu_{\rm CP} = \{X_{\nu 1}, X_{\nu 2}\}$ of remnant gCP transformations, the given matrix Ω_ν provides the Takagi factorisation of the first element, i.e., $X_{\nu 1} = \Omega_\nu \, \Omega_\nu^T$.[5] The 4 inequivalent groups of cases considered in our analysis are indicated in bold.

- Group A of cases: $\{G_e, G_\nu\} = \{Z_2^{TU}, Z_2^S \times H^\nu_{\rm CP}\}$ with $H^\nu_{\rm CP} = \{1, S\}$,
- Group B of cases: $\{G_e, G_\nu\} = \{Z_2^{TU}, Z_2^S \times H^\nu_{\rm CP}\}$ with $H^\nu_{\rm CP} = \{U, SU\}$,
- Group C of cases: $\{G_e, G_\nu\} = \{Z_2^{TU}, Z_2^U \times H^\nu_{\rm CP}\}$ with $H^\nu_{\rm CP} = \{1, U\}$,
- Group D of cases: $\{G_e, G_\nu\} = \{Z_2^{TU}, Z_2^U \times H^\nu_{\rm CP}\}$ with $H^\nu_{\rm CP} = \{S, SU\}$.

An individual case is specified by the choice of a pair of residual symmetries and of the permutation matrices P_e and P_ν. For each case, one has expressions for $\sin^2\theta_{ij}$ in terms of θ^ν, θ^e and δ^e of the

type of Eqs. (4.56) – (4.58). Moreover, exploiting sum rules for $\cos\delta$ analogous to that in Eq. (4.59) and computing the rephasing invariant (cf. Eq. (1.8))

$$\mathcal{J}_{\rm CP} = {\rm Im}\left\{(U_{\rm PMNS})^*_{e1}\,(U_{\rm PMNS})^*_{\mu 3}\,(U_{\rm PMNS})_{e3}\,(U_{\rm PMNS})_{\mu 1}\right\}\,, \tag{4.63}$$

which determines the magnitude of CPV effects in neutrino oscillations and which in the standard parametrisation of the PMNS matrix is proportional to $\sin\delta$,

$$\mathcal{J}_{\rm CP} = \frac{1}{8}\sin 2\theta_{12}\sin 2\theta_{23}\sin 2\theta_{13}\cos\theta_{13}\sin\delta\,, \tag{4.64}$$

we know the value of δ for any θ^ν, θ^e and δ^e. Similarly, making use of the two charged lepton rephasing invariants,[6] associated with the Majorana phases [199–202],

$$I_1 = {\rm Im}\left\{(U_{\rm PMNS})^*_{e1}\,(U_{\rm PMNS})_{e2}\right\} \quad \text{and} \quad I_2 = {\rm Im}\left\{(U_{\rm PMNS})^*_{e1}\,(U_{\rm PMNS})_{e3}\right\}\,, \tag{4.65}$$

and the corresponding real parts

$$R_1 = {\rm Re}\left\{(U_{\rm PMNS})^*_{e1}\,(U_{\rm PMNS})_{e2}\right\} \quad \text{and} \quad R_2 = {\rm Re}\left\{(U_{\rm PMNS})^*_{e1}\,(U_{\rm PMNS})_{e3}\right\}\,, \tag{4.66}$$

which in the standard parametrisation of the PMNS matrix read:

$$I_1 = \sin\theta_{12}\cos\theta_{12}\cos^2\theta_{13}\sin\left(\alpha_{21}/2\right)\,, \quad I_2 = \cos\theta_{12}\sin\theta_{13}\cos\theta_{13}\sin\left(\alpha_{31}/2-\delta\right)\,, \tag{4.67}$$

$$R_1 = \sin\theta_{12}\cos\theta_{12}\cos^2\theta_{13}\cos\left(\alpha_{21}/2\right)\,, \quad R_2 = \cos\theta_{12}\sin\theta_{13}\cos\theta_{13}\cos\left(\alpha_{31}/2-\delta\right)\,, \tag{4.68}$$

we also obtain the values of α_{21} and α_{31} for any θ^ν, θ^e and δ^e.

Further, we scan randomly over $\theta^\nu \in [0,\pi)$, $\theta^e \in [0,\pi)$ and $\delta^e \in [0,2\pi)$ and calculate the values of $\sin^2\theta_{ij}$ and the CPV phases. We require the $\sin^2\theta_{ij}$ to lie in the corresponding 3σ ranges given in Table 1.2.[7] The obtained values of $\sin^2\theta_{ij}$ and δ can be characterised by a certain value of a χ^2 function, constructed as follows:

$$\chi^2\left(\vec{x}\right) = \sum_{i=1}^{4}\chi^2_i\left(x_i\right)\,, \tag{4.69}$$

where $\vec{x} = \{x_i\} = \{\sin^2\theta_{12}, \sin^2\theta_{13}, \sin^2\theta_{23}, \delta\}$ and χ^2_i are one-dimensional projections for NO and IO taken from Ref. [38] (see also Fig. 1.1). We take here a conservative approach and treat both orderings on an equal footing. To see the restrictions on the mixing parameters imposed by flavour and CP symmetries we consider all 15 different pairs of the mixing parameters. For each pair we divide the plane into bins and find a minimum of the χ^2 function in each bin. We present results in terms of heat maps with colour denoting the minimal value of χ^2. The results obtained in each case are discussed in the following subsection.

[5] $X_{\nu 2}$ is instead factorised as $X_{\nu 2} = \tilde{\Omega}_\nu\,\tilde{\Omega}_\nu^T$, with $\tilde{\Omega}_\nu = \Omega_\nu\,{\rm diag}(1,i,i)$, as follows from $X_{\nu 2} = \rho(g_\nu)\,X_{\nu 1} = \Omega_\nu\,\Omega_\nu^\dagger\,\rho(g_\nu)\,\Omega_\nu\,\Omega_\nu^T = \Omega_\nu\,\rho(g_\nu)^{\rm d}\,\Omega_\nu^T$, with $\rho(g_\nu)^{\rm d}$ defined in Eq. (4.18).

[6] In their general form, when one keeps explicit the unphysical phases ξ_j in the Majorana condition $C\,\overline{\nu_j}^T = \xi_j\,\nu_j$, $j = 1,2,3$, the rephasing invariants related to the Majorana phases involve ξ_j and are invariant under phase transformations of both the charged lepton and neutrino fields (see, for example, Eqs. (22) – (28) in Ref. [199]). We have set $\xi_j = 1$.

[7] These ranges are overall wider than those in Table 1.3, meaning points found are unchanged up to the χ^2 landscape.

4.3.4 Results and Discussion

We now systematically go through all different potentially viable cases and summarise their particular features. In each case we concentrate on results for the ordering for which a better compatibility with the global data is attained. Note that results for NO and IO differ only i) due to the fact that the 3σ ranges of $\sin^2\theta_{13}$ and $\sin^2\theta_{23}$ depend slightly on the ordering and ii) in the respective χ^2 landscapes. Moreover, we present numerical and graphical results for the Majorana phases obtained for $k_1 = k_2 = 0$, where k_1 and k_2 are defined in Eq. (4.26). However, one should keep in mind that all four (k_1, k_2) pairs, where $k_i = 0, 1$, are allowed, meaning Majorana phases are constrained mod π. Whenever $k_{1(2)} = 1$, the predicted range for $\alpha_{21(31)}$ shifts by π. The values of the k_i are important for the predictions of the neutrinoless double beta decay effective Majorana mass, which we present in Section 4.4.

Group A: $\{G_e, G_\nu\} = \{Z_2^{TU}, Z_2^S \times H_{\rm CP}^\nu\}$ with $H_{\rm CP}^\nu = \{1, S\}$. Using the corresponding matrices Ω_e and Ω_ν from Table 4.1 and the master formula of Eq. (4.27), we find the following form of the PMNS matrix (up to permutations of rows and columns and the phases in the matrix Q_ν):

$$U_{\rm PMNS}^{\rm A} = \frac{1}{2\sqrt{3}} \begin{pmatrix} \sqrt{6}\, e^{-\frac{i\pi}{6}} & \sqrt{3}\, e^{i\theta^\nu} & \sqrt{3}\, e^{-i\theta^\nu} \\ \sqrt{2}\, c^e e^{\frac{i\pi}{3}} + 2\, s^e e^{-i\delta^e} & a_1\left(\theta^\nu, \theta^e, \delta^e\right) & a_2\left(\theta^\nu, \theta^e, \delta^e\right) \\ 2\, c^e - \sqrt{2}\, s^e e^{\frac{i\pi}{3}} e^{i\delta^e} & a_3\left(\theta^\nu, \theta^e, \delta^e\right) & a_4\left(\theta^\nu, \theta^e, \delta^e\right) \end{pmatrix}, \tag{4.70}$$

with $c^e \equiv \cos\theta^e$, $s^e \equiv \sin\theta^e$, $c^\nu \equiv \cos\theta^\nu$, $s^\nu \equiv \sin\theta^\nu$ and

$$a_1\left(\theta^\nu, \theta^e, \delta^e\right) = \left[\sqrt{3} c^\nu + \left(2 - i\sqrt{3}\right) s^\nu\right] c^e + \sqrt{2}\left(s^\nu - \sqrt{3}\, c^\nu\right) s^e e^{-i\delta^e}, \tag{4.71}$$

$$a_2\left(\theta^\nu, \theta^e, \delta^e\right) = \left[\sqrt{3} s^\nu - \left(2 - i\sqrt{3}\right) c^\nu\right] c^e - \sqrt{2}\left(c^\nu + \sqrt{3}\, s^\nu\right) s^e e^{-i\delta^e}, \tag{4.72}$$

$$a_3\left(\theta^\nu, \theta^e, \delta^e\right) = \sqrt{2}\left(s^\nu - \sqrt{3}\, c^\nu\right) c^e - \left[\sqrt{3} c^\nu + \left(2 - i\sqrt{3}\right) s^\nu\right] s^e e^{i\delta^e}, \tag{4.73}$$

$$a_4\left(\theta^\nu, \theta^e, \delta^e\right) = -\sqrt{2}\left(c^\nu + \sqrt{3}\, s^\nu\right) c^e - \left[\sqrt{3}\, s^\nu - \left(2 - i\sqrt{3}\right) c^\nu\right] s^e e^{i\delta^e}. \tag{4.74}$$

From Eq. (4.70), we see that the absolute values of the elements of the first row are fixed. Namely, the modulus of the first element is equal to $1/\sqrt{2}$, while the moduli of the second and third elements equal $1/2$. Taking into account Eqs. (4.50) and (4.51), this implies that there are only two potentially viable cases: i) with $|(U_{\rm PMNS})_{\mu 1}| = |(U_{\rm PMNS})_{\mu 2}| = 1/2$ and $|(U_{\rm PMNS})_{\mu 3}| = 1/\sqrt{2}$, and ii) with $|(U_{\rm PMNS})_{\tau 1}| = |(U_{\rm PMNS})_{\tau 2}| = 1/2$ and $|(U_{\rm PMNS})_{\tau 3}| = 1/\sqrt{2}$.

• **Case A1: $|(U_{\rm PMNS})_{\mu 1}| = |(U_{\rm PMNS})_{\mu 2}| = 1/2$, $|(U_{\rm PMNS})_{\mu 3}| = 1/\sqrt{2}$ ($P_e = P_{213}$, $P_\nu = P_{321}$).** In this case we obtain

$$\sin^2\theta_{23} = \frac{1}{2\left(1 - \sin^2\theta_{13}\right)} = \frac{1}{2}\left(1 + \sin^2\theta_{13}\right) + \mathcal{O}\left(\sin^4\theta_{13}\right). \tag{4.75}$$

This means that only a narrow interval $\sin^2\theta_{23} \in [0.510, 0.512]$ is allowed using the 3σ region for $\sin^2\theta_{13}$. From the equality $|(U_{\rm PMNS})_{\mu 1}| = 1/2$, which we find to hold in this case, it follows that $\cos\delta$ satisfies the following sum rule:

$$\cos\delta = \frac{1 - 4\sin^2\theta_{12}\cos^2\theta_{23} - 4\cos^2\theta_{12}\sin^2\theta_{23}\sin^2\theta_{13}}{2\sin 2\theta_{12}\sin 2\theta_{23}\sin\theta_{13}}, \tag{4.76}$$

where the mixing angles in addition are correlated among themselves. We find that $\sin^2\theta_{13}$ is constrained to lie in the interval $(0.0213, 0.0240(2)]$ for NO (IO) and, hence, $\sin^2\theta_{23}$ in $[0.5109, 0.5123(4)]$. This range of values of $\sin^2\theta_{23}$ is not compatible with its 2σ range. Moreover, $\sin^2\theta_{12}$ is found to be between approximately 0.345 and 0.354, which is outside its 2σ range as well. In what concerns the CPV phases, the predicted values of δ are distributed around 0, namely, $\delta \in [-0.11\pi, 0.11\pi]$, while $\alpha_{21} \in (0.93\pi, 1.07\pi)$ mod π, and the values of α_{31} fill the whole range, i.e., $\alpha_{31} \in [0, 2\pi)$. These numbers, presented for the NO spectrum, remain practically unchanged for the IO spectrum. However, the global minimum $\chi^2_{\rm min}$ of the χ^2 function, defined in Eq. (4.69), yields approximately 22 (19) for NO (IO), which implies that this case is strongly disfavoured by the global data.

- **Case A2: $|(U_{\rm PMNS})_{\tau 1}| = |(U_{\rm PMNS})_{\tau 2}| = 1/2$, $|(U_{\rm PMNS})_{\tau 3}| = 1/\sqrt{2}$ ($P_e = P_\nu = P_{321}$).** This case shares the predicted ranges for $\sin^2\theta_{12}$, $\sin^2\theta_{13}$, α_{21} and α_{31} with case A1, but differs in the predictions for $\sin^2\theta_{23}$ and δ. Again, there is a correlation between $\sin^2\theta_{13}$ and $\sin^2\theta_{23}$:

$$\sin^2\theta_{23} = \frac{1 - 2\sin^2\theta_{13}}{2\left(1 - \sin^2\theta_{13}\right)} = \frac{1}{2}\left(1 - \sin^2\theta_{13}\right) + \mathcal{O}\left(\sin^4\theta_{13}\right) , \tag{4.77}$$

which, in particular, implies that $\sin^2\theta_{23} \in [0.4877(6), 0.4891]$, which is not compatible with its 2σ range. We also find that $|(U_{\rm PMNS})_{\tau 1}| = 1/2$. This equality leads to the following sum rule:

$$\cos\delta = \frac{4\sin^2\theta_{12}\sin^2\theta_{23} + 4\cos^2\theta_{12}\cos^2\theta_{23}\sin^2\theta_{13} - 1}{2\sin 2\theta_{12}\sin 2\theta_{23}\sin\theta_{13}} . \tag{4.78}$$

It is worth noting that we should always keep in mind the correlations between the mixing angles in expressions of this type. The values of δ in this case lie around π, in the interval $[0.89\pi, 1.11\pi]$. As in the previous case, the global minimum of χ^2 is somewhat large, $\chi^2_{\rm min} \simeq 18.5$ (15) for NO (IO), meaning that this case is also strongly disfavoured.

Group B: $\{G_e, G_\nu\} = \{Z_2^{TU}, Z_2^S \times H^\nu_{\rm CP}\}$ with $H^\nu_{\rm CP} = \{U, SU\}$. For this choice of the residual symmetries, the PMNS matrix reads (up to permutations of rows and columns and the phases in the matrix Q_ν):

$$U^{\rm B}_{\rm PMNS} = \frac{1}{2\sqrt{3}} \begin{pmatrix} \sqrt{6}\, e^{\frac{i\pi}{3}} & \sqrt{3}\,(c^\nu + s^\nu)\, e^{\frac{i\pi}{3}} & \sqrt{3}\,(s^\nu - c^\nu)\, e^{\frac{i\pi}{3}} \\ -\sqrt{2}\, c^e e^{-\frac{i\pi}{6}} + 2\, i\, s^e e^{-i\delta^e} & b_1\left(\theta^\nu, \theta^e, \delta^e\right) & b_2\left(\theta^\nu, \theta^e, \delta^e\right) \\ 2\, i\, c^e + \sqrt{2}\, s^e e^{-\frac{i\pi}{6}} e^{i\delta^e} & b_3\left(\theta^\nu, \theta^e, \delta^e\right) & b_4\left(\theta^\nu, \theta^e, \delta^e\right) \end{pmatrix} , \tag{4.79}$$

with

$$b_1\left(\theta^\nu, \theta^e, \delta^e\right) = (3s^\nu - c^\nu)\, c^e e^{-\frac{i\pi}{6}} - 2\sqrt{2}\, i\, c^\nu s^e e^{-i\delta^e} , \tag{4.80}$$

$$b_2\left(\theta^\nu, \theta^e, \delta^e\right) = -\,(3c^\nu + s^\nu)\, c^e e^{-\frac{i\pi}{6}} - 2\sqrt{2}\, i\, s^\nu s^e e^{-i\delta^e} , \tag{4.81}$$

$$b_3\left(\theta^\nu, \theta^e, \delta^e\right) = -2\sqrt{2}\, i\, c^\nu c^e - (3s^\nu - c^\nu)\, s^e e^{-\frac{i\pi}{6}} e^{i\delta^e} , \tag{4.82}$$

$$b_4\left(\theta^\nu, \theta^e, \delta^e\right) = -2\sqrt{2}\, i\, s^\nu c^e + (3c^\nu + s^\nu)\, s^e e^{-\frac{i\pi}{6}} e^{i\delta^e} . \tag{4.83}$$

Equation (4.79) implies that the absolute value of one element of the PMNS matrix is predicted to be $1/\sqrt{2}$. Thus, we have four potentially viable cases.

• **Case B1: $|(U_{\rm PMNS})_{\mu 2}| = 1/\sqrt{2}$ ($P_e = P_\nu = P_{213}$).** Note that from Eqs. (4.50) and (4.51) it follows that this magnitude of the fixed element is inside its 3σ range for NO, but slightly outside the corresponding range for IO. Hence, we will focus on the results for NO. The characteristic feature of this case is the following sum rule for $\cos\delta$:

$$\cos\delta = \frac{2\cos^2\theta_{12}\cos^2\theta_{23} + 2\sin^2\theta_{12}\sin^2\theta_{23}\sin^2\theta_{13} - 1}{\sin 2\theta_{12}\sin 2\theta_{23}\sin\theta_{13}}\,, \tag{4.84}$$

which arises from the equality of $|(U_{\rm PMNS})_{\mu 2}|$ to $1/\sqrt{2}$. The pair correlations between the mixing parameters in this case are summarised in Fig. 4.1. The colour palette corresponds to values of χ^2 for NO. As can be seen, while all values of $\sin^2\theta_{13}$ in its 3σ range are allowed, the parameters $\sin^2\theta_{12}$ and $\sin^2\theta_{23}$ are found to lie in $[0.250, 0.308]$ and $[0.381, 0.425)$ intervals, respectively. The predicted values of δ span the range $[0.68\pi, 1.32\pi]$. Thus, CPV effects in neutrino oscillations due to the phase δ can be suppressed. The Majorana phases instead are distributed in relatively narrow regions, namely $\alpha_{21} \in [-0.16\pi, 0.16\pi]$ and $\alpha_{31} \in (-0.13\pi, 0.13\pi)$ mod π. In addition, δ is strongly correlated with α_{21} and α_{31}, which in turn exhibit a strong correlation between themselves. Finally, $\chi^2_{\rm min} \simeq 7$ for both NO and IO, i.e., this case is compatible with the global data.[8]

• **Case B2: $|(U_{\rm PMNS})_{\tau 2}| = 1/\sqrt{2}$ ($P_e = P_{321}$, $P_\nu = P_{213}$).** Note that this value of $|(U_{\rm PMNS})_{\tau 2}|$ is compatible at 3σ with the global data in the case of IO spectrum, but not in the case of NO spectrum, as can be seen from Eqs. (4.50) and (4.51). Thus, below we present results for the IO spectrum only. As in case B1, the whole 3σ range for $\sin^2\theta_{13}$ is allowed. The obtained ranges of values of α_{21} and α_{31} are the same of the preceding case. The range for $\sin^2\theta_{12}$ differs somewhat from that obtained in case B1, and it reads $\sin^2\theta_{12} \in [0.250, 0.328]$.[9] The predictions for $\sin^2\theta_{23}$ and δ are different. Now the following sum rule, derived from $|(U_{\rm PMNS})_{\tau 2}| = 1/\sqrt{2}$, holds:

$$\cos\delta = \frac{1 - 2\cos^2\theta_{12}\sin^2\theta_{23} - 2\sin^2\theta_{12}\cos^2\theta_{23}\sin^2\theta_{13}}{\sin 2\theta_{12}\sin 2\theta_{23}\sin\theta_{13}}\,. \tag{4.85}$$

The values of δ are concentrated in $[-0.38\pi, 0.38\pi]$. For $\sin^2\theta_{23}$ we find the range $(0.575, 0.636]$. The correlations between the phases are of the same type as in case B1. We summarise the results in Fig. 4.2. Finally, $\chi^2_{\rm min} \simeq 6$ in the case of IO and $\chi^2_{\rm min} \simeq 12.5$ for NO, which reflects incompatibility of this case at more than 3σ for the NO spectrum. This occurs mainly due to the predicted values of $\sin^2\theta_{23}$, which are outside its 2σ range for NO.

• **Case B3: $|(U_{\rm PMNS})_{\mu 3}| = 1/\sqrt{2}$ ($P_e = P_{213}$, $P_\nu = P_{321}$).** Since $|(U_{\rm PMNS})_{\mu 3}| = 1/\sqrt{2}$, the angles θ_{13} and θ_{23} are correlated as in case A1, i.e., according to Eq. (4.75). For IO this leads to $\sin^2\theta_{23} \in [0.5097, 0.5124]$ due to the fact that the whole 3σ range of $\sin^2\theta_{13}$ is found to be allowed, as can be seen from Fig. 4.3. Note that this range is outside the 2σ range of $\sin^2\theta_{23}$. In addition, we find that the whole 3σ range of the values of $\sin^2\theta_{12}$ can be reproduced. In contrast to case A1, $|(U_{\rm PMNS})_{\mu 1}|$

[8] The apparent contradiction between the obtained value of $\chi^2_{\rm min} \simeq 7$, which suggests compatibility also for IO, and the expectation of $\chi^2_{\rm min} \gtrsim 9$, according to Eq. (4.51), arises from the way we construct the χ^2 function (see Eq. (4.69)), which does not explicitly include covariances between the oscillation parameters.

[9] This difference is related to the fact that the 3σ range of $\sin^2\theta_{23}$ for IO, which reads $[0.384, 0.636]$, is not symmetric with respect to 0.5. The asymmetry of 0.02 translates to increase of the allowed range of $\sin^2\theta_{12}$ by approximately 0.02. This can be better understood from the top right plots in Figs. 4.1 and 4.2.

does not equal 1/2, but depends on θ^ν in the following way:

$$|(U_{\rm PMNS})_{\mu 1}|^2 = \frac{1 - \sin 2\theta^\nu}{4}. \tag{4.86}$$

From this equation we find

$$\cos\delta = \frac{1 - 4\sin^2\theta_{12}\cos^2\theta_{23} - 4\cos^2\theta_{12}\sin^2\theta_{23}\sin^2\theta_{13} - \sin 2\theta^\nu}{2\sin 2\theta_{12}\sin 2\theta_{23}\sin\theta_{13}}\,, \tag{4.87}$$

i.e., $\cos\delta$ depends on θ^ν explicitly (not only via θ_{12}, θ_{23} and θ_{13}). Any value of δ between 0 and 2π turns out to be allowed (see Fig. 4.3). The Majorana phases, however, are constrained to lie in the following intervals: $\alpha_{21} \in [-0.23\pi, 0.23\pi]$ and $\alpha_{31} \in (-0.18\pi, 0.18\pi)$, mod π. Moreover, both phases α_{21} and α_{31} are correlated in one and the same peculiar way with the phase δ. The correlation between α_{21} and α_{31} is similar to those in cases B1 and B2 (cf. Figs. 4.1 and 4.2). Due to the predicted values of $\sin^2\theta_{23}$, which belong to the upper octant, IO is preferred over NO in this analysis, the corresponding $\chi^2_{\rm min}$ being approximately 5 and 8.5.

• **Case B4: $|(U_{\rm PMNS})_{\tau 3}| = 1/\sqrt{2}$ ($P_e = P_\nu = P_{321}$).** The predicted ranges of all the mixing parameters are the same of case B3, except for $\sin^2\theta_{23}$, which respects the relation in Eq. (4.77), and thus belongs to $[0.4876, 0.4903]$ in the case of IO spectrum. As in the previous case, this interval falls outside the 2σ range of $\sin^2\theta_{23}$. The results obtained in this case for the IO spectrum are presented in Fig. 4.4. Similarly to the preceding case, we find

$$|(U_{\rm PMNS})_{\tau 1}|^2 = \frac{1 - \sin 2\theta^\nu}{4}\,, \tag{4.88}$$

which leads to

$$\cos\delta = \frac{\sin 2\theta^\nu + 4\sin^2\theta_{12}\sin^2\theta_{23} + 4\cos^2\theta_{12}\cos^2\theta_{23}\sin^2\theta_{13} - 1}{2\sin 2\theta_{12}\sin 2\theta_{23}\sin\theta_{13}}\,. \tag{4.89}$$

The correlation between the Majorana phases is similar to that in the previous case. Also in this case, $\chi^2_{\rm min} \simeq 4.5$ for IO is lower than that of approximately 6.5 for NO, the reason being again the predicted range of $\sin^2\theta_{23}$.

Group C: $\{G_e, G_\nu\} = \{Z_2^{TU}, Z_2^U \times H^\nu_{\rm CP}\}$ with $H^\nu_{\rm CP} = \{1, U\}$. Using the corresponding matrices Ω_e and Ω_ν given in Table 4.1 and Eq. (4.27), we obtain the following form of the PMNS matrix (up to permutations of rows and columns and the phases in the matrix Q_ν):

$$U^{\rm C}_{\rm PMNS} = \frac{1}{2}\begin{pmatrix} e^{i\frac{\pi}{3}} & \sqrt{3}\,c^\nu e^{-i\frac{\pi}{6}} & \sqrt{3}\,s^\nu e^{-i\frac{\pi}{6}} \\ \sqrt{3}\,c^e e^{-i\frac{\pi}{6}} & c^\nu c^e e^{i\frac{\pi}{3}} - 2\,s^\nu s^e e^{-i\delta^e} & s^\nu c^e e^{i\frac{\pi}{3}} + 2\,c^\nu s^e e^{-i\delta^e} \\ -\sqrt{3}\,s^e e^{-i\frac{\pi}{6}} e^{i\delta^e} & -2\,s^\nu c^e - c^\nu s^e e^{i\frac{\pi}{3}} e^{i\delta^e} & 2\,c^\nu c^e - s^\nu s^e e^{i\frac{\pi}{3}} e^{i\delta^e} \end{pmatrix}. \tag{4.90}$$

Thus, this pair of residual symmetries leads the absolute value of the fixed element to be 1/2. Taking into account the uncertainties in the values of the neutrino mixing parameters, Eqs. (4.50) and (4.51), we have to consider five potentially viable cases corresponding to $(U_{\rm PMNS})_{e2}$, $(U_{\rm PMNS})_{\mu 1}$, $(U_{\rm PMNS})_{\tau 1}$, $(U_{\rm PMNS})_{\mu 2}$ or $(U_{\rm PMNS})_{\tau 2}$ being the fixed element.

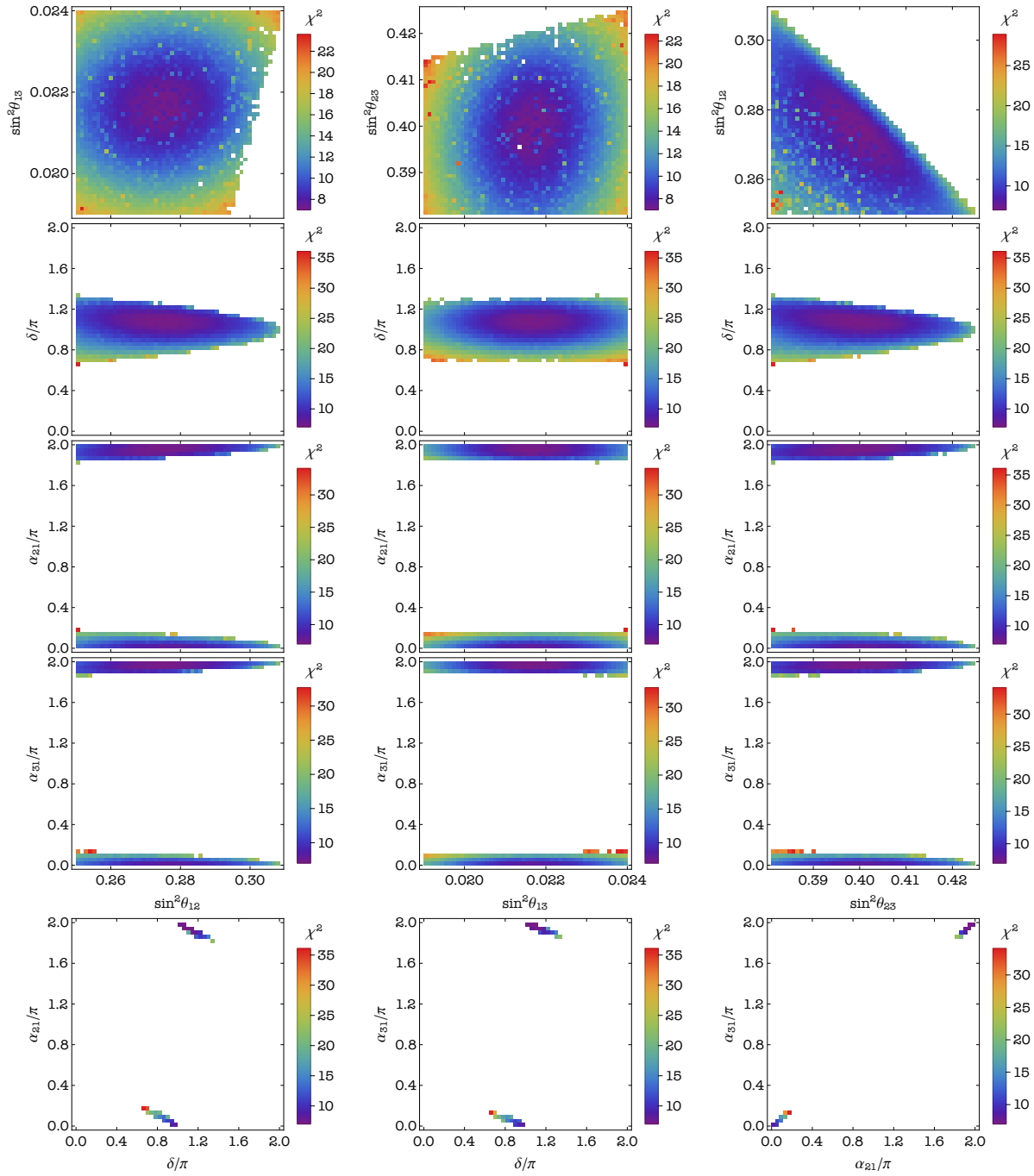

Figure 4.1: Correlations between the neutrino mixing parameters in case B1, for a mass spectrum with NO. The values of all the three mixing angles are required to lie in their respective 3σ ranges.

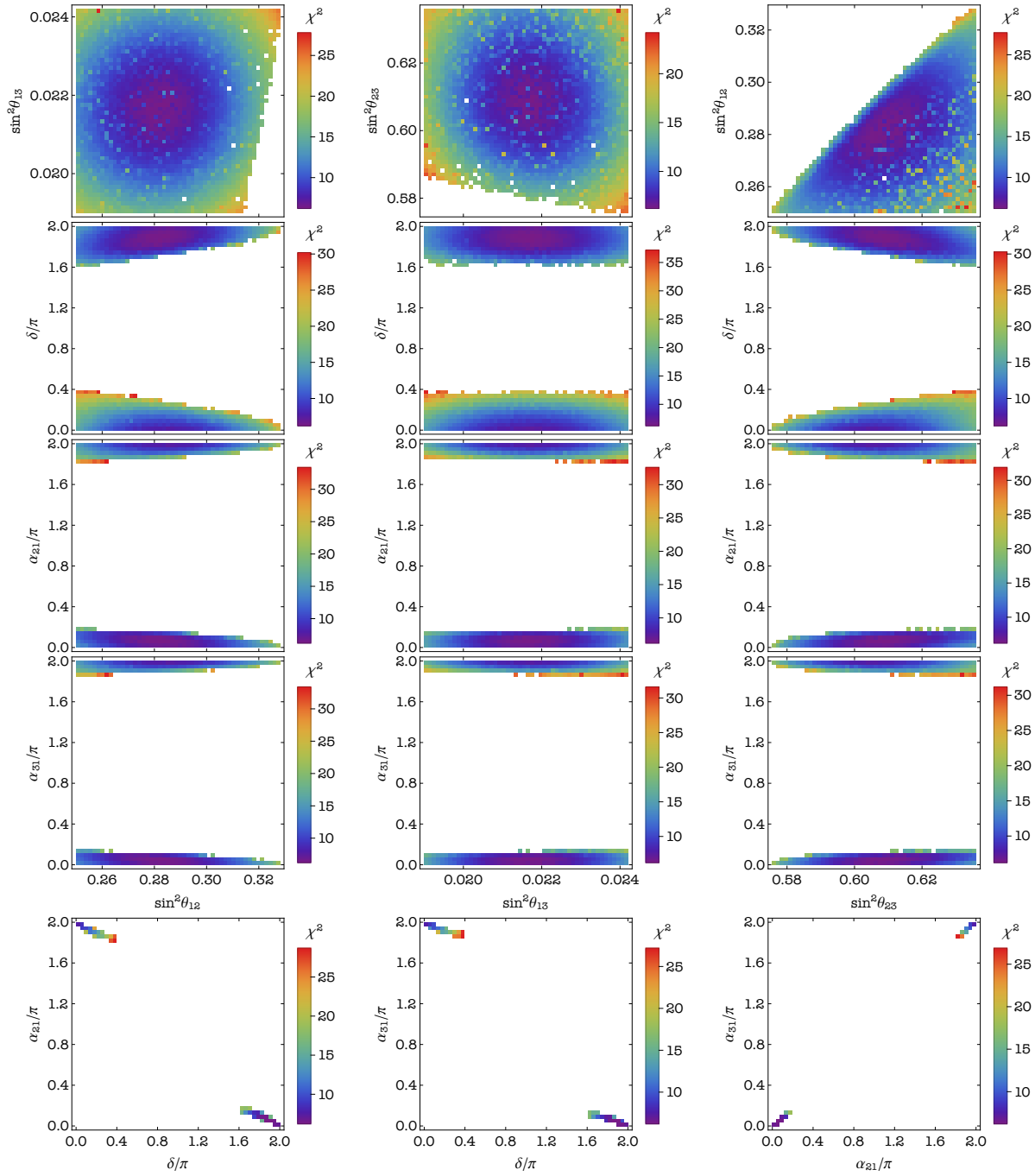

Figure 4.2: Correlations between the neutrino mixing parameters in case B2, for a mass spectrum with IO. The values of all the three mixing angles are required to lie in their respective 3σ ranges.

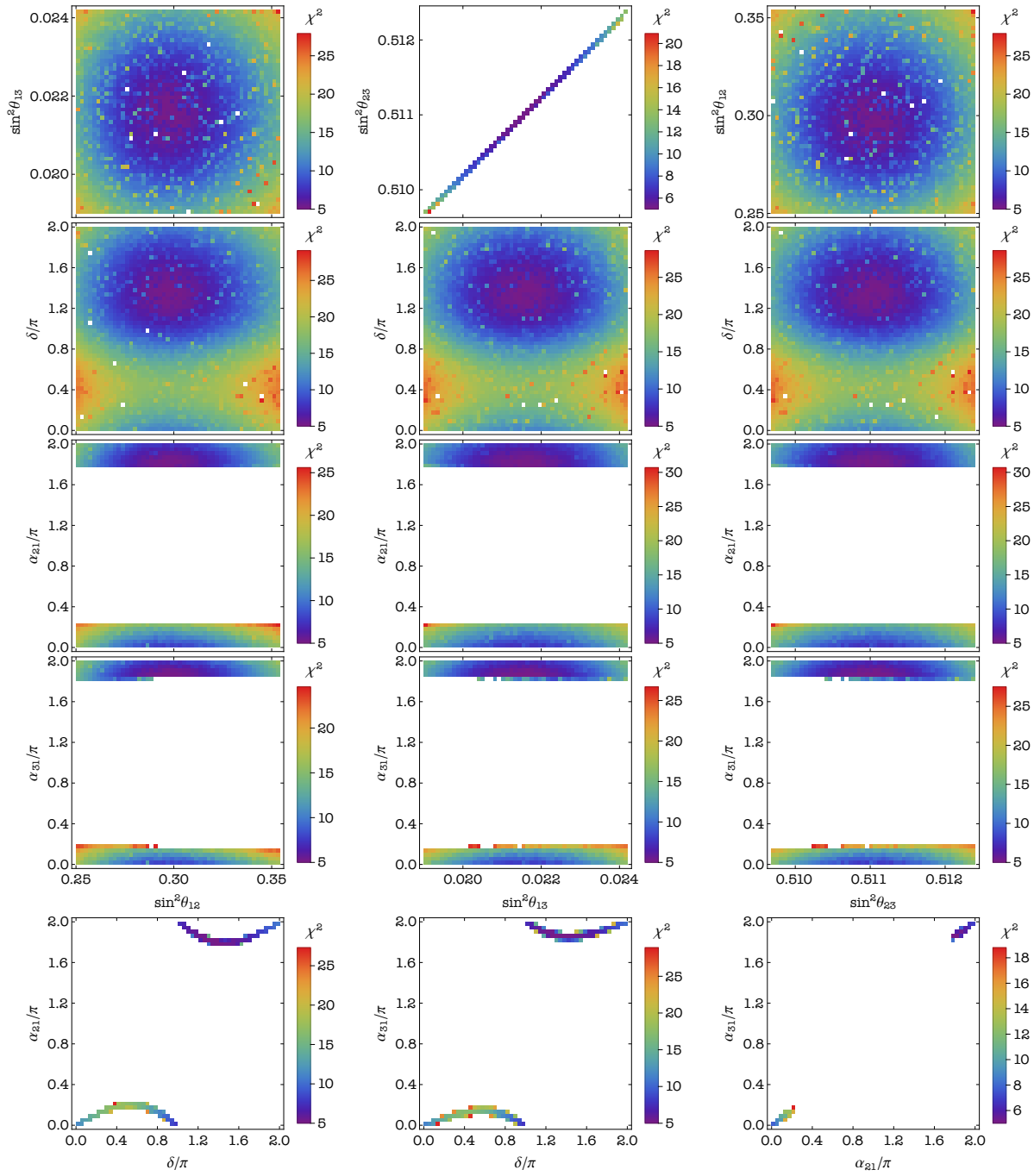

Figure 4.3: Correlations between the neutrino mixing parameters in case B3, for a mass spectrum with IO. The values of all the three mixing angles are required to lie in their respective 3σ ranges. Note that this case is not compatible with the 2σ range of $\sin^2\theta_{23}$.

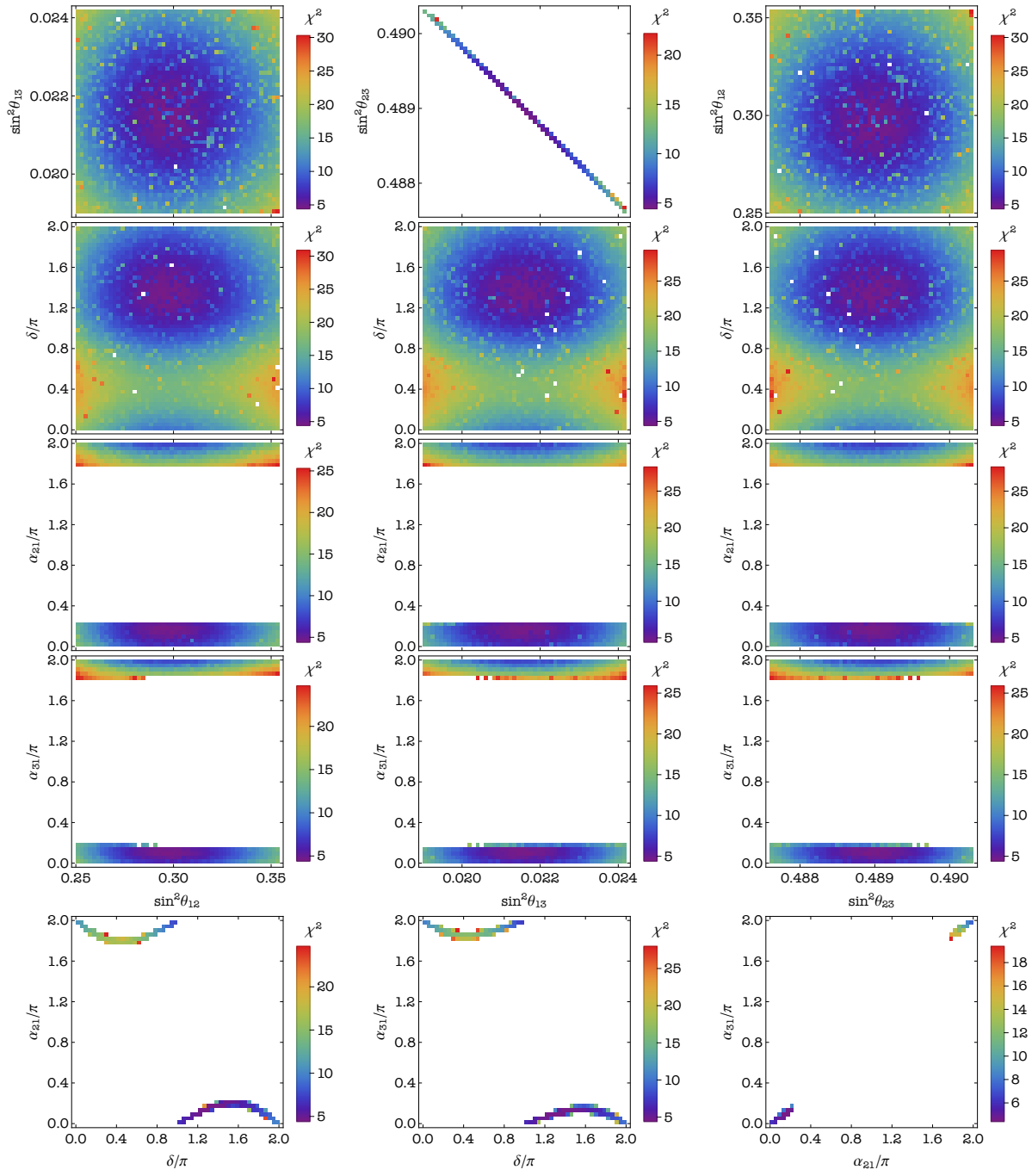

Figure 4.4: Correlations between the neutrino mixing parameters in case B4, for a mass spectrum with IO. The values of all the three mixing angles are required to lie in their respective 3σ ranges. Note that this case is not compatible with the 2σ range of $\sin^2\theta_{23}$.

• **Case C1: $|(U_{\rm PMNS})_{e2}| = 1/2$ ($P_e = P_{123}$, $P_\nu = P_{213}$).** Fixing $(U_{\rm PMNS})_{e2}$ leads to the following relation between $\sin^2\theta_{13}$ and $\sin^2\theta_{12}$:

$$\sin^2\theta_{12} = \frac{1}{4\left(1-\sin^2\theta_{13}\right)} = \frac{1}{4}\left(1+\sin^2\theta_{13}\right) + \mathcal{O}\left(\sin^4\theta_{13}\right) . \tag{4.91}$$

Since this case allows for the whole 3σ range of $\sin^2\theta_{13}$ (see Fig. 4.5), we find $\sin^2\theta_{12} \in (0.2548, 0.2562)$. Note that this narrow interval is outside the 2σ range of $\sin^2\theta_{12}$. At the same time, this case reproduces the whole 3σ range of the values of $\sin^2\theta_{23}$. From

$$|(U_{\rm PMNS})_{\mu 2}|^2 = \frac{3\cos^2\theta^e}{4} , \tag{4.92}$$

we obtain

$$\cos\delta = \frac{4\cos^2\theta_{12}\cos^2\theta_{23} + 4\sin^2\theta_{12}\sin^2\theta_{23}\sin^2\theta_{13} - 3\cos^2\theta^e}{2\sin 2\theta_{12}\sin 2\theta_{23}\sin\theta_{13}} , \tag{4.93}$$

i.e., $\cos\delta$ explicitly depends on θ^e, and eventually δ is not constrained. Instead the Majorana phase α_{21} is predicted to be exactly π (exactly 0) for $k_1 = 0$ ($k_1 = 1$). While the second Majorana phase α_{31} itself remains unconstrained, the difference $\alpha_{31} - 2\delta = 0$ (π) for $k_2 = 0$ ($k_2 = 1$), i.e., we have a strong linear correlation between δ and α_{31} (see Fig. 4.5). The reason for these values of α_{21} and $\alpha_{31} - 2\delta$ is the following. In the standard parametrisation of the PMNS matrix, α_{21} and the combination $(\alpha_{31} - 2\delta)$ may be extracted from the phases of the first row of the PMNS matrix, as can be seen from Eqs. (4.65) – (4.68). In case C1, none of the phases of the first row elements of the PMNS matrix depend (mod π) on the free parameters θ^ν, θ^e and δ^e. Namely, the phases of $(U_{\rm PMNS})_{e1}$, $(U_{\rm PMNS})_{e2}$ and $(U_{\rm PMNS})_{e3}$ are fixed (mod π and up to a global phase) to be $-\pi/6$, $\pi/3$ and $-\pi/6$, respectively. Notice that only in groups B and C the relative phases of the first row can be predicted (mod π) to be independent of θ^ν, θ^e and δ^e. Furthermore, case C1 stands out since it is, out of these relevant cases, the only one which survives the constraints on the magnitudes of the PMNS matrix elements given in Eqs. (4.50) and (4.51). Finally, $\chi^2_{\rm min} \simeq 7$ for both mass orderings.

• **Case C2: $|(U_{\rm PMNS})_{\mu 1}| = 1/2$ ($P_e = P_{213}$, $P_\nu = P_{123}$).** The correlations between the mixing parameters obtained in this case for NO are summarised in Fig. 4.6 (the results for IO are very similar). This case accounts for the whole 3σ range of $\sin^2\theta_{13}$, but constrains the values of the two other angles. Namely, we find $\sin^2\theta_{12} \in [0.285, 0.354]$ and $\sin^2\theta_{23} \in [0.381, 0.524]$. For this case, Eq. (4.76) is valid, since $|(U_{\rm PMNS})_{\mu 1}| = 1/2$ as in case A1. As a consequence, we find δ to be constrained: $\delta \in (-0.38\pi, 0.38\pi)$. Both Majorana phases are distributed in relatively narrow intervals: $\alpha_{21} \in (0.85\pi, 1.15\pi)$ and $\alpha_{31} \in [0.91\pi, 1.09\pi]$, mod π. The phase δ is correlated with each of the two Majorana phases in a similar way. The latter in turn are correlated linearly between themselves. Overall, NO is slightly preferred over IO in this case. The corresponding values of $\chi^2_{\rm min}$ read 4.5 and 5.5, respectively.

• **Case C3: $|(U_{\rm PMNS})_{\tau 1}| = 1/2$ ($P_e = P_{321}$, $P_\nu = P_{123}$).** This case shares some of the predictions of case C2. Namely, the whole 3σ range of $\sin^2\theta_{13}$ is allowed, and the ranges of α_{21} and α_{31} are the same as in the preceding case, as can be seen from Fig. 4.7, in which we present the results for the IO neutrino mass spectrum. The interval of values of $\sin^2\theta_{12}$ differs somewhat from that of case C2 and reads $\sin^2\theta_{12} \in [0.279, 0.354]$. The predictions for $\sin^2\theta_{23}$ and δ, however, are very different from those of case

C2. The allowed values of $\sin^2\theta_{23}$ are concentrated mostly in the upper octant, $\sin^2\theta_{23} \in [0.475, 0.636]$. The sum rule for $\cos\delta$ in Eq. (4.78) is valid in this case, since $|(U_{\rm PMNS})_{\tau 1}| = 1/2$, and we find the values of δ to be symmetrically distributed around π in the interval $[0.60\pi, 1.40\pi]$. The pairwise correlations between the CPV phases are of the same type as in case C2 (taking into account an approximate shift of δ by π, as suggested by Figs. 4.6 and 4.7). Due to the predicted range of $\sin^2\theta_{23}$, this case is favoured by the data for IO, for which $\chi^2_{\rm min} \simeq 1.5$, while for NO we find $\chi^2_{\rm min} \simeq 8.5$.

• **Case C4: $|(U_{\rm PMNS})_{\mu 2}| = 1/2$ ($P_e = P_\nu = P_{213}$).** From Eqs. (4.50) and (4.51) it follows that the value of $|(U_{\rm PMNS})_{\mu 2}| = 1/2$ is allowed at 3σ only for IO. Thus, below we present results obtained in the IO case. In the case under consideration there are no constraints on the ranges of $\sin^2\theta_{12}$ and $\sin^2\theta_{13}$. The atmospheric angle is, in turn, found to lie in the upper octant, $\sin^2\theta_{23} \in (0.505, 0.636]$. As can be seen in Fig. 4.8, $\delta \in [-0.54\pi, 0.54\pi]$, which is a consequence of the following correlation between $\cos\delta$ and the mixing angles:

$$\cos\delta = \frac{4\cos^2\theta_{12}\cos^2\theta_{23} + 4\sin^2\theta_{12}\sin^2\theta_{23}\sin^2\theta_{13} - 1}{2\sin 2\theta_{12}\sin 2\theta_{23}\sin\theta_{13}}\,, \tag{4.94}$$

obtained from $|(U_{\rm PMNS})_{\mu 2}| = 1/2$. There is also a peculiar correlation between $\sin^2\theta_{23}$ and δ. The phases $\alpha_{21} \in [0.73\pi, 1.27\pi]$ and $\alpha_{31} \in [-0.18\pi, 0.18\pi]$ mod π. The values of all the three phases are highly correlated among themselves. The predicted values of $\sin^2\theta_{23}$ in the upper octant lead to $\chi^2_{\rm min} \simeq 8.5$ for NO (see footnote 8), while $\chi^2_{\rm min} \simeq 2$ for IO.

• **Case C5: $|(U_{\rm PMNS})_{\tau 2}| = 1/2$ ($P_e = P_{321}$, $P_\nu = P_{213}$).** The last case of this group, analogously to case C4, does not constrain the ranges of $\sin^2\theta_{12}$ and $\sin^2\theta_{13}$. Moreover, it leads to almost the same allowed ranges of α_{21} and α_{31} as in the previous case, $\alpha_{21} \in (0.74\pi, 1.26\pi)$ and $\alpha_{31} \in [-0.16\pi, 0.16\pi]$, mod π. The differences are in predictions for $\sin^2\theta_{23}$ and δ. Now the atmospheric angle lies in the lower octant, namely, for NO we find $\sin^2\theta_{23} \in [0.381, 0.494]$. The condition $|(U_{\rm PMNS})_{\tau 2}| = 1/2$ gives rise to the following sum rule:

$$\cos\delta = \frac{1 - 4\cos^2\theta_{12}\sin^2\theta_{23} - 4\sin^2\theta_{12}\cos^2\theta_{23}\sin^2\theta_{13}}{2\sin 2\theta_{12}\sin 2\theta_{23}\sin\theta_{13}}\,. \tag{4.95}$$

The allowed values of δ span the range $[0.51\pi, 1.49\pi]$. The correlations between the mixing parameters in this case are summarised in Fig. 4.9 for NO. Finally, we have $\chi^2_{\rm min} \simeq 0.5$ for both orderings.

Group D: $\{G_e, G_\nu\} = \{Z_2^{TU}, Z_2^U \times H^\nu_{\rm CP}\}$ with $H^\nu_{\rm CP} = \{S, SU\}$. For this last group of cases, we find that the PMNS matrix takes the following form (up to permutations of rows and columns and the phases in the matrix Q_ν):

$$U^{\rm D}_{\rm PMNS} = \frac{1}{2\sqrt{3}} \begin{pmatrix} -\sqrt{3}\, e^{-\frac{i\pi}{6}} & \sqrt{3}\left(\sqrt{2}\, c^\nu + i\, s^\nu\right) e^{-\frac{i\pi}{6}} & \sqrt{3}\left(\sqrt{2}\, s^\nu - i\, c^\nu\right) e^{-\frac{i\pi}{6}} \\ 3\, c^e e^{\frac{i\pi}{3}} & d_1\left(\theta^\nu, \theta^e, \delta^e\right) & d_2\left(\theta^\nu, \theta^e, \delta^e\right) \\ -3\, s^e e^{\frac{i\pi}{3}} e^{i\delta^e} & d_3\left(\theta^\nu, \theta^e, \delta^e\right) & d_4\left(\theta^\nu, \theta^e, \delta^e\right) \end{pmatrix}, \tag{4.96}$$

where

$$d_1\left(\theta^\nu, \theta^e, \delta^e\right) = \left(\sqrt{2}\, c^\nu + i\, s^\nu\right) c^e e^{\frac{i\pi}{3}} + 2\left(c^\nu - i\sqrt{2}\, s^\nu\right) s^e e^{-i\delta^e}\,, \tag{4.97}$$

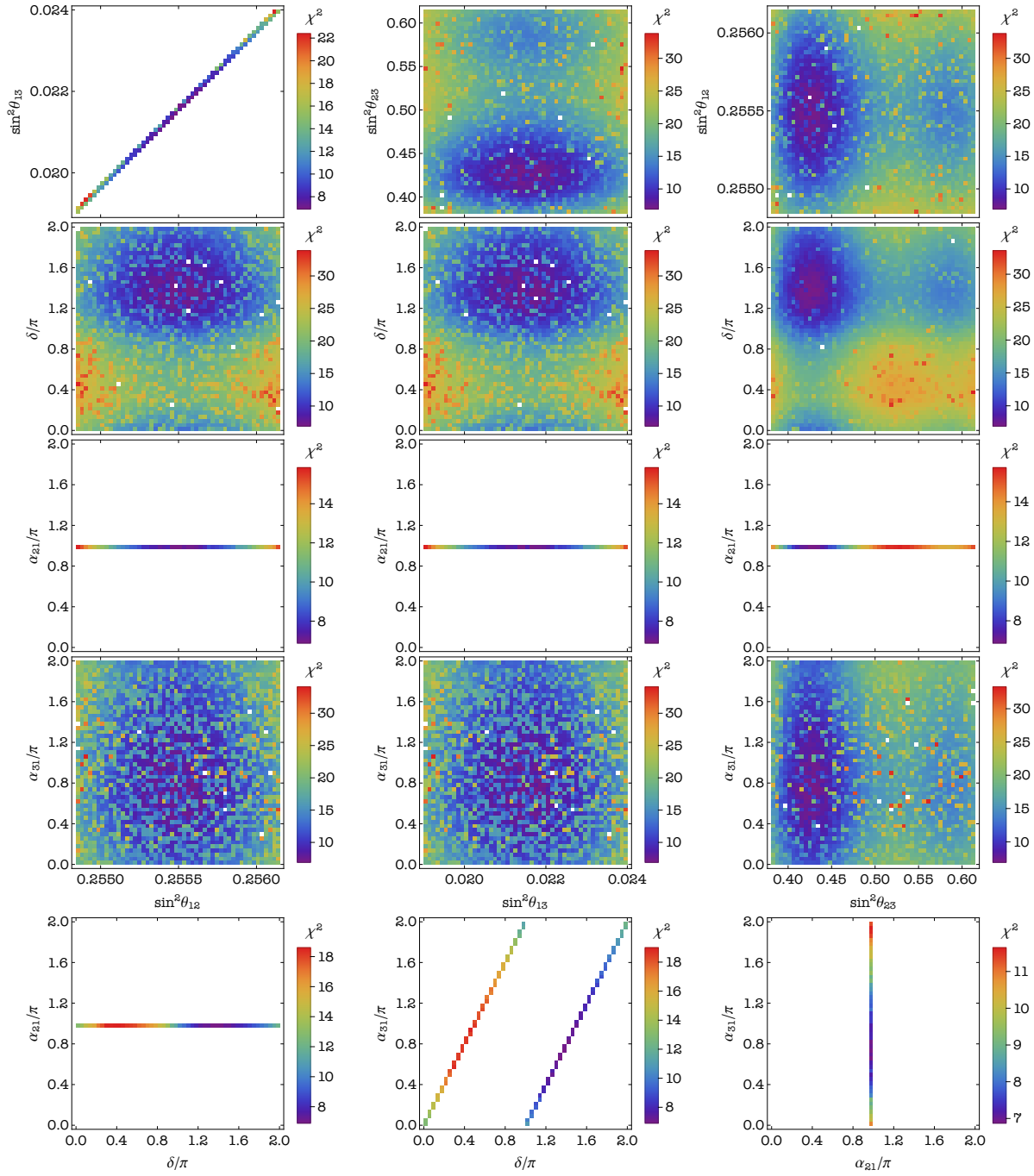

Figure 4.5: Correlations between the neutrino mixing parameters in case C1, for a mass spectrum with NO. The values of all the three mixing angles are required to lie in their respective 3σ ranges. Note that this case is not compatible with the 2σ range of $\sin^2\theta_{12}$.

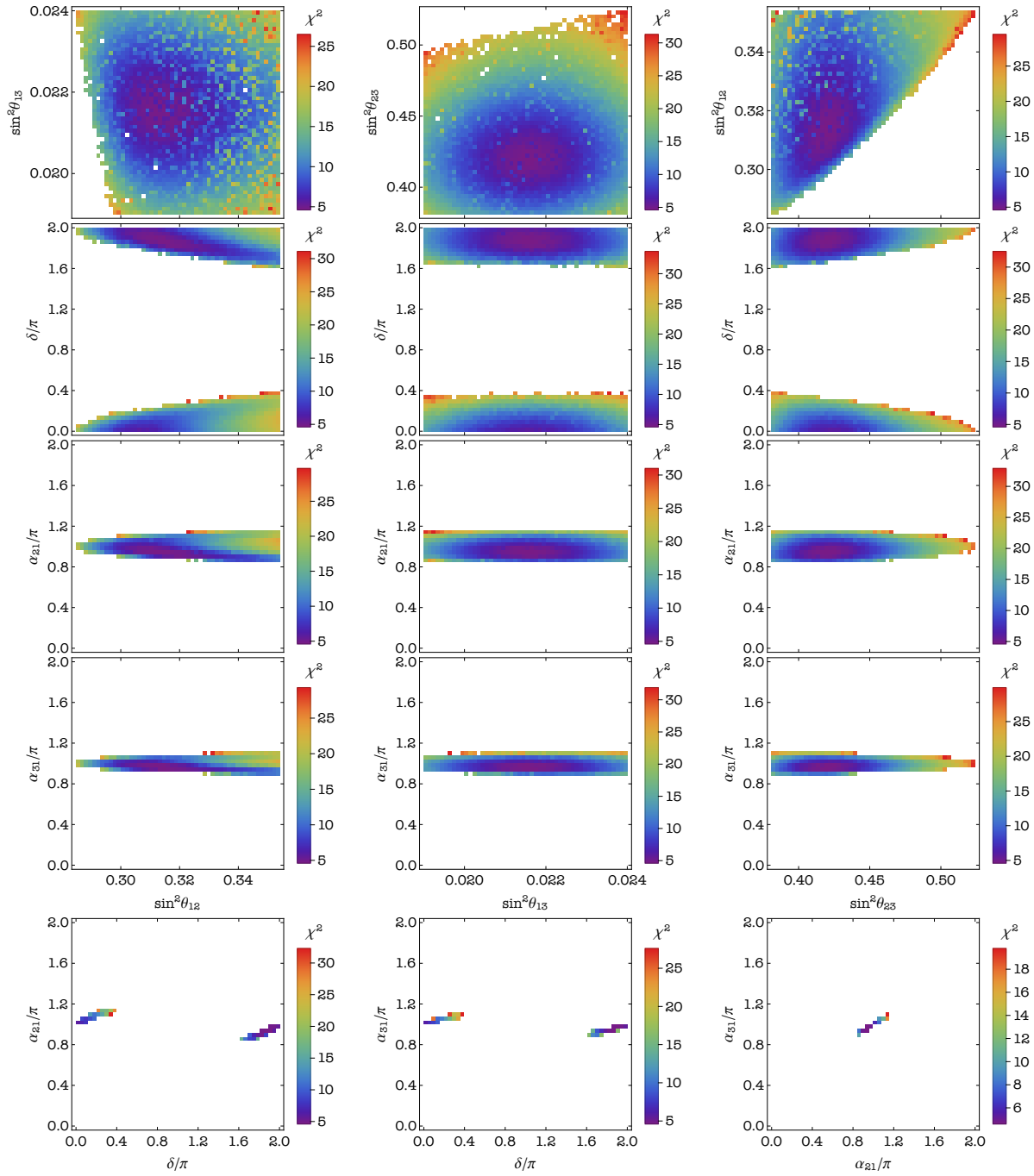

Figure 4.6: Correlations between the neutrino mixing parameters in case C2, for a mass spectrum with NO. The values of all the three mixing angles are required to lie in their respective 3σ ranges.

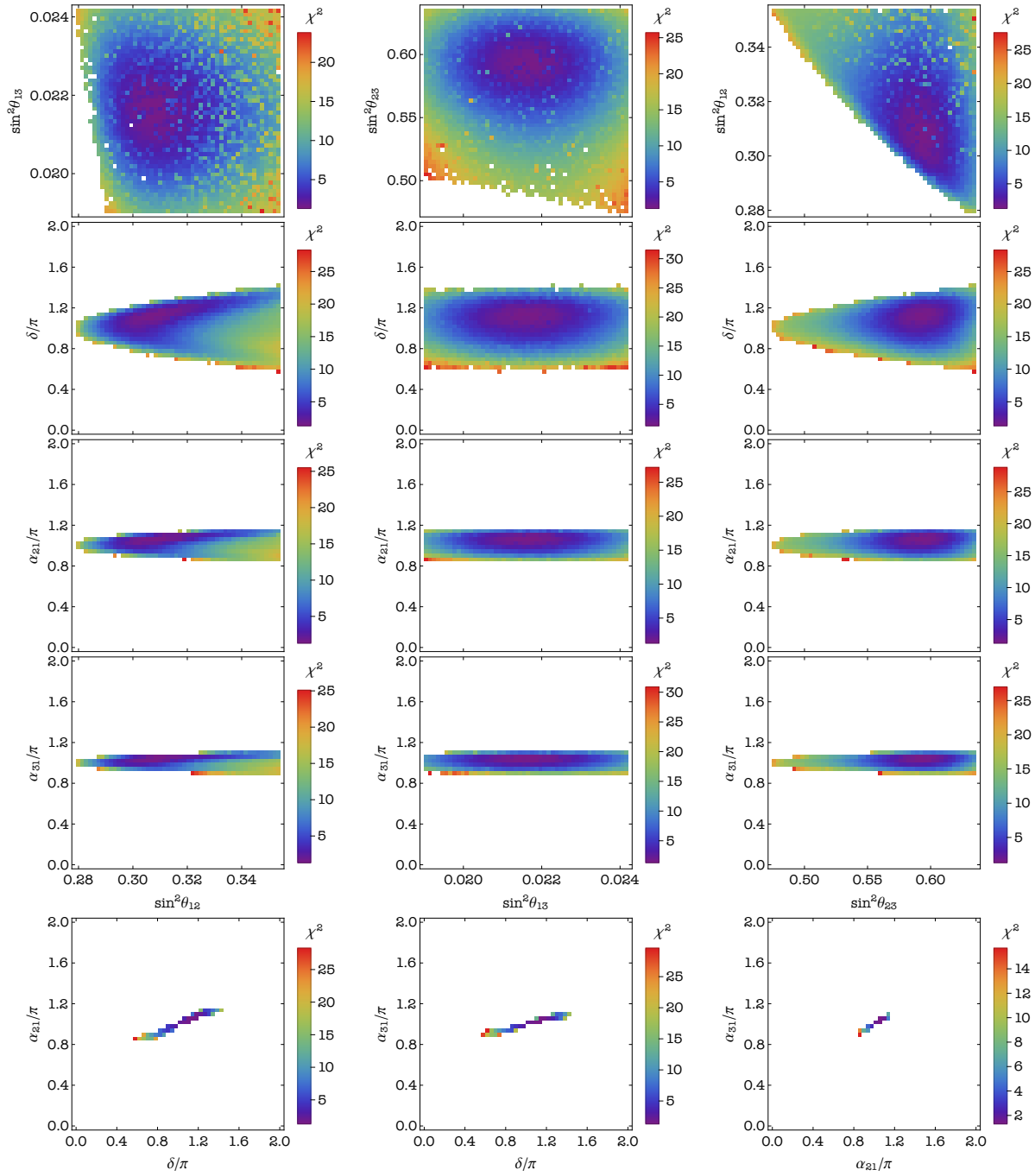

Figure 4.7: Correlations between the neutrino mixing parameters in case C3, for a mass spectrum with IO. The values of all the three mixing angles are required to lie in their respective 3σ ranges.

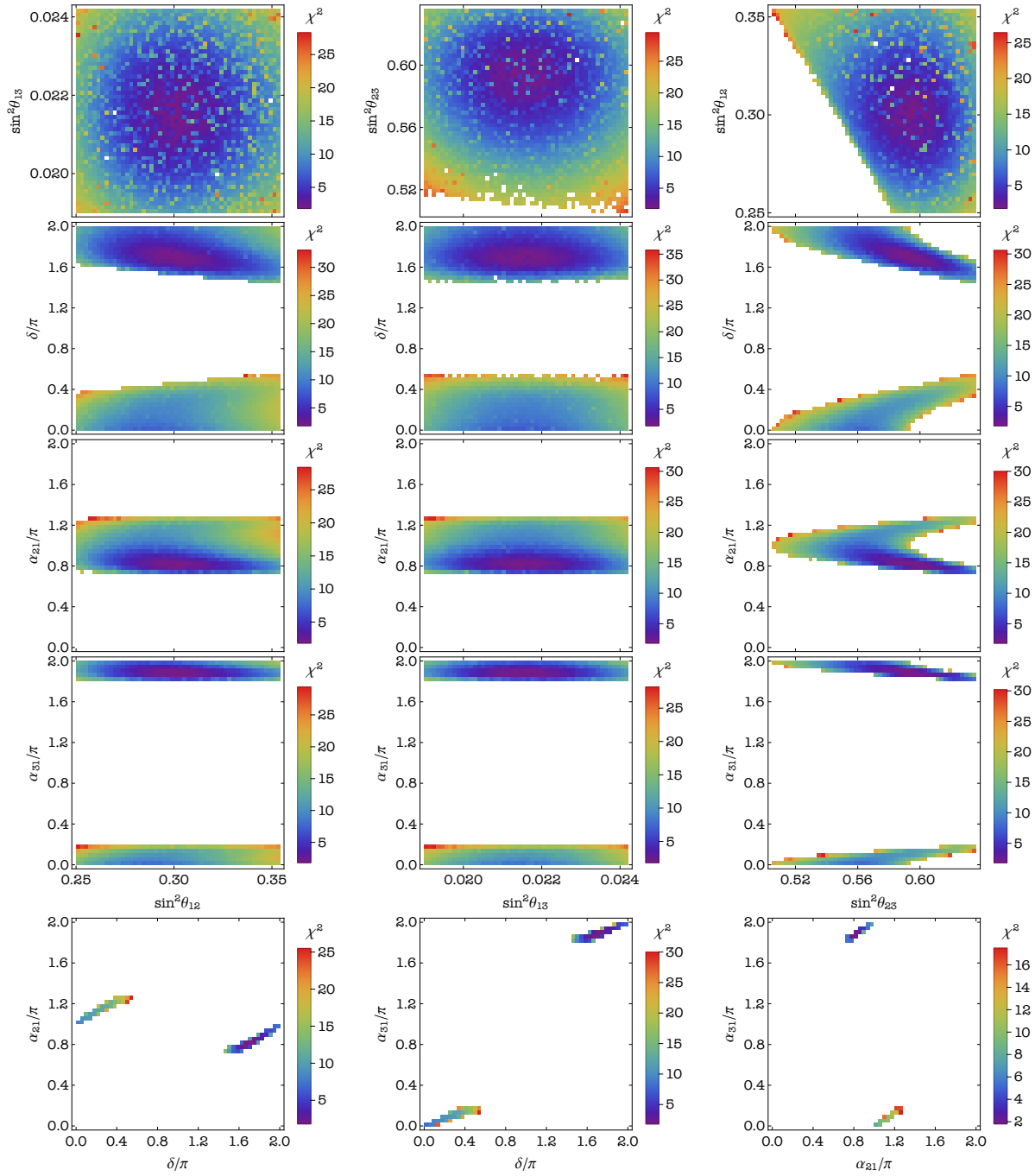

Figure 4.8: Correlations between the neutrino mixing parameters in case C4, for a mass spectrum with IO. The values of all the three mixing angles are required to lie in their respective 3σ ranges.

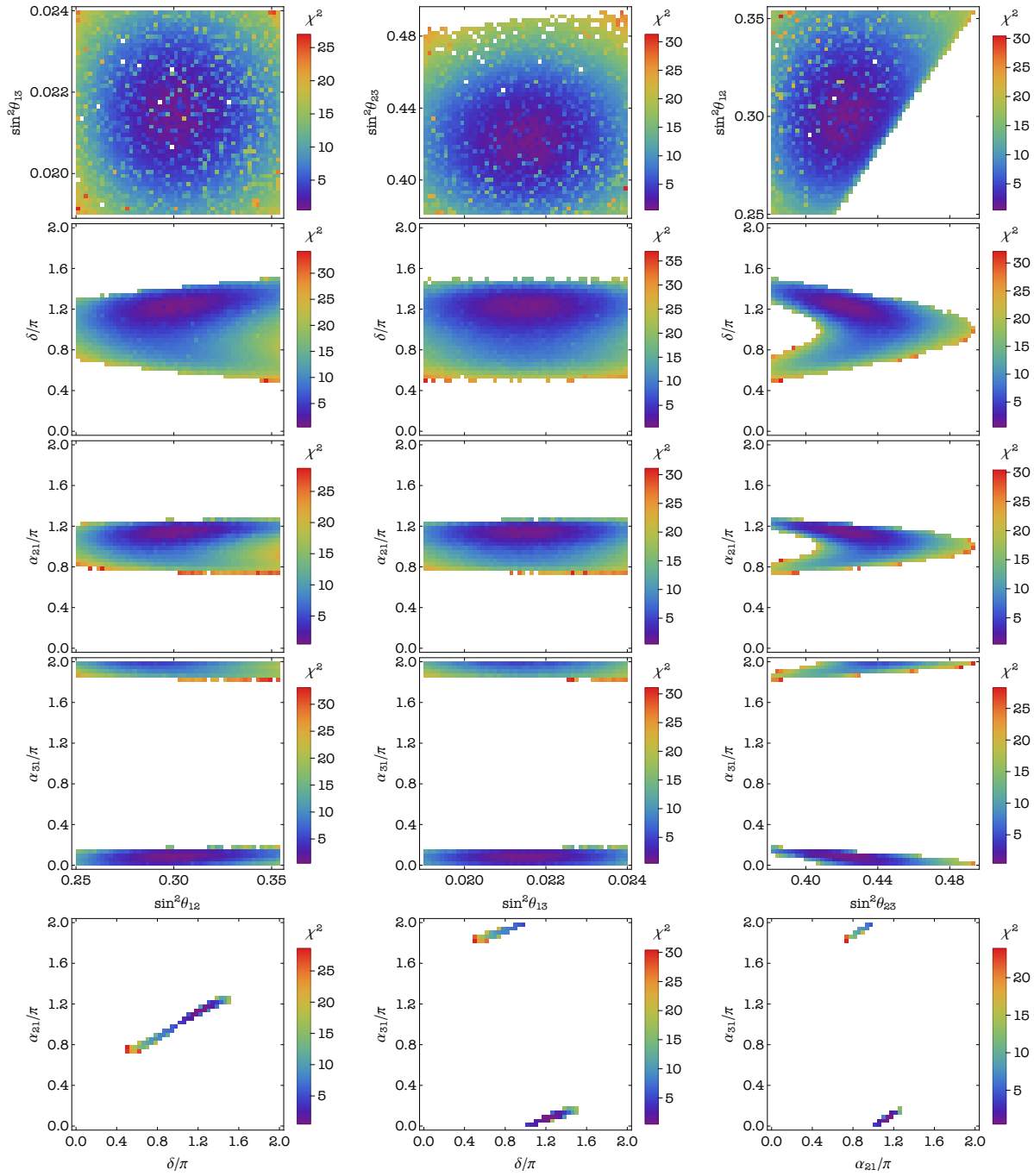

Figure 4.9: Correlations between the neutrino mixing parameters in case C5, for a mass spectrum with NO. The values of all the three mixing angles are required to lie in their respective 3σ ranges.

$$d_2\left(\theta^\nu, \theta^e, \delta^e\right) = \left(\sqrt{2}\, s^\nu - i\, c^\nu\right) c^e e^{\frac{i\pi}{3}} + 2\left(s^\nu + i\sqrt{2}\, c^\nu\right) s^e e^{-i\delta^e}\,, \tag{4.98}$$

$$d_3\left(\theta^\nu, \theta^e, \delta^e\right) = 2\left(c^\nu - i\sqrt{2}\, s^\nu\right) c^e - \left(\sqrt{2}\, c^\nu + i\, s^\nu\right) s^e e^{\frac{i\pi}{3}} e^{i\delta^e}\,, \tag{4.99}$$

$$d_4\left(\theta^\nu, \theta^e, \delta^e\right) = 2\left(s^\nu + i\sqrt{2}\, c^\nu\right) c^e - \left(\sqrt{2}\, s^\nu - i\, c^\nu\right) s^e e^{\frac{i\pi}{3}} e^{i\delta^e}\,. \tag{4.100}$$

Therefore, the absolute value of the fixed element of the neutrino mixing matrix yields 1/2. Thus, we have again five potentially viable cases.

• **Case D1: $|(U_{\rm PMNS})_{e2}| = 1/2$ ($P_e = P_{123}$, $P_\nu = P_{213}$).** In this case we find

$$\sin^2\theta_{13} = \frac{3 - \cos 2\theta^\nu}{8}\,, \tag{4.101}$$

which implies that $\sin^2\theta_{13}$ can have values between 1/4 and 1/2. Thus, this case is ruled out.

• **Case D2: $|(U_{\rm PMNS})_{\mu 1}| = 1/2$ ($P_e = P_{213}$, $P_\nu = P_{123}$).** This case allows for the whole 3σ range of $\sin^2\theta_{13}$ and, in the case of NO, for the following ranges of $\sin^2\theta_{12}$ and $\sin^2\theta_{23}$: $\sin^2\theta_{12} \in [0.284, 0.354]$ and $\sin^2\theta_{23} \in [0.381, 0.512]$. The sum rule for $\cos\delta$ in Eq. (4.76) holds, since $|(U_{\rm PMNS})_{\mu 1}| = 1/2$. We find $\delta \in [-0.37\pi, 0.37\pi]$. In what concerns the Majorana phases, α_{21} spans a relatively broad interval $[0.25\pi, 1.75\pi]$, while $\alpha_{31} \in [-0.48\pi, 0.48\pi]$ (both mod π). There are very particular correlations between $\alpha_{21(31)}$ and all the other mixing parameters in this case, as can be seen in Fig. 4.10, in which we summarise the results for NO. Finally, $\chi^2_{\rm min} \simeq 4.5$ for NO, and $\chi^2_{\rm min} \simeq 5.5$ for IO.

• **Case D3: $|(U_{\rm PMNS})_{\tau 1}| = 1/2$ ($P_e = P_{321}$, $P_\nu = P_{123}$).** As in the previous case, the whole 3σ range of $\sin^2\theta_{13}$ is reproduced. The allowed ranges of $\sin^2\theta_{12}$, α_{21} and α_{31} are very similar to those of case D2. Namely, in the case of IO spectrum we have $\sin^2\theta_{12} \in [0.279, 0.354]$, while $\alpha_{21} \in [0.21\pi, 1.79\pi]$ and $\alpha_{31} \in (-0.53\pi, 0.53\pi)$ mod π. Instead, the values of $\sin^2\theta_{23}$ occupy mostly the upper octant, $\sin^2\theta_{23} \in [0.488, 0.636]$. The sum rule in Eq. (4.78), which holds in this case since $|(U_{\rm PMNS})_{\tau 1}| = 1/2$, leads to the values of δ distributed around π in a rather broad range, $\delta \in (0.59\pi, 1.41\pi)$. The correlations between the Majorana phases and δ are as in the previous case, but again with an approximate shift of δ by π (see Fig. 4.11). The minimal value $\chi^2_{\rm min} \simeq 1.5$ in the IO case, while for the NO spectrum we get approximately 8.5. This difference is due to the allowed values of $\sin^2\theta_{23}$.

• **Case D4: $|(U_{\rm PMNS})_{\mu 2}| = 1/2$ ($P_e = P_\nu = P_{213}$).** This case can account only for a part of the 3σ range of $\sin^2\theta_{13}$, namely, $\sin^2\theta_{13} \in [0.0214, 0.0240(2)]$ for NO (IO) spectrum. The constraints on two other angles are more severe. We find that only a narrow region of the values of $\sin^2\theta_{23}$, which falls outside its 2σ range, is allowed, namely, $\sin^2\theta_{23} \in [0.505, 0.512]$. For the solar mixing angle we have $\sin^2\theta_{12} \in [0.345, 0.354]$, which is also outside the 2σ range of this parameter. The sum rule in Eq. (4.94), which is also valid in this case, constrains δ to lie in a narrow interval around 0: $\delta \in [-0.11\pi, 0.11\pi]$. The Majorana phases are also distributed in narrow intervals, namely $\alpha_{21} \in (0.83\pi, 1.17\pi)$ and $\alpha_{31} \in [0.92\pi, 1.08\pi]$ mod π. However, the global minimum of χ^2 is somewhat large in this case for both NO and IO orderings. Namely, we find $\chi^2_{\rm min} \simeq 22$ (19) for NO (IO), i.e., this case is strongly disfavoured by global data.

• **Case D5: $|(U_{\rm PMNS})_{\tau 2}| = 1/2$ ($P_e = P_{321}$, $P_\nu = P_{213}$).** This last case shares the predicted ranges for $\sin^2\theta_{12}$, $\sin^2\theta_{13}$, α_{21} and α_{31} with case D4. Therefore, this case is also not compatible with the 2σ range of $\sin^2\theta_{12}$. For $\sin^2\theta_{23}$ instead we find the narrow interval in the lower octant, $\sin^2\theta_{23} \in [0.488, 0.495]$, which lies outside the 2σ range of $\sin^2\theta_{23}$. We find $\cos\delta$ to satisfy the sum rule in Eq. (4.95), which in this case gives us the values of δ in a narrow interval around π, $\delta \in [0.89\pi, 1.11\pi]$. Finally, we find $\chi^2_{\rm min} \simeq 18.5$ (15) for NO (IO), which implies that this case is also strongly disfavoured.

The PMNS matrix in case A2 is related with that in case A1 by the permutation matrix P_{312} as $U^{\rm A2}_{\rm PMNS} = P_{312}\, U^{\rm A1}_{\rm PMNS}$. Given that $P_{312} = P_{132}P_{321}$, one can see that these matrices are related by $\mu - \tau$ interchange, after an unphysical exchange of the first and third rows of $U^{\rm A1}_{\rm PMNS}$ has been performed (which amounts to a redefinition of the free parameter θ^e, as shown in Eq. (4.61)). The same also holds for the following pairs of cases: (B1, B2), (B3, B4), (C2, C3), (C4, C5), (D2, D3) and (D4, D5). As can be seen from the discussion above and Figs. 4.1 – 4.4 and 4.6 – 4.11, cases inside a pair share some qualitative features. Namely, i) the predicted ranges of $\sin^2\theta_{12}$, $\sin^2\theta_{13}$, α_{21} and α_{31} are approximately the same; ii) the predicted range of $\sin^2\theta_{23}$ gets approximately reflected around 1/2, i.e., $\sin^2\theta_{23} \to 1 - \sin^2\theta_{23}$; iii) the predicted range of the CPV phase δ experiences an approximate shift by π, i.e., $\delta \to \delta + \pi$.

In Tables 4.2 and 4.3 we summarise the predicted ranges of the mixing parameters obtained in all the phenomenologically viable cases discussed above. The corresponding best-fit values together with $\chi^2_{\rm min}$ are presented in Tables 4.4 and 4.5. Finally, in Table 4.6 we show whether the cases compatible with the 3σ ranges of the three mixing angles are also compatible with their corresponding 2σ ranges.

The results shown in Tables 4.2 – 4.5 allow to assess the possibilities to critically test the predictions of the viable cases of the model and to distinguish between them. The *current* global-fit 1σ uncertainties on the measured values of $\sin^2\theta_{12}$, $\sin^2\theta_{13}$ and $\sin^2\theta_{23}$ are 4.4%, 3.8% and 5.2%, respectively [39]. These uncertainties are foreseen to be further reduced by the currently active and/or future planned experiments. The Daya Bay collaboration plans to determine $\sin^2\theta_{13}$ with 1σ uncertainty of 3% [203]. The uncertainties on $\sin^2\theta_{12}$ and $\sin^2\theta_{23}$ are planned to be reduced significantly. The parameter $\sin^2\theta_{12}$ is foreseen to be measured with 1σ relative error of 0.7% in the JUNO experiment [204, 205]. In the proposed upgrade of the (currently taking data) T2K experiment [206, 207], for example, θ_{23} is estimated to be determined with a 1σ error of 1.7°, 0.5° or 0.7° if the best-fit value of $\sin^2\theta_{23} = 0.50$, 0.43 or 0.60, respectively. This implies that for these three values of $\sin^2\theta_{23}$ the 1σ error would be 5% for $\sin^2\theta_{23} = 0.50$, and 2% for $\sin^2\theta_{23} = 0.43$ or 0.60. This error on $\sin^2\theta_{23}$ will be further reduced in the future planned T2HK [208] and DUNE [209] experiments. If $\delta = 3\pi/2$, the CP-conserving case of $\sin\delta = 0$ would be disfavoured for the NO mass spectrum in the same experiment at least at 3σ CL. Higher precision measurements of δ are planned to be performed in the T2HK and DUNE experiments.

We turn now to the possibilities to discriminate experimentally between the different cases listed in Tables 4.2 – 4.5 using the prospective data on $\sin^2\theta_{12}$, $\sin^2\theta_{13}$, $\sin^2\theta_{23}$ and δ. One starts by noting that the predicted ranges for $\sin^2\theta_{12}$, $\sin^2\theta_{13}$, $\sin^2\theta_{23}$ and δ in cases A1 and A2 practically coincide with the predictions respectively in cases D4 and D5. However, cases A1, D4 and cases A2, D5 are strongly disfavoured by data: for a NO (IO) neutrino mass spectrum, A1 and D4 present $\chi^2_{\rm min} = 22.0$ (19.0),

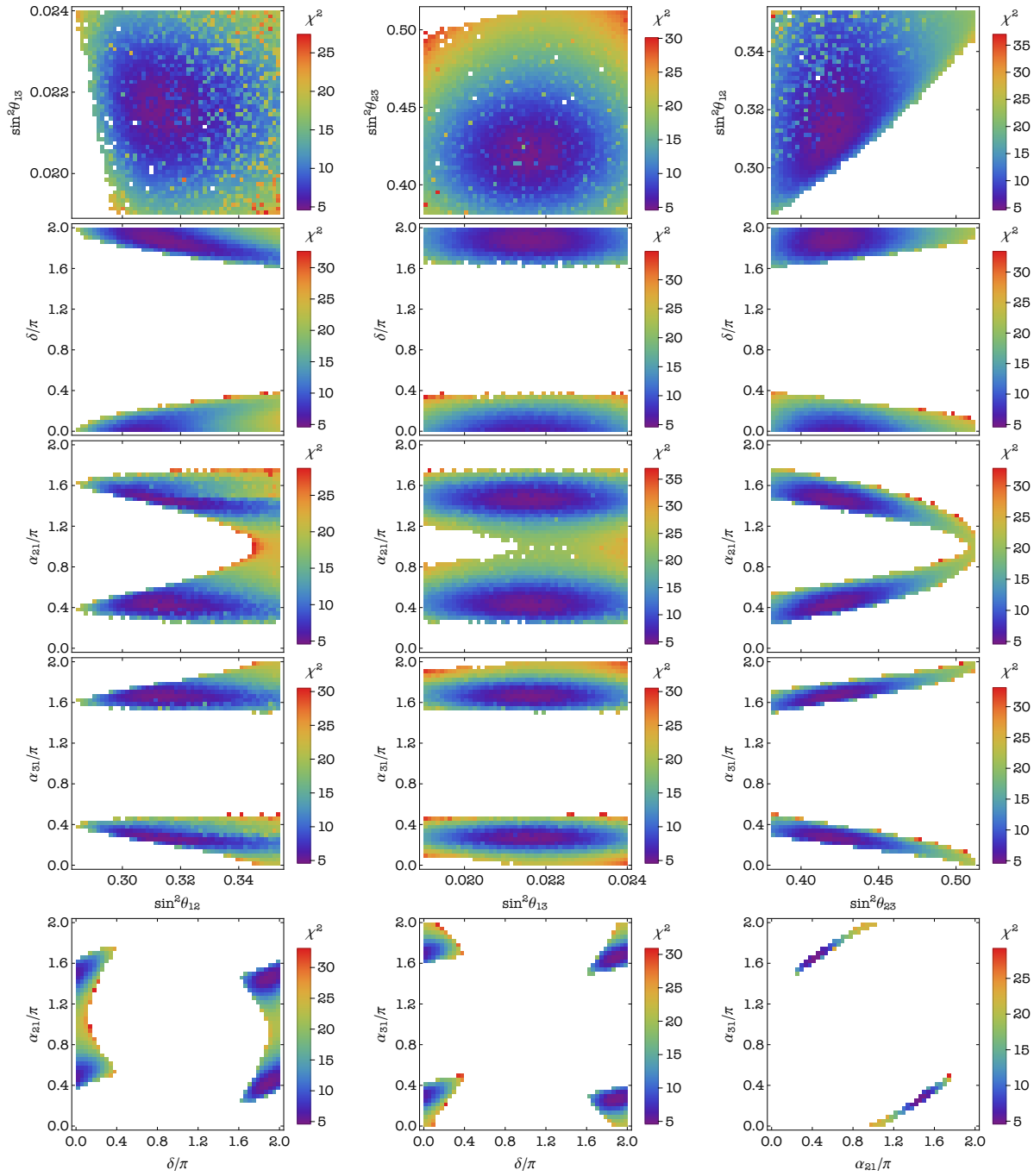

Figure 4.10: Correlations between the neutrino mixing parameters in case D2, for a mass spectrum with NO. The values of all the three mixing angles are required to lie in their respective 3σ ranges.

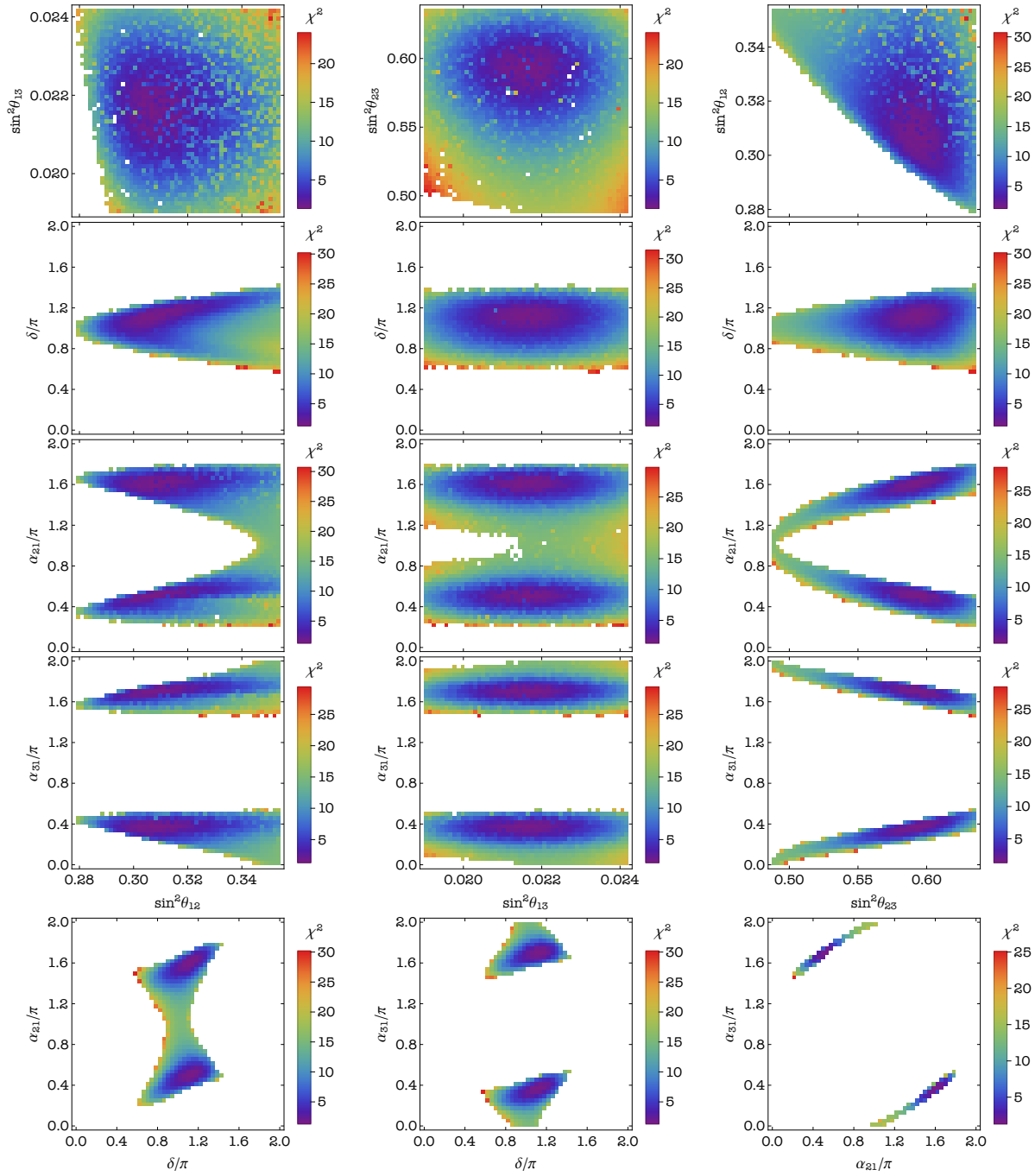

Figure 4.11: Correlations between the neutrino mixing parameters in case D3, for a mass spectrum with IO. The values of all the three mixing angles are required to lie in their respective 3σ ranges.

while for A2 and D5 $\chi^2_{\rm min} = 18.5$ (15.0). In all these cases, $\sin^2\theta_{12}$ in particular is predicted to lie in the interval (0.345,0.354) compatible with its 3σ range and, given the best-fit value of $\sin^2\theta_{12}$ and prospective JUNO precision on $\sin^2\theta_{12}$, it is very probable that future more precise data on $\sin^2\theta_{12}$ will rule out these scenarios.

It follows also from Tables 4.4 and 4.5 that the combined results on the best-fit values of $\sin^2\theta_{12}$, $\sin^2\theta_{23}$ and δ we have obtained in the different viable cases (excluding A1, A2, D4 and D5) differ significantly. Assuming, for example, that the experimentally determined best-fit values of $\sin^2\theta_{12}$ and $\sin^2\theta_{23}$ will coincide with those found by us for a given viable case, it is not difficult to convince oneself inspecting Tables 4.4 and 4.5 that the cited prospective 1σ errors on $\sin^2\theta_{12}$ and $\sin^2\theta_{23}$ will allow to discriminate between the different viable cases identified in our study. More specifically, considering as an example only the case of NO neutrino mass spectrum, the prospective high precision measurement of $\sin^2\theta_{12}$ will allow to discriminate between case C1 and all other cases B1 – B4, C2 – C5, D2 and D3. The same measurement will make it possible to distinguish i) between case B1 and all the other cases except B2, ii) between case B2 and all the other cases except B1, B3 and B4, and similarly iii) between case B3 and all the other cases except B2, B4, C4 and C5. However, the differences between the best-fit values of $\sin^2\theta_{23}$ in cases B1, B2 and B3 (or B4) are sufficiently large, which would permit to distinguish between these three cases if $\sin^2\theta_{23}$ were measured with the prospective precision. It follows from Table 4.4, however, that it would be very challenging to discriminate between cases B3 and B4: it will require extremely high precision measurement of $\sin^2\theta_{23}$. These two cases would be ruled out, however, if the experimentally determined best-fit value of $\sin^2\theta_{23}$ differs significantly from the results for $\sin^2\theta_{23}$ we have obtained in the B3 and B4 cases, namely 0.511 and 0.489, respectively.

In the remaining cases C2 – C5 and D2 – D3, the results we have obtained for $\sin^2\theta_{12}$, as Table 4.5 shows, are very similar. However, the predictions for the pair $\sin^2\theta_{23}$ and δ differ significantly in cases C2 or D2, and C3 or D3. The cases within each pair would be ruled out if the experimentally determined values of $\sin^2\theta_{23}$ and δ differ significantly from the predicted best-fit values.

The planned future high-precision measurements of $\sin^2\theta_{12}$ and $\sin^2\theta_{23}$, together with more precise data on the Dirac phase δ, will make it possible to critically test the predictions of the cases listed in Tables 4.2 – 4.5. We schematically summarise in Fig. 4.12 the predicted 3σ allowed regions in the plane $(\sin^2\theta_{23}, \sin^2\theta_{12})$ for all viable cases from Figs. 4.1 – 4.11. In this figure we also present the best-fit point in each case used in the preceding discussion. When future more precise data on $\sin^2\theta_{23}$ and $\sin^2\theta_{12}$ become available, the experimentally allowed region in the $(\sin^2\theta_{23}, \sin^2\theta_{12})$ plane will shrink, and only a limited number of cases, if any, will remain viable. A comprehensive analysis of the possibilities to distinguish between the different viable cases found in our work in the considered S_4 model can only be done when more precise data first of all on $\sin^2\theta_{12}$ and $\sin^2\theta_{23}$, and then on δ, will be available.

$H^{\nu}_{\rm CP}$	Case (p.f.e.)	$\frac{\sin^2\theta_{12}}{10^{-1}}$	$\frac{\sin^2\theta_{13}}{10^{-2}}$	$\frac{\sin^2\theta_{23}}{10^{-1}}$	δ/π	α_{21}/π (mod 1)	α_{31}/π (mod 1)
$\{1, S\}$	A1	$3.45 - 3.54$	$2.13 - 2.40$	$5.11 - 5.12$	$[0, 0.11] \cup [1.89, 2]$	$[0, 0.07] \cup [0.93, 1]$	$0 - 1$
	(μ3)	$3.44 - 3.54$	$2.13 - 2.42$	$5.11 - 5.12$	$[0, 0.12] \cup [1.88, 2]$	$[0, 0.07] \cup [0.93, 1]$	$0 - 1$
	A2	$3.45 - 3.54$	$2.13 - 2.40$	$4.88 - 4.89$	$0.89 - 1.11$	$[0, 0.07] \cup [0.93, 1]$	$0 - 1$
	(τ3)	$3.44 - 3.54$	$2.13 - 2.42$	$4.88 - 4.89$	$0.88 - 1.12$	$[0, 0.07] \cup [0.93, 1]$	$0 - 1$
$\{U, SU\}$	B1	$2.50 - 3.08$	Full 3σ	$3.81 - 4.25$	$0.68 - 1.32$	$[0, 0.16] \cup [0.84, 1]$	$[0, 0.13] \cup [0.88, 1]$
	(μ2)	$2.50 - 3.06$	Full 3σ	$3.84 - 4.25$	$0.69 - 1.31$	$[0, 0.16] \cup [0.84, 1]$	$[0, 0.12] \cup [0.88, 1]$
	B2	$2.50 - 3.03$	Full 3σ	$5.76 - 6.15$	$[0, 0.30] \cup [1.70, 2]$	$[0, 0.16] \cup [0.84, 1]$	$[0, 0.12] \cup [0.88, 1]$
	(τ2)	$2.50 - 3.28$	Full 3σ	$5.76 - 6.36$	$[0, 0.38] \cup [1.61, 2]$	$[0, 0.17] \cup [0.83, 1]$	$[0, 0.13] \cup [0.87, 1]$
	B3	Full 3σ	Full 3σ	$5.10 - 5.12$	$0 - 2$	$[0, 0.23] \cup [0.77, 1]$	$[0, 0.18] \cup [0.83, 1]$
	(μ3)	Full 3σ	Full 3σ	$5.10 - 5.12$	$0 - 2$	$[0, 0.23] \cup [0.77, 1]$	$[0, 0.18] \cup [0.82, 1]$
	B4	Full 3σ	Full 3σ	$4.88 - 4.90$	$0 - 2$	$[0, 0.23] \cup [0.77, 1]$	$[0, 0.17] \cup [0.83, 1]$
	(τ3)	Full 3σ	Full 3σ	$4.88 - 4.90$	$0 - 2$	$[0, 0.23] \cup [0.77, 1]$	$[0, 0.18] \cup [0.82, 1]$

Table 4.2: Ranges of the mixing parameters for the viable cases, i.e., those cases for which the predicted values of all the three mixing angles lie inside their respective 3σ allowed ranges. The cases presented here correspond to $G_e = Z_2^{g_e}$ and $G_\nu = Z_2^{g_\nu} \times H^{\nu}_{\rm CP}$ with $\{g_e, g_\nu\} = \{TU, S\}$, for which the magnitude of the fixed element is $1/\sqrt{2}$ (p.f.e. denotes the position of the fixed element in $U_{\rm PMNS}$). Within each case, the upper and lower rows refer to NO and IO, respectively.

$H^{\nu}_{\rm CP}$	Case (p.f.e.)	$\frac{\sin^2\theta_{12}}{10^{-1}}$	$\frac{\sin^2\theta_{13}}{10^{-2}}$	$\frac{\sin^2\theta_{23}}{10^{-1}}$	δ/π	α_{21}/π (mod 1)	α_{31}/π (mod 1)
$\{1, U\}$	C1	$2.55 - 2.56$	Full 3σ	Full 3σ	$0 - 2$	0 (exactly)	$0 - 1$
	($e2$)	$2.55 - 2.56$	Full 3σ	Full 3σ	$0 - 2$	0 (exactly)	$0 - 1$
	C2	$2.85 - 3.54$	Full 3σ	$3.81 - 5.24$	$[0, 0.38] \cup [1.62, 2]$	$[0, 0.15] \cup [0.85, 1]$	$[0, 0.09] \cup [0.91, 1]$
	($\mu 1$)	$2.86 - 3.54$	Full 3σ	$3.84 - 5.25$	$[0, 0.37] \cup [1.63, 2]$	$[0, 0.15] \cup [0.85, 1]$	$[0, 0.09] \cup [0.91, 1]$
	C3	$2.87 - 3.54$	Full 3σ	$4.75 - 6.15$	$0.63 - 1.37$	$[0, 0.15] \cup [0.86, 1]$	$[0, 0.09] \cup [0.91, 1]$
	($\tau 1$)	$2.79 - 3.54$	Full 3σ	$4.75 - 6.36$	$0.60 - 1.40$	$[0, 0.15] \cup [0.85, 1]$	$[0, 0.09] \cup [0.91, 1]$
	C4	Full 3σ	Full 3σ	$5.06 - 6.15$	$[0, 0.48] \cup [1.52, 2]$	$[0, 0.25] \cup [0.75, 1]$	$[0, 0.16] \cup [0.84, 1]$
	($\mu 2$)	Full 3σ	Full 3σ	$5.05 - 6.36$	$[0, 0.54] \cup [1.45, 2]$	$[0, 0.27] \cup [0.73, 1]$	$[0, 0.18] \cup [0.82, 1]$
	C5	Full 3σ	Full 3σ	$3.81 - 4.94$	$0.51 - 1.49$	$[0, 0.26] \cup [0.74, 1]$	$[0, 0.17] \cup [0.84, 1]$
	($\tau 2$)	Full 3σ	Full 3σ	$3.84 - 4.94$	$0.52 - 1.48$	$[0, 0.25] \cup [0.74, 1]$	$[0, 0.16] \cup [0.84, 1]$
$\{S, SU\}$	D2	$2.84 - 3.54$	Full 3σ	$3.81 - 5.12$	$[0, 0.38] \cup [1.63, 2]$	$0 - 1$	$[0, 0.48] \cup [0.52, 1]$
	($\mu 1$)	$2.85 - 3.54$	Full 3σ	$3.84 - 5.12$	$[0, 0.37] \cup [1.63, 2]$	$0 - 1$	$[0, 0.48] \cup [0.52, 1]$
	D3	$2.87 - 3.54$	Full 3σ	$4.88 - 6.15$	$0.63 - 1.37$	$0 - 1$	$[0, 0.47] \cup [0.52, 1]$
	($\tau 1$)	$2.79 - 3.54$	Full 3σ	$4.88 - 6.36$	$0.59 - 1.41$	$0 - 1$	$0 - 1$
	D4	$3.45 - 3.54$	$2.14 - 2.40$	$5.05 - 5.12$	$[0, 0.11] \cup [1.89, 2]$	$[0, 0.16] \cup [0.83, 1]$	$[0, 0.08] \cup [0.92, 1]$
	($\mu 2$)	$3.45 - 3.54$	$2.14 - 2.42$	$5.05 - 5.12$	$[0, 0.11] \cup [1.89, 2]$	$[0, 0.17] \cup [0.83, 1]$	$[0, 0.08] \cup [0.91, 1]$
	D5	$3.45 - 3.54$	$2.13 - 2.40$	$4.88 - 4.95$	$0.89 - 1.11$	$[0, 0.16] \cup [0.83, 1]$	$[0, 0.08] \cup [0.92, 1]$
	($\tau 2$)	$3.45 - 3.54$	$2.13 - 2.42$	$4.88 - 4.95$	$0.88 - 1.11$	$[0, 0.17] \cup [0.83, 1]$	$[0, 0.09] \cup [0.91, 1]$

Table 4.3: The same as in Table 4.2, but for $G_e = Z_2^{g_e}$ and $G_\nu = Z_2^{g_\nu} \times H^{\nu}_{\rm CP}$ with $\{g_e, g_\nu\} = \{TU, U\}$. In this case the magnitude of the fixed element is $1/2$.

$H^{\nu}_{\rm CP}$	Case (p.f.e.)	$\frac{\sin^2\theta_{12}}{10^{-1}}$	$\frac{\sin^2\theta_{13}}{10^{-2}}$	$\frac{\sin^2\theta_{23}}{10^{-1}}$	δ/π	α_{21}/π (mod 1)	α_{31}/π (mod 1)	$\chi^2_{\rm min}$
$\{1, S\}$	A1	3.54	2.18	5.11	1.96	0.97	0.43	22.0
	(μ3)	3.53	2.19	5.11	1.95	0.97	0.89	19.0
	A2	3.54	2.18	4.89	1.05	0.03	0.01	18.5
	(τ3)	3.53	2.20	4.89	1.04	0.02	0.67	15.0
$\{U, SU\}$	B1	2.74	2.17	3.99	1.09	0.94	0.96	7.0
	(μ2)	2.75	2.18	4.01	1.07	0.96	0.97	7.0
	B2	2.83	2.17	6.09	1.89	0.07	0.05	12.5
	(τ2)	2.83	2.17	6.09	1.89	0.07	0.05	6.0
	B3	2.95	2.15	5.11	1.36	0.80	0.85	8.5
	(μ3)	2.95	2.15	5.11	1.36	0.80	0.85	5.0
	B4	2.93	2.16	4.89	1.38	0.19	0.13	6.5
	(τ3)	2.97	2.16	4.89	1.31	0.16	0.11	4.5

Table 4.4: Best-fit values of the mixing parameters and the corresponding value of the χ^2 function, $\chi^2_{\rm min}$, for the viable cases, i.e., those cases for which the predicted values of all the three mixing angles lie inside their respective 3σ allowed ranges. The cases presented here correspond to $G_e = Z_2^{g_e}$ and $G_\nu = Z_2^{g_\nu} \times H^{\nu}_{\rm CP}$ with $\{g_e, g_\nu\} = \{TU, S\}$, for which the magnitude of the fixed element is $1/\sqrt{2}$ (p.f.e. denotes the position of the fixed element in $U_{\rm PMNS}$). Within each case, the upper and lower rows refer to NO and IO, respectively.

$H^\nu_{\rm CP}$	Case (p.f.e.)	$\frac{\sin^2\theta_{12}}{10^{-1}}$	$\frac{\sin^2\theta_{13}}{10^{-2}}$	$\frac{\sin^2\theta_{23}}{10^{-1}}$	δ/π	α_{21}/π (mod 1)	α_{31}/π (mod 1)	$\chi^2_{\rm min}$
$\{1, U\}$	C1	2.56	2.16	4.25	1.32	0	0.64	7.0
	($e2$)	2.56	2.16	5.85	1.36	0	0.73	7.0
	C2	3.15	2.16	4.19	1.86	0.93	0.96	4.5
	($\mu1$)	3.14	2.16	4.24	1.88	0.94	0.96	5.5
	C3	3.11	2.16	5.92	1.15	0.07	0.05	8.5
	($\tau1$)	3.08	2.17	5.93	1.13	0.06	0.04	1.5
	C4	3.00	2.14	5.95	1.69	0.81	0.88	8.5
	($\mu2$)	3.00	2.14	5.95	1.69	0.81	0.88	2.0
	C5	3.01	2.15	4.21	1.25	0.15	0.10	0.5
	($\tau2$)	2.99	2.17	4.26	1.22	0.13	0.09	0.5
$\{S, SU\}$	D2	3.13	2.15	4.20	1.88	0.43	0.65	4.5
	($\mu1$)	3.15	2.17	4.23	1.87	0.43	0.66	5.5
	D3	3.11	2.17	5.91	1.14	0.61	0.38	8.5
	($\tau1$)	3.06	2.16	5.96	1.12	0.50	0.69	1.5
	D4	3.54	2.18	5.11	1.96	0.97	0.98	22.0
	($\mu2$)	3.53	2.20	5.11	1.95	0.97	0.98	19.0
	D5	3.54	2.19	4.89	1.05	0.03	0.02	18.5
	($\tau2$)	3.53	2.19	4.89	1.04	0.03	0.01	15.0

Table 4.5: The same as in Table 4.4, but for $G_e = Z_2^{g_e}$ and $G_\nu = Z_2^{g_\nu} \times H^\nu_{\rm CP}$ with $\{g_e, g_\nu\} = \{TU, U\}$. In this case the magnitude of the fixed element is 1/2.

		A1	A2	B1	B2	B3	B4	C1	C2	C3	C4	C5	D2	D3	D4	D5
2σ	NO	✗	✗	✓	✗	✗	✗	✗	✓	✗	✗	✓	✓	✗	✗	✗
	IO	✗	✗	✓	✓	✗	✗	✗	✓	✓	✓	✓	✓	✓	✗	✗

Table 4.6: Compatibility of the cases under consideration with the 2σ experimentally allowed ranges of the three neutrino mixing angles for both types of the neutrino mass spectrum.

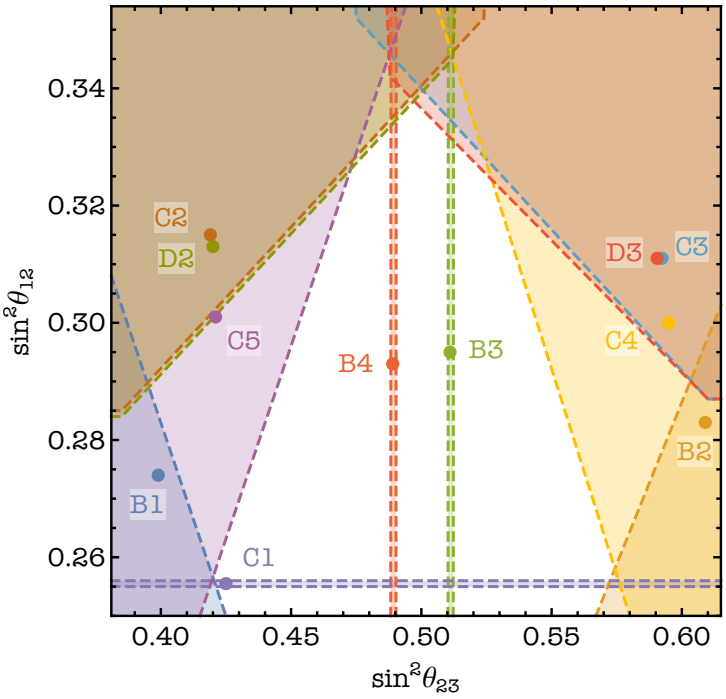

Figure 4.12: Summary of the predicted allowed regions in the $(\sin^2\theta_{23}, \sin^2\theta_{12})$ plane and the corresponding best-fit points in cases B1 – B4, C1 – C5, D2 and D3 for the NO neutrino mass spectrum. The values of all the three mixing angles are required to lie in their respective 3σ ranges.

Finally, we note that the sum rules for $\sin^2\theta_{23}$ ($\sin^2\theta_{12}$ in case C1) and $\cos\delta$ obtained here can be obtained from those derived in Ref. [176] for certain values of the parameters $\sin^2\theta^{\circ}_{ij}$ (defined within). In Ref. [176] only flavour symmetry, without gCP symmetry, has been considered. As we have seen in Section 4.2.1, a gCP symmetry does not allow for a free phase δ^{ν} coming from the neutrino sector, which is present otherwise. This, in turn, leads to the fact that in certain cases the free parameter $\sin\hat{\theta}^{\nu}_{ij}$ of Ref. [176] (see Eq. (213) within) gets fixed by the gCP symmetry. Thus, we find additional correlations between the θ_{ij} and between the θ_{ij} and $\cos\delta$ in these cases. The correspondence between the phenomenologically viable cases of the present study and the cases considered in Ref. [176] can be found in Appendix B.2.

4.4 Neutrinoless Double Beta Decay

As we have seen, in the class of models investigated in the present chapter, the Dirac and Majorana CPV phases, δ and α_{21}, α_{31}, are (statistically) predicted to lie in specific, in most cases relatively narrow, intervals and their values are strongly correlated. The only exception is case C1, in which the exact predictions $\alpha_{21} = 0$ or π and $(\alpha_{31} - 2\delta) = 0$ or π hold. These results make it possible to derive predictions for the absolute value of the neutrinoless double beta decay effective Majorana mass $\langle m \rangle$, as a function of the lightest neutrino mass, in the scenario where the exchange of three light Majorana neutrinos provides the dominant contribution to the decay rate (see preceding chapter).

In what follows, we obtain predictions for $|\langle m\rangle|$ using the phenomenologically viable neutrino mixing patterns found in Section 4.3.4. In Figs. 4.13 – 4.16 we present $|\langle m\rangle|$ as a function of the lightest neutrino mass $m_{\rm min}$ in cases B1 – B4, C1 – C3, C4 and C5, and D2 and D3. The solid and dashed lines limit the found allowed regions of $|\langle m\rangle|$ calculated using the predicted ranges for θ_{12}, θ_{13}, α_{21}, $(\alpha_{31}-2\delta)$. In the left panels we require the predicted values of $\sin^2\theta_{12}$, $\sin^2\theta_{13}$ and $\sin^2\theta_{23}$ to lie in their corresponding experimentally-allowed 3σ intervals, while in the right panels we require them to be inside the corresponding 2σ ranges. The mass-squared differences Δm^2_{21} and $\Delta m^2_{31(23)}$ in the case of NO (IO) spectrum are varied in the ranges given in Table 1.2. Here, the light-blue (light-red) areas in the left and right panels are obtained by varying the neutrino oscillation parameters θ_{12}, θ_{13}, Δm^2_{21} and $\Delta m^2_{31(23)}$ in their full 3σ and 2σ NO (IO) ranges, respectively, and varying the phases α_{21} and $(\alpha_{31}-2\delta)$ in the interval $[0, 2\pi)$. The horizontal brown and grey bands indicate the upper limits on $|\langle m\rangle|$ set by KamLAND-Zen and GERDA Phase II, respectively.[10] The vertical grey line represents the prospective upper limit on $m_{\rm min} \lesssim 0.2$ eV from the KATRIN experiment [158].

Several comments are in order. Firstly, for given values of (k_1, k_2) and a given ordering we find $|\langle m\rangle|$ to be inside of a band, which occupies a certain part of the allowed parameter space. Secondly, we note that most cases are compatible with both 3σ and 2σ ranges of all the mixing angles for both neutrino mass orderings (see Table 4.6). There are several exceptions. Namely, cases B2, C3, C4 and D3, in which, due to the correlations imposed by the employed symmetry, the predictions for $\sin^2\theta_{23}$ for the NO spectrum are not compatible with its 2σ allowed range (see Tables 4.2 and 4.3). Moreover, there is incompatibility for both orderings of cases B3 and B4 with the allowed 2σ ranges of $\sin^2\theta_{23}$ (see Table 4.2), and of case C1 with the 2σ range of $\sin^2\theta_{12}$ (see Table 4.3). Thirdly, the predictions for $|\langle m\rangle|$ compatible with the 3σ ranges of all the mixing angles are almost the same for the following pairs of cases: (B1, B2), (B3, B4), (C2, C3), (C4, C5) and (D2, D3). As discussed at the end of Section 4.3.4, the cases in each pair share some qualitative features, in particular, the allowed ranges of θ_{12}, θ_{13}, α_{21} and $(\alpha_{31}-2\delta)$ are approximately equal. We note also that case C1 stands out by having relatively narrow bands for $|\langle m\rangle|$ due to the predicted values of $\alpha_{21} = k_1\,\pi$ and $(\alpha_{31}-2\delta) = k_2\,\pi$. Finally, the results shown in Figs. 4.13 – 4.16 and derived using the predictions for the CPV phases and the mixing angles θ_{12} and θ_{13} in the case when the predicted values of all three mixing angles are compatible with their respective 3σ ranges, can be obtained analytically in the limiting cases of normal hierarchical, inverted hierarchical and quasi-degenerate spectra. This can be done by using the approximate expressions [25, 211]

$$|\langle m\rangle| \simeq \left|\sqrt{\Delta m^2_{21}}\,\sin^2\theta_{12}\cos^2\theta_{13}\,e^{i\alpha_{21}} + \sqrt{\Delta m^2_{31}}\,\sin^2\theta_{13}\,e^{i(\alpha_{31}-2\delta)}\right| \quad \text{(NH)}\,, \tag{4.102}$$

$$|\langle m\rangle| \simeq \sqrt{\Delta m^2_{23}}\,\cos^2\theta_{13}\left|\cos^2\theta_{12} + \sin^2\theta_{12}\,e^{i\alpha_{21}}\right| \quad \text{(IH)}, \tag{4.103}$$

$$|\langle m\rangle| \simeq m_{\rm min}\left|\cos^2\theta_{12} + \sin^2\theta_{12}\,e^{i\alpha_{21}}\right| \quad \text{(QD)}\,, \tag{4.104}$$

the values of Δm^2_{21} and $\Delta m^2_{31(23)}$ quoted in Table 1.2 and the results on $\sin^2\theta_{12}$, $\sin^2\theta_{13}$, δ, α_{21} and α_{31} given in Tables 4.2 and 4.3.

[10] The KamLAND-Zen limit considered is the one given in Eq. (3.4) while the GERDA Phase II limit plotted corresponds to $|\langle m\rangle| < (0.15 - 0.33)$ eV [210]. A more recent limit, $|\langle m\rangle| < (0.12 - 0.26)$ eV [151] exists. For our purposes, it does not differ significantly from the one used here.

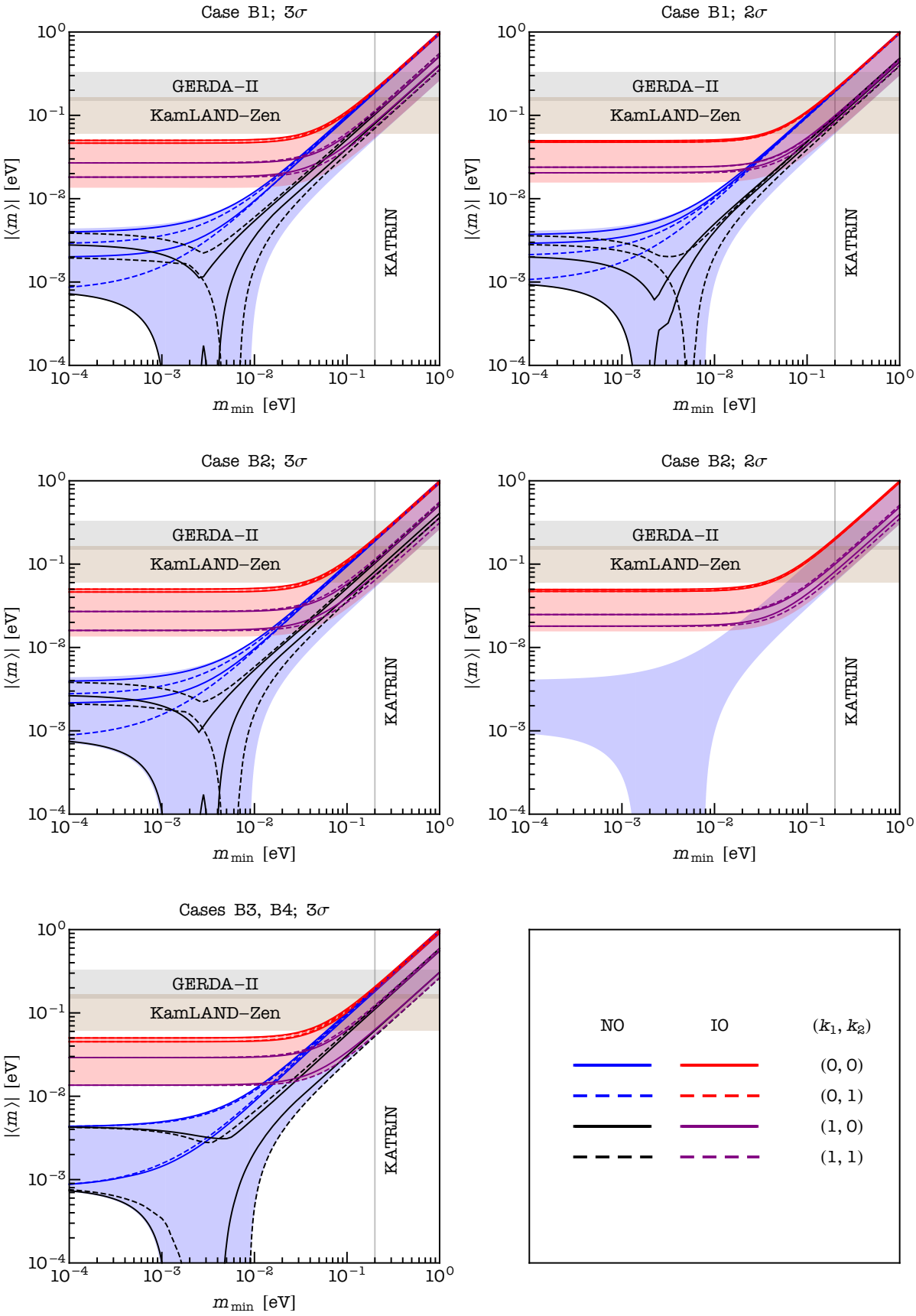

Figure 4.13: The magnitude of the effective Majorana mass versus the lightest neutrino mass. Lines limit the allowed regions of $|\langle m \rangle|$, calculated using the predictions of cases B1 – B4 and compatible with the 3σ (left panels) and 2σ (right panels) ranges of all mixing angles. Cases B3 and B4 are compatible with the 3σ ranges of the mixing angles, but not with their 2σ ranges.

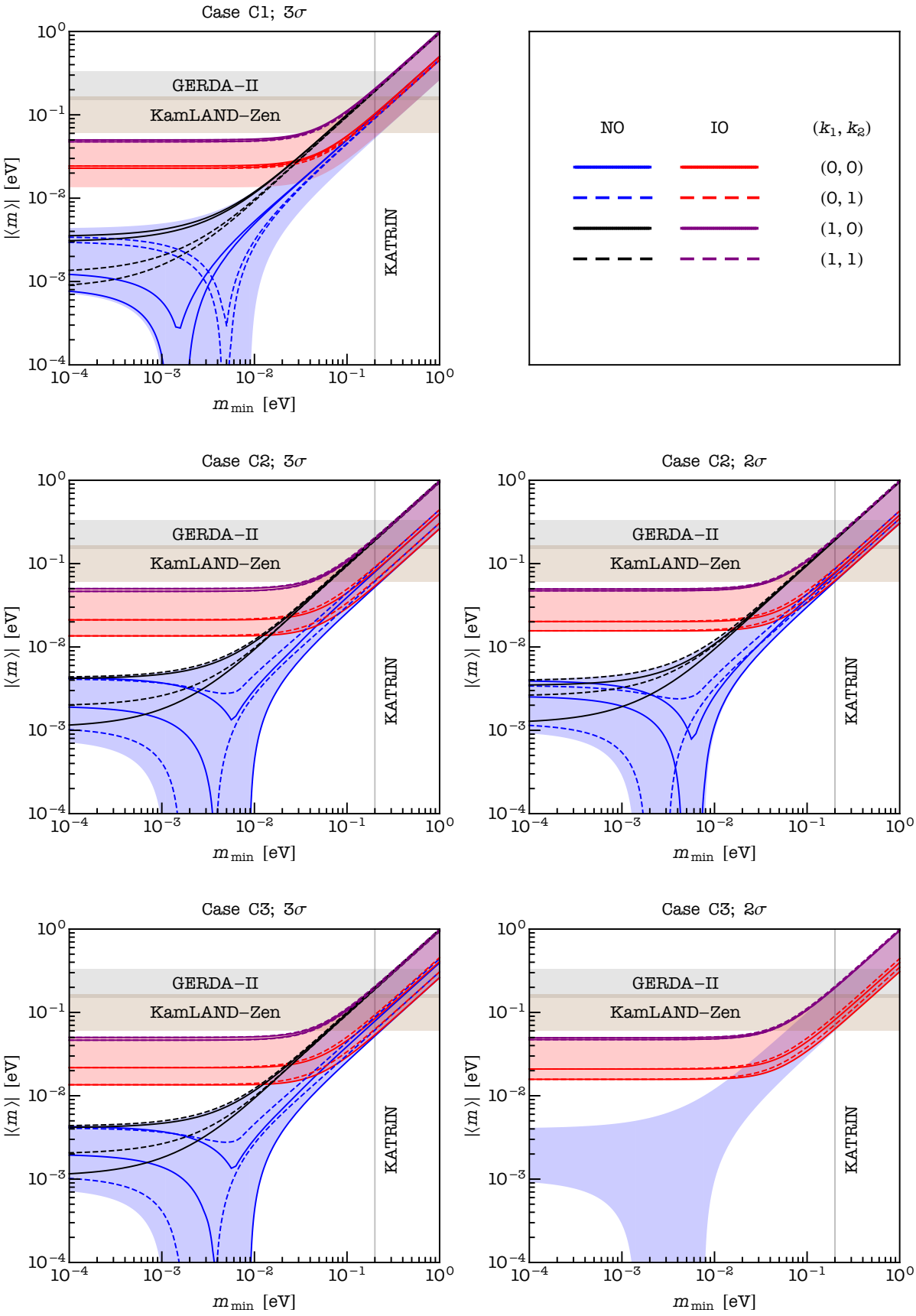

Figure 4.14: The same as in Fig. 4.13, but for cases C1 – C3. Case C1 is compatible with the 3σ ranges of the mixing angles, but not with their 2σ ranges.

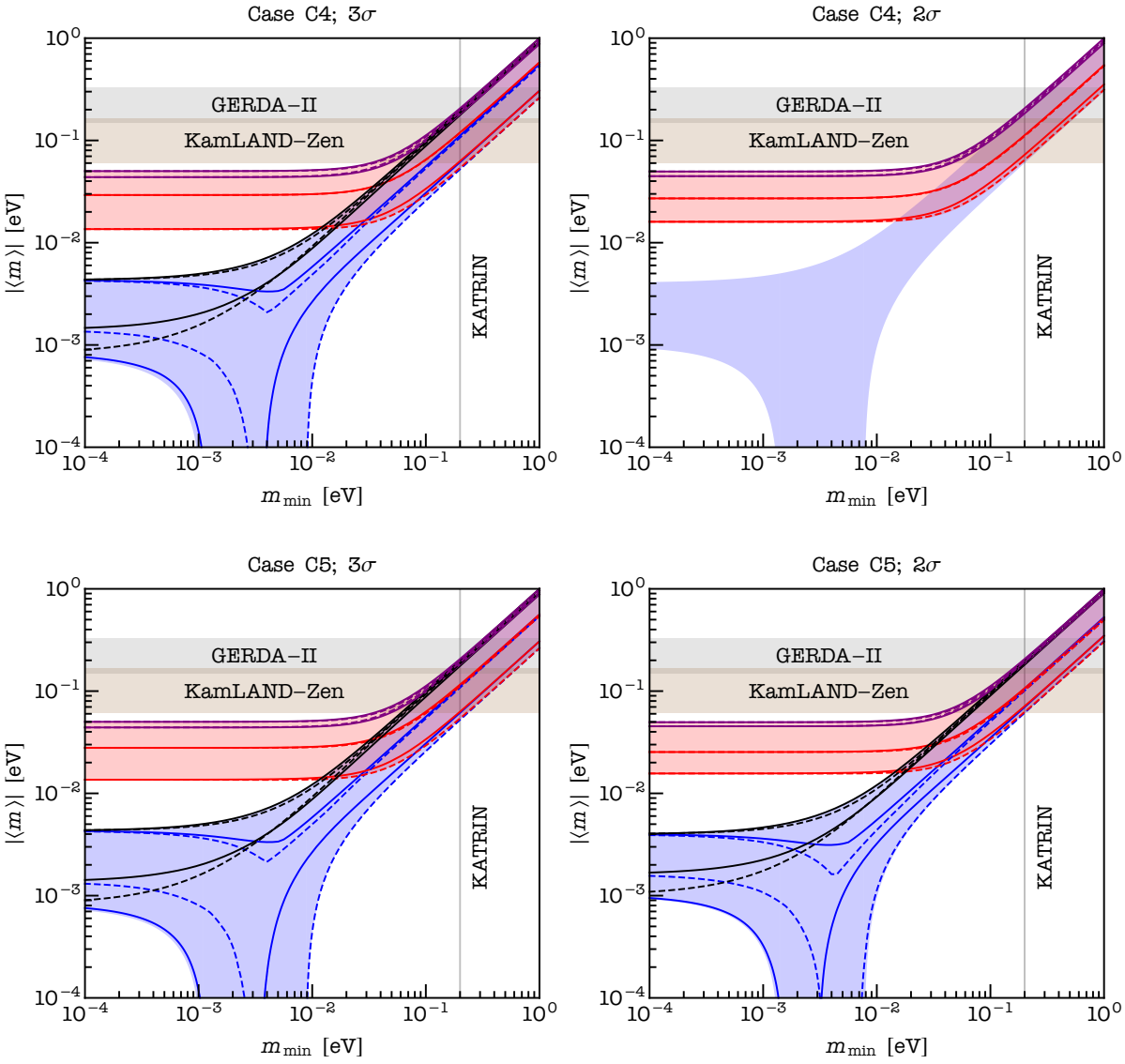

Figure 4.15: The same as in Fig. 4.13, but for cases C4 and C5.

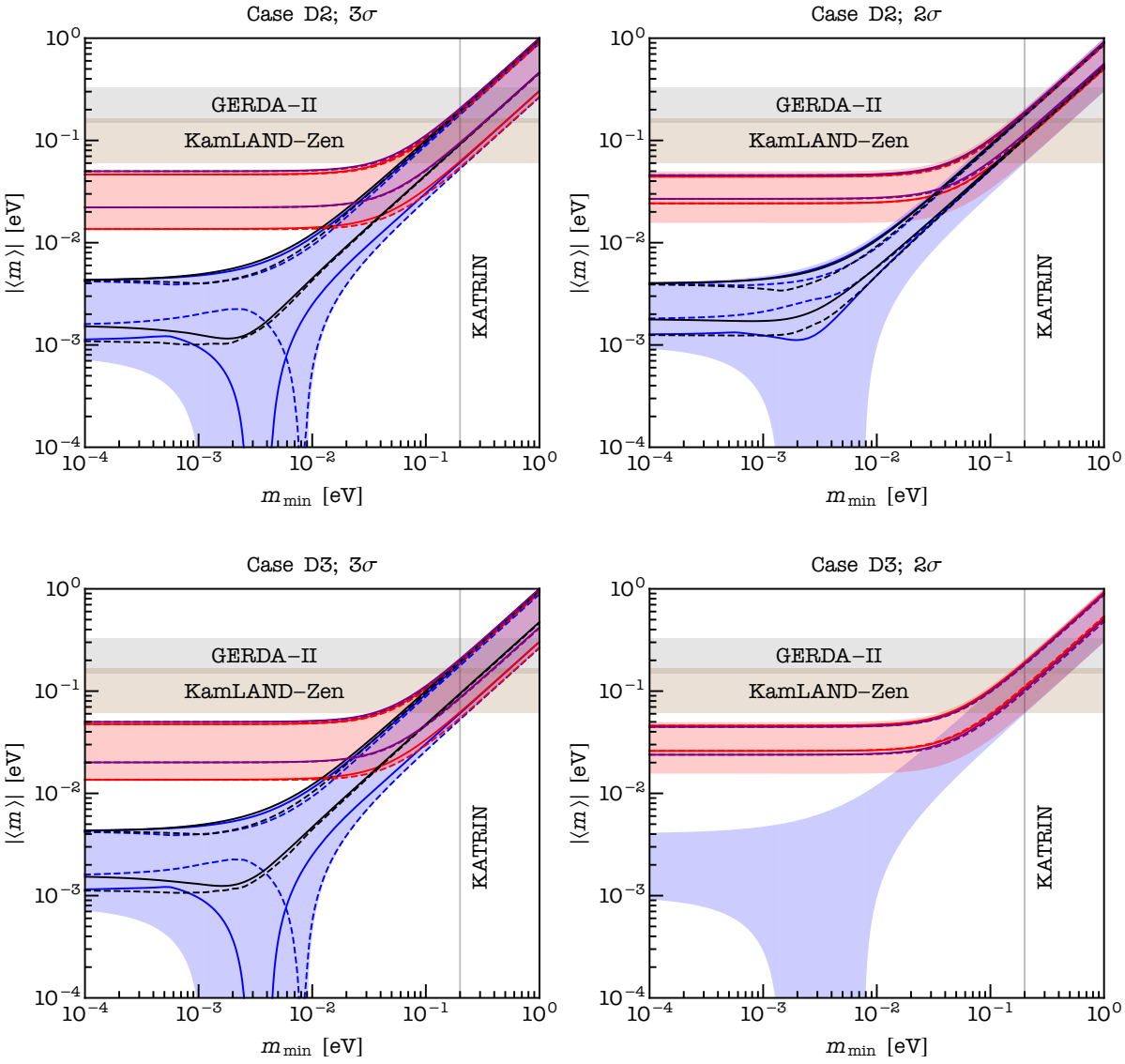

Figure 4.16: The same as in Fig. 4.13, but for cases D2 and D3.

4.5 Chapter Summary

In the present chapter we have derived predictions for neutrino mixing and CPV phases in a class of models based on S_4 lepton flavour symmetry combined with a generalised CP symmetry $H_{\rm CP}$, which are broken to residual $Z_2^{g_e}$ and $Z_2^{g_\nu} \times H_{\rm CP}^\nu$ symmetries in the charged lepton and neutrino sectors, respectively. We have shown that in this class of models the three neutrino mixing angles, θ_{12}, θ_{23} and θ_{13}, the Dirac and the two Majorana CP violation (CPV) phases, δ and α_{21}, α_{31}, are functions of altogether three parameters – two mixing angles and a phase, θ^e, θ^ν and δ^e.

We have found that effectively there are 4 distinct groups of cases to be considered. In all four groups of cases the PMNS matrix is predicted to contain one constant element which does not depend on the free parameters θ^e, θ^ν and δ^e. The magnitude of this element is equal to $1/\sqrt{2}$ in the "Group A" cases of $\{G_e, G_\nu\} = \{Z_2^{TU}, Z_2^S \times H_{\rm CP}^\nu\}$ with $H_{\rm CP}^\nu = \{1, S\}$, and in the "Group B" cases of $\{G_e, G_\nu\} = \{Z_2^{TU}, Z_2^S \times H_{\rm CP}^\nu\}$ with $H_{\rm CP}^\nu = \{U, SU\}$; and it is equal to $1/2$ in the "Group C" cases of $\{G_e, G_\nu\} = \{Z_2^{TU}, Z_2^U \times H_{\rm CP}^\nu\}$ with $H_{\rm CP}^\nu = \{1, U\}$, and in the "Group D" cases of $\{G_e, G_\nu\} = \{Z_2^{TU}, Z_2^U \times H_{\rm CP}^\nu\}$ with $H_{\rm CP}^\nu = \{S, SU\}$. In the approach employed, the PMNS matrix is determined up to permutations of columns and rows. Taking into account neutrino oscillation data, only 4 elements can have an absolute value equal to $1/\sqrt{2} \simeq 0.707$, and only 5 elements can have an absolute value equal to $1/2$. These potential 18 cases are reduced to 15 due to further constraints in the A and D groups. From these, 4 are strongly disfavoured by data and one is left with 11 viable cases. The results of the statistical analysis for such cases are presented graphically in Figs. 4.1 – 4.11. The predicted ranges of the neutrino mixing parameters and the their corresponding best-fit values are summarised in Tables 4.2 – 4.5.

As a consequence of the fact that, in the class of models we consider, the six PMNS matrix parameters, θ_{12}, θ_{23}, θ_{13}, δ, α_{21} and α_{31}, are fitted with the three parameters, θ^e, θ^ν and δ^e, it is not surprising that there are strong correlations i) between the values of the Dirac phase δ and the values of the two Majorana phases α_{21} and α_{31}, which in turn are correlated between themselves (Figs. 4.1, 4.2, 4.6 – 4.9), and depending on the case ii) either between the values of θ_{12} and θ_{13} (Fig. 4.5), or between the values of θ_{23} and θ_{13} (Figs. 4.3 and 4.4) or else between the values of θ_{12} and θ_{23} (Figs. 4.1, 4.2, 4.6 – 4.11). In certain cases our results showed strong correlations between the predicted values of θ_{23} and the Dirac phase δ and/or the Majorana phases $\alpha_{21,31}$ (Figs. 4.8 – 4.11).

In the cases of i) Group B with $|(U_{\rm PMNS})_{\mu 2}| = 1/\sqrt{2}$, or $|(U_{\rm PMNS})_{\tau 2}| = 1/\sqrt{2}$, ii) Group C with $|(U_{\rm PMNS})_{\mu 1}| = 1/2$, or $|(U_{\rm PMNS})_{\tau 1}| = 1/2$, or $|(U_{\rm PMNS})_{\mu 2}| = 1/2$, or $|(U_{\rm PMNS})_{\tau 2}| = 1/2$, and iii) Group D with $|(U_{\rm PMNS})_{\mu 1}| = 1/2$, or $|(U_{\rm PMNS})_{\tau 1}| = 1/2$, the cosine of the Dirac phase δ satisfies a sum rule by which it is expressed in terms of the three neutrino mixing angles θ_{12}, θ_{23} and θ_{13}. Taking into account the ranges and correlations of the predicted values of the three neutrino mixing angles, δ is predicted to lie in certain, in most of the discussed cases rather narrow, intervals (Section 4.3.4).

We have derived also predictions for the Majorana CPV phases α_{21} and α_{31} in all viable cases. With one exception – the case of $|(U_{\rm PMNS})_{e2}| = 1/2$ of Group C – the values of α_{21} and α_{31}, as we have indicated earlier, are strongly correlated between themselves. In case C1 there is a strong linear correlation between α_{31} and δ. Using the predictions for the Dirac and Majorana CPV phases allowed us to derive predictions

for the magnitude of the neutrinoless double beta decay effective Majorana mass, $|\langle m \rangle|$, as a function of the lightest neutrino mass for all the viable cases belonging to Groups B, C and D. They are presented graphically in Figs. 4.13 – 4.16.

All viable cases in the class of S_4 models here investigated have distinct predictions for the set of observables $\sin^2\theta_{12}$, $\sin^2\theta_{23}$, $\sin^2\theta_{13}$, the Dirac phase δ and the absolute value of one element of the PMNS neutrino mixing matrix. Using future more precise data on $\sin^2\theta_{12}$, $\sin^2\theta_{23}$, $\sin^2\theta_{13}$ and the Dirac phase δ, which will allow also to determine the absolute values of the elements of the PMNS matrix with a better precision, will make it possible to test and discriminate symmetry breaking predictions.

5 Modular Invariance

As we have seen, a popular approach to explaining the observed mixing patterns consists in assuming the presence of a spontaneously broken discrete flavour symmetry. However, in concrete models, such breaking typically requires the introduction of a plethora of scalar fields (flavons) with a set of particularly aligned vacuum expectation values. Arranging for such an alignment usually calls for the construction of rather "baroque" scalar potentials. In the modular symmetry approach, the VEV of the modulus τ may be the only source of symmetry breaking, bypassing the need for many flavon fields. Leading-order predictions may be derived by treating τ as a spurion.

In the present chapter we follow Ref. [93] and investigate the consequences of the presence of modular invariance in the lepton sector. We focus on the action of the finite modular group Γ_4, which is isomorphic to the group of permutations of four objects S_4. After reviewing the necessary formalism, we explicitly construct the generators of modular forms of level $N = 4$. We then investigate two minimal models where neutrino masses arise from the dimension 5 Weinberg operator and where no flavons are introduced.

5.1 The Framework

As in Ref. [91], we consider the infinite groups $\Gamma(N)$,

$$\Gamma(N) \equiv \left\{ \gamma = \begin{pmatrix} a & b \\ c & d \end{pmatrix} \,\middle|\, a, b, c, d \in \mathbb{Z} \wedge \det\gamma = 1 \wedge \gamma = \begin{pmatrix} 1 & 0 \\ 0 & 1 \end{pmatrix} \pmod N \right\}, \tag{5.1}$$

where N is a positive integer. The group $\Gamma(1) \simeq \mathrm{SL}(2,\mathbb{Z})$ is the modular group and $\Gamma(N > 1)$ are normal subgroups of $\Gamma(1)$. Taking the quotient of $\Gamma(1)$ and $\Gamma(2)$ by $\{\mathbb{1}, -\mathbb{1}\}$ we obtain the groups of linear fractional transformations, $\overline{\Gamma}(N) \equiv \Gamma(N)/\{\mathbb{1}, -\mathbb{1}\}$ for $N = 1, 2$, and $\overline{\Gamma}(N > 2) \equiv \Gamma(N)$. Elements of $\overline{\Gamma}(N)$ act on a complex variable τ as:

$$\tau \to \gamma\tau = \frac{a\tau + b}{c\tau + d}, \quad \text{with } \gamma = \begin{pmatrix} a & b \\ c & d \end{pmatrix} \in \overline{\Gamma}(N), \tag{5.2}$$

and it can be shown that the upper half-plane $\{\tau \in \mathbb{C} \,|\, \mathrm{Im}(\tau) > 0\}$ is mapped to itself under this action. The complex variable τ is henceforth restricted to have positive imaginary part.

We are interested in studying physical actions which are invariant under transformations of the finite modular groups Γ_N. These discrete groups are obtained from the quotient of two of the aforementioned infinite groups, namely $\Gamma_N \equiv \overline{\Gamma}(1)/\overline{\Gamma}(N)$. The group $\overline{\Gamma}(1)$ is generated by two elements S and T acting

on τ as

$$S:\ \tau \to -1/\tau\,, \qquad S = \begin{pmatrix} 0 & 1 \\ -1 & 0 \end{pmatrix}\,, \tag{5.3}$$

$$T:\ \tau \to \tau + 1\,, \qquad T = \begin{pmatrix} 1 & 1 \\ 0 & 1 \end{pmatrix}\,, \tag{5.4}$$

and satisfying

$$S^2 \,=\, (ST)^3 \,=\, \mathbb{1}\,. \tag{5.5}$$

The presentation of the groups Γ_N can be obtained from that of $\overline{\Gamma}(1)$ by extending it with the condition $T^N = \mathbb{1}$, see Eq. (5.1). Thus, the generators S and T of Γ_N obey

$$S^2 \,=\, (ST)^3 \,=\, T^N \,=\, \mathbb{1}\,. \tag{5.6}$$

We consider modular-invariant $\mathcal{N} = 1$ global supersymmetric (SUSY) actions [212, 213],

$$\mathcal{S} \,=\, \int d^4x\, d^2\theta\, d^2\overline{\theta}\ K(\chi_i, \overline{\chi}_i; \tau, \overline{\tau}) + \int d^4x\, d^2\theta\ W(\chi_i; \tau) + \text{h.c.}\,, \tag{5.7}$$

where χ_i denotes the set of matter chiral superfields of the theory.[1] The physical action $\mathcal{S}$ is required to be invariant under the action of Γ_N. Under an element of this group, one has the following transformations of τ and of the fields χ_i:

$$\begin{cases} \tau \,\to\, \gamma\tau = \dfrac{a\tau + b}{c\tau + d} \\[2ex] \chi_i \,\to\, (c\tau + d)^{-k_i}\, \rho_i(\gamma)\, \chi_i \end{cases}\,, \qquad \text{with } \gamma = \begin{pmatrix} a & b \\ c & d \end{pmatrix} \in \Gamma_N\,, \tag{5.8}$$

where ρ_i are unitary representation matrices and the k_i are integers. The fields χ_i are said to carry weigth $-k_i$. We require that the superpotential W remains invariant under Γ_N and that the Kähler potential is changed at most by a Kähler transformation. To satisfy this last condition, we work with the Kähler:

$$K(\chi_i, \overline{\chi}_i; \tau, \overline{\tau}) = -h\, \Lambda_0^2\, \log(-i(\tau - \overline{\tau})) + \sum_i \frac{|\chi_i|^2}{(-i(\tau - \overline{\tau}))^{k_i}}\,, \tag{5.9}$$

with $h > 0$ and Λ_0 a mass parameter. After τ develops a VEV, it gives rise to kinetic terms for the matter fields,

$$\mathcal{L} \,\supset\, \sum_i \frac{\partial_\mu \overline{\chi}_i\, \partial^\mu \chi_i}{(2\,\text{Im}\langle\tau\rangle)^{k_i}}\,. \tag{5.10}$$

These terms can be made canonical by rescaling the fields χ_i, which in practice amounts to a redefinition of superpotential parameters. The superpotential reads

$$W(\chi_i; \tau) = \sum_n \sum_{\{i_1, \ldots, i_n\}} \left(Y_{\{i_1, \ldots, i_n\}}(\tau)\ \chi_{i_1} \cdots \chi_{i_n}\right)_{\mathbf{1}}\,, \tag{5.11}$$

and should remain unchanged under Γ_N.

[1] Following Ref. [91], we turn off gauge interactions and treat τ as a dimensionless spurion.

Given the field transformations in Eq. (5.8), the functions $Y_{\{i_1,\ldots,i_n\}}(\tau)$ in (5.11) must transform under Γ_N as (we omit the indices $i_1, \ldots, i_n$):

$$\begin{cases} \tau \;\to\; \gamma\tau = \dfrac{a\tau+b}{c\tau+d} \\ \\ Y(\tau) \;\to\; Y(\gamma\tau) = (c\tau+d)^{2k_Y}\,\rho_Y(\gamma)\,Y(\tau) \end{cases} , \qquad \text{with } \gamma = \begin{pmatrix} a & b \\ c & d \end{pmatrix} \in \Gamma_N\,, \tag{5.12}$$

where the unitary matrix $\rho_Y(\gamma)$ and the non-negative integer k_Y, as will shortly be shown, must satisfy specific conditions.

Holomorphic functions $f(\tau)$ satisfying $f(\gamma\tau) = (c\tau+d)^{2k} f(\tau)$ with $\gamma \in \Gamma(N)$ and $k \in \mathbb{N}_0$ are said to be modular forms of weight $2k$ and level N. For $k = 0$, the modular forms are constant functions, while for $k < 0$ modular forms do not exist. Modular forms are important objects in the present construction since, under Γ_N, modular forms of weight $2k_Y$ and level N transform in the way we require $Y(\tau)$ in Eq. (5.12) to transform. The requirement of invariance of the superpotential then implies that the functions $Y(\tau)$ are modular forms of level N. Their weights must cancel those of the fields in Eq. (5.11), $2k_Y - k_{i_1} - \ldots - k_{i_n} = 0$. Additionally, the tensor product $\rho_Y \otimes \rho_{i_1} \otimes \ldots \otimes \rho_{i_1}$ should contain at least one singlet. The subscript **1** in Eq. (5.11) indicates a sum (with independent coefficients) of all possible singlets one can extract from this product.

The effects of invariance under Γ_N for $N = 2$ and $N = 3$ have been studied in Refs. [91, 92]. The group Γ_2 is isomorphic to S_3 while $\Gamma_3 \simeq A_4$ (see also [214, 215]). In what follows we consider invariance under the group $\Gamma_4 \simeq S_4$, whose generators satisfy the following presentation rules:

$$S^2 \;=\; (ST)^3 \;=\; T^4 \;=\; \mathbb{1}\,. \tag{5.13}$$

For a generic value of $\langle\tau\rangle$, Γ_4 will be fully broken. It is important to remark that the leading-order results obtained with this approach are susceptible to corrections from a small number of sources, namely from SUSY breaking and corrections to the Kähler potential. In generalisations of our approach where flavons are introduced, additional corrections are expected from vacuum (mis)alignment.

5.1.1 Generators of Modular Forms of Level $N = 4$

The functions $Y(\tau)$ are modular forms of level $N = 4$ and weight $2k_Y$. The dimension of the space of modular forms of level 4 and weight $2k$ is $4k + 1$. Thus, the space of (level 4) forms which carry the lowest non-trivial weight, $2k = 2$, has dimension $4k + 1 = 5$. It proves useful to explicitly find a basis $\{Y_1(\tau), \ldots, Y_5(\tau)\}$ of this lowest weight space, since modular forms of higher weights can be constructed from homogeneous polynomials in these five modular forms Y_i $(i = 1, \ldots, 5)$.

A starting point in this search is the recognition of certain properties of the Dedekind eta function $\eta(z \in \mathbb{C})$, defined as:

$$\eta(z) \;\equiv\; q^{1/24} \prod_{k=1}^{\infty} (1 - q^k)\,, \qquad \text{with } q = e^{2\pi i\, z}\,. \tag{5.14}$$

The η function satisfies $\eta(z+1) = e^{i\pi/12}\,\eta(z)$ and $\eta(-1/z) = \sqrt{-iz}\,\eta(z)$, as well as the identity (see, e.g., [216]):

$$\eta\left(z+\frac{1}{2}\right) = e^{i\pi/24}\,\frac{\eta^3(2z)}{\eta(z)\eta(4z)}\,. \tag{5.15}$$

One sees that the set

$$\{\eta_i\} = \left\{\eta\left(\tau+\frac{1}{2}\right),\,\eta\left(4\tau\right),\,\eta\left(\frac{\tau}{4}\right),\,\eta\left(\frac{\tau+1}{4}\right),\,\eta\left(\frac{\tau+2}{4}\right),\,\eta\left(\frac{\tau+3}{4}\right)\right\} \tag{5.16}$$

respects a certain notion of closure under the action of Γ_4 generators S and T, since under their action one has:

$$S: \quad \begin{cases} \eta\left(\tau+\frac{1}{2}\right) & \to & \frac{1}{\sqrt{2}}\sqrt{-i\tau}\,\eta\left(\frac{\tau+2}{4}\right) \\ \eta\left(4\tau\right) & \to & \frac{1}{2}\sqrt{-i\tau}\,\eta\left(\frac{\tau}{4}\right) \\ \eta\left(\frac{\tau}{4}\right) & \to & 2\sqrt{-i\tau}\,\eta\left(4\tau\right) \\ \eta\left(\frac{\tau+1}{4}\right) & \to & e^{-i\pi/6}\sqrt{-i\tau}\,\eta\left(\frac{\tau+3}{4}\right) \\ \eta\left(\frac{\tau+2}{4}\right) & \to & \sqrt{2}\sqrt{-i\tau}\,\eta\left(\tau+\frac{1}{2}\right) \\ \eta\left(\frac{\tau+3}{4}\right) & \to & e^{i\pi/6}\sqrt{-i\tau}\,\eta\left(\frac{\tau+1}{4}\right) \end{cases} \tag{5.17}$$

and

$$T: \quad \begin{cases} \eta\left(\tau+\frac{1}{2}\right) & \to & e^{i\pi/12}\,\eta\left(\tau+\frac{1}{2}\right) \\ \eta\left(4\tau\right) & \to & e^{i\pi/3}\,\eta\left(4\tau\right) \\ \eta\left(\frac{\tau}{4}\right) & \to & \eta\left(\frac{\tau+1}{4}\right) \\ \eta\left(\frac{\tau+1}{4}\right) & \to & \eta\left(\frac{\tau+2}{4}\right) \\ \eta\left(\frac{\tau+2}{4}\right) & \to & \eta\left(\frac{\tau+3}{4}\right) \\ \eta\left(\frac{\tau+3}{4}\right) & \to & e^{i\pi/12}\,\eta\left(\frac{\tau}{4}\right)\,. \end{cases} \tag{5.18}$$

The transformations under S of the elements $\eta(\tau+1/2)$ and $\eta((\tau+2)/4)$ can be derived by making use of the relation (5.15). Up to multiplicative factors, this set is closed under S and T. Furthermore, each element is taken into itself (up to a factor) by the (left-)actions of S^2, $(ST)^3$ and T^4. The above suggests that the desired $k=1$ modular forms can be written as linear combinations of the logarithmic derivatives of the elements of the set $\{\eta_i\}$. We define:

$$\begin{aligned} Y(a_1,\ldots,a_6|\tau) &\equiv \frac{d}{d\tau}\left(\sum_{i=1}^{6} a_i\,\log\eta_i(\tau)\right) \\ &= a_1\frac{\eta'(\tau+1/2)}{\eta(\tau+1/2)} + 4\,a_2\frac{\eta'(4\tau)}{\eta(4\tau)} + \frac{1}{4}\Bigg[a_3\frac{\eta'(\tau/4)}{\eta(\tau/4)} \\ &\quad + a_4\frac{\eta'((\tau+1)/4)}{\eta((\tau+1)/4)} + a_5\frac{\eta'((\tau+2)/4)}{\eta((\tau+2)/4)} + a_6\frac{\eta'((\tau+3)/4)}{\eta((\tau+3)/4)}\Bigg]. \end{aligned} \tag{5.19}$$

The use of logarithmic derivatives allows one to eliminate the multiplicative factors in the transformations (5.17) and (5.18) by requiring $\sum_i a_i = 0$. We are thus left with five independent linear combinations of the η_i'/η_i, as expected. Under the action of the generators S and T this function transforms as:

$$S:\ Y(a_1,\ldots,a_6|\tau)\ \to\ Y(a_1,a_2,a_3,a_4,a_5,a_6|-1/\tau)\ =\ \tau^2\, Y(a_5,a_3,a_2,a_6,a_1,a_4|\tau)\,, \tag{5.20}$$

$$T:\ Y(a_1,\ldots,a_6|\tau)\ \to\ Y(a_1,a_2,a_3,a_4,a_5,a_6|\tau+1)\ =\ Y(a_1,a_2,a_6,a_3,a_4,a_5|\tau)\,. \tag{5.21}$$

We find a basis for lowest weight modular forms,

$$\begin{aligned}
Y_1(\tau) &\equiv Y(1,1,\omega,\omega^2,\omega,\omega^2|\tau)\,,\\
Y_2(\tau) &\equiv Y(1,1,\omega^2,\omega,\omega^2,\omega|\tau)\,,\\
Y_3(\tau) &\equiv Y(1,-1,-1,-1,1,1|\tau)\,,\\
Y_4(\tau) &\equiv Y(1,-1,-\omega^2,-\omega,\omega^2,\omega|\tau)\,,\\
Y_5(\tau) &\equiv Y(1,-1,-\omega,-\omega^2,\omega,\omega^2|\tau)\,,
\end{aligned} \tag{5.22}$$

where $\omega \equiv e^{2\pi i/3}$. These five linearly independent forms $Y_i(\tau)$ arrange themselves into two irreducible representations of $\Gamma_4 \simeq S_4$, a doublet $\mathbf{2}$ and a triplet $\mathbf{3'}$,

$$Y_{\mathbf{2}}(\tau)\ \equiv\ \begin{pmatrix} Y_1(\tau) \\ Y_2(\tau) \end{pmatrix}\,, \qquad Y_{\mathbf{3'}}(\tau)\ \equiv\ \begin{pmatrix} Y_3(\tau) \\ Y_4(\tau) \\ Y_5(\tau) \end{pmatrix}\,. \tag{5.23}$$

The multiplets $Y_{\mathbf{2}}$ and $Y_{\mathbf{3'}}$ transform under Γ_4 as indicated in Eq. (5.12). In Appendix A.1 we specify our basis choice for the representation matrices $\rho(\gamma)$ of S_4 and we list the Clebsch-Gordan coefficients for this basis in Appendix A.2. In Appendix C.1 we give the q-expansions of (combinations of) the five functions defined in Eq. (5.22).

Multiplets transforming in the other representations of S_4 can be obtained from tensor products of $Y_{\mathbf{2}}$ and $Y_{\mathbf{3'}}$. The representations $\mathbf{1}$ and $\mathbf{3}$ arise at weight $2k = 4$, while the $\mathbf{1'}$ representation first arises at weight 6. Since we can form 15 combinations Y_iY_j, one may expect 15 independent (level 4) forms at weight $2k = 4$. However, the dimension of the space of these forms is $4k + 1 = 9$. In fact, we find 6 constraints between the several Y_iY_j, which we list in Appendix C.2. These constraints reduce the 15 potentially independent combinations to 9 truly independent ones, which are organised in the following representations of S_4:

$$\begin{aligned}
Y^{(4)}_{\mathbf{1}} &= Y_1Y_2 \ \sim\ \mathbf{1}\,,\\
Y^{(4)}_{\mathbf{2}} &= (Y_2^2,\, Y_1^2)^T \ \sim\ \mathbf{2}\,,\\
Y^{(4)}_{\mathbf{3}} &= (Y_1Y_4 - Y_2Y_5,\, Y_1Y_5 - Y_2Y_3,\, Y_1Y_3 - Y_2Y_4)^T \ \sim\ \mathbf{3}\,,\\
Y^{(4)}_{\mathbf{3'}} &= (Y_1Y_4 + Y_2Y_5,\, Y_1Y_5 + Y_2Y_3,\, Y_1Y_3 + Y_2Y_4)^T \ \sim\ \mathbf{3'}\,.
\end{aligned} \tag{5.24}$$

5.2 Phenomenology

To understand how invariance under the subgroup Γ_4 of the modular group may play a role in determining lepton masses and mixing, one needs to specify the S_4 representations ρ_i and the modular

		H_u	H_d	L	$E^c_{1,2,3}$
$\mathrm{SU}(2)_L \times \mathrm{U}(1)_Y$		$(\mathbf{2}, 1/2)$	$(\mathbf{2}, -1/2)$	$(\mathbf{2}, -1/2)$	$(\mathbf{1}, 1)$
Γ_4	ρ_i	ρ_d	ρ_u	ρ_L	$\rho_{1,2,3}$
	k_i	k_u	k_d	k_L	$k_{1,2,3}$

Table 5.1: Transformation properties of the relevant MSSM chiral superfields under the gauge group and under the Γ_4 discrete modular symmetry. The ρ_i denote the representations of the fields transforming under S_4 and the k_i correspond to (minus) their modular weights.

weights $-k_i$ of the relevant fields χ_i, which transform as indicated in Eq. (5.8). In what follows, we search for choices of representations and weights which are in line with a certain notion of minimality.

In a minimal approach, the superpotential W includes only the Yukawa interactions of the Minimal Supersymmetric Standard Model (MSSM) and the SUSY Weinberg operator as the origin of (Majorana) neutrino masses:

$$W \,=\, \alpha \left(\hat{E}^c\, \hat{L}\, \hat{H}_d\, f_E(Y_{\mathbf{2}}, Y_{\mathbf{3}'})\right)_{\mathbf{1}} + \frac{g}{\Lambda} \left(\hat{L}\, \hat{H}_u\, \hat{L}\, \hat{H}_u\, f_W(Y_{\mathbf{2}}, Y_{\mathbf{3}'})\right)_{\mathbf{1}}, \tag{5.25}$$

where, as mentioned before, different coefficients are implied for different singlet combinations (we drop hats denoting superfields in what follows). No flavons are present in the above superpotential. Recall also that the functions $Y_{\mathbf{2}} = Y_{\mathbf{2}}(\tau)$ and $Y_{\mathbf{3}'} = Y_{\mathbf{3}'}(\tau)$ have definite transformation properties under Γ_4. After the breaking of modular symmetry we obtain:

$$W \,\to\, \lambda_{ij}\, E^c_i\, (L_j\, H_d) + c_{ij}\, (L_i\, H_u)\, (L_j\, H_u)\,, \tag{5.26}$$

which leads to the Lagrangian terms (cf. Eq. (1.13))

$$\mathcal{L} \,\supset\, -\frac{1}{2} \left(M_\nu\right)_{ij} \overline{\nu^C_{iR}}\, \nu_{jL} - \left(M_e\right)_{ij} \overline{\ell_{iL}}\, \ell_{jR} + \text{h.c.}\,, \tag{5.27}$$

written in terms of four-spinors, where $M_e \equiv v_d\, \lambda^\dagger$ and $M_\nu \equiv 2\, c\, v_u^2$, with $\langle H_u \rangle = (0, v_u)^T$ and $\langle H_d \rangle = (v_d, 0)^T$.[2]

The generic assignments of representations and weights to the MSSM fields present in Eq. (5.25) are defined in Table 5.1. We will keep the Higgs sector assignments trivial for simplicity. We will also take lepton doublets (singlets) to transform as three (one) dimensional representations of S_4, as is customary. Minimal models are then built by adhering to the following guidelines:

- No flavons are introduced,
- Neutrino masses arise from the dimension 5 Weinberg operator,
- Higgs multiplets transform trivially $\rho_{u,d} \sim \mathbf{1}$ under Γ_4, with $k_{u,d} = 0$,
- Lepton $\mathrm{SU}(2)_L$ doublets transform as a triplet $\rho_L \sim \mathbf{3}$ or $\mathbf{3}'$ under Γ_4,
- Lepton $\mathrm{SU}(2)_L$ singlets transform as singlets $\rho_{1,2,3} \sim \mathbf{1}$ or $\mathbf{1}'$ under Γ_4, and

[2] In the decoupling limit of the MSSM (e.g. when the heavier Higgs scalar states have masses exceeding ~ 1 TeV), the lightest Higgs boson couplings to charged leptons (and, for that matter, also to quarks) differ insignificantly from those of the Standard Model Higgs.

- Lowest possible weights are chosen such that a rank 3 charged-lepton mass matrix M_e is possible without imposing additional "shaping" symmetries.

Given the above conditions, we further expand the superpotential as:

$$W = \sum_i \alpha_i \left(E_i^c\, L\, H_d\, Y_{\mathbf{2}}^{a_i}\, Y_{\mathbf{3'}}^{b_i}\right)_{\mathbf{1}} + \frac{g}{\Lambda}\left(L\, H_u\, L\, H_u\, Y_{\mathbf{2}}^{c}\, Y_{\mathbf{3'}}^{d}\right)_{\mathbf{1}}, \tag{5.28}$$

where the integer, non-negative exponents of the modular forms satisfy $2(a_i+b_i) = k_L+k_i+k_d = k_L+k_i$ and $2(c+d) = 2(k_L+k_u) = 2k_L$. In order to obtain some non-trivial structure in the Weinberg operator, we assume that $k_L > 0$. We explore in what follows two minimal choices of weights and representations, corresponding to $k_L = 1$ (model I) and $k_L = 2$ (model II).

5.2.1 Model I ($k_L = 1$)

The choices $k_L = 1$ and $k_u = 0$ along with the fact that $\rho_L \sim \mathbf{3}$ or $\rho_L \sim \mathbf{3'}$ are enough to determine the structure of the Weinberg operator and hence of the neutrino mass matrix M_ν.

On the charged lepton side, the cancellation-of-weights condition $2(a_i + b_i) = 1 + k_i$ implies that the k_i are odd, $k_i \in \{-1, 1, 3, \ldots\}$. To avoid having rank$(\lambda) < 3$, one must make sure that different singlets can be extracted from each term in W. If two lepton singlet superfields share the same weight and representation under Γ_4, the rank of the charged-lepton mass matrix is lower than its possible maximum. If some $k_i = -1$, then $a_i = b_i = 0$ and no singlet can be formed for that generation. If instead $k_i = 1$, a singlet can only be formed if $\rho_i \sim \mathbf{1'}$ $(\mathbf{1})$ when $\rho_L \sim \mathbf{3}$ $(\mathbf{3'})$. We summarise in Table 5.2 the weight and representation assignments of the minimal model allowing for rank$(\lambda) = 3$.

	H_u	H_d	L	E_1^c	E_2^c	E_3^c
ρ_i	$\mathbf{1}$	$\mathbf{1}$	$\mathbf{3}$ $\mathbf{3'}$	$\mathbf{1'}$ $\mathbf{1}$	$\mathbf{1}$ $\mathbf{1'}$	$\mathbf{1'}$ $\mathbf{1}$
k_i	0	0	1	1	3	3

Table 5.2: Transformation properties of chiral superfields under Γ_4, for the minimal model with $k_L = 1$ (model I). Both lines of lepton assignments lead to the same results.

With the weight assignments of Table 5.2, the superpotential reads:

$$\begin{aligned} W^{\mathrm{I}} = {} & \alpha_1 \left(E_1^c\, L\, Y_{\mathbf{2}}\right)_{\mathbf{1}} H_d + \alpha_2 \left(E_1^c\, L\, Y_{\mathbf{3'}}\right)_{\mathbf{1}} H_d \\ & + \beta_1 \left(E_2^c\, L\, Y_{\mathbf{2}}^2\right)_{\mathbf{1}} H_d + \beta_2 \left(E_2^c\, L\, Y_{\mathbf{2}}\, Y_{\mathbf{3'}}\right)_{\mathbf{1}} H_d + \beta_3 \left(E_2^c\, L\, Y_{\mathbf{3'}}^2\right)_{\mathbf{1}} H_d \\ & + \gamma_1 \left(E_3^c\, L\, Y_{\mathbf{2}}^2\right)_{\mathbf{1}} H_d + \gamma_2 \left(E_3^c\, L\, Y_{\mathbf{2}}\, Y_{\mathbf{3'}}\right)_{\mathbf{1}} H_d + \gamma_3 \left(E_3^c\, L\, Y_{\mathbf{3'}}^2\right)_{\mathbf{1}} H_d \\ & + \frac{g_1}{\Lambda}\left(L^2\, Y_{\mathbf{2}}\right)_{\mathbf{1}} H_u^2 + \frac{g_2}{\Lambda}\left(L^2\, Y_{\mathbf{3'}}\right)_{\mathbf{1}} H_u^2 . \end{aligned} \tag{5.29}$$

Making use of the Clebsch-Gordan coefficients given in Appendix A.2 and of the $\Gamma_4 \simeq S_4$ representation choices in Table 5.2 we find that only some terms in Eq. (5.29) contain non-zero singlets. We are left with

$$W^{\mathrm{I}} = \alpha \left(E_1^c\, L\, Y_{\mathbf{3'}}\right)_{\mathbf{1}} H_d + \beta \left(E_2^c\, L\, Y_{\mathbf{3'}}^2\right)_{\mathbf{1}} H_d + \gamma \left(E_3^c\, L\, Y_{\mathbf{2}}\, Y_{\mathbf{3'}}\right)_{\mathbf{1}} H_d + \frac{g_1}{\Lambda}\left(L^2\, Y_{\mathbf{2}}\right)_{\mathbf{1}} H_u^2 , \tag{5.30}$$

where $\alpha \equiv \alpha_2$, $\beta \equiv \beta_2 + \beta_3$ and $\gamma \equiv \gamma_2$. It is interesting to note that the constraints listed in Appendix C.2 imply that the singlets of the β_2 and β_3 terms coincide. This superpotential gives rise to the mass matrices:

$$M_\nu^{\rm I} = \frac{2 g_1 v_u^2}{\Lambda} \begin{pmatrix} 0 & Y_1 & Y_2 \\ Y_1 & Y_2 & 0 \\ Y_2 & 0 & Y_1 \end{pmatrix} , \tag{5.31}$$

and

$$M_e^{\rm I} = v_d \begin{pmatrix} \alpha\, Y_3 & \alpha\, Y_5 & \alpha\, Y_4 \\ \beta\,(Y_1 Y_4 - Y_2 Y_5) & \beta\,(Y_1 Y_3 - Y_2 Y_4) & \beta\,(Y_1 Y_5 - Y_2 Y_3) \\ \gamma\,(Y_1 Y_4 + Y_2 Y_5) & \gamma\,(Y_1 Y_3 + Y_2 Y_4) & \gamma\,(Y_1 Y_5 + Y_2 Y_3) \end{pmatrix}^\dagger . \tag{5.32}$$

Specifying values for the parameters α, β, γ, and τ determines both mass matrices up to global factors,[3] and hence determines mass ratios as well as lepton mixing.

After performing a numerical search, it seems this minimal model does not allow to reproduce known data. As a benchmark, we find the point $\alpha = 0.1$, $\beta = 1$, $\gamma = 2 \times 10^{-4}$, and $\tau = 0.1 + 0.985 i$, which accommodates a neutrino mass spectrum with inverted ordering, but does not provide an acceptable value for $\sin^2\theta_{12}$. For this point, we have

$$\begin{aligned} \frac{m_e}{m_\mu} &\simeq 0.0045\,, \qquad \sin^2\theta_{12} \simeq 0.497\,, \qquad \delta \simeq 1.47\pi\,, \\ \frac{m_\mu}{m_\tau} &\simeq 0.0522\,, \qquad \sin^2\theta_{13} \simeq 0.021\,, \qquad \alpha_{21} \simeq 1.00\pi\,, \\ r &\simeq 0.0308\,, \qquad \sin^2\theta_{23} \simeq 0.496\,, \qquad \alpha_{31} \simeq 0.53\pi\,. \end{aligned} \tag{5.33}$$

The obtained predictions are to be compared with neutrino oscillation data and information on charged-lepton mass ratios, which we collect for convenience in Table 5.3 (see also Table 1.3).

5.2.2 Model II ($k_L = 2$)

As before, the choices $k_L = 2$ and $k_u = 0$ along with the fact that $\rho_L \sim \mathbf{3}$ or $\rho_L \sim \mathbf{3'}$ are enough to determine the structure of M_ν.

On the charged lepton side, the cancellation-of-weights condition $2(a_i + b_i) = 2 + k_i$ implies that the k_i are even, $k_i \in \{-2, 0, 2, \ldots\}$. If some $k_i = -2$, then again $a_i = b_i = 0$ and no singlet can be formed for that generation. If instead $k_i = 0$, a singlet can only be formed if $\rho_i \sim \mathbf{1'}$ ($\mathbf{1}$) when $\rho_L \sim \mathbf{3}$ ($\mathbf{3'}$). We summarise in Table 5.4 the weight and representation assignments of the minimal model allowing for $\mathrm{rank}(\lambda) = 3$.

With the weight assignments of Table 5.4, the charged-lepton Yukawa part of the superpotential matches that of the case $k_L = 1$, leading to the same charged-lepton mass matrix as the one given in Eq. (5.32), i.e. $M_e^{\rm II} = M_e^{\rm I}$.

The Weinberg operator part of the superpotential reads instead:

$$W^{\rm II} \supset \frac{g_1}{\Lambda} \left(L^2\, Y_{\mathbf{2}}^2\right)_{\mathbf{1}} H_u^2 + \frac{g_2}{\Lambda} \left(L^2\, Y_{\mathbf{2}}\, Y_{\mathbf{3'}}\right)_{\mathbf{1}} H_u^2 + \frac{g_3}{\Lambda} \left(L^2\, Y_{\mathbf{3'}}^2\right)_{\mathbf{1}} H_u^2 . \tag{5.34}$$

[3] The parameters α, β and γ can be made real through the rephasing of the singlet fields E_i^c. One of them may be taken outside of the matrix $M_e^{\rm I}$ as a global factor. It is assumed that the correct charged-lepton mass scale is reproduced by an appropriate choice of this global factor, after v_d has been specified.

Parameter	Best-fit value and 1σ range	
m_e/m_μ	0.0048 ± 0.0002	
m_μ/m_τ	0.0565 ± 0.0045	
	NO	IO
$\delta m^2/(10^{-5}\text{ eV})$	$7.34^{+0.17}_{-0.14}$	
$\lvert\Delta m^2\rvert/(10^{-3}\text{ eV})$	$2.455^{+0.035}_{-0.032}$	$2.441^{+0.033}_{-0.035}$
$r \equiv \delta m^2/\lvert\Delta m^2\rvert$	0.0299 ± 0.0008	0.0301 ± 0.0008
$\sin^2\theta_{12}$	$0.304^{+0.014}_{-0.013}$	$0.303^{+0.014}_{-0.013}$
$\sin^2\theta_{13}$	$0.0214^{+0.0009}_{-0.0007}$	$0.0218^{+0.0008}_{-0.0007}$
$\sin^2\theta_{23}$	$0.551^{+0.019}_{-0.070}$	$0.557^{+0.017}_{-0.024}$
δ/π	$1.32^{+0.23}_{-0.18}$	$1.52^{+0.14}_{-0.15}$

Table 5.3: Best-fit values and 1σ ranges for neutrino oscillation parameters, obtained from the 2018 global analysis of Ref. [39], and for charged-lepton mass ratios, given at the scale 2×10^{16} GeV with the $\tan\beta$ averaging described in Ref. [91], obtained from Ref. [217]. The parameters entering the definition of r are $\delta m^2 \equiv m_2^2 - m_1^2$ and $\Delta m^2 \equiv m_3^2 - (m_1^2 + m_2^2)/2$. The best-fit value and 1σ range of δ did not drive the numerical searches here reported.

	H_u	H_d	L	E_1^c	E_2^c	E_3^c
ρ_i	$\mathbf{1}$	$\mathbf{1}$	$\mathbf{3}$ $\mathbf{3'}$	$\mathbf{1'}$ $\mathbf{1}$	$\mathbf{1}$ $\mathbf{1'}$	$\mathbf{1'}$ $\mathbf{1}$
k_i	0	0	2	0	2	2

Table 5.4: Transformation properties of chiral superfields under Γ_4, for the minimal model with $k_L = 2$ (model II). Both lines of lepton assignments lead to the same results.

The first term in Eq. (5.34) contributes with two different non-zero singlets, since $L^2 \sim \mathbf{1} \oplus \mathbf{2} \oplus \mathbf{3} \oplus \mathbf{3'}$ with vanishing antisymmetric $\mathbf{3'}$, $Y_\mathbf{2}^2 \sim \mathbf{1} \oplus \mathbf{1'} \oplus \mathbf{2}$ with vanishing antisymmetric $\mathbf{1'}$, and singlets may be obtained from both the $\mathbf{1} \otimes \mathbf{1}$ and the $\mathbf{2} \otimes \mathbf{2}$ combinations. The second term contributes with a third singlet, as $Y_\mathbf{2} Y_{\mathbf{3'}} \sim \mathbf{3} \oplus \mathbf{3'}$ and thus a singlet is obtained from the $\mathbf{3} \otimes \mathbf{3}$ combination. The third term contains all the three singlets: $\mathbf{1} \otimes \mathbf{1}$, $\mathbf{2} \otimes \mathbf{2}$, and $\mathbf{3} \otimes \mathbf{3}$. Due to the constraints in Appendix C.2, there are only three independent singlets which enter the Weinberg operator part of W^{II}. Explicitly, using the Clebsch-Gordan coefficients of Appendix A.2:

$$
\begin{aligned}
W^{\text{II}} \supset \frac{1}{\Lambda} \Big[& g\, Y_1 Y_2 (L_1^2 + 2 L_2 L_3) \\
& + g' \left(Y_1^2 (L_2^2 + 2 L_1 L_3) + Y_2^2 (L_3^2 + 2 L_2 L_3) \right) \\
& + g'' \Big((Y_1 Y_4 - Y_2 Y_5)(L_1^2 - L_2 L_3) + (Y_1 Y_5 - Y_2 Y_3)(L_2^2 - L_1 L_3) \\
& \qquad + (Y_1 Y_3 - Y_2 Y_4)(L_3^2 - L_1 L_2) \Big) \Big] H_u^2 \,,
\end{aligned}
\tag{5.35}
$$

which gives rise to the mass matrix:

$$M_\nu^{\rm II} = \frac{2g'v_u^2}{\Lambda}\left[\begin{pmatrix}(g/g')Y_1Y_2 & Y_2^2 & Y_1^2\\ Y_2^2 & Y_1^2 & (g/g')Y_1Y_2\\ Y_1^2 & (g/g')Y_1Y_2 & Y_2^2\end{pmatrix} + \frac{1}{2}\frac{g''}{g'}\begin{pmatrix}2(Y_1Y_4-Y_2Y_5) & -(Y_1Y_3-Y_2Y_4) & -(Y_1Y_5-Y_2Y_3)\\ -(Y_1Y_3-Y_2Y_4) & 2(Y_1Y_5-Y_2Y_3) & -(Y_1Y_4-Y_2Y_5)\\ -(Y_1Y_5-Y_2Y_3) & -(Y_1Y_4-Y_2Y_5) & 2(Y_1Y_3-Y_2Y_4)\end{pmatrix}\right]. \tag{5.36}$$

Specifying values for the parameters α, β, γ, g/g', g''/g' and τ determines both mass matrices up to global factors,[4] and hence determines mass ratios as well as lepton mixing.

Through numerical search, we find that this minimal model is successful in accommodating the data. We find a first benchmark, $\alpha = 0.1$, $\beta = 1$, $\gamma = 2.3\times10^{-4}$, $g/g' = -0.99 - 0.52i$, $g''/g' = 0.15 - 0.06i$, and $\tau = 0.04 + 1.11i$, which admits a neutrino mass spectrum with normal ordering, with

$$\begin{aligned}\frac{m_e}{m_\mu} &\simeq 0.0048\,, \qquad \sin^2\theta_{12} \simeq 0.288\,, \qquad \delta \simeq 0.88\pi\,,\\ \frac{m_\mu}{m_\tau} &\simeq 0.0593\,, \qquad \sin^2\theta_{13} \simeq 0.021\,, \qquad \alpha_{21} \simeq 1.46\pi\,,\\ r &\simeq 0.0299\,, \qquad \sin^2\theta_{23} \simeq 0.553\,, \qquad \alpha_{31} \simeq 1.09\pi\,.\end{aligned} \tag{5.37}$$

These results are in good agreement with the values of Table 5.3, except in what regards the experimental hint of $\delta \sim 3\pi/2$.

We find a second benchmark, $\alpha = 0.11$, $\beta = 1$, $\gamma = 2.3\times10^{-4}$, $g/g' = -6.2-1.5i$, $g''/g' = -0.03+0.03i$, and $\tau = -0.09 + 0.96i$, also admitting a neutrino mass spectrum with normal ordering, for which the values of δ and of other measured parameters are less than 2σ away from the best-fit values of Table 5.3:

$$\begin{aligned}\frac{m_e}{m_\mu} &\simeq 0.0048\,, \qquad \sin^2\theta_{12} \simeq 0.292\,, \qquad \delta \simeq 1.64\pi\,,\\ \frac{m_\mu}{m_\tau} &\simeq 0.0560\,, \qquad \sin^2\theta_{13} \simeq 0.021\,, \qquad \alpha_{21} \simeq 0.10\pi\,,\\ r &\simeq 0.0298\,, \qquad \sin^2\theta_{23} \simeq 0.493\,, \qquad \alpha_{31} \simeq 1.10\pi\,.\end{aligned} \tag{5.38}$$

For this second benchmark, in order to fit the individual mass-squared differences δm^2 and Δm^2, we set the global factor $2g'v_u^2/\Lambda \simeq 0.0037$ eV. In this case, the neutrino masses read $m_1 \simeq 0.042$ eV, $m_2 \simeq 0.043$ eV, and $m_3 \simeq 0.066$ eV. A distinctive feature of this framework is the prediction of the Dirac and Majorana CPV phases. One is then in a position to extract a prediction for the effective Majorana mass $|\langle m\rangle|$ which controls the rate of neutrinoless double beta decay (see Chapter 3). Using the values in (5.38) we find $|\langle m\rangle| \simeq 0.042$ eV. This value can be probed by new-generation experiments which are working towards the $|\langle m\rangle| \sim 10^{-2}$ eV frontier.

In this setup, the correlations between pairs of mixing angles, phases and mass ratios are non-trivial, as is suggested, in particular, by comparing the predictions for $\sin^2\theta_{23}$ and δ in Eqs. (5.37) and (5.38). The existence and the success of the above benchmark warrants further exploration of the present framework.

[4] As before, α, β and γ can be made real and one of them may be taken outside of $M_e^{\rm II} = M_e^{\rm I}$ as a global factor.

5.3 Chapter Summary

In this chapter we have explored the consequences of the presence of modular invariance in the lepton sector via the action of the finite modular group $\Gamma_4 \simeq S_4$ which is a subgroup of $\mathrm{SL}(2,\mathbb{Z})$. Fields carrying a non-trivial modular weight transform with a scale factor in addition to the usual unitary rotation. To build an invariant action, modular forms are introduced to provide compensating factors. For a fixed scaling (modular) weight, these forms make up a finite-dimensional space. In section 5.1.1, we have detailed the construction of a basis $\{Y_1, \ldots, Y_5\}$ for the lowest weight modular forms of level 4 (corresponding to $\Gamma_4 \simeq S_4$), necessary to the generation of higher weight forms. We have additionally shown how the weight 2 and 4 forms organise themselves into different multiplets of S_4, and that they satisfy non-trivial constraints which guarantee the correct dimensionality of higher-weight spaces (see Appendix C.2).

We have then studied supersymmetric models of lepton masses and mixing based on the breaking of the $\Gamma_4 \simeq S_4$ modular invariance. Focusing on minimality as a guiding principle, we considered models where neutrino Majorana masses have their origin in the Weinberg operator and where no flavons are introduced. The expectation value of the modulus τ is the only source of symmetry breaking. We describe two minimal models, differing in the weight $-k_L$ of the lepton doublet under modular transformations. While the first model (model I, $k_L = 1$) does not seem to be able to reproduce the data, the second model (model II, $k_L = 2$) successfully accommodates charged-lepton masses and neutrino oscillation data. Deviations of individual parameters from best-fit values are found to be below the 2σ level for the benchmark of Eq. (5.38). Since in the present scheme the mass matrices are fully determined by the VEV $\langle\tau\rangle$ and by superpotential parameters – see Eqs. (5.31), (5.32) and (5.36) – the values of the Dirac and Majorana CPV phases can be predicted. For the benchmark of Eq. (5.38), which corresponds to a neutrino mass spectrum with normal ordering, a prediction for the effective Majorana mass $|\langle m\rangle| \simeq 0.042$ eV is possible. This value can be probed by new-generation experiments working towards the $|\langle m\rangle| \sim 10^{-2}$ eV frontier.

In closing, a systematic exploration of this predictive paradigm is desirable. Such a future analysis is expected to include, in particular, a description of the origin of neutrino masses via, e.g., the seesaw mechanism.

Summary and Conclusions 6

Symmetries are a powerful tool to build and constrain physical theories. In particular, symmetry principles may be behind the smallness of neutrino masses and the peculiarities of the pattern of neutrino mixing. To understand whether this is the case, one invariably needs precise experimental input.

We are entering, at present, a precision era for neutrino physics. It is not unreasonable to expect that future data will resolve the neutrino mass spectrum ordering, pinpoint the absolute neutrino mass scale, and disentangle the nature of massive neutrinos. It is also hoped that more and more precise data will help clarify the origins of the observed neutrino mixing pattern and allow for a glimpse into the mechanism behind neutrino mass generation.

In the present thesis, we have explored possible roles of different symmetries in connection to the flavour puzzle, namely: lepton number symmetry, Froggatt-Nielsen symmetry, non-Abelian discrete flavour symmetries combined with generalised CP symmetries, and modular symmetry.

We have found that a Froggatt-Nielsen construction may mimic approximate lepton number conservation. In the minimal case where only two right-handed neutrino fields are present, the Froggatt-Nielsen charge assignments are able to constrain CP violation phases (see Figs. 2.2 and 2.1). Furthermore, in such a symmetry-protected scenario, mass terms of right-handed neutrinos need not involve high scales and interesting phenomenology is possible, such as lepton flavour violating signals (see Fig. 2.3) or direct production of the new pseudo-Dirac particle at colliders.

Still in connection with lepton number symmetry, we have considered the process of neutrinoless double beta decay in the standard 3ν-exchange scenario. We have determined conditions on the lightest neutrino mass, taking into account updated confidence intervals for neutrino oscillation parameters, such that the effective Majorana mass exceeds the 5×10^{-3} eV and 10^{-3} eV values (see Fig. 3.3 and Figs. 3.4 and 3.5, respectively). Further, we have looked into specific values of Majorana phases which are not CP conserving but are instead in line with very predictive models of lepton flavour (see Figs. 3.7, 3.8 and 3.9). For such pairs of Majorana phases and in the case of normal ordering, the effective mass is found to be bounded from below with the lower bound at or above the meV value.

The aforementioned predictive scenarios consistently combine non-Abelian discrete symmetries with so-called generalised CP symmetries. Different breaking patterns of the assumed high-scale symmetry lead to different predictions for lepton mixing and CPV phases. Some degree of flexibility is required to accommodate the best-fit values of neutrino mixing angles. We have explored a scenario based on

the group S_4 which predicts testable correlations between oscillation parameters (see Figs. 4.1 – 4.11 and Fig. 4.12), having identified all phenomenologically viable cases following from the considered flavour and generalised CP breaking pattern. In this setup, predictions for the effective Majorana mass governing neutrinoless double beta decay have also been obtained (see Figs. 4.13 – 4.16).

Finally, a new type of symmetry – modular symmetry – which may shape lepton mass matrices and thus neutrino masses and mixing has been discussed. Working in a supersymmetric context, it can be seen as a generalisation of flavour symmetries when modular weights of superfields are non-vanishing. In a bottom-up approach, we have described minimal models based on the finite modular group $\Gamma_4 \simeq S_4$. For this group, we have explicitly constructed the generators of modular forms of lowest level, and next-to-lowest level, and seen how they arrange into multiplets (see Eqs. 5.22 – 5.24). We have also provided a benchmark successfully accommodating the current data (see Eq. 5.38). Future exploration of this approach to models of lepton flavour with invariance under either Γ_4 or other finite modular groups Γ_N is warranted. Such an analysis is expected to include a description of the origin of neutrino masses, as well as a systematic analysis of possible weight assignments and mass matrix structures.

Borrowing the words of Wigner, the appropriateness of gauge symmetry for the description of fundamental interactions may be seen as a wonderful gift from Nature. Perhaps we are also gifted with a new symmetry principle, suitable for the description of the flavour sector. The question of whether or not we deserve it remains unanswered.

S_4 Group Theory

A

A.1 Presentation and Basis

As indicated in Section 4.3.1, S_4 is the symmetric group of permutations of four objects. It contains $4! = 24$ elements and admits five irreducible representations $\mathbf{1}$, $\mathbf{1'}$, $\mathbf{2}$, $\mathbf{3}$ and $\mathbf{3'}$ (see also [72]). Throughout Section 1.3 and Chapter 4, the following presentation of this finite group in terms of three generators S, T, and U has been considered (cf. (4.41)):

$$S^2 = T^3 = U^2 = (ST)^3 = (SU)^2 = (TU)^2 = (STU)^4 = 1\,. \tag{A.1}$$

Notice that this presentation reduces to that of the group $A_4 \subset S_4$ of even permutations of four objects if one drops the U generator. The representation basis for this presentation has been given in Eq. (1.21).

While the above group presentation is common, it proves convenient for the discussion of modular symmetry (see Chapter 5) to consider also a presentation given in terms of two generators S and T (cf. Eq. (5.13)),

$$S^2 \;=\; (ST)^3 \;=\; T^4 \;=\; \mathbb{1}\,. \tag{A.2}$$

Here, and in the next subsection of this appendix, the S and T generators will refer to those defined through this equation, and not to the ones in Eq. (A.1).

We will use the group theoretical results of Ref. [218]. The two S_4 generators therein, which we denote here with primes, satisfy $S'^4 = T'^3 = (S'T'^2)^2 = 1$. We define $S \equiv S'T'^2$, $T \equiv S'$, which imply the inverse relations $S' = T$ and $T' = ST$. Then, S and T furnish the presentation (A.2) of S_4, useful to the discussion of modular invariance. Making use of this identification and of the results in Appendix A of Ref. [218], we find an explicit basis for the irreducible representations of S_4, which we employ in our discussion:

$$\mathbf{1}: \quad \rho(S) = 1, \quad \rho(T) = 1\,, \tag{A.3}$$

$$\mathbf{1'}: \quad \rho(S) = -1, \quad \rho(T) = -1\,, \tag{A.4}$$

$$\mathbf{2}: \quad \rho(S) = \begin{pmatrix} 0 & \omega \\ \omega^2 & 0 \end{pmatrix}, \quad \rho(T) = \begin{pmatrix} 0 & 1 \\ 1 & 0 \end{pmatrix}\,, \tag{A.5}$$

$$\mathbf{3}: \quad \rho(S) = \frac{1}{3}\begin{pmatrix} -1 & 2\omega^2 & 2\omega \\ 2\omega & 2 & -\omega^2 \\ 2\omega^2 & -\omega & 2 \end{pmatrix}, \quad \rho(T) = \frac{1}{3}\begin{pmatrix} -1 & 2\omega & 2\omega^2 \\ 2\omega & 2\omega^2 & -1 \\ 2\omega^2 & -1 & 2\omega \end{pmatrix}\,, \tag{A.6}$$

$$\mathbf{3'}: \quad \rho(S) = -\frac{1}{3}\begin{pmatrix} -1 & 2\omega^2 & 2\omega \\ 2\omega & 2 & -\omega^2 \\ 2\omega^2 & -\omega & 2 \end{pmatrix}, \quad \rho(T) = -\frac{1}{3}\begin{pmatrix} -1 & 2\omega & 2\omega^2 \\ 2\omega & 2\omega^2 & -1 \\ 2\omega^2 & -1 & 2\omega \end{pmatrix}, \tag{A.7}$$

where as usual $\omega = e^{2\pi i/3}$.

A.2 Clebsch-Gordan Coefficients

After establishing a dictionary between S_4 presentations with two generators S and T in the previous section, we can directly use the Clebsch-Gordan coefficients from Ref. [218], since no change of basis on the representation matrices has been performed. We reproduce the coefficients here for completeness. Entries of each multiplet entering the tensor product are denoted by α_i and β_i.

$$\begin{aligned}
\mathbf{1} \otimes \mathbf{r} &= \mathbf{r} &&\sim \alpha\,\beta_i \\
\mathbf{1'} \otimes \mathbf{1'} &= \mathbf{1} &&\sim \alpha\,\beta \\
\mathbf{1'} \otimes \mathbf{2} &= \mathbf{2} &&\sim \begin{pmatrix} \alpha\,\beta_1 \\ -\alpha\,\beta_2 \end{pmatrix} \\
\mathbf{1'} \otimes \mathbf{3} &= \mathbf{3'} &&\sim \begin{pmatrix} \alpha\,\beta_1 \\ \alpha\,\beta_2 \\ \alpha\,\beta_3 \end{pmatrix} \\
\mathbf{1'} \otimes \mathbf{3'} &= \mathbf{3} &&\sim \begin{pmatrix} \alpha\,\beta_1 \\ \alpha\,\beta_2 \\ \alpha\,\beta_3 \end{pmatrix}
\end{aligned} \tag{A.8}$$

$$\mathbf{2} \otimes \mathbf{2} = \mathbf{1} \oplus \mathbf{1'} \oplus \mathbf{2} \quad \begin{cases} \mathbf{1} &\sim \alpha_1\beta_2 + \alpha_2\beta_1 \\ \mathbf{1'} &\sim \alpha_1\beta_2 - \alpha_2\beta_1 \\ \mathbf{2} &\sim \begin{pmatrix} \alpha_2\,\beta_2 \\ \alpha_1\,\beta_1 \end{pmatrix} \end{cases}$$

$$\mathbf{2} \otimes \mathbf{3} = \mathbf{3} \oplus \mathbf{3'} \quad \begin{cases} \mathbf{3} &\sim \begin{pmatrix} \alpha_1\,\beta_2 + \alpha_2\,\beta_3 \\ \alpha_1\,\beta_3 + \alpha_2\,\beta_1 \\ \alpha_1\,\beta_1 + \alpha_2\,\beta_2 \end{pmatrix} \\ \mathbf{3'} &\sim \begin{pmatrix} \alpha_1\,\beta_2 - \alpha_2\,\beta_3 \\ \alpha_1\,\beta_3 - \alpha_2\,\beta_1 \\ \alpha_1\,\beta_1 - \alpha_2\,\beta_2 \end{pmatrix} \end{cases} \tag{A.9}$$

$$\mathbf{2} \otimes \mathbf{3'} = \mathbf{3} \oplus \mathbf{3'} \quad \begin{cases} \mathbf{3} &\sim \begin{pmatrix} \alpha_1\,\beta_2 - \alpha_2\,\beta_3 \\ \alpha_1\,\beta_3 - \alpha_2\,\beta_1 \\ \alpha_1\,\beta_1 - \alpha_2\,\beta_2 \end{pmatrix} \\ \mathbf{3'} &\sim \begin{pmatrix} \alpha_1\,\beta_2 + \alpha_2\,\beta_3 \\ \alpha_1\,\beta_3 + \alpha_2\,\beta_1 \\ \alpha_1\,\beta_1 + \alpha_2\,\beta_2 \end{pmatrix} \end{cases}$$

$$\mathbf{3}\otimes\mathbf{3}=\mathbf{3'}\otimes\mathbf{3'}=\mathbf{1}\oplus\mathbf{2}\oplus\mathbf{3}\oplus\mathbf{3'}\quad\begin{cases}\mathbf{1} & \sim & \alpha_1\beta_1+\alpha_2\beta_3+\alpha_3\beta_2\\ \mathbf{2} & \sim & \begin{pmatrix}\alpha_2\beta_2+\alpha_1\beta_3+\alpha_3\beta_1\\ \alpha_3\beta_3+\alpha_1\beta_2+\alpha_2\beta_1\end{pmatrix}\\ \mathbf{3} & \sim & \begin{pmatrix}2\alpha_1\beta_1-\alpha_2\beta_3-\alpha_3\beta_2\\ 2\alpha_3\beta_3-\alpha_1\beta_2-\alpha_2\beta_1\\ 2\alpha_2\beta_2-\alpha_1\beta_3-\alpha_3\beta_1\end{pmatrix}\\ \mathbf{3'} & \sim & \begin{pmatrix}\alpha_2\beta_3-\alpha_3\beta_2\\ \alpha_1\beta_2-\alpha_2\beta_1\\ \alpha_3\beta_1-\alpha_1\beta_3\end{pmatrix}\end{cases}\tag{A.10}$$

$$\mathbf{3}\otimes\mathbf{3'}=\mathbf{1'}\oplus\mathbf{2}\oplus\mathbf{3}\oplus\mathbf{3'}\quad\begin{cases}\mathbf{1'} & \sim & \alpha_1\beta_1+\alpha_2\beta_3+\alpha_3\beta_2\\ \mathbf{2} & \sim & \begin{pmatrix}\alpha_2\beta_2+\alpha_1\beta_3+\alpha_3\beta_1\\ -\alpha_3\beta_3-\alpha_1\beta_2-\alpha_2\beta_1\end{pmatrix}\\ \mathbf{3} & \sim & \begin{pmatrix}\alpha_2\beta_3-\alpha_3\beta_2\\ \alpha_1\beta_2-\alpha_2\beta_1\\ \alpha_3\beta_1-\alpha_1\beta_3\end{pmatrix}\\ \mathbf{3'} & \sim & \begin{pmatrix}2\alpha_1\beta_1-\alpha_2\beta_3-\alpha_3\beta_2\\ 2\alpha_3\beta_3-\alpha_1\beta_2-\alpha_2\beta_1\\ 2\alpha_2\beta_2-\alpha_1\beta_3-\alpha_3\beta_1\end{pmatrix}\end{cases}\tag{A.11}$$

A.3 Conjugate Pairs of S_4 Elements

As detailed in Section 4.2.2, residual flavour symmetries $Z_2^{g_e}$ and $Z_2^{g_\nu}$ which are conjugate to each other lead to the same form of the PMNS matrix. For $G_f = S_4$, there are nine group elements of order two, given in Eqs. (4.42) and (4.43), which generate Z_2 subgroups. The resulting 81 pairs of elements $\{g_e, g_\nu\}$ can themselves be partitioned, under the conjugacy relation of Eq. (4.28), into nine equivalence classes. Using the generators in the presentation of Eq. (A.1), employed throughout Chapter 4, these classes explicitly read:

- $\boldsymbol{\{S,S\}}$, $\{TST^2, TST^2\}$, $\{T^2ST, T^2ST\}$;
- $\boldsymbol{\{U,U\}}$, $\{SU, SU\}$, $\{T^2U, T^2U\}$, $\{TU, TU\}$, $\{ST^2SU, ST^2SU\}$, $\{STSU, STSU\}$;
- $\boldsymbol{\{T^2ST,S\}}$, $\{TST^2, S\}$, $\{T^2ST, TST^2\}$, $\{S, T^2ST\}$, $\{S, TST^2\}$, $\{TST^2, T^2ST\}$;
- $\boldsymbol{\{S,U\}}$, $\{S, SU\}$, $\{TST^2, T^2U\}$, $\{T^2ST, TU\}$, $\{TST^2, ST^2SU\}$, $\{T^2ST, STSU\}$;
- $\boldsymbol{\{U,S\}}$, $\{SU, S\}$, $\{T^2U, TST^2\}$, $\{TU, T^2ST\}$, $\{ST^2SU, TST^2\}$, $\{STSU, T^2ST\}$;
- $\boldsymbol{\{SU,U\}}$, $\{U, SU\}$, $\{ST^2SU, T^2U\}$, $\{STSU, TU\}$, $\{T^2U, ST^2SU\}$, $\{TU, STSU\}$;
- $\boldsymbol{\{S,TU\}}$, $\{S, STSU\}$, $\{S, T^2U\}$, $\{TST^2, TU\}$, $\{S, ST^2SU\}$, $\{T^2ST, U\}$, $\{T^2ST, SU\}$, $\{TST^2, U\}$, $\{T^2ST, T^2U\}$, $\{TST^2, SU\}$, $\{T^2ST, ST^2SU\}$, $\{TST^2, STSU\}$;
- $\boldsymbol{\{TU,S\}}$, $\{STSU, S\}$, $\{T^2U, S\}$, $\{TU, TST^2\}$, $\{ST^2SU, S\}$, $\{U, T^2ST\}$, $\{SU, T^2ST\}$, $\{U, TST^2\}$, $\{T^2U, T^2ST\}$, $\{SU, TST^2\}$, $\{ST^2SU, T^2ST\}$, $\{STSU, TST^2\}$;

- $\boldsymbol{\{TU, U\}}$, $\{STSU, U\}$, $\{STSU, SU\}$, $\{TU, SU\}$, $\{T^2U, U\}$, $\{TU, T^2U\}$, $\{ST^2SU, U\}$, $\{U, TU\}$, $\{TU, ST^2SU\}$, $\{SU, STSU\}$, $\{U, T^2U\}$, $\{T^2U, TU\}$, $\{U, ST^2SU\}$, $\{SU, T^2U\}$, $\{SU, ST^2SU\}$, $\{T^2U, STSU\}$, $\{ST^2SU, STSU\}$, $\{ST^2SU, TU\}$, $\{STSU, ST^2SU\}$, $\{STSU, T^2U\}$, $\{SU, TU\}$, $\{ST^2SU, SU\}$, $\{T^2U, SU\}$, $\{U, STSU\}$;

where in boldface we have identified a representative pair of elements for each class, matching the choice made in Eqs. (4.44) and (4.45).

S_4 Flavour and gCP

B

B.1 Equivalent Cases

Following the discussion in Section 4.3.2, we note that a necessary condition for two matrices U_{PMNS} and U'_{PMNS} to be equivalent is for them to have the same magnitude of the fixed element. Indeed, for the 4 cases under consideration in said section the absolute value of one element is $1/\sqrt{2}$.

Generically, for $P_e = P'_e$ and $P_\nu = P'_\nu$, two matrices U_{PMNS} and U'_{PMNS} are equivalent if the products $\Omega_e^\dagger\,\Omega_\nu$ and $\Omega_e'^\dagger\,\Omega'_\nu$ can be related in the following way:

$$\Omega_e^\dagger\,\Omega_\nu = \text{diag}(e^{i\phi_1}, e^{i\phi_2}, e^{i\phi_3})\,U_{23}(\theta^e_\circ, \delta^e_\circ)\,\Omega_e'^\dagger\,\Omega'_\nu\,R_{23}(\theta^\nu_\circ)\;\text{diag}(1, i^k, i^k)\,, \tag{B.1}$$

with ϕ_i, $\delta^e_\circ$ and $\theta^e_\circ$, $\theta^\nu_\circ$ some fixed phases and angles, respectively, and $k = 0, 1, 2, 3$. If this relation holds, from Eq. (4.27) we have

$$\begin{aligned} U_{\text{PMNS}} &= P_e\,U_{23}(\theta^e, \delta^e)\;\text{diag}(e^{i\phi_1}, e^{i\phi_2}, e^{i\phi_3})\,U_{23}(\theta^e_\circ, \delta^e_\circ)\,\Omega_e'^\dagger\,\Omega'_\nu\,R_{23}(\theta^\nu_\circ)\;\text{diag}(1, i^k, i^k)\,R_{23}(\theta^\nu)\,P_\nu\,Q_\nu \\ &= P_e\;\text{diag}(e^{i\phi_1}, e^{i\phi_2}, e^{i\phi_3})\,U_{23}(\theta^e, \tilde{\delta}^e)\,U_{23}(\theta^e_\circ, \delta^e_\circ)\,\Omega_e'^\dagger\,\Omega'_\nu\,R_{23}(\hat{\theta}^\nu)\,P_\nu\,\hat{Q}_\nu\,, \end{aligned} \tag{B.2}$$

with

$$\tilde{\delta}^e = \delta^e + \phi_2 - \phi_3\,, \quad \hat{\theta}^\nu = \theta^\nu_\circ + \theta^\nu \quad \text{and} \quad \hat{Q}_\nu = P_\nu^T\;\text{diag}(1, i^k, i^k)\,P_\nu\,Q_\nu\,. \tag{B.3}$$

Now, using

$$U_{23}(\theta^e, \tilde{\delta}^e)\,U_{23}(\theta^e_\circ, \delta^e_\circ) = \text{diag}(1, e^{i\alpha}, e^{-i\alpha})\,U_{23}(\hat{\theta}^e, \hat{\delta}^e)\,, \tag{B.4}$$

where (see for instance Ref. [176], Appendix B)

$$\alpha = \arg\left\{\cos\theta^e\cos\theta^e_\circ - \sin\theta^e\sin\theta^e_\circ\,e^{i(\delta^e_\circ - \tilde{\delta}^e)}\right\}\,, \tag{B.5}$$

$$\beta = \arg\left\{\sin\theta^e\cos\theta^e_\circ\,e^{-i\tilde{\delta}^e} + \cos\theta^e\sin\theta^e_\circ\,e^{-i\delta^e_\circ}\right\}\,, \tag{B.6}$$

$$\cos\hat{\theta}^e = \left|\cos\theta^e\cos\theta^e_\circ - \sin\theta^e\sin\theta^e_\circ\,e^{i(\delta^e_\circ - \tilde{\delta}^e)}\right|\,, \tag{B.7}$$

$$\sin\hat{\theta}^e = \left|\sin\theta^e\cos\theta^e_\circ\,e^{-i\tilde{\delta}^e} + \cos\theta^e\sin\theta^e_\circ\,e^{-i\delta^e_\circ}\right|\,, \tag{B.8}$$

$$\hat{\delta}^e = \alpha - \beta\,, \tag{B.9}$$

we obtain

$$U_{\text{PMNS}} = Q_e\,P_e\,U_{23}(\hat{\theta}^e, \hat{\delta}^e)\,\Omega_e'^\dagger\,\Omega'_\nu\,R_{23}(\hat{\theta}^\nu)\,P_\nu\,\hat{Q}_\nu\,, \tag{B.10}$$

with $Q_e = P_e\;\text{diag}\left(e^{i\phi_1}, e^{i(\phi_2+\alpha)}, e^{i(\phi_3-\alpha)}\right)\,P_e^T$ being a matrix of unphysical phases. Thus, up to this matrix, U_{PMNS} and U'_{PMNS} are the same.

We now return to the specific case under analysis in Section 4.3.2. Taking $\{G_e, G_\nu\} = \{Z_2^{TU}, Z_2^S \times H_{\rm CP}^\nu\}$ with $H_{\rm CP}^\nu = \{U, SU\}$ as a reference case, denoting the corresponding diagonalising matrices as Ω_e' and Ω_ν' and taking Ω_e and Ω_ν to be the diagonalising matrices in one of the three remaining cases under consideration, we summarise the values of ϕ_i, $\delta_\circ^e$, $\theta_\circ^e$, $\theta_\circ^\nu$ and k for which Eq. (B.1) holds in Table B.1.

$(g_e,\, g_\nu,\, H_{\rm CP}^\nu)$	$(S,\, TU,\, \{U,T\})$	$(S,\, TU,\, \{STS, T^2STU\})$	$(TU,\, S,\, \{TST^2U, T^2STU\})$
ϕ_1	$\pi/6$	$-\pi/3$	$-\pi/2$
ϕ_2	$-\arctan\sqrt{1+2\sqrt{2}/3}$	$-\arctan\left(\sqrt{2}+\sqrt{3}\right)$	$\operatorname{arccot}(2)$
ϕ_3	$\arctan\left(3\sqrt{3}+2\sqrt{6}\right)$	$\operatorname{arccot}\left(2\sqrt{2}+\sqrt{3}\right)$	$\arctan(2)$
$\delta_\circ^e$	$\operatorname{arccot}\left(5/\sqrt{3}\right)$	$\pi/3$	$\arctan\left(\left(5\sqrt{3}-6\right)/13\right)$
$\theta_\circ^e$	$\arctan\sqrt{\left(11-6\sqrt{2}\right)/7}$	$\arctan\left(\sqrt{2}+\sqrt{3}\right)$	$\pi-\arctan\left(2/\sqrt{5}\right)$
$\theta_\circ^\nu$	$\pi-\arctan\left(3-2\sqrt{2}\right)$	$\pi/4$	$\pi/4$
k	0	1	3

Table B.1: The values of the parameters ϕ_i, $\delta_\circ^e$, $\theta_\circ^e$, $\theta_\circ^\nu$ and k for which Eq. (B.1) holds, proving the equivalence of the PMNS matrix in a given case to the PMNS matrix in the reference case of $(g_e,\, g_\nu,\, H_{\rm CP}^\nu) = (TU,\, S,\, \{U, SU\})$.

B.2 Correspondence with Earlier Results

The sum rules found for $\cos\delta$ or $\sin^2\theta_{23}$ ($\sin^2\theta_{12}$ in case C1) can be formally obtained from sum rules derived in Ref. [176]. In certain cases, this requires an additional input which is provided by the residual gCP symmetry $H_{\rm CP}^\nu$ considered in Chapter 4. We describe this correspondence below.

i) Cases **B1**, **C4** and **D4** of the present study correspond to case C8 in [176], since for all these cases $(U_{\rm PMNS})_{\mu 2}$ is fixed. The sum rule for $\cos\delta$ in case B1, Eq. (4.84), follows from that of case C8 in [176] (see Table 4 therein) for $\sin^2\theta_{23}^\circ = 1/2$, while the sum rule in Eq. (4.94), valid in cases C4 and D4, can be obtained from the same sum rule found in [176], but for $\sin^2\theta_{23}^\circ = 3/4$. As should be, these two values of $\sin^2\theta_{23}^\circ$ follow from $G_f = S_4$, when it is broken to two different non-equivalent specific pairs of residual $\{Z_2^{g_e}, Z_2^{g_\nu}\}$ flavour symmetries (see Table 10 in [176]).

ii) Cases **B2**, **C5** and **D5** correspond to case C1 in [176], since for all of them $(U_{\rm PMNS})_{\tau 2}$ is fixed. The sum rule for $\cos\delta$ in case B2, Eq. (4.85), follows from that of case C1 in [176] (see Table 4 therein) for $\sin^2\theta_{23}^\circ = 1/2$, while the sum rule in Eq. (4.95), valid in cases C5 and D5, can be obtained from the same rule found in [176], but for $\sin^2\theta_{23}^\circ = 1/4$. Again, these values of $\sin^2\theta_{23}^\circ$ are fixed uniquely by $G_f = S_4$ and the specific choice of the residual symmetries here considered.

iii) Cases **A1** and **B3** of the present study correspond to case C2 in [176], since for these cases $(U_{\rm PMNS})_{\mu 3}$ is fixed. The expression for $\sin^2\theta_{23}$ in Eq. (4.75) follows from the corresponding expression for case C2 in Table 6 of [176] with $\sin^2\theta_{23}^\circ = 1/2$. This value is in agreement with Table 10 of [176]. Moreover, the sum rule for $\cos\delta$ in Eq. (4.76) in case A1 can be obtained from the sum rule for case

C2 in Table 4 of [176] with $\sin^2\theta^\circ_{23} = 1/2$ and $\sin^2\hat{\theta}^\nu_{12} = 1/2$.[1] The value of $\sin^2\hat{\theta}^\nu_{12}$, which was an arbitrary free parameter in [176], is fixed by the gCP symmetry employed in the present study. Finally, we note that the expression for $\cos\delta$ in Eq. (4.87) valid in case B3 can formally be obtained from the corresponding expression in case C2 of Table 4 in [176] by setting $\hat{\theta}^\nu_{12} = \theta^\nu - \pi/4$.

iv) Analogously, cases **A2** and **B4** correspond to case C7 in [176]. Equation (4.77) can be obtained from the corresponding formula in Table 6 of [176] for $\sin^2\theta^\circ_{23} = 1/2$, which agrees with the result in Table 10 therein. The sum rule in Eq. (4.78) follows from that in case C7 in Table 4 of [176] with $\sin^2\theta^\circ_{23} = 1/2$ and $\sin^2\hat{\theta}^\nu_{12} = 1/2$, where again the value of $\sin^2\hat{\theta}^\nu_{12}$, which in [176] is a free parameter, here is fixed by the gCP symmetry. Similarly to the previous clause, Eq. (4.89) can formally be derived from the corresponding expression in case C7 of Table 4 in [176] setting $\hat{\theta}^\nu_{12} = \theta^\nu - \pi/4$.

v) Case **C1** corresponds to case C5 in [176], in which all possible residual flavour symmetries $G_e = Z_2$ and $G_\nu = Z_2$ have been considered. The expression for $\sin^2\theta_{12}$ in Eq. (4.91) follows from that of case C5 in Table 6 in [176] with $\sin^2\theta^\circ_{12} = 1/4$. This value of $\sin^2\theta^\circ_{12}$ is found for $G_f = S_4$ and the specific choice of the residual symmetries (see Table 10 in [176]). Moreover, Eq. (4.93) for $\cos\delta$ can formally be obtained from the corresponding formula in case C5 of Table 4 in [176] by setting $\sin^2\hat{\theta}^e_{23} = \sin^2\theta^e$.

vi) Cases **C2** and **D2** correspond to case C4 of [176]. The sum rule for $\cos\delta$ in Eq. (4.76), valid in cases C2 and D2, follows from that of case C4 in [176] (see Table 4 therein) for $\sin^2\theta^\circ_{12} = 1/4$, which is in agreement with Table 10 in [176].

vii) Cases **C3** and **D3** correspond to case C3 in [176]. Equation (4.78) for $\cos\delta$, which holds in these cases, can be obtained from the corresponding sum rule for case C3 from Table 4 in [176] with $\sin^2\theta^\circ_{13} = 1/4$, a value which can be found in Table 10 of the same reference.

[1] In Eq. (85) of Ref. [176], $\cos^2\theta^\circ_{23}$ should read $\cos\theta^\circ_{23}$. This typo does not affect the corresponding sum rule for $\cos\delta$ in Eq. (86) and in Table 4 of [176].

C Modular Forms

C.1 q-expansions of Lowest Weight $N = 4$ Modular Forms

The five linearly independent modular forms in Eq. (5.22) admit the expansions:

$$-\frac{8i}{3\pi}\,Y_1(\tau) \;=\; 1 - 24y - 72y^2 + 288y^3 + 216y^4 + \dots\,, \tag{C.1}$$

$$-\frac{8i}{3\pi}\,Y_2(\tau) \;=\; 1 + 24y - 72y^2 - 288y^3 + 216y^4 + \dots\,, \tag{C.2}$$

$$\frac{4i}{\pi}\,Y_3(\tau) \;=\; 1 - 8z + 64z^3 + 32z^4 + 192z^5 - 512z^7 + 384z^8 + \dots\,, \tag{C.3}$$

$$\frac{2i}{\pi}\,\left[Y_4(\tau) + Y_5(\tau)\right] \;=\; 1 + 4z - 32z^3 + 32z^4 - 96z^5 + 256z^7 + 384z^8 + \dots\,, \tag{C.4}$$

$$\frac{i}{\pi}\,\left[Y_4(\tau) - Y_5(\tau)\right] \;=\; 2\sqrt{3}\,z\left(1 + 8z^2 - 24z^4 - 64z^6 + \dots\right)\,, \tag{C.5}$$

where $y \equiv i\sqrt{q/3}$, $z \equiv e^{i\pi/4}(q/4)^{1/4}$, and as usual $q = e^{2\pi i\,\tau}$.

C.2 Forms of Higher Weight and Constraints

Through tensor products of $Y_{\mathbf{2}}$ and $Y_{\mathbf{3'}}$, one can find the multiplets:

$$\begin{aligned}
Y_{\mathbf{1}}^{(4)} &= Y_1 Y_2 \sim \mathbf{1}\,,\\
Y_{\mathbf{1}}^{(4)'} &= Y_3^2 + 2\,Y_4 Y_5 \sim \mathbf{1}\,,\\
Y_{\mathbf{2}}^{(4)} &= (Y_2^2,\, Y_1^2)^T \sim \mathbf{2}\,,\\
Y_{\mathbf{2}}^{(4)'} &= (Y_4^2 + 2Y_3Y_5,\, Y_5^2 + 2Y_3Y_4)^T \sim \mathbf{2}\,,\\
Y_{\mathbf{3}}^{(4)} &= (Y_1Y_4 - Y_2Y_5,\, Y_1Y_5 - Y_2Y_3,\, Y_1Y_3 - Y_2Y_4)^T \sim \mathbf{3}\,,\\
Y_{\mathbf{3}}^{(4)'} &= (Y_3^2 - Y_4Y_5,\, Y_5^2 - Y_3Y_4,\, Y_4^2 - Y_3Y_5)^T \sim \mathbf{3}\,,\\
Y_{\mathbf{3'}}^{(4)} &= (Y_1Y_4 + Y_2Y_5,\, Y_1Y_5 + Y_2Y_3,\, Y_1Y_3 + Y_2Y_4)^T \sim \mathbf{3'}\,.
\end{aligned} \tag{C.6}$$

Not all of these multiplets are expected to be independent. Indeed, from the q-expansions of the $Y_i(\tau)$ given in Appendix C.1 we find 6 constraints between the 15 different $Y_i(\tau)Y_j(\tau)$ products:

$$\begin{aligned}
&\frac{1}{3}\left(Y_3^2+2Y_4Y_5\right)=Y_1Y_2\,, \qquad &&-\frac{1}{\sqrt{3}}\left(Y_3^2-Y_4Y_5\right)=Y_1Y_4-Y_2Y_5\,,\\
&\frac{1}{3}\left(Y_4^2+2Y_3Y_5\right)=Y_2^2\,, \qquad &&-\frac{1}{\sqrt{3}}\left(Y_5^2-Y_3Y_4\right)=Y_1Y_5-Y_2Y_3\,,\\
&\frac{1}{3}\left(Y_5^2+2Y_3Y_4\right)=Y_1^2\,, \qquad &&-\frac{1}{\sqrt{3}}\left(Y_4^2-Y_3Y_5\right)=Y_1Y_3-Y_2Y_4\,.
\end{aligned} \tag{C.7}$$

These constraints imply that $Y_{\mathbf{1}}^{(4)}$ and $Y_{\mathbf{1}}^{(4)'}$, $Y_{\mathbf{2}}^{(4)}$ and $Y_{\mathbf{2}}^{(4)'}$, and $Y_{\mathbf{3}}^{(4)}$ and $Y_{\mathbf{3}}^{(4)'}$ in Eq. (C.6) denote the same multiplets, and only one of each pair is kept in our discussion, cf. Eq. (5.24).

In Ref. [91] it is argued that the presence of a covariant constraint similar to the ones given in Eq. (C.7) signals the non-linear realisation of the discrete symmetry.

Bibliography

[1] E. P. Wigner, *The Unreasonable Effectiveness of Mathematics in the Natural Sciences*, *Commun. Pur. Appl. Math.* **13** (1960) 1.

[2] J. Haller, A. Hoecker, R. Kogler, K. Mönig, T. Peiffer and J. Stelzer, *Update of the global electroweak fit and constraints on two-Higgs-doublet models*, [arXiv:1803.01853], and Gfitter (2018), http://cern.ch/gfitter.

[3] G. Altarelli, *The Higgs and the Excessive Success of the Standard Model*, *Frascati Phys. Ser.* **58** (2014) 102 [arXiv:1407.2122].

[4] ATLAS collaboration, G. Aad et al., *Observation of a new particle in the search for the Standard Model Higgs boson with the ATLAS detector at the LHC*, *Phys. Lett.* **B716** (2012) 1 [arXiv:1207.7214].

[5] CMS collaboration, S. Chatrchyan et al., *Observation of a new boson at a mass of 125 GeV with the CMS experiment at the LHC*, *Phys. Lett.* **B716** (2012) 30 [arXiv:1207.7235].

[6] A. Pich, *Effective field theory: Course*, in *Probing the Standard Model of Particle Interactions. Les Houches Summer School in Theoretical Physics, 68th session, France*, pp. 949–1049, 1998, [arXiv:hep-ph/9806303].

[7] S. Weinberg, *Baryon and Lepton Nonconserving Processes*, *Phys. Rev. Lett.* **43** (1979) 1566.

[8] L. J. Hall, H. Murayama and N. Weiner, *Neutrino mass anarchy*, *Phys. Rev. Lett.* **84** (2000) 2572 [arXiv:hep-ph/9911341].

[9] B. Pontecorvo, *Mesonium and anti-mesonium*, *Sov. Phys. JETP* **6** (1957) 429 [Also in: *Zh. Eksp. Teor. Fiz.* **33** (1957) 549].

[10] B. Pontecorvo, *Inverse beta processes and nonconservation of lepton charge*, *Sov. Phys. JETP* **7** (1958) 172 [Also in: *Zh. Eksp. Teor. Fiz.* **34** (1957) 247].

[11] Z. Maki, M. Nakagawa and S. Sakata, *Remarks on the unified model of elementary particles*, *Prog. Theor. Phys.* **28** (1962) 870.

[12] B. Pontecorvo, *Neutrino Experiments and the Problem of Conservation of Leptonic Charge*, *Sov. Phys. JETP* **26** (1968) 984 [Also in: *Zh. Eksp. Teor. Fiz.* **53** (1967) 1717].

[13] V. N. Gribov and B. Pontecorvo, *Neutrino astronomy and lepton charge*, *Phys. Lett.* **28B** (1969) 493.

[14] S. Eliezer and A. R. Swift, *Experimental Consequences of $\nu_e - \nu_\mu$ Mixing in Neutrino Beams*, *Nucl. Phys.* **B105** (1976) 45.

[15] H. Fritzsch and P. Minkowski, *Vector-Like Weak Currents, Massive Neutrinos, and Neutrino Beam Oscillations*, *Phys. Lett.* **62B** (1976) 72.

[16] S. M. Bilenky and B. Pontecorvo, *Quark-Lepton Analogy and Neutrino Oscillations*, *Phys. Lett.* **61B** (1976) 248.

[17] S. M. Bilenky and B. Pontecorvo, *The Quark-Lepton Analogy and the Muonic Charge*, *Yad. Fiz.* **24** (1976) 603 [Also in: *Sov. J. Nucl. Phys.* **24** (1976) 316].

[18] S. M. Bilenky and B. Pontecorvo, *Again on Neutrino Oscillations*, *Lett. Nuovo Cim.* **17** (1976) 569.

[19] B. Kayser, *On the Quantum Mechanics of Neutrino Oscillation*, *Phys. Rev.* **D24** (1981) 110.

[20] S. M. Bilenky, J. Hosek and S. T. Petcov, *On Oscillations of Neutrinos with Dirac and Majorana Masses*, *Phys. Lett.* **94B** (1980) 495.

[21] L. Wolfenstein, *Neutrino Oscillations in Matter*, *Phys. Rev.* **D17** (1978) 2369.

[22] P. Langacker, S. T. Petcov, G. Steigman and S. Toshev, *On the Mikheev-Smirnov-Wolfenstein (MSW) Mechanism of Amplification of Neutrino Oscillations in Matter*, *Nucl. Phys.* **B282** (1987) 589.

[23] S. P. Mikheyev and A. Y. Smirnov, *Resonance Amplification of Oscillations in Matter and Spectroscopy of Solar Neutrinos*, *Sov. J. Nucl. Phys.* **42** (1985) 913.

[24] C. Giunti and C. W. Kim, *Fundamentals of Neutrino Physics and Astrophysics*. Oxford University Press, UK, 2007.

[25] K. Nakamura and S. T. Petcov in C. Patrignani et al. (Particle Data Group collaboration), *Review of Particle Physics*, *Chin. Phys.* **C40** (2016) 100001 and 2017 update.

[26] Super-Kamiokande collaboration, Y. Fukuda et al., *Evidence for oscillation of atmospheric neutrinos*, *Phys. Rev. Lett.* **81** (1998) 1562 [arXiv:hep-ex/9807003].

[27] SNO collaboration, Q. R. Ahmad et al., *Measurement of the rate of $\nu_e + d \to p + p + e^-$ interactions produced by ^8B solar neutrinos at the Sudbury Neutrino Observatory*, *Phys. Rev. Lett.* **87** (2001) 071301 [arXiv:nucl-ex/0106015].

[28] J. Schechter and J. W. F. Valle, *Neutrino Masses in SU(2)× U(1) Theories*, *Phys. Rev.* **D22** (1980) 2227.

[29] M. Doi, T. Kotani, H. Nishiura, K. Okuda and E. Takasugi, *CP Violation in Majorana Neutrinos*, *Phys. Lett.* **102B** (1981) 323.

[30] P. I. Krastev and S. T. Petcov, *Resonance Amplification and T-Violation Effects in Three Neutrino Oscillations in the Earth*, *Phys. Lett.* **B205** (1988) 84.

[31] C. Jarlskog, *Commutator of the Quark Mass Matrices in the Standard Electroweak Model and a Measure of Maximal CP Violation*, *Phys. Rev. Lett.* **55** (1985) 1039.

[32] F. Capozzi, G. L. Fogli, E. Lisi, A. Marrone, D. Montanino and A. Palazzo, *Status of three-neutrino oscillation parameters, circa 2013*, *Phys. Rev.* **D89** (2014) 093018 [arXiv:1312.2878].

[33] D. V. Forero, M. Tortola and J. W. F. Valle, *Neutrino oscillations refitted*, *Phys. Rev.* **D90** (2014) 093006 [arXiv:1405.7540].

[34] M. C. Gonzalez-Garcia, M. Maltoni and T. Schwetz, *Updated fit to three neutrino mixing: status of leptonic CP violation*, *JHEP* **11** (2014) 052 [arXiv:1409.5439].

[35] F. Capozzi, E. Lisi, A. Marrone, D. Montanino and A. Palazzo, *Neutrino masses and mixings: Status of known and unknown 3ν parameters*, *Nucl. Phys.* **B908** (2016) 218 [arXiv:1601.07777].

[36] I. Esteban, M. C. Gonzalez-Garcia, M. Maltoni, I. Martinez-Soler and T. Schwetz, *Updated fit to three neutrino mixing: exploring the accelerator-reactor complementarity*, *JHEP* **01** (2017) 087 [arXiv:1611.01514], and NuFIT 3.2 (2018), www.nu-fit.org.

[37] P. F. de Salas, D. V. Forero, C. A. Ternes, M. Tortola and J. W. F. Valle, *Status of neutrino oscillations 2018: 3σ hint for normal mass ordering and improved CP sensitivity*, *Phys. Lett.* **B782** (2018) 633 [arXiv:1708.01186].

[38] F. Capozzi, E. Di Valentino, E. Lisi, A. Marrone, A. Melchiorri and A. Palazzo, *Global constraints on absolute neutrino masses and their ordering*, *Phys. Rev.* **D95** (2017) 096014 [arXiv:1703.04471].

[39] F. Capozzi, E. Lisi, A. Marrone and A. Palazzo, *Current unknowns in the three neutrino framework*, *Prog. Part. Nucl. Phys.* **102** (2018) 48 [arXiv:1804.09678].

[40] G. L. Fogli, E. Lisi, A. Marrone, A. Palazzo and A. M. Rotunno, *Hints of $\theta_{13} > 0$ from global neutrino data analysis*, *Phys. Rev. Lett.* **101** (2008) 141801 [arXiv:0806.2649].

[41] E. Majorana, *Teoria simmetrica dell'elettrone e del positrone*, *Nuovo Cim.* **14** (1937) 171.

[42] Y. B. Zeldovich, *On the neutrino charge of elementary particles*, *Dokl. Akad. Nauk SSSR* **91** (1953) 1317 reproduced in the book "Selected works of Yakov Borisovich Zeldovich. Volume II: Particles, nuclei, and the universe", J. P. Ostriker, G. I. Barenblatt, and R. A. Sunyaev, eds.

[43] E. J. Konopinski and H. M. Mahmoud, *The Universal Fermi interaction*, *Phys. Rev.* **92** (1953) 1045.

[44] S. T. Petcov, *On Pseudo-Dirac Neutrinos, Neutrino Oscillations and Neutrinoless Double β-Decay*, *Phys. Lett.* **110B** (1982) 245.

[45] S. T. Petcov and W. Rodejohann, *Flavor symmetry $L_e - L_\mu - L_\tau$, atmospheric neutrino mixing and CP violation in the lepton sector*, *Phys. Rev.* **D71** (2005) 073002 [arXiv:hep-ph/0409135].

[46] L. Wolfenstein, *Different Varieties of Massive Dirac Neutrinos*, *Nucl. Phys.* **B186** (1981) 147.

[47] P. Minkowski, *$\mu \to e\gamma$ at a Rate of One Out of 10^9 Muon Decays?*, *Phys. Lett.* **67B** (1977) 421.

[48] T. Yanagida, *Horizontal Symmetry and Masses of Neutrinos*, *Conf. Proc.* **C7902131** (1979) 95.

[49] S. L. Glashow, *The Future of Elementary Particle Physics*, *NATO Sci. Ser. B* **61** (1980) 687.

[50] M. Gell-Mann, P. Ramond and R. Slansky, *Complex Spinors and Unified Theories*, *Conf. Proc.* **C790927** (1979) 315 [arXiv:1306.4669].

[51] R. N. Mohapatra and G. Senjanovic, *Neutrino Mass and Spontaneous Parity Violation*, *Phys. Rev. Lett.* **44** (1980) 912.

[52] W. Konetschny and W. Kummer, *Nonconservation of Total Lepton Number with Scalar Bosons*, *Phys. Lett.* **70B** (1977) 433.

[53] G. Lazarides, Q. Shafi and C. Wetterich, *Proton Lifetime and Fermion Masses in an SO(10) Model*, *Nucl. Phys.* **B181** (1981) 287.

[54] T. P. Cheng and L.-F. Li, *Neutrino Masses, Mixings and Oscillations in SU(2)$\times$U(1) Models of Electroweak Interactions*, *Phys. Rev.* **D22** (1980) 2860.

[55] R. N. Mohapatra and G. Senjanovic, *Neutrino Masses and Mixings in Gauge Models with Spontaneous Parity Violation*, *Phys. Rev.* **D23** (1981) 165.

[56] R. Foot, H. Lew, X. G. He and G. C. Joshi, *Seesaw Neutrino Masses Induced by a Triplet of Leptons*, *Z. Phys.* **C44** (1989) 441.

[57] A. Zee, *Quantum Numbers of Majorana Neutrino Masses*, *Nucl. Phys.* **B264** (1986) 99.

[58] K. S. Babu, *Model of 'Calculable' Majorana Neutrino Masses*, *Phys. Lett.* **B203** (1988) 132.

[59] K. S. Babu and E. Ma, *Radiative Mechanisms for Generating Quark and Lepton Masses: Some Recent Developments*, *Mod. Phys. Lett.* **A4** (1989) 1975.

[60] E. Ma, *Pathways to naturally small neutrino masses*, *Phys. Rev. Lett.* **81** (1998) 1171 [arXiv:hep-ph/9805219].

[61] A. Broncano, M. B. Gavela and E. E. Jenkins, *The Effective Lagrangian for the seesaw model of neutrino mass and leptogenesis*, *Phys. Lett.* **B552** (2003) 177 [arXiv:hep-ph/0210271], [Erratum: *Phys. Lett.* **B636** (2006) 332].

[62] C. N. Leung and S. T. Petcov, *A Comment on the Coexistence of Dirac and Majorana Massive Neutrinos*, *Phys. Lett.* **125B** (1983) 461.

[63] S. C. Chuliá, E. Ma, R. Srivastava and J. W. F. Valle, *Dirac Neutrinos and Dark Matter Stability from Lepton Quarticity*, *Phys. Lett.* **B767** (2017) 209 [arXiv:1606.04543].

[64] A. D. Sakharov, *Violation of CP Invariance, C asymmetry, and baryon asymmetry of the universe*, *Pisma Zh. Eksp. Teor. Fiz.* **5** (1967) 32 [Also in: *Usp. Fiz. Nauk* **161** (1991) 61].

[65] M. Fukugita and T. Yanagida, *Baryogenesis Without Grand Unification*, *Phys. Lett.* **B174** (1986) 45.

[66] F. R. Klinkhamer and N. S. Manton, *A Saddle Point Solution in the Weinberg-Salam Theory*, *Phys. Rev.* **D30** (1984) 2212.

[67] V. A. Kuzmin, V. A. Rubakov and M. E. Shaposhnikov, *On the Anomalous Electroweak Baryon Number Nonconservation in the Early Universe*, *Phys. Lett.* **155B** (1985) 36.

[68] B. Kayser, *Majorana Neutrinos and their Electromagnetic Properties*, *Phys. Rev.* **D26** (1982) 1662.

[69] C. D. Froggatt and H. B. Nielsen, *Hierarchy of Quark Masses, Cabibbo Angles and CP Violation*, *Nucl. Phys.* **B147** (1979) 277.

[70] K. S. Babu, *TASI Lectures on Flavor Physics*, in *Proceedings of TASI 2008, Boulder, USA*, pp. 49–123, 2010, [arXiv:0910.2948].

[71] G. Altarelli and F. Feruglio, *Discrete Flavor Symmetries and Models of Neutrino Mixing*, *Rev. Mod. Phys.* **82** (2010) 2701 [arXiv:1002.0211].

[72] H. Ishimori, T. Kobayashi, H. Ohki, Y. Shimizu, H. Okada and M. Tanimoto, *Non-Abelian Discrete Symmetries in Particle Physics*, *Prog. Theor. Phys. Suppl.* **183** (2010) 1 [arXiv:1003.3552].

[73] S. F. King and C. Luhn, *Neutrino Mass and Mixing with Discrete Symmetry*, *Rept. Prog. Phys.* **76** (2013) 056201 [arXiv:1301.1340].

[74] S. F. King, A. Merle, S. Morisi, Y. Shimizu and M. Tanimoto, *Neutrino Mass and Mixing: from Theory to Experiment*, *New J. Phys.* **16** (2014) 045018 [arXiv:1402.4271].

[75] C. S. Lam, *Mass Independent Textures and Symmetry*, *Phys. Rev.* **D74** (2006) 113004 [arXiv:hep-ph/0611017].

[76] T. Fukuyama and H. Nishiura, *Mass matrix of Majorana neutrinos*, [arXiv:hep-ph/9702253].

[77] R. N. Mohapatra and S. Nussinov, *Bimaximal neutrino mixing and neutrino mass matrix*, *Phys. Rev.* **D60** (1999) 013002 [arXiv:hep-ph/9809415].

[78] P. F. Harrison, D. H. Perkins and W. G. Scott, *Tri-bimaximal mixing and the neutrino oscillation data*, *Phys. Lett.* **B530** (2002) 167 [arXiv:hep-ph/0202074].

[79] G. Altarelli and F. Feruglio, *Tri-bimaximal neutrino mixing from discrete symmetry in extra dimensions*, *Nucl. Phys.* **B720** (2005) 64 [arXiv:hep-ph/0504165].

[80] C. S. Lam, *Determining Horizontal Symmetry from Neutrino Mixing*, *Phys. Rev. Lett.* **101** (2008) 121602 [arXiv:0804.2622].

[81] G. C. Branco, L. Lavoura and M. N. Rebelo, *Majorana Neutrinos and CP Violation in the Leptonic Sector*, *Phys. Lett.* **B180** (1986) 264.

[82] G. Ecker, W. Grimus and H. Neufeld, *A Standard Form for Generalized CP Transformations*, *J. Phys.* **A20** (1987) L807.

[83] H. Neufeld, W. Grimus and G. Ecker, *Generalized CP Invariance, Neutral Flavor Conservation and the Structure of the Mixing Matrix*, *Int. J. Mod. Phys.* **A3** (1988) 603.

[84] W. Grimus and M. N. Rebelo, *Automorphisms in gauge theories and the definition of CP and P*, *Phys. Rept.* **281** (1997) 239 [arXiv:hep-ph/9506272].

[85] P. F. Harrison and W. G. Scott, *μ-τ reflection symmetry in lepton mixing and neutrino oscillations*, *Phys. Lett.* **B547** (2002) 219 [arXiv:hep-ph/0210197].

[86] W. Grimus and L. Lavoura, *A Nonstandard CP transformation leading to maximal atmospheric neutrino mixing*, *Phys. Lett.* **B579** (2004) 113 [arXiv:hep-ph/0305309].

[87] F. Feruglio, C. Hagedorn and R. Ziegler, *Lepton Mixing Parameters from Discrete and CP Symmetries*, *JHEP* **07** (2013) 027 [arXiv:1211.5560].

[88] M. Holthausen, M. Lindner and M. A. Schmidt, *CP and Discrete Flavour Symmetries*, *JHEP* **04** (2013) 122 [arXiv:1211.6953].

[89] M.-C. Chen, M. Fallbacher, K. T. Mahanthappa, M. Ratz and A. Trautner, *CP Violation from Finite Groups*, *Nucl. Phys.* **B883** (2014) 267 [arXiv:1402.0507].

[90] G.-J. Ding, S. F. King, C. Luhn and A. J. Stuart, *Spontaneous CP violation from vacuum alignment in S_4 models of leptons*, *JHEP* **05** (2013) 084 [arXiv:1303.6180].

[91] F. Feruglio, *Are neutrino masses modular forms?*, [arXiv:1706.08749], to appear in the book "From my vast repertoire: the legacy of Guido Altarelli", S. Forte, A. Levy, and G. Ridolfi, eds.

[92] T. Kobayashi, K. Tanaka and T. H. Tatsuishi, *Neutrino mixing from finite modular groups*, *Phys. Rev.* **D98** (2018) 016004 [arXiv:1803.10391].

[93] J. T. Penedo and S. T. Petcov, *Lepton Masses and Mixing from Modular S_4 Symmetry*, [arXiv:1806.11040].

[94] J. C. Criado and F. Feruglio, *Modular Invariance Faces Precision Neutrino Data*, [arXiv:1807.01125].

[95] T. Kobayashi, N. Omoto, Y. Shimizu, K. Takagi, M. Tanimoto and T. H. Tatsuishi, *Modular A_4 invariance and neutrino mixing*, [arXiv:1808.03012].

[96] J. T. Penedo, S. T. Petcov and T. Yanagida, *Low-Scale Seesaw and the CP Violation in Neutrino Oscillations*, *Nucl. Phys.* **B929** (2018) 377 [arXiv:1712.09922].

[97] A. Ibarra, E. Molinaro and S. T. Petcov, *TeV Scale See-Saw Mechanisms of Neutrino Mass Generation, the Majorana Nature of the Heavy Singlet Neutrinos and $(\beta\beta)_{0\nu}$-Decay*, *JHEP* **09** (2010) 108 [arXiv:1007.2378].

[98] A. Ibarra, E. Molinaro and S. T. Petcov, *Low Energy Signatures of the TeV Scale See-Saw Mechanism*, *Phys. Rev.* **D84** (2011) 013005 [arXiv:1103.6217].

[99] D. N. Dinh, A. Ibarra, E. Molinaro and S. T. Petcov, *The $\mu - e$ Conversion in Nuclei, $\mu \to e\gamma, \mu \to 3e$ Decays and TeV Scale See-Saw Scenarios of Neutrino Mass Generation*, *JHEP* **08** (2012) 125 [arXiv:1205.4671], [Erratum: *JHEP* **09** (2013) 023].

[100] C. G. Cely, A. Ibarra, E. Molinaro and S. T. Petcov, *Higgs Decays in the Low Scale Type I See-Saw Model*, *Phys. Lett.* **B718** (2013) 957 [arXiv:1208.3654].

[101] S. Antusch, M. Blennow, E. Fernandez-Martinez and J. Lopez-Pavon, *Probing non-unitary mixing and CP-violation at a Neutrino Factory*, *Phys. Rev.* **D80** (2009) 033002 [arXiv:0903.3986].

[102] M. Shaposhnikov, *A Possible symmetry of the νMSM*, *Nucl. Phys.* **B763** (2007) 49 [arXiv:hep-ph/0605047].

[103] J. Kersten and A. Yu. Smirnov, *Right-Handed Neutrinos at CERN LHC and the Mechanism of Neutrino Mass Generation*, *Phys. Rev.* **D76** (2007) 073005 [arXiv:0705.3221].

[104] J. Sato and T. Yanagida, *Low-energy predictions of lopsided family charges*, *Phys. Lett.* **B493** (2000) 356 [arXiv:hep-ph/0009205].

[105] Y. Kaneta, M. Tanimoto and T. T. Yanagida, *Dirac CP phase in the neutrino mixing matrix and the Froggatt-Nielsen mechanism with* $\det[M_\nu] = 0$, *Phys. Lett.* **B770** (2017) 546 [arXiv:1701.08938].

[106] P. Binetruy, S. Lavignac, S. T. Petcov and P. Ramond, *Quasidegenerate neutrinos from an Abelian family symmetry*, *Nucl. Phys.* **B496** (1997) 3 [arXiv:hep-ph/9610481].

[107] M. Malinsky, J. C. Romao and J. W. F. Valle, *Novel supersymmetric SO(10) seesaw mechanism*, *Phys. Rev. Lett.* **95** (2005) 161801 [arXiv:hep-ph/0506296].

[108] D. Wyler and L. Wolfenstein, *Massless Neutrinos in Left-Right Symmetric Models*, *Nucl. Phys.* **B218** (1983) 205.

[109] R. N. Mohapatra, *Mechanism for Understanding Small Neutrino Mass in Superstring Theories*, *Phys. Rev. Lett.* **56** (1986) 561.

[110] R. N. Mohapatra and J. W. F. Valle, *Neutrino Mass and Baryon Number Nonconservation in Superstring Models*, *Phys. Rev.* **D34** (1986) 1642.

[111] J. A. Casas and A. Ibarra, *Oscillating neutrinos and $\mu \to e, \gamma$*, *Nucl. Phys.* **B618** (2001) 171 [arXiv:hep-ph/0103065].

[112] A. Ibarra and G. G. Ross, *Neutrino phenomenology: The Case of two right-handed neutrinos*, *Phys. Lett.* **B591** (2004) 285 [arXiv:hep-ph/0312138].

[113] A. Ibarra and G. G. Ross, *Neutrino properties from Yukawa structure*, *Phys. Lett.* **B575** (2003) 279 [arXiv:hep-ph/0307051].

[114] K. Nakayama, F. Takahashi and T. T. Yanagida, *Neutrino CP phases from Sneutrino Chaotic Inflation*, *Phys. Lett.* **B773** (2017) 179 [arXiv:1705.04796].

[115] W. Buchmuller and T. Yanagida, *Quark lepton mass hierarchies and the baryon asymmetry*, *Phys. Lett.* **B445** (1999) 399 [arXiv:hep-ph/9810308].

[116] S. Antusch and O. Fischer, *Testing sterile neutrino extensions of the Standard Model at future lepton colliders*, *JHEP* **05** (2015) 053 [arXiv:1502.05915].

[117] A. Das and N. Okada, *Bounds on heavy Majorana neutrinos in type-I seesaw and implications for collider searches*, *Phys. Lett.* **B774** (2017) 32 [arXiv:1702.04668].

[118] F. F. Deppisch, P. S. Bhupal Dev and A. Pilaftsis, *Neutrinos and Collider Physics*, *New J. Phys.* **17** (2015) 075019 [arXiv:1502.06541].

[119] M. Drewes, B. Garbrecht, D. Gueter and J. Klarić, *Testing the low scale seesaw and leptogenesis*, *JHEP* **08** (2017) 018 [arXiv:1609.09069].

[120] A. Das, P. S. B. Dev and C. S. Kim, *Constraining Sterile Neutrinos from Precision Higgs Data*, *Phys. Rev.* **D95** (2017) 115013 [arXiv:1704.00880].

[121] E. Fernandez-Martinez, J. Hernandez-Garcia and J. Lopez-Pavon, *Global constraints on heavy neutrino mixing*, *JHEP* **08** (2016) 033 [arXiv:1605.08774].

[122] M. Blennow, P. Coloma, E. Fernandez-Martinez, J. Hernandez-Garcia and J. Lopez-Pavon, *Non-Unitarity, sterile neutrinos, and Non-Standard neutrino Interactions*, *JHEP* **04** (2017) 153 [arXiv:1609.08637].

[123] S. T. Petcov, *The Processes $\mu \to e + \gamma$, $\mu \to e + e + \bar{e}$, $\nu' \to \nu + \gamma$ in the Weinberg-Salam Model with Neutrino Mixing*, *Sov. J. Nucl. Phys.* **25** (1977) 340 [Erratum: *Yad. Fiz.* **25** (1977) 1336].

[124] MEG collaboration, A. M. Baldini et al., *Search for the lepton flavour violating decay $\mu^+ \to e^+\gamma$ with the full dataset of the MEG experiment*, *Eur. Phys. J.* **C76** (2016) 434 [arXiv:1605.05081].

[125] SINDRUM collaboration, U. Bellgardt et al., *Search for the Decay $\mu^+ \to e^+e^+e^-$*, *Nucl. Phys.* **B299** (1988) 1.

[126] SINDRUM II collaboration, C. Dohmen et al., *Test of lepton flavor conservation in $\mu \to e$ conversion on titanium*, *Phys. Lett.* **B317** (1993) 631.

[127] SINDRUM II collaboration, W. H. Bertl et al., *A Search for μ-e conversion in muonic gold*, *Eur. Phys. J.* **C47** (2006) 337.

[128] MEG II collaboration, P. W. Cattaneo, *The MEGII detector*, *JINST* **12** (2017) C06022 [arXiv:1705.10224].

[129] A. Blondel et al., *Research Proposal for an Experiment to Search for the Decay $\mu \to eee$*, [arXiv:1301.6113].

[130] Mu2e collaboration, L. Bartoszek et al., *Mu2e Technical Design Report*, [arXiv:1501.05241].

[131] COMET collaboration, Y. Kuno, *A search for muon-to-electron conversion at J-PARC: The COMET experiment*, *PTEP* **2013** (2013) 022C01.

[132] R. J. Barlow, *The PRISM/PRIME project*, *Nucl. Phys. Proc. Suppl.* **218** (2011) 44.

[133] BaBar collaboration, B. Aubert et al., *Searches for Lepton Flavor Violation in the Decays $\tau^\pm \to e^\pm\gamma$ and $\tau^\pm \to \mu^\pm\gamma$*, *Phys. Rev. Lett.* **104** (2010) 021802 [arXiv:0908.2381].

[134] K. Hayasaka et al., *Search for Lepton Flavor Violating Tau Decays into Three Leptons with 719 Million Produced $\tau^+\tau^-$ Pairs*, *Phys. Lett.* **B687** (2010) 139 [arXiv:1001.3221].

[135] Particle Data Group collaboration, M. Carena *et al.* in C. Patrignani et al., *Review of Particle Physics*, *Chin. Phys.* **C40** (2016) 100001 and 2017 update.

[136] S. M. Bilenky and S. T. Petcov, *Massive Neutrinos and Neutrino Oscillations*, *Rev. Mod. Phys.* **59** (1987) 671 [Errata: *Rev. Mod. Phys.* **61** (1989) 169, *Rev. Mod. Phys.* **60** (1988) 575].

[137] A. Halprin, S. T. Petcov and S. P. Rosen, *Effects of Light and Heavy Majorana Neutrinos in Neutrinoless Double Beta Decay*, *Phys. Lett.* **125B** (1983) 335.

[138] W. C. Haxton and G. J. Stephenson, *Double beta Decay*, *Prog. Part. Nucl. Phys.* **12** (1984) 409.

[139] J. Lopez-Pavon, E. Molinaro and S. T. Petcov, *Radiative Corrections to Light Neutrino Masses in Low Scale Type I Seesaw Scenarios and Neutrinoless Double Beta Decay*, *JHEP* **11** (2015) 030 [arXiv:1506.05296].

[140] P. S. Bhupal Dev, P. Millington, A. Pilaftsis and D. Teresi, *Flavour Covariant Transport Equations: an Application to Resonant Leptogenesis*, *Nucl. Phys.* **B886** (2014) 569 [arXiv:1404.1003].

[141] Planck collaboration, P. A. R. Ade et al., *Planck 2015 results. XIII. Cosmological parameters*, *Astron. Astrophys.* **594** (2016) A13 [arXiv:1502.01589].

[142] M. Fukugita and T. Yanagida, *Resurrection of grand unified theory baryogenesis*, *Phys. Rev. Lett.* **89** (2002) 131602 [arXiv:hep-ph/0203194].

[143] W.-C. Huang, H. Päs and S. Zeissner, *Neutrino assisted GUT baryogenesis - revisited*, *Phys. Rev.* **D97** (2018) 055040 [arXiv:1608.04354].

[144] J. T. Penedo and S. T. Petcov, *The 10^{-3} eV Frontier in Neutrinoless Double Beta Decay*, [arXiv:1806.03203].

[145] S. Pascoli and S. T. Petcov, *Majorana Neutrinos, Neutrino Mass Spectrum and the $|\langle m\rangle| \sim 10^{-3}$ eV Frontier in Neutrinoless Double Beta Decay*, *Phys. Rev.* **D77** (2008) 113003 [arXiv:0711.4993].

[146] J. D. Vergados, H. Ejiri and F. Šimkovic, *Neutrinoless double beta decay and neutrino mass*, *Int. J. Mod. Phys.* **E25** (2016) 1630007 [arXiv:1612.02924].

[147] S. Dell'Oro, S. Marcocci, M. Viel and F. Vissani, *Neutrinoless double beta decay: 2015 review*, *Adv. High Energy Phys.* **2016** (2016) 2162659 [arXiv:1601.07512].

[148] J. Schechter and J. W. F. Valle, *Neutrinoless Double beta Decay in SU(2)×U(1) Theories*, *Phys. Rev.* **D25** (1982) 2951.

[149] M. Duerr, M. Lindner and A. Merle, *On the Quantitative Impact of the Schechter-Valle Theorem*, *JHEP* **06** (2011) 091 [arXiv:1105.0901].

[150] A. S. Barabash, *Double Beta Decay: Historical Review of 75 Years of Research*, *Phys. Atom. Nucl.* **74** (2011) 603 [arXiv:1104.2714].

[151] M. Agostini et al., *Improved Limit on Neutrinoless Double-β Decay of ^{76}Ge from GERDA Phase II*, *Phys. Rev. Lett.* **120** (2018) 132503 [arXiv:1803.11100].

[152] CUORE collaboration, C. Alduino et al., *First Results from CUORE: A Search for Lepton Number Violation via $0\nu\beta\beta$ Decay of ^{130}Te*, *Phys. Rev. Lett.* **120** (2018) 132501 [arXiv:1710.07988].

[153] KamLAND-Zen collaboration, A. Gando et al., *Search for Majorana Neutrinos near the Inverted Mass Hierarchy Region with KamLAND-Zen*, *Phys. Rev. Lett.* **117** (2016) 082503 [arXiv:1605.02889], [Addendum: *Phys. Rev. Lett.* **117** (2016) 109903].

[154] S. Pascoli and S. T. Petcov, *The SNO solar neutrino data, neutrinoless double beta decay and neutrino mass spectrum*, *Phys. Lett.* **B544** (2002) 239 [arXiv:hep-ph/0205022], [Addendum: *Phys. Lett.* **B580** (2004) 280].

[155] F. Iachello, J. Kotila and J. Barea, *Quenching of g_A and its impact in double beta decay*, *PoS* **NEUTEL2015** (2015) 047.

[156] Troitsk collaboration, V. N. Aseev et al., *An upper limit on electron antineutrino mass from Troitsk experiment*, *Phys. Rev.* **D84** (2011) 112003 [arXiv:1108.5034].

[157] C. Kraus et al., *Final results from phase II of the Mainz neutrino mass search in tritium beta decay*, *Eur. Phys. J.* **C40** (2005) 447 [arXiv:hep-ex/0412056].

[158] K. Eitel, *Direct neutrino mass experiments*, *Nucl. Phys. Proc. Suppl.* **143** (2005) 197.

[159] Planck collaboration, N. Aghanim et al., *Planck intermediate results. XLVI. Reduction of large-scale systematic effects in HFI polarization maps and estimation of the reionization optical depth*, *Astron. Astrophys.* **596** (2016) A107 [arXiv:1605.02985].

[160] S. M. Koksbang and S. Hannestad, *Constraining dynamical neutrino mass generation with cosmological data*, *JCAP* **1709** (2017) 014 [arXiv:1707.02579].

[161] S.-F. Ge and M. Lindner, *Extracting Majorana properties from strong bounds on neutrinoless double beta decay*, *Phys. Rev.* **D95** (2017) 033003 [arXiv:1608.01618].

[162] Z.-z. Xing and Z.-h. Zhao, *The effective neutrino mass of neutrinoless double-beta decays: how possible to fall into a well*, *Eur. Phys. J.* **C77** (2017) 192 [arXiv:1612.08538].

[163] L. Wolfenstein, *CP Properties of Majorana Neutrinos and Double beta Decay*, *Phys. Lett.* **107B** (1981) 77.

[164] B. Kayser, *CPT, CP, and c Phases and their Effects in Majorana Particle Processes*, *Phys. Rev.* **D30** (1984) 1023.

[165] S. M. Bilenky, N. P. Nedelcheva and S. T. Petcov, *Some Implications of the CP Invariance for Mixing of Majorana Neutrinos*, *Nucl. Phys.* **B247** (1984) 61.

[166] G.-J. Ding and Y.-L. Zhou, *Predicting lepton flavor mixing from* $\Delta(48)$ *and generalized CP symmetries*, *Chin. Phys.* **C39** (2015) 021001 [arXiv:1312.5222].

[167] G.-J. Ding and Y.-L. Zhou, *Lepton mixing parameters from* $\Delta(48)$ *family symmetry and generalised CP*, *JHEP* **06** (2014) 023 [arXiv:1404.0592].

[168] S. F. King and T. Neder, *Lepton mixing predictions including Majorana phases from* $\Delta(6n^2)$ *flavour symmetry and generalised CP*, *Phys. Lett.* **B736** (2014) 308 [arXiv:1403.1758].

[169] G.-J. Ding and S. F. King, *Generalized CP and* $\Delta(96)$ *family symmetry*, *Phys. Rev.* **D89** (2014) 093020 [arXiv:1403.5846].

[170] C. Hagedorn, A. Meroni and E. Molinaro, *Lepton mixing from* $\Delta(3n^2)$ *and* $\Delta(6n^2)$ *and CP*, *Nucl. Phys.* **B891** (2015) 499 [arXiv:1408.7118].

[171] G.-J. Ding, S. F. King and T. Neder, *Generalised CP and* $\Delta(6n^2)$ *family symmetry in semi-direct models of leptons*, *JHEP* **12** (2014) 007 [arXiv:1409.8005].

[172] G.-J. Ding and S. F. King, *Generalized CP and* $\Delta(3n^2)$ *Family Symmetry for Semi-Direct Predictions of the PMNS Matrix*, *Phys. Rev.* **D93** (2016) 025013 [arXiv:1510.03188].

[173] J. T. Penedo, S. T. Petcov and A. V. Titov, *Neutrino mixing and leptonic CP violation from S_4 flavour and generalised CP symmetries*, *JHEP* **12** (2017) 022 [arXiv:1705.00309].

[174] S. T. Petcov, *Predicting the values of the leptonic CP violation phases in theories with discrete flavour symmetries*, *Nucl. Phys.* **B892** (2015) 400 [arXiv:1405.6006].

[175] I. Girardi, S. T. Petcov and A. V. Titov, *Predictions for the Leptonic Dirac CP Violation Phase: a Systematic Phenomenological Analysis*, *Eur. Phys. J.* **C75** (2015) 345 [arXiv:1504.00658].

[176] I. Girardi, S. T. Petcov, A. J. Stuart and A. V. Titov, *Leptonic Dirac CP Violation Predictions from Residual Discrete Symmetries*, *Nucl. Phys.* **B902** (2016) 1 [arXiv:1509.02502].

[177] D. Marzocca, S. T. Petcov, A. Romanino and M. C. Sevilla, *Nonzero $|U_{e3}|$ from Charged Lepton Corrections and the Atmospheric Neutrino Mixing Angle*, *JHEP* **05** (2013) 073 [arXiv:1302.0423].

[178] M. Tanimoto, *Neutrinos and flavor symmetries*, *AIP Conf. Proc.* **1666** (2015) 120002.

[179] P. Ballett, S. F. King, C. Luhn, S. Pascoli and M. A. Schmidt, *Testing atmospheric mixing sum rules at precision neutrino facilities*, *Phys. Rev.* **D89** (2014) 016016 [arXiv:1308.4314].

[180] S.-F. Ge, D. A. Dicus and W. W. Repko, *Residual Symmetries for Neutrino Mixing with a Large θ_{13} and Nearly Maximal δ_D*, *Phys. Rev. Lett.* **108** (2012) 041801 [arXiv:1108.0964].

[181] S.-F. Ge, D. A. Dicus and W. W. Repko, *Z_2 Symmetry Prediction for the Leptonic Dirac CP Phase*, *Phys. Lett.* **B702** (2011) 220 [arXiv:1104.0602].

[182] S. Antusch, S. F. King, C. Luhn and M. Spinrath, *Trimaximal mixing with predicted θ_{13} from a new type of constrained sequential dominance*, *Nucl. Phys.* **B856** (2012) 328 [arXiv:1108.4278].

[183] I. Girardi, S. T. Petcov and A. V. Titov, *Determining the Dirac CP Violation Phase in the Neutrino Mixing Matrix from Sum Rules*, *Nucl. Phys.* **B894** (2015) 733 [arXiv:1410.8056].

[184] I. Girardi, S. T. Petcov and A. V. Titov, *Predictions for the Dirac CP Violation Phase in the Neutrino Mixing Matrix*, *Int. J. Mod. Phys.* **A30** (2015) 1530035 [arXiv:1504.02402], [Also in: *Adv. Ser. Direct. High Energy Phys.* **25** (2015) 69].

[185] A. D. Hanlon, S.-F. Ge and W. W. Repko, *Phenomenological consequences of residual Z_2^s and $\overline{Z}_2^s$ symmetries*, *Phys. Lett.* **B729** (2014) 185 [arXiv:1308.6522].

[186] G.-J. Ding, S. F. King and A. J. Stuart, *Generalised CP and A_4 Family Symmetry*, *JHEP* **12** (2013) 006 [arXiv:1307.4212].

[187] C.-C. Li and G.-J. Ding, *Lepton Mixing in A_5 Family Symmetry and Generalized CP*, *JHEP* **05** (2015) 100 [arXiv:1503.03711].

[188] A. Di Iura, C. Hagedorn and D. Meloni, *Lepton mixing from the interplay of the alternating group A_5 and CP*, *JHEP* **08** (2015) 037 [arXiv:1503.04140].

[189] P. Ballett, S. Pascoli and J. Turner, *Mixing angle and phase correlations from A_5 with generalized CP and their prospects for discovery*, *Phys. Rev.* **D92** (2015) 093008 [arXiv:1503.07543].

[190] C.-Y. Yao and G.-J. Ding, *CP Symmetry and Lepton Mixing from a Scan of Finite Discrete Groups*, *Phys. Rev.* **D94** (2016) 073006 [arXiv:1606.05610].

[191] I. Girardi, A. Meroni, S. T. Petcov and M. Spinrath, *Generalised geometrical CP violation in a T' lepton flavour model*, *JHEP* **02** (2014) 050 [arXiv:1312.1966].

[192] J. Turner, *Predictions for leptonic mixing angle correlations and nontrivial Dirac CP violation from A_5 with generalized CP symmetry*, *Phys. Rev.* **D92** (2015) 116007 [arXiv:1507.06224].

[193] I. Girardi, S. T. Petcov and A. V. Titov, *Predictions for the Majorana CP Violation Phases in the Neutrino Mixing Matrix and Neutrinoless Double Beta Decay*, *Nucl. Phys.* **B911** (2016) 754 [arXiv:1605.04172].

[194] J.-N. Lu and G.-J. Ding, *Alternative Schemes of Predicting Lepton Mixing Parameters from Discrete Flavor and CP Symmetry*, *Phys. Rev.* **D95** (2017) 015012 [arXiv:1610.05682].

[195] A. V. Titov, *Phenomenology of the Discrete Symmetry Approach to Neutrino Mixing and Leptonic CP Violation*, Ph.D. thesis, SISSA, Trieste, 2017.

[196] C. Hagedorn, S. F. King and C. Luhn, *A SUSY GUT of Flavour with $S_4 \times SU(5)$ to NLO*, *JHEP* **06** (2010) 048 [arXiv:1003.4249].

[197] C.-C. Li and G.-J. Ding, *Deviation from bimaximal mixing and leptonic CP phases in S_4 family symmetry and generalized CP*, *JHEP* **08** (2015) 017 [arXiv:1408.0785].

[198] S. F. King and C. Luhn, *A New family symmetry for SO(10) GUTs*, *Nucl. Phys.* **B820** (2009) 269 [arXiv:0905.1686].

[199] S. M. Bilenky, S. Pascoli and S. T. Petcov, *Majorana neutrinos, neutrino mass spectrum, CP violation and neutrinoless double beta decay. 1. The Three neutrino mixing case*, *Phys. Rev.* **D64** (2001) 053010 [arXiv:hep-ph/0102265].

[200] J. F. Nieves and P. B. Pal, *Minimal Rephasing Invariant CP Violating Parameters With Dirac and Majorana Fermions*, *Phys. Rev.* **D36** (1987) 315.

[201] J. A. Aguilar-Saavedra and G. C. Branco, *Unitarity triangles and geometrical description of CP violation with Majorana neutrinos*, *Phys. Rev.* **D62** (2000) 096009 [arXiv:hep-ph/0007025].

[202] J. F. Nieves and P. B. Pal, *Rephasing invariant CP violating parameters with Majorana neutrinos*, *Phys. Rev.* **D64** (2001) 076005 [arXiv:hep-ph/0105305].

[203] Daya Bay collaboration, J. Ling, *Precision Measurement of $\sin^2(2\theta_{13})$ and $|\Delta m^2_{ee}|$ from Daya Bay*, *PoS* **ICHEP2016** (2016) 467.

[204] JUNO collaboration, F. An et al., *Neutrino Physics with JUNO*, *J. Phys.* **G43** (2016) 030401 [arXiv:1507.05613].

[205] Y.-F. Li, *Overview of the Jiangmen Underground Neutrino Observatory (JUNO)*, *Int. J. Mod. Phys. Conf. Ser.* **31** (2014) 1460300 [arXiv:1402.6143].

[206] T2K collaboration, K. Abe et al., *Neutrino oscillation physics potential of the T2K experiment*, *PTEP* **2015** (2015) 043C01 [arXiv:1409.7469].

[207] K. Abe et al., *Proposal for an Extended Run of T2K to* 20×10^{21} *POT*, [arXiv:1609.04111].

[208] Hyper-Kamiokande Proto-Collaboration collaboration, K. Abe et al., *Physics potential of a long-baseline neutrino oscillation experiment using a J-PARC neutrino beam and Hyper-Kamiokande*, *PTEP* **2015** (2015) 053C02 [arXiv:1502.05199].

[209] DUNE collaboration, R. Acciarri et al., *Long-Baseline Neutrino Facility (LBNF) and Deep Underground Neutrino Experiment (DUNE)*, [arXiv:1512.06148].

[210] M. Agostini et al., *Background-free search for neutrinoless double-β decay of ^{76}Ge with GERDA*, *Nature* **544** (2017) 47 [arXiv:1703.00570].

[211] S. T. Petcov, *Theory prospective on leptonic CP violation*, *Nucl. Phys.* **B908** (2016) 279.

[212] S. Ferrara, D. Lust, A. D. Shapere and S. Theisen, *Modular Invariance in Supersymmetric Field Theories*, *Phys. Lett.* **B225** (1989) 363.

[213] S. Ferrara, D. Lust and S. Theisen, *Target Space Modular Invariance and Low-Energy Couplings in Orbifold Compactifications*, *Phys. Lett.* **B233** (1989) 147.

[214] R. de Adelhart Toorop, F. Feruglio and C. Hagedorn, *Finite Modular Groups and Lepton Mixing*, *Nucl. Phys.* **B858** (2012) 437 [arXiv:1112.1340].

[215] R. de Adelhart Toorop, *A flavour of family symmetries in a family of flavour models*, Ph.D. thesis, Leiden U., Leiden, Netherlands, 2012.

[216] G. Köhler, *Eta Products and Theta Series Identities*, Springer Monographs in Mathematics. Springer Berlin Heidelberg, 2011.

[217] G. Ross and M. Serna, *Unification and fermion mass structure*, *Phys. Lett.* **B664** (2008) 97 [arXiv:0704.1248].

[218] F. Bazzocchi, L. Merlo and S. Morisi, *Fermion Masses and Mixings in a S(4)-based Model*, *Nucl. Phys.* **B816** (2009) 204 [arXiv:0901.2086].